

Resonant Processes in a Frozen Gas

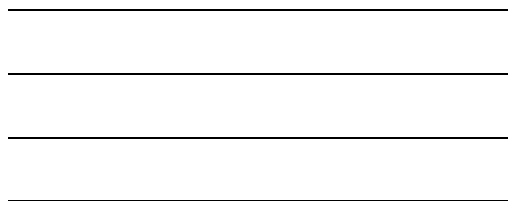
Jeremy Shane Frasier
Charlottesville, Virginia

B.S. University of Virginia, 1996

A Dissertation presented to the Graduate Faculty of the
University of Virginia in Candidacy for the Degree of Doctor of
Philosophy

Department of Physics

University of Virginia
May, 2001



© Copyright by
Jeremy Shane Frasier
All Rights Reserved
May, 2001

Acknowledgements

First I would like to thank my advisor, Vittorio Celli, for agreeing to take me on as a student and for finding an interesting and novel problem on which to work.

Thanks to Michael Fowler, we were lucky enough to have Tom Blum work with us during the summer of 1998. We made a great deal of progress and submitted our first publication on this work that summer, in large part because of Tom's diligent efforts. He also kept me from becoming lazy while my advisor was away.

Tom Gallagher first brought the results of his experiments to our attention, and he was always willing to discuss this work with us. He also provided me with the opportunity to travel to the University of Paris and work with Vladimir Akulin during the spring of 1999.

Ziad Maassarani, Tim Newman, and Mike Robinson provided many useful discussions. Bryan Wright was always willing to lend his considerable computer expertise. Bobby Anderson and Jay Lowell kindly provided the raw data for the figures that appear in their theses. Jay also donated a postscript file he created of the energy levels of rubidium, which saved me the enormous trouble of recreating that figure from scratch.

Acknowledgement is made to the Thomas F. and Kate Miller Jeffress Memorial Trust for the support of this research. I was supported by a Dissertation Year Fellowship from the Graduate School of Arts and Sciences during the fall and spring semesters of the 1999–2000 school year. During the 1996–1999 school years I was supported by a Presidential Fellowship and a Hugh P. Kelly Fellowship from the Department of Physics.

Abstract

In this thesis are presented analytical results and numerical simulations concerning resonant processes in a frozen gas. This work was begun with the intent of modeling experiments involving energy transfer due to dipole-dipole interactions between ultracold Rydberg atoms, and the subsequent propagation of dipolar excitons. However, the results and the techniques developed to obtain them are more generally applicable to a wide variety of problems.

We start by studying a simplified model that considers only the energy transfer process in an infinite medium of randomly distributed atoms. This model is very instructive, because it gives a simplified arena in which to develop the techniques that are used again and again throughout the thesis. Exact analytical results are obtained for the time evolution of energy transfer, its dependence on the detuning from resonance, and the localization distance over which the transfer process is effective. The result for the initial rate of energy transfer turns out to have general validity. This soluble model also provides an excellent means for testing the numerical simulations that are carried out for a finite sample.

When we allow for the propagation of dipolar excitons, it is no longer possible to obtain exact analytical solutions, but an approximation has been found that agrees quite well with the numerical simulations for the amplitude of the overall process. Simulations are necessary to find the sample-averaged probability of the overall process, and also to take into account the dependence of the results on the sample shape.

In the experiments we wish to model, the atomic states are degenerate with respect to the sign of the projection of total angular momentum in the direction of the applied electric field. We show that, in one case of interest, this degeneracy simply leads to a

rescaling of the dipole-dipole interaction in the final formulas for the simple model.

Contents

1	Introduction	1
2	Sparse $ss' \rightarrow pp'$ Processes — The Simple Model	10
2.1	Introduction	10
2.2	Basic equations	11
2.3	Averaging over atom positions	12
2.4	The averaged signal and lineshape	16
2.4.1	The Laplace and Fourier transforms	17
2.4.2	Inverting the Laplace transform	17
2.4.3	A numerical method using Eq. (2.25)	21
2.4.4	Comparison of the three methods	24
2.4.5	Plots and discussion	25
2.5	Averaging more complicated interaction potentials	27
2.5.1	Interaction potential of aligned dipoles	30
2.5.2	Effect of a different radial dependence on the initial rise	31
2.6	Summary	32
3	Localization in the Simple Model	34
3.1	Introduction	34
3.2	The function $\langle \mathcal{S}(\Delta, \mathbf{r}, t) \rangle$	35
3.2.1	Computation of the Laplace transform of $\langle \mathcal{S}(\Delta, \mathbf{r}, t) \rangle$	35
3.2.2	Inverting the Laplace transform	36
3.2.3	A check on the result for $\langle \tilde{\mathcal{S}}(\Delta, \mathbf{r}, \alpha) \rangle$	37

3.2.4	Plots	38
3.3	The moments of $\langle \mathcal{S}(\Delta, \mathbf{r}, t) \rangle$	40
3.3.1	Computation of $\tilde{\mathcal{M}}_p(\Delta, \alpha)$	40
3.3.2	Inverting the Laplace transform	42
3.3.3	A more convenient form for $\mathcal{M}_p(\Delta, t)$	44
3.3.4	A check on the result for $\mathcal{M}_p(\Delta, t)$	47
3.3.5	Plots	47
3.4	Summary	48
4	Sparse $ss' \rightarrow pp'$ Processes with U Interaction	55
4.1	Introduction	55
4.2	The Cayley tree approximation	56
4.2.1	Justification of the Cayley tree approximation	56
4.2.2	Cayley tree approximation with the U process only	58
4.2.3	Cayley tree approximation with U and V processes in the absence of Δ	61
4.2.4	Cayley tree approximation with U and V processes in the presence of Δ	62
4.3	The Hubbard approximation	62
4.3.1	Computation of $\langle 1/f \rangle$	63
4.3.2	Computation of $\langle 1/f_0 \rangle$	65
4.3.3	Computation of $\langle a_0(\Delta, t) ^2 \rangle$ with the U process only at resonance	66
4.4	The coherent potential approximation	71
4.4.1	Computation of $\langle 1/f \rangle$	71
4.4.2	Computation of $\langle 1/f_0 \rangle$	71
4.5	Comparison of the Cayley, Hubbard, and CPA approximations	72
4.6	Plots	74
4.6.1	The averaged amplitude $\langle a_0 \rangle$ as a function of time	74
4.6.2	The averaged amplitude $\langle a_0 \rangle$ as a function of frequency	79
4.7	Summary	83
5	Analogy With Spin Glasses	89
5.1	Introduction	89
5.2	The rubidium system as a spin glass	89

5.2.1	Spin glass Hamiltonian and equations of motion	89
5.2.2	Reduction to the sparse limit	91
5.2.3	Another spin glass Hamiltonian for the rubidium system	91
5.3	Spin glass model for the cesium system	93
5.4	Summary	94
6	The Effect of Spin	95
6.1	Introduction	95
6.2	Matrix elements for the $ss' \rightarrow pp'$ and $sp \rightarrow ps$ processes	96
6.2.1	The dipole-dipole interaction	96
6.2.2	Dipolar matrix elements	97
6.2.3	A change of basis	99
6.2.4	The $ss' \rightarrow pp'$ and $sp \rightarrow ps$ matrix elements	100
6.3	Determining the potential	101
6.3.1	States and probability amplitudes with spin included	102
6.3.2	Equations of motion	103
6.3.3	Dirac matrices	106
6.3.4	Separability	108
6.3.5	Averaging the $ss' \rightarrow pp'$ process when $ m_j = 3/2$ for the p' atom	112
6.4	Summary	116
7	Numerical Simulations	117
7.1	Introduction	117
7.2	Review of theoretical model	117
7.3	Description of method	119
7.4	The effect of many s' atoms	121
7.4.1	The chemical argument	121
7.4.2	Extrapolation to many s' atoms	122
7.5	Results of simulations for the signal	124
7.6	Results of simulations for the width	130
7.7	Comparison with experimental data	130
7.8	Summary	133

8 Final Thoughts

List of Figures

1.1	The s , s' , p , and p' energy levels of Rb as a function of electric field	3
1.2	Illustration of the $ss' \rightarrow pp'$ and $sp \rightarrow ps$ processes	4
1.3	Experimental signal as a function of time	5
1.4	Experimental lineshape as a function of detuning	7
2.1	Signal as a function of time	26
2.2	Resonance width as a function of time	28
2.3	Saturation lineshape	29
3.1	The quantity $r^2 \langle \mathcal{S}(\Delta, \mathbf{r}, t = \infty) \rangle$ as a function of r for several values of Δ	39
3.2	The moments $\mathcal{M}_p(0, t)$ for $p = -2, -1, 1$, and 2	49
3.3	The moments $\mathcal{M}_p(v, t)$ for $p = -2, -1, 1$, and 2	50
3.4	The moments $\mathcal{M}_p(2v, t)$ for $p = -2, -1, 1$, and 2	51
3.5	The localization lengths $l_p(0, t)$ for $p = -2, -1, 1$, and 2	52
3.6	The localization lengths $l_p(v, t)$ for $p = -2, -1, 1$, and 2	53
3.7	The localization lengths $l_p(2v, t)$ for $p = -2, -1, 1$, and 2	54
4.1	Averaged signal as a function of time for the Hubbard approximation	70
4.2	Real part of $\langle a_0(\Delta, \omega) \rangle$ for $u = 0$	75
4.3	Real part of $\langle a_0(\Delta, \omega) \rangle$ for $u = 0.25v$	76
4.4	Real part of $\langle a_0(\Delta, \omega) \rangle$ for $u = v$	77
4.5	Real part of $\langle a_0(\Delta, \omega) \rangle$ for $u = 4v$	78
4.6	Real part of $\langle a_0(\Delta, t) \rangle$	80
4.7	Imaginary part of $\langle a_0(\Delta, t) \rangle$	81

4.8	Real part of $\langle a_0(\Delta, \omega) \rangle$ for $u = 0$ — comparison with simulation	84
4.9	Real part of $\langle a_0(\Delta, \omega) \rangle$ for $u = 0.25v$ — comparison with simulation	85
4.10	Real part of $\langle a_0(\Delta, \omega) \rangle$ for $u = v$ — comparison with simulation	86
4.11	Real part of $\langle a_0(\Delta, \omega) \rangle$ for $u = 4v$ — comparison with simulation	87
7.1	Comparison of simulation with exact results	125
7.2	Averaged signal as a function of time for $u = 0.25v$	126
7.3	Averaged signal as a function of time for $u = v$	127
7.4	Averaged signal as a function of time for $u = 2v$	128
7.5	Averaged signal as a function of time for $u = 4v$	129
7.6	Width as a function of time for $u = 4v$	131
7.7	Width as a function of u/v	132
7.8	Experimental signal as a function of time — larger density	134
7.9	Experimental signal as a function of time — smaller density	135
7.10	Experimental width as a function of time	136

List of Tables

6.1	Decomposition of p and p' states	100
6.2	Matrix elements for the $ss' \rightarrow pp'$ process ($ m_j = 3/2$)	101
6.3	Matrix elements for the $ss' \rightarrow pp'$ process ($ m_j = 1/2$)	102
6.4	Matrix elements for the $sp \rightarrow ps$ process	102
6.5	The P matrix for the $ss' \rightarrow pp'$ process ($ m_j = 3/2$)	107
6.6	The P matrix for the $ss' \rightarrow pp'$ process ($ m_j = 1/2$)	107
6.7	The P matrix for the $sp \rightarrow ps$ process	108
6.8	Projections of P onto the Dirac matrices for the $ss' \rightarrow pp'$ process ($ m_j = 3/2$) . . .	108
6.9	Projections of P onto the Dirac matrices for the $ss' \rightarrow pp'$ process ($ m_j = 1/2$) . . .	109
6.10	Projections of P onto the Dirac matrices for the $sp \rightarrow ps$ process	109

Chapter 1

Introduction

Frozen gases are a new and in many ways ideal laboratory to test our understanding of quantum theory in a complex system. With present technology one can manipulate and detect electronic processes with an extraordinary selectivity and precision. Furthermore, the translational temperature of the gas can be lowered to the point where it can be ignored when discussing electronic processes. Frozen Rydberg gases have the added advantages that their states are well understood and many processes occur on a microsecond time scale, easily allowing for time-resolved spectroscopy.

Pioneering experiments on resonant processes in these gases have been carried out by Anderson *et al.* [5, 6] and Mourachko *et al.* [45, 44]. The present work was motivated by the desire to understand those experiments and the subsequent work of Lowell *et al.* [40] highlighting the dynamic aspects of these resonant, many particle systems. The measurements of Anderson *et al.* and Lowell *et al.* are performed on mixtures of cold (about 150 μK) ^{85}Rb atoms initially prepared in the $25s_{1/2}$ and $33s_{1/2}$ states, henceforth to be called the s and s' states respectively. There are initially N atoms in the s state and N' atoms in the s' state. A dipole matrix element μ connects the state s to the state p , and another dipole matrix element μ' connects the state s' to the state p' , where p refers to the $24p_{1/2}$ state and p' refers to the $34p_{3/2}$ state. Dipole-dipole interactions cause $ss' \rightarrow pp'$ interactions to occur, and then $sp \rightarrow ps$ and $s'p' \rightarrow p's'$ flippings become possible.¹ The number of p' states is measured after a given time has elapsed, up to about 5 μs . As a function of time, the number of p' states rises rapidly at first and then slowly saturates. The energy of a pp' pair can be swept

¹Although the $s'p' \rightarrow p's'$ process is present, it is smaller than the $sp \rightarrow ps$ process by a factor of 16 in this case and can therefore be neglected to a first approximation, except when $N \ll N'$.

through resonance with an ss' pair, where $\epsilon_{s'} + \epsilon_s = \epsilon_{p'} + \epsilon_p$, via the Stark effect by the application of an electric field.² At any one time the resonance lineshape can be obtained as a function of the detuning $\Delta = \epsilon_{p'} + \epsilon_p - \epsilon_{s'} - \epsilon_s$, which is a known function of the applied electric field.

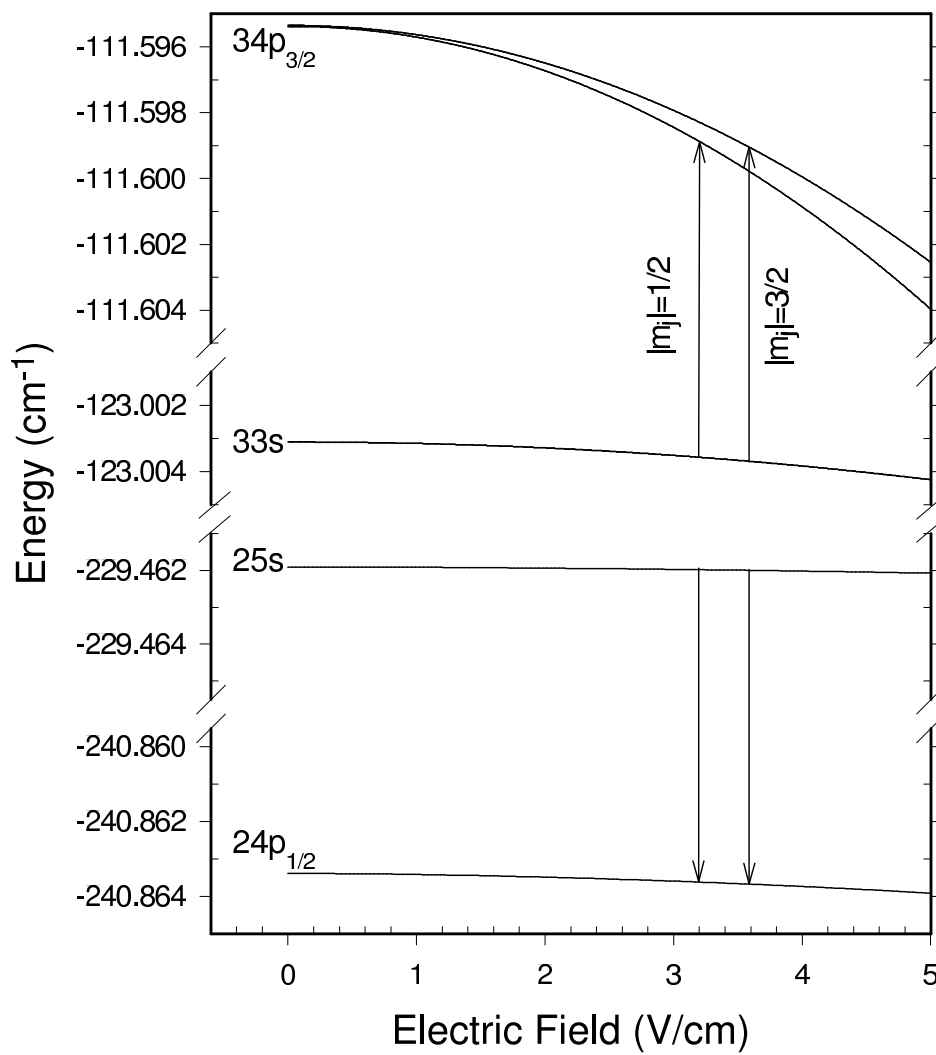
Figure 1.1 shows the s , s' , p , and p' energies as a function of the applied electric field. This figure is a slightly modified version of Fig. 3.1 on page 54 of Ref. [40]. Because the p' state is in the $j = 3/2$ state, there are actually two resonances. One corresponds to the two $|m_j| = 1/2$ states, and the other corresponds to the two $|m_j| = 3/2$ states. To a first approximation the two resonances can be treated separately.

Figure 1.2 is a schematic of the $ss' \rightarrow pp'$ and $sp \rightarrow ps$ processes. In this illustration the circles represent atoms in an s state and the ovals represent atoms in a p state. In addition, the black shapes represent primed states, while the grey shapes represent unprimed states. The first panel shows a single atom in the s' state surrounded by atoms in the s state. In going from the first to the second panel an ss' pair has made the $ss' \rightarrow pp'$ transition via an interaction potential V . In the third panel an sp pair has made the $sp \rightarrow ps$ transition via an interaction potential U . In the final panel the pp' pair has made the $ss' \rightarrow pp'$ transition, and the system has returned to the initial state of the first panel.

Several features of the experimental data present a challenge to theorists and are investigated in this thesis. The first feature we wish to understand is the rapid rise followed by slow approach to saturation of the signal. This behavior can be seen in Fig. 1.3, which is a plot of the experimental data taken from Fig. 3.8 on page 71 of Ref. [40] with all the data points shown. Each individual interaction between pairs of atoms leads to a coherent oscillatory behavior, but as we will see in Chapter 2, averaging the $ss' \rightarrow pp'$ interaction over the random positions of the atoms greatly smooths out the signal. The effective incoherence brought about by the $sp \rightarrow ps$ process (the “walking away” discussed by Mourachko *et al.* [45, 44]) completes the smoothing out of the on-resonance signal but has less effect on the off-resonance signal.

We also want to understand the width of the lineshape in the detuning Δ as a function of time. Fig. 1.4 shows a plot of the experimental data for the lineshape as a function of detuning for an interaction time of $1.78 \mu\text{s}$. These data are taken from Fig. 3.9 on page 74 of Ref. [40]. We note the presence of two resonances, which as was stated before correspond to the $|m_j| = 1/2$ and $|m_j| = 3/2$ states of the p' atom. The behavior of the collisional resonance width as a function of temperature

²For a discussion of the Stark effect in hydrogenic atoms, see pages 228–241 of Ref. [9] or pages 164–171 of Ref. [19].

Figure 1.1: The s , s' , p , and p' energy levels of Rb as a function of electric field.

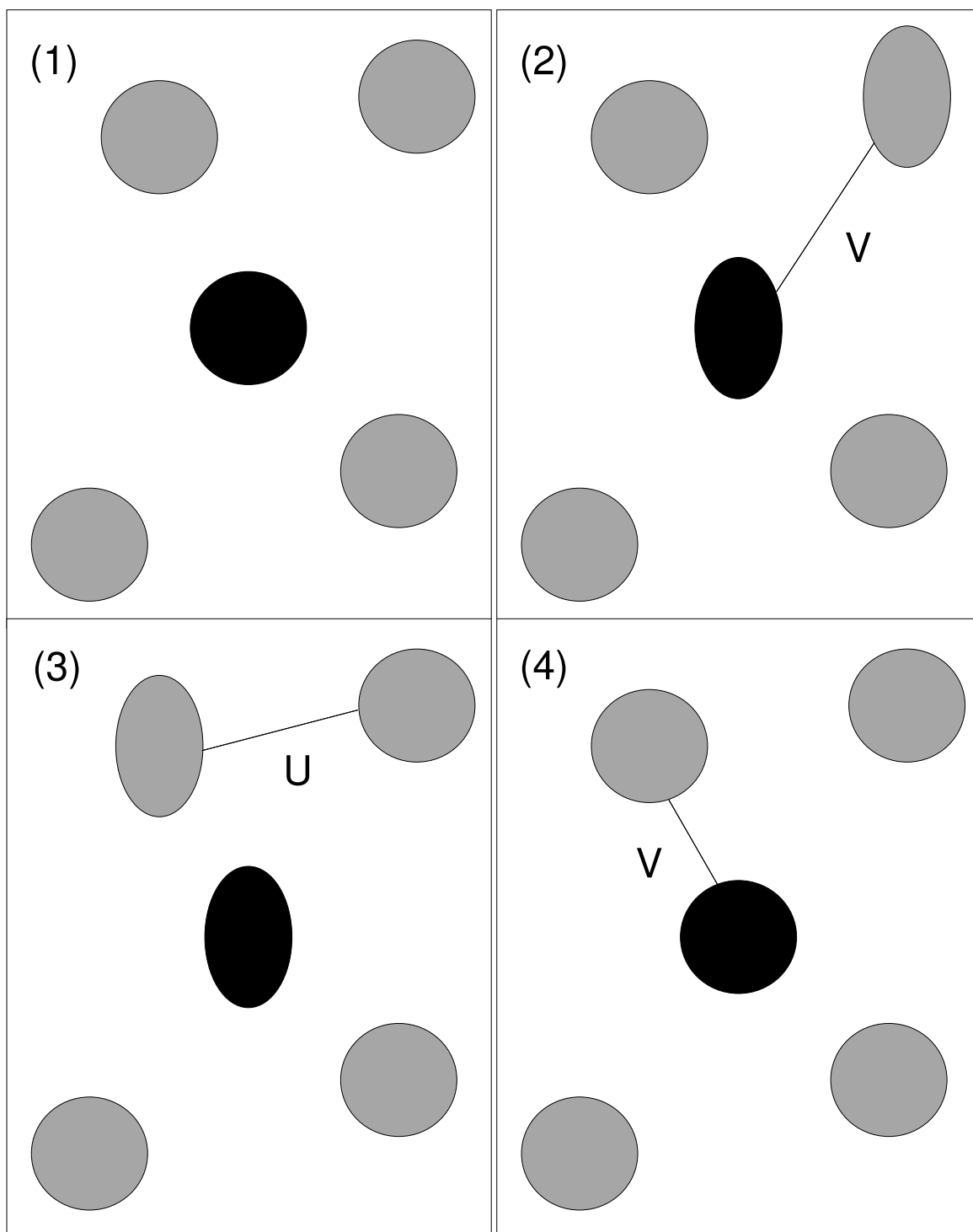


Figure 1.2: The circles represent atoms in an s state and the ovals represent atoms in a p state. The black shapes are in primed states, while the grey shapes are in unprimed states. The first panel shows a single atom in the s' state surrounded by atoms in the s state. In the second panel an ss' pair has made the $ss' \rightarrow pp'$ transition via an interaction potential V . In the third panel an sp pair has made the $sp \rightarrow ps$ transition via an interaction potential U . In the final panel the pp' pair has made the $ss' \rightarrow pp'$ transition, and the system is again in its initial state.

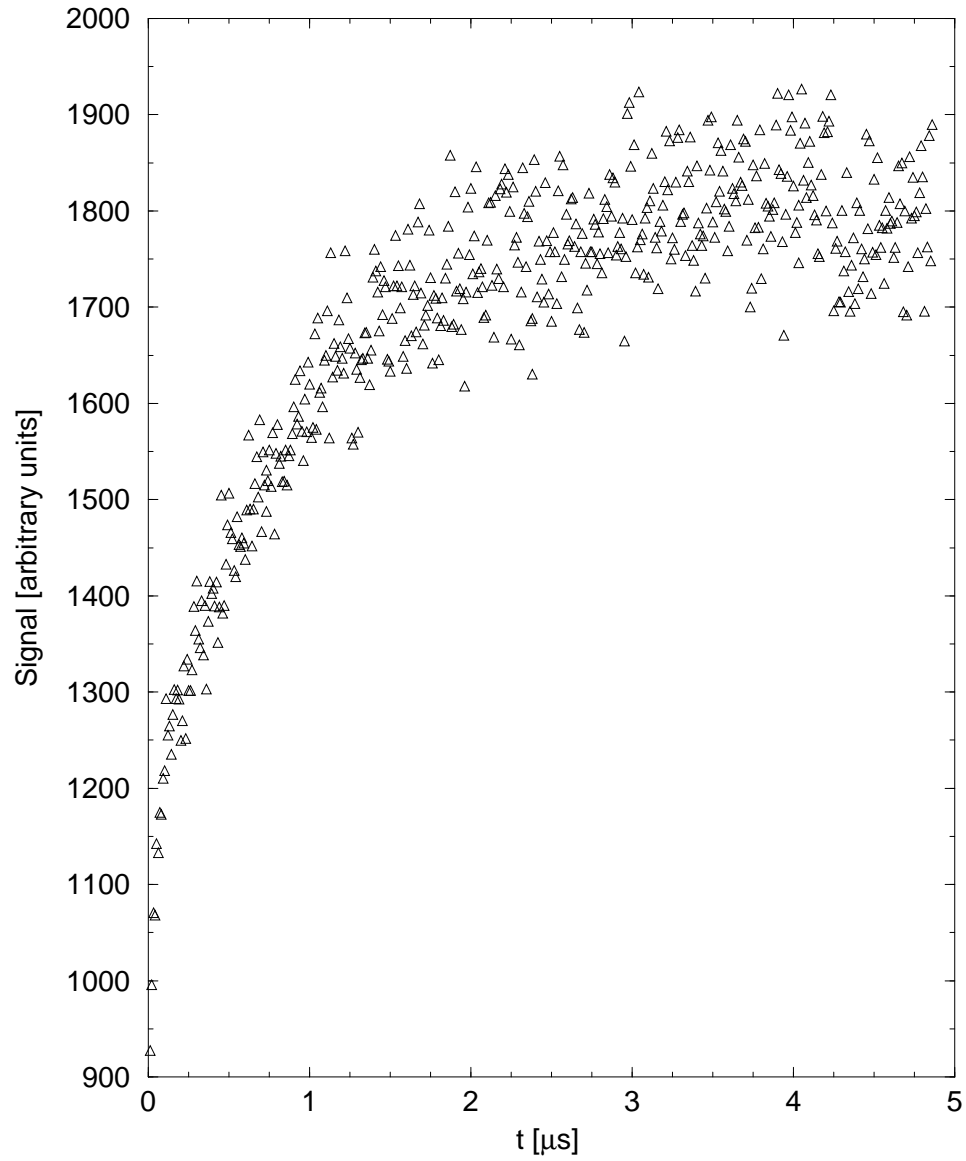


Figure 1.3: A representative plot of the experimental signal as a function of time. The data are taken from Fig. 3.8 on page 71 of Ref. [40] with all the data points shown.

for hot (i.e., roughly room temperature) Rydberg gases is known to be

$$\Delta\nu \propto T^{3/4}, \quad (1.1)$$

as can be found in Ref. [21] or on page 293 of Ref. [22]. This result agrees quite well with experiments on such gases,³ and is obtained by considering only two-body collisions. Simply plugging the temperature 150 μK into this result gives a width that is smaller than the room temperature width by a factor of about 2×10^4 . The experimental results, however, show a reduction in the width of only a factor of ten. Thus we can conclude that the resonance effects of the frozen gas are not determined by two-body interactions alone.

It was surmised by Anderson *et al.* [6] that the linewidth must be of the order of the average interaction energy. This interaction splits the ss' - pp' degeneracy and the subsequent migration of the p state to other atoms broadens the energy of this “elementary excitation” into a band, as appropriate to an amorphous solid. Cluster calculations were performed to illustrate this band formation [40], but averaging over atom positions was done by order-of-magnitude arguments only. Mourachko *et al.* [45, 44] pointed out, in connection with their experiments on a different system, that the “walking away” of the p excitation from its original location should be regarded as a diffusion process, and dynamical equations for the resonance transition in the presence of this diffusion were written down [3, 44].

The present work builds on these earlier insights, but goes considerably further in the process of accurately averaging over atomic positions. It turns out that this averaging (effectively, a phase averaging) itself produces an $\exp(-\sqrt{\gamma_{eq}t})$ dependence at large times, characteristic of a diffusive process [18]. We discuss in detail in Chapter 2 a particular case that cleanly shows the effects of randomness and phase averaging. In this simple case, the averaging process can be carried out exactly. For the practically important r^{-3} interaction potential, one can proceed in a mathematically elegant way and obtain closed formulas that can be evaluated by a computer package such as *Mathematica*, or in some cases by hand. It appears to be a fortunate coincidence that the r^{-3} potential accurately describes the dipole-dipole interactions that are so prevalent in nature. Some aspects of this approach are easily extended to more general interactions; however, the r^{-3} dependence has special properties which, when coupled with the assumption of a random distribution of atoms, lead

³See, for example, pages 309–310 of Ref. [22].

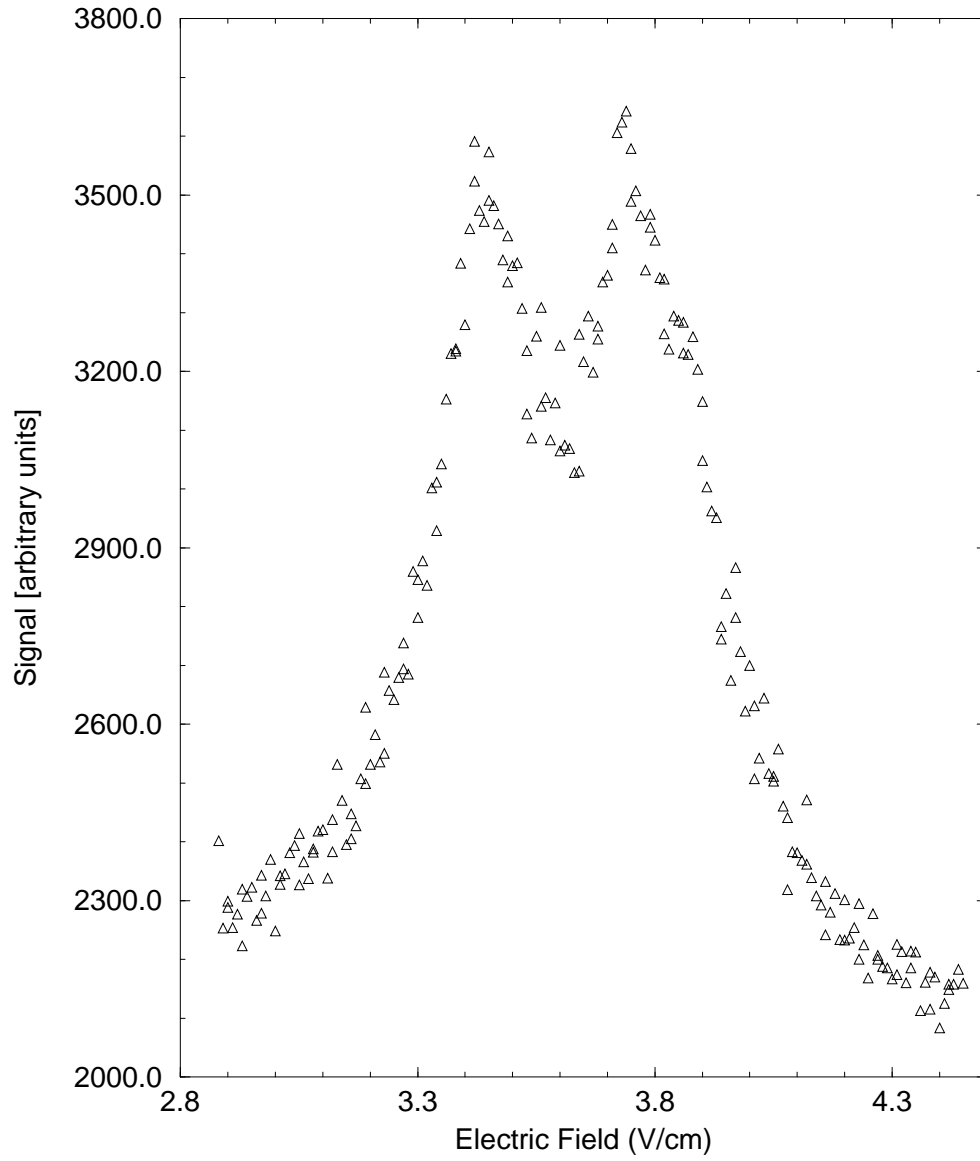


Figure 1.4: A representative plot of the experimental lineshape as a function of applied electric field. The detuning Δ varies linearly with the field. The data are taken from Fig. 3.9 on page 74 of Ref. [40].

to relatively simple results.

Although this work was stimulated by experiments on Rydberg atoms, it is generally applicable to resonances induced by dipole-dipole interactions. These may be common in highly excited gases and in molecular systems. Frozen, resonant gases may even exist in interstellar clouds.

First, in Chapter 2, we discuss a single s' atom interacting resonantly with a surrounding gas of s atoms, without any possibility for the s atom to interact with p atoms through an $sp \rightarrow ps$ process. When the result is averaged over the positions of the s atoms, it corresponds to a “sparse” system of s' atoms, i.e. a system where $N' \ll N$. We do not know of an existing experiment to which this treatment applies, so this section can be viewed as a theoretical prediction of the outcome of a possible experiment. Our purpose here is also one of exposition, since this example allows us to introduce in the simplest context some of the mathematical techniques used throughout the rest of this thesis. Some plots of the results are presented, and in the final sections of this chapter we consider the effect of interaction potentials more complicated than just a simple $1/r^3$ potential.

In Chapter 3 we continue with our discussion of the simple model of Chapter 2 by examining the issue of localization. We study localization in this system because we need to have some idea of the relative importance of close pairs of atoms, as well as some idea of the effective range of the $1/r^3$ interaction. Naively, it seems that the close pairs are dominant and that the range of the $1/r^3$ potential is infinite because $1/r^3$ diverges at $r = 0$ and yet the integral $\int d^3r/r^3$ over all space diverges at both limits.

In Chapter 4 we come one step closer to the actual system used in the experiments by allowing the $sp \rightarrow ps$ process to take place. This renders the problem analytically insoluble but we consider several approximations, each of which allows us to make some progress. When compared with the results of numerical simulations, we see that the coherent potential approximation compares most favorably.

In Chapter 5, we introduce an effective spin Hamiltonian which fully models the Rb system of Anderson *et al.* [5, 6] and Lowell *et al.* [40] for all values of N and N' , as well as for any strength of the resonant process $ss' \rightarrow pp'$ and of the mixing processes $sp \rightarrow ps$ and $s'p' \rightarrow p's'$. This Hamiltonian corresponds to a system of two interpenetrating spin glasses. We show its equivalence to the results of Chapter 4 in the sparse limit ($N' \ll N$). We then derive an entirely equivalent but seemingly more cumbersome Hamiltonian to describe this system. This second derivation embodies a more general technique, which we demonstrate by constructing a spin Hamiltonian that describes

the cesium system studied by Mourachko *et al.* [45, 44].

In Chapter 6 we take into account fully the complication introduced by the consideration of spin, and we determine exactly what the spin-dependent interatomic potentials are for the $sp \rightarrow ps$ and $ss' \rightarrow pp'$ processes in the experiment we are modeling [6, 40].

In Chapter 7 we discuss numerical simulations of the system we are considering. We start by describing in detail how the simulations are carried out, then we present the results, including comparisons of the simulations with the experimental data.

The limitations of the present theory and some of the many possible extensions are discussed in Chapter 8.

Chapter 2

Sparse $ss' \rightarrow pp'$ Processes — The Simple Model

2.1 Introduction

In this chapter we discuss a single s' atom interacting resonantly with a surrounding gas of s atoms, without any possibility for the s atom to interact with p atoms through an $sp \rightarrow ps$ process. In Section 2.2 we write down and solve the Schrödinger equation for a given spatial configuration of the s atoms. Then in Section 2.3 this result is averaged over the positions of the s atoms, so that it corresponds to a sparse system of s' atoms where $N' \ll N$. In Section 2.4 we compute the averaged signal and the lineshape. Specifically, in Sections 2.4.1 and 2.4.2 we start from the Laplace transform of the signal and develop series expansions for the signal as a function of time. We also discuss the use of the fast Fourier transform to obtain the signal as a function of time. In Section 2.4.3 we develop a numerical method to compute the averaged signal and lineshape that works exceedingly well, and in Section 2.4.4 we discuss the good and bad points of the three methods. Next, in Section 2.4.5 we present plots of the averaged signal and lineshape. In Section 2.5 we consider the effect of interaction potentials more complicated than just a simple $1/r^3$ potential. Finally, we summarize the results of this chapter in Section 2.6.

2.2 Basic equations

We consider one atom at the origin, initially in the state s' , in interaction with a gas of N randomly distributed s atoms through an $ss' \rightarrow pp'$ process. Like Mourachko *et al.* [45], we describe the system by the equations

$$i\dot{a}_0 = \Delta a_0 + \sum_{k=1}^N V_k c_k, \quad (2.1a)$$

$$i\dot{c}_k = V_k a_0. \quad (2.1b)$$

Here $a_0(\Delta, t)$ is the amplitude of the state in which the atom at the origin is in state s' and all other atoms are in state s , while $c_k(\Delta, t)$ (with k running from 1 to N) is the amplitude of the state in which the atom at the origin is in state p' and the atom at \mathbf{r}_k is in state p , while all the others remain in state s . The quantity V_k is the interaction potential and $\Delta = \epsilon'_p + \epsilon_p - \epsilon'_s - \epsilon_s$ is the detuning from resonance. For simplicity, we will assume for now that V_k is of the dipole-dipole form

$$V_k = \frac{\mu\mu'}{r_k^3}, \quad (2.2)$$

and we will discuss later in Section 2.5 what happens when the interaction potential has a different dependence on r or contains an angular dependence. Furthermore, the atoms are sufficiently cold that during the time scale of interest they move only a very small fraction of their separation, and therefore V_k can be taken to be independent of time. As the temperature increases one approaches the opposite limit, where binary collisions control the resonant process [57].

The set of differential equations (2.1a) and (2.1b) can easily be solved with the initial condition $a_0(\Delta, t=0) = 1$ and $c_k(\Delta, t=0) = 0$ for all k , yielding

$$c_k(\Delta, t) = -\frac{2iV_k e^{-i\Delta t/2} \sin(\sqrt{\Delta^2 + 4\mathcal{V}^2}t/2)}{\sqrt{\Delta^2 + 4\mathcal{V}^2}}, \quad (2.3)$$

with

$$\mathcal{V}^2 = \sum_{k=1}^N V_k^2. \quad (2.4)$$

Eq. (2.1b) then gives

$$a_0(\Delta, t) = e^{-i\Delta t/2} \left[\cos\left(\sqrt{\Delta^2 + 4\mathcal{V}^2}t/2\right) - i\frac{\Delta}{\sqrt{\Delta^2 + 4\mathcal{V}^2}} \sin\left(\sqrt{\Delta^2 + 4\mathcal{V}^2}t/2\right) \right]. \quad (2.5)$$

The experiment detects transitions to any one of the p' states (or, equivalently, to any one of the p states), and is thus a measure of

$$\begin{aligned} S(\Delta, t) &= 1 - |a_0(\Delta, t)|^2 = \sum_k |c_k(\Delta, t)|^2 \\ &= \frac{4\mathcal{V}^2 \sin^2\left(\sqrt{\Delta^2 + 4\mathcal{V}^2}t/2\right)}{\Delta^2 + 4\mathcal{V}^2}. \end{aligned} \quad (2.6)$$

We see that the signal $S(\Delta, t)$ exhibits Rabi oscillations.

We apply this result to a system of N' atoms, initially in state s' , randomly dispersed among a much larger number, N , of s atoms. In this sparse limit, the experimental signal is proportional to N' times the sample average of $S(\Delta, t)$, and the sample average is equivalent to an ensemble average over the atomic positions \mathbf{r}_k that are hidden in \mathcal{V}^2 (see Eq. (2.8) below). In general, averaging is more easily done on the Laplace transform of the signal, which in this case is

$$\begin{aligned} \tilde{S}(\Delta, \alpha) &= \int_0^\infty e^{-\alpha t} S(\Delta, t) dt \\ &= \frac{1}{\alpha} \frac{2\mathcal{V}^2}{\alpha^2 + \Delta^2 + 4\mathcal{V}^2} \\ &= \frac{1}{2\alpha} \left(1 - \frac{\alpha^2 + \Delta^2}{\alpha^2 + \Delta^2 + 4\mathcal{V}^2} \right). \end{aligned} \quad (2.7)$$

This Laplace transform can also be found as Eq. (5.9) on page 28 of Ref. [51].

2.3 Averaging over atom positions

To compute ensemble averages we use the following result, valid in the limit $N \gg 1$, for a random distribution of the variables \mathbf{r}_k :¹

$$\langle e^{-\beta V^2} \rangle = \frac{1}{\Omega^N} \int d^3r_1 \dots d^3r_N \exp \left[-\beta \sum_{k=1}^N V^2(r_k) \right]$$

¹The procedure here is, in effect, that used in the derivation of the second virial coefficient. See, for example, page 421 of Ref. [49].

$$\begin{aligned}
&= \left\{ \frac{1}{\Omega} \int d^3r \exp[-\beta V^2(r)] \right\}^N \\
&= \left\{ 1 - \frac{1}{\Omega} \int d^3r [1 - e^{-\beta V^2(r)}] \right\}^N \\
&\rightarrow \exp \left\{ -\frac{N}{\Omega} \int d^3r [1 - e^{-\beta V^2(r)}] \right\}, \tag{2.8}
\end{aligned}$$

where Ω is the volume of the gas in the trap and

$$\langle X \rangle = \frac{1}{\Omega^N} \int d^3r_1 \dots d^3r_N X. \tag{2.9}$$

In particular, for the dipolar interaction $V(r) = \mu\mu'/r^3$, we have

$$\int d^3r [1 - e^{-\beta(\mu\mu')^2/r^6}] = \frac{4\pi^{3/2}}{3} \mu\mu' \sqrt{\beta}, \tag{2.10}$$

leading to

$$\langle e^{-\beta \mathcal{V}^2} \rangle = e^{-v\sqrt{\beta}}, \tag{2.11}$$

where

$$v = \frac{4\pi^{3/2}}{3} \frac{N}{\Omega} \mu\mu'. \tag{2.12}$$

For the typical densities in the experiments of Anderson *et al.* [6] and Lowell *et al.* [40], v is on the order of MHz. Since v has the units of an energy, it must be of order $\mu\mu'N/\Omega$ on dimensional grounds. It is still remarkable, however, that Eq. (2.12) gives simply and exactly the quantity v that will enter in all the averaged quantities in this section.²

Using Eq. (2.11), we can evaluate the average of any function $F(\mathcal{V}^2)$. We simply need to determine the probability distribution of the variable \mathcal{V}^2 , which we will denote as $P(\mathcal{V}^2)$. By definition, we have

$$P(\mathcal{V}^2) = \left\langle \delta \left(\mathcal{V}^2 - \sum_{k=1}^N \left(\frac{\mu\mu'}{r_k^3} \right)^2 \right) \right\rangle. \tag{2.13}$$

We proceed by writing the delta function as a Fourier transform over the dummy variable q . This leads to

$$P(\mathcal{V}^2) = \int_{-\infty}^{\infty} \frac{dq}{2\pi} e^{iq\mathcal{V}^2} \left\langle \exp \left[-iq \sum_{k=1}^N \left(\frac{\mu\mu'}{r_k^3} \right)^2 \right] \right\rangle. \tag{2.14}$$

²In this section we perform an average over many configurations of randomly positioned atoms. The corresponding dipolar sums for regular lattices are discussed in Refs. [13] and [20].

The average can now be performed using Eq. (2.11), and we have

$$P(\mathcal{V}^2) = \int_{-\infty}^{\infty} \frac{dq}{2\pi} \exp\left(iq\mathcal{V}^2 - \sqrt{iqv}\right). \quad (2.15)$$

The remaining integral requires a little finesse to evaluate. First, we split the integral into two parts, so that

$$P_1(\mathcal{V}^2) = \int_0^{\infty} \frac{dq}{2\pi} \exp\left(iq\mathcal{V}^2 - \sqrt{iqv}\right), \quad (2.16)$$

and

$$\begin{aligned} P_2(\mathcal{V}^2) &= \int_{-\infty}^0 \frac{dq}{2\pi} \exp\left(iq\mathcal{V}^2 - \sqrt{iqv}\right) \\ &= \int_0^{\infty} \frac{dq}{2\pi} \exp\left(-iq\mathcal{V}^2 - \sqrt{-iqv}\right) \\ &= [P_1(\mathcal{V}^2)]^*. \end{aligned} \quad (2.17)$$

Now we note that

$$\begin{aligned} P(\mathcal{V}^2) &= P_1(\mathcal{V}^2) + P_2(\mathcal{V}^2) \\ &= 2 \operatorname{Re} \int_0^{\infty} \frac{dq}{2\pi} \exp\left(iq\mathcal{V}^2 - \sqrt{iqv}\right). \end{aligned} \quad (2.18)$$

Changing variables to $\sigma = \sqrt{-iq\mathcal{V}^2} = e^{-i\pi/4} \sqrt{q\bar{x}}$, we see that $q = i\sigma^2/\mathcal{V}^2$ and hence

$$\begin{aligned} P(\mathcal{V}^2) &= \frac{2}{\pi} \frac{1}{\mathcal{V}^2} \operatorname{Re} \left[i \int_0^{\infty} d\sigma \sigma \exp\left(-\sigma^2 - \frac{iv\sigma}{\sqrt{\mathcal{V}^2}}\right) \right] \\ &= \frac{2}{\pi} \frac{1}{\sqrt{\mathcal{V}^2}} \operatorname{Re} \left[\left(-\frac{\partial}{\partial v}\right) \int_0^{\infty} d\sigma \exp\left(-\sigma^2 - \frac{iv\sigma}{\sqrt{\mathcal{V}^2}}\right) \right]. \end{aligned} \quad (2.19)$$

This can be rewritten as

$$P(\mathcal{V}^2) = \frac{2}{\pi} \frac{1}{\sqrt{\mathcal{V}^2}} \left(-\frac{\partial}{\partial v}\right) \int_0^{\infty} d\sigma \exp(-\sigma^2) \cos\left(\frac{v\sigma}{\sqrt{\mathcal{V}^2}}\right), \quad (2.20)$$

and the remaining integral is easily looked up in tables, such as Ref. [25]. One finds that

$$\int_0^{\infty} dx \exp(-\beta x^2) \cos(bx) = \frac{1}{2} \sqrt{\frac{\pi}{\beta}} \exp\left(-\frac{b^2}{4\beta}\right), \quad (2.21)$$

and hence we have

$$P(\mathcal{V}^2) = \frac{1}{\sqrt{\pi}} \frac{1}{\sqrt{\mathcal{V}^2}} \left(-\frac{\partial}{\partial v} \right) \exp\left(-\frac{v^2}{4\mathcal{V}^2}\right). \quad (2.22)$$

When the derivative is evaluated we are left with

$$P(\mathcal{V}^2) = \frac{1}{2\sqrt{\pi}} \frac{v}{\mathcal{V}^3} \exp\left(-\frac{v^2}{4\mathcal{V}^2}\right). \quad (2.23)$$

It is interesting to note that $P(\mathcal{V}^2)$ is not Gaussian, and the central limit theorem does not apply, because $P(V) \propto V^{-2}$ does not have a root mean square value. In fact, $P(V)$ is not even normalizable.

Therefore, using Eq. (2.23) we can compute the average of any function $F(\mathcal{V}^2)$ as

$$\langle F(\mathcal{V}^2) \rangle = \int_0^\infty d(\mathcal{V}^2) P(\mathcal{V}^2) F(\mathcal{V}^2). \quad (2.24)$$

We can further define $y^2 = v^2/\mathcal{V}^2$, and then by a simple change of variable the average of F can be written in the form

$$\langle F(\mathcal{V}^2) \rangle = \int_0^\infty dy \frac{1}{\sqrt{\pi}} \exp\left(-\frac{y^2}{4}\right) F\left(\frac{y^2}{\mathcal{V}^2}\right), \quad (2.25)$$

which agrees with the result derived by an alternative method in Ref. [18].

This last set of relations implies that we can average a function $F(\mathcal{V}^2)$ over the positions of the interacting dipoles (atoms in our case) by replacing \mathcal{V}^2 with v^2/y^2 and integrating over the kernel $\exp(-y^2/4)/\sqrt{\pi}$. This trick is not always useful as such, because it can lead to highly oscillatory integrals. However, if the function F has suitable analytic properties, then the integration path of Eq. (2.25) can be shifted in the complex y plane in such a way that the oscillations are damped out and the integral is rather easy to evaluate numerically. An example of this procedure is discussed in detail in Section 2.4.3.

2.4 The averaged signal and lineshape

The average over atomic positions can be obtained in closed form for the Laplace transform of the signal, $\langle \tilde{S}(\Delta, \alpha) \rangle$. Starting from Eq. (2.7) in the form

$$\tilde{S}(\Delta, \alpha) = \frac{1}{2\alpha} - \frac{\alpha^2 + \Delta^2}{2\alpha} \int_0^\infty d\beta e^{-\beta(\alpha^2 + \Delta^2 + 4v^2)}, \quad (2.26)$$

and using Eq. (2.11), we obtain

$$\begin{aligned} \langle \tilde{S}(\Delta, \alpha) \rangle &= \frac{1}{2\alpha} - \frac{A^2}{2\alpha} \int_0^\infty d\beta e^{-\beta A^2 - 2v\sqrt{\beta}} \\ &= \frac{\sqrt{\pi}}{2} \frac{v}{\alpha A} \exp\left(\frac{v^2}{A^2}\right) \operatorname{erfc}\left(\frac{v}{A}\right), \end{aligned} \quad (2.27)$$

where $A^2 = \alpha^2 + \Delta^2$. For the sake of completeness, and because it will be used later on, we note that a similar result can be obtained for $\langle \tilde{a}_0(\Delta, \alpha) \rangle$ by applying the same method to Eq. (2.5). One finds

$$\langle \tilde{a}_0(\Delta, \alpha) \rangle = \frac{1}{\alpha + i\Delta} - \frac{\sqrt{\pi}}{2} \frac{v}{(\alpha + i\Delta)^{3/2} \sqrt{\alpha}} \exp\left[\frac{v^2}{4\alpha(\alpha + i\Delta)}\right] \operatorname{erfc}\left[\frac{v}{2\sqrt{\alpha(\alpha + i\Delta)}}\right]. \quad (2.28)$$

The problem is then to invert the Laplace transform of Eq. (2.27). As is shown in Section 2.4.1, it is possible in this case to convert the Laplace transform to a Fourier transform, which can then be inverted numerically by a fast Fourier transform algorithm. A more convenient inversion method was presented in Ref. [18] and is described in more detail in Section 2.4.2. It leads to an expression for $\langle S(\Delta, t) \rangle$ in terms of generalized hypergeometric functions, which can be conveniently handled by *Mathematica*.

A third method to obtain $\langle S(\Delta, t) \rangle$ is to apply Eq. (2.25) directly to $\langle \tilde{S}(\Delta, \alpha) \rangle$ as given by Eq. (2.6). The remaining integral is difficult to perform numerically, as we already noted, but this difficulty can be circumvented as is shown in Section 2.4.3. The advantages and limitations of the three numerical methods for evaluating $\langle S(\Delta, t) \rangle$ are compared in Section 2.4.4.

Plots of $\langle S(\Delta, t) \rangle$ are presented and discussed in Section 2.4.5. Readers who are not interested in mathematical methods can proceed directly to Section 2.4.5.

2.4.1 The Laplace and Fourier transforms

We see from Eq. (7.1.6) on page 297 of Ref. [2] that

$$\begin{aligned} e^{z^2} \operatorname{erfc}(z) &= e^{z^2} - \frac{2}{\sqrt{\pi}} \sum_{n=0}^{\infty} \frac{2^n}{(2n+1)!!} z^{2n+1} \\ &= \sum_{n=0}^{\infty} \frac{z^{2n}}{\Gamma(n+1)} - \frac{2}{\sqrt{\pi}} \sum_{n=0}^{\infty} \frac{4^n \Gamma(n+1)}{\Gamma(2n+2)} z^{2n+1}. \end{aligned} \quad (2.29)$$

Now we use the fact that

$$\Gamma(2z) = \frac{1}{2\sqrt{\pi}} 2^{2z} \Gamma(z) \Gamma\left(z + \frac{1}{2}\right), \quad (2.30)$$

and we find

$$\begin{aligned} e^{z^2} \operatorname{erfc}(z) &= \sum_{n=0}^{\infty} \frac{z^{2n}}{\Gamma(n+1)} - \sum_{n=0}^{\infty} \frac{z^{2n+1}}{\Gamma\left(n + \frac{3}{2}\right)} \\ &= \sum_{n=0}^{\infty} \frac{(-z)^n}{\Gamma\left(\frac{n}{2} + 1\right)}. \end{aligned} \quad (2.31)$$

Therefore Eq. (2.27) gives

$$\langle \tilde{S}(\Delta, \alpha) \rangle = \frac{\sqrt{\pi}}{2} \sum_{n=0}^{\infty} \frac{1}{\Gamma\left(\frac{n+2}{2}\right)} (-1)^n \frac{v^{n+1}}{\alpha A^{n+1}}. \quad (2.32)$$

This equation shows that $\langle \tilde{S}(\Delta, \alpha) \rangle$ can be analytically continued to complex α with $\operatorname{Re} \alpha > 0$, although it has a branch cut ending at essential singularities located at $\alpha = i\Delta$ and $\alpha = -i\Delta$. In particular, the Fourier transform is obtained by putting $\alpha = \omega/i$. We have obtained $\langle S(\Delta, t) \rangle$ by inverting this Fourier transform numerically using a fast Fourier transform routine. However, the following method of inverting the Laplace transform is much more convenient, for reasons that are explained in Section 2.4.4.

2.4.2 Inverting the Laplace transform

According to Eq. (2.66) of Ref. [51], the inverse Laplace transform of

$$\frac{1}{\alpha^{2\mu} (\alpha^2 + a^2)^\nu} \quad (2.33)$$

is

$$\frac{t^{2\mu+2\nu-1}}{\Gamma(2\mu+2\nu)} {}_1F_2 \left(\nu; \mu + \nu, \mu + \nu + \frac{1}{2}; -\frac{a^2 t^2}{4} \right), \quad (2.34)$$

where the function ${}_pF_q(a_1, a_2, \dots, a_p; b_1, b_2, \dots, b_q; z)$ is a generalized hypergeometric function, and is defined on pages 750–751 of Ref. [62] to be

$${}_pF_q(a_1, a_2, \dots, a_p; b_1, b_2, \dots, b_q; z) = \frac{\prod_{i=1}^q \Gamma(b_i)}{\prod_{j=1}^p \Gamma(a_j)} \sum_{k=0}^{\infty} \frac{\prod_{l=1}^p \Gamma(a_l + k)}{\prod_{m=1}^q \Gamma(b_m + k)} \frac{z^k}{\Gamma(k+1)}. \quad (2.35)$$

Hence we find that the inverse Laplace transform of $\langle \tilde{S}(\Delta, \alpha) \rangle$ is

$$\langle S(\Delta, t) \rangle = \frac{\sqrt{\pi}}{2} \sum_{n=0}^{\infty} (-1)^n \frac{(vt)^{n+1}}{\Gamma(\frac{n+2}{2}) \Gamma(n+2)} {}_1F_2 \left(\frac{n+1}{2}; \frac{n+2}{2}, \frac{n+3}{2}; -\frac{\Delta^2 t^2}{4} \right). \quad (2.36)$$

Expanding ${}_1F_2$ using Eq. (2.35) yields

$$\begin{aligned} \langle S(\Delta, t) \rangle &= \frac{\sqrt{\pi}}{2} vt \sum_{n=0}^{\infty} \frac{(-vt)^n}{\Gamma(\frac{n+2}{2}) \Gamma(n+2)} \frac{\Gamma(\frac{n+2}{2}) \Gamma(\frac{n+3}{2})}{\Gamma(\frac{n+1}{2})} \times \\ &\quad \sum_{m=0}^{\infty} \frac{\Gamma(\frac{n+2m+1}{2})}{\Gamma(\frac{n+2m+2}{2}) \Gamma(\frac{n+2m+3}{2}) \Gamma(m+1)} \left(-\frac{\Delta^2 t^2}{4} \right)^m \\ &= \frac{\sqrt{\pi}}{2} vt \sum_{n=0}^{\infty} \sum_{m=0}^{\infty} (-vt)^n \frac{\Gamma(\frac{n+3}{2})}{\Gamma(n+2) \Gamma(\frac{n+1}{2})} \times \\ &\quad \frac{\Gamma(\frac{n+2m+1}{2})}{\Gamma(\frac{n+2m+2}{2}) \Gamma(\frac{n+2m+3}{2}) \Gamma(m+1)} \left(-\frac{\Delta^2 t^2}{4} \right)^m \\ &= \frac{\sqrt{\pi}}{2} vt \sum_{n=0}^{\infty} \sum_{m=0}^{\infty} (-vt)^n \frac{n+1}{2} \frac{1}{\Gamma(n+2)} \times \\ &\quad \frac{1}{\Gamma(\frac{n+2m+2}{2}) (\frac{n+2m+1}{2}) \Gamma(m+1)} \left(-\frac{\Delta^2 t^2}{4} \right)^m \\ &= \frac{\sqrt{\pi}}{2} vt \sum_{n=0}^{\infty} \sum_{m=0}^{\infty} \frac{(-1)^{n+m} v^n \Delta^{2m} t^{n+2m}}{4^m \Gamma(n+1) \Gamma(m+1) \Gamma(\frac{n+2m+2}{2}) (n+2m+1)}, \quad (2.37) \end{aligned}$$

which can also be obtained directly by expanding Eq. (2.27) in $1/\alpha$ and then taking the inverse Laplace transform term by term.

For some purposes, it is convenient to rearrange Eq. (2.37) in the form of a series in powers of the detuning squared. To achieve this, we use the second line of this equation and find

$$\langle S(\Delta, t) \rangle = \sum_{m=0}^{\infty} \left(-\frac{\Delta^2 t^2}{4} \right)^m \frac{1}{\Gamma(m+1)} Z_m, \quad (2.38)$$

where

$$\begin{aligned}
Z_m &= \frac{\sqrt{\pi}}{2} vt \sum_{n=0}^{\infty} (-vt)^n \frac{\Gamma\left(\frac{n+3}{2}\right) \Gamma\left(\frac{n+2m+1}{2}\right)}{\Gamma(n+2) \Gamma\left(\frac{n+1}{2}\right) \Gamma\left(\frac{n+2m+2}{2}\right) \Gamma\left(\frac{n+2m+3}{2}\right)} \\
&= \frac{\sqrt{\pi}}{2} vt \sum_{n=0}^{\infty} (-vt)^{2n} \frac{\Gamma\left(n+\frac{3}{2}\right) \Gamma\left(n+m+\frac{1}{2}\right)}{\Gamma(2n+2) \Gamma\left(n+\frac{1}{2}\right) \Gamma(n+m+1) \Gamma\left(n+m+\frac{3}{2}\right)} + \\
&\quad \frac{\sqrt{\pi}}{2} vt \sum_{n=0}^{\infty} (-vt)^{2n+1} \frac{\Gamma(n+2) \Gamma(n+m+1)}{\Gamma(2n+3) \Gamma(n+1) \Gamma\left(n+m+\frac{3}{2}\right) \Gamma(n+m+2)}. \quad (2.39)
\end{aligned}$$

Again using Eq. (2.30), we see that

$$\begin{aligned}
Z_m &= \frac{\sqrt{\pi}}{2} vt \sum_{n=0}^{\infty} \frac{2\sqrt{\pi}}{4^{n+1}} (v^2 t^2)^n \frac{\Gamma\left(n+\frac{3}{2}\right) \Gamma\left(n+m+\frac{1}{2}\right)}{\Gamma(n+1) \Gamma\left(n+\frac{3}{2}\right) \Gamma\left(n+\frac{1}{2}\right) \Gamma(n+m+1) \Gamma\left(n+m+\frac{3}{2}\right)} - \\
&\quad \frac{\sqrt{\pi}}{2} \sum_{n=0}^{\infty} \frac{2\sqrt{\pi}}{4^{n+3/2}} (v^2 t^2)^{n+1} \frac{\Gamma(n+2) \Gamma(n+m+1)}{\Gamma\left(n+\frac{3}{2}\right) \Gamma(n+2) \Gamma(n+1) \Gamma\left(n+m+\frac{3}{2}\right) \Gamma(n+m+2)} \\
&= \frac{\pi}{4} vt \sum_{n=0}^{\infty} \left(\frac{v^2 t^2}{4}\right)^n \frac{\Gamma\left(n+m+\frac{1}{2}\right)}{\Gamma(n+1) \Gamma\left(n+\frac{1}{2}\right) \Gamma(n+m+1) \Gamma\left(n+m+\frac{3}{2}\right)} - \\
&\quad \frac{\pi}{2} \frac{v^2 t^2}{4} \sum_{n=0}^{\infty} \left(\frac{v^2 t^2}{4}\right)^n \frac{\Gamma(n+m+1)}{\Gamma\left(n+\frac{3}{2}\right) \Gamma(n+1) \Gamma\left(n+m+\frac{3}{2}\right) \Gamma(n+m+2)} \\
&= \frac{\pi}{4} vt \frac{\Gamma\left(m+\frac{1}{2}\right)}{\Gamma\left(\frac{1}{2}\right) \Gamma(m+1) \Gamma\left(m+\frac{3}{2}\right)} {}_1F_3\left(m+\frac{1}{2}; \frac{1}{2}, m+1, m+\frac{3}{2}; \frac{v^2 t^2}{4}\right) - \\
&\quad \frac{\pi}{8} v^2 t^2 \frac{\Gamma(m+1)}{\Gamma\left(\frac{3}{2}\right) \Gamma\left(m+\frac{3}{2}\right) \Gamma(m+2)} {}_1F_3\left(m+1; \frac{3}{2}, m+\frac{3}{2}, m+2; \frac{v^2 t^2}{4}\right) \\
&= \frac{\sqrt{\pi}}{4} vt \frac{1}{\left(m+\frac{1}{2}\right) \Gamma(m+1)} {}_1F_3\left(m+\frac{1}{2}; \frac{1}{2}, m+1, m+\frac{3}{2}; \frac{v^2 t^2}{4}\right) - \\
&\quad \frac{\sqrt{\pi}}{4} v^2 t^2 \frac{1}{(m+1) \Gamma\left(m+\frac{3}{2}\right)} {}_1F_3\left(m+1; \frac{3}{2}, m+\frac{3}{2}, m+2; \frac{v^2 t^2}{4}\right). \quad (2.40)
\end{aligned}$$

Thus the expression for the signal becomes

$$\begin{aligned}
\langle S(\Delta, t) \rangle &= \sum_{m=0}^{\infty} \left(-\frac{\Delta^2 t^2}{4}\right)^m \frac{1}{\Gamma(m+1)} \times \\
&\quad \left[\frac{\sqrt{\pi}}{4} vt \frac{1}{\left(m+\frac{1}{2}\right) \Gamma(m+1)} {}_1F_3\left(m+\frac{1}{2}; \frac{1}{2}, m+1, m+\frac{3}{2}; \frac{v^2 t^2}{4}\right) - \right. \\
&\quad \left. \frac{\sqrt{\pi}}{4} v^2 t^2 \frac{1}{(m+1) \Gamma\left(m+\frac{3}{2}\right)} {}_1F_3\left(m+1; \frac{3}{2}, m+\frac{3}{2}, m+2; \frac{v^2 t^2}{4}\right) \right] \\
&= \sum_{m=0}^{\infty} \left(-\frac{\Delta^2 t^2}{4}\right)^m \times
\end{aligned}$$

$$\left\{ \frac{\sqrt{\pi}}{4} vt \frac{1}{(m + \frac{1}{2}) [\Gamma(m + 1)]^2} {}_1F_3 \left(m + \frac{1}{2}; \frac{1}{2}, m + 1, m + \frac{3}{2}; \frac{v^2 t^2}{4} \right) - \frac{\sqrt{\pi}}{4} v^2 t^2 \frac{1}{\Gamma(m + \frac{3}{2}) \Gamma(m + 2)} {}_1F_3 \left(m + 1; \frac{3}{2}, m + \frac{3}{2}, m + 2; \frac{v^2 t^2}{4} \right) \right\}. \quad (2.41)$$

If we consider the signal at resonance, then the expression in Eq. (2.41) simplifies considerably.

We note that only the $m = 0$ term contributes when $\Delta = 0$. Thus we have

$$\begin{aligned} \langle S(\Delta = 0, t) \rangle &= \frac{\sqrt{\pi}}{4} vt \frac{1}{\frac{1}{2} [\Gamma(1)]^2} {}_1F_3 \left(\frac{1}{2}; \frac{1}{2}, 1, \frac{3}{2}; \frac{v^2 t^2}{4} \right) - \\ &\quad \frac{\sqrt{\pi}}{4} v^2 t^2 \frac{1}{\Gamma(\frac{3}{2}) \Gamma(2)} {}_1F_3 \left(1; \frac{3}{2}, \frac{3}{2}, 2; \frac{v^2 t^2}{4} \right) \\ &= \frac{\sqrt{\pi}}{2} vt {}_0F_2 \left(; 1, \frac{3}{2}; \frac{v^2 t^2}{4} \right) - \frac{1}{2} v^2 t^2 {}_1F_3 \left(1; \frac{3}{2}, \frac{3}{2}, 2; \frac{v^2 t^2}{4} \right). \end{aligned} \quad (2.42)$$

We further note that

$$\begin{aligned} \frac{1}{2} v^2 t^2 {}_1F_3 \left(1; \frac{3}{2}, \frac{3}{2}, 2; \frac{v^2 t^2}{4} \right) &= \frac{1}{2} v^2 t^2 \Gamma\left(\frac{3}{2}\right) \Gamma\left(\frac{3}{2}\right) \Gamma(2) \times \\ &\quad \sum_{n=0}^{\infty} \frac{\Gamma(n+1)}{\Gamma(n+1) \Gamma(n+\frac{3}{2}) \Gamma(n+\frac{3}{2}) \Gamma(n+2)} \left(\frac{v^2 t^2}{4} \right)^n \\ &= \frac{\pi}{2} \sum_{n=0}^{\infty} \frac{1}{\Gamma(n+\frac{3}{2}) \Gamma(n+\frac{3}{2}) \Gamma(n+2)} \left(\frac{v^2 t^2}{4} \right)^{n+1} \\ &= \frac{\pi}{2} \left[\sum_{n=0}^{\infty} \frac{1}{\Gamma(n+\frac{1}{2}) \Gamma(n+\frac{1}{2}) \Gamma(n+1)} \left(\frac{v^2 t^2}{4} \right)^n - \frac{1}{\pi} \right] \\ &= \frac{\pi}{2} \frac{1}{\Gamma(\frac{1}{2}) \Gamma(\frac{1}{2})} {}_0F_2 \left(; \frac{1}{2}, \frac{1}{2}; \frac{v^2 t^2}{4} \right) - \frac{1}{2} \\ &= \frac{1}{2} {}_0F_2 \left(; \frac{1}{2}, \frac{1}{2}; \frac{v^2 t^2}{4} \right) - \frac{1}{2}. \end{aligned} \quad (2.43)$$

Thus the signal at resonance can be written as

$$\langle S(\Delta = 0, t) \rangle = \frac{\sqrt{\pi}}{2} vt {}_0F_2 \left(; 1, \frac{3}{2}; \frac{v^2 t^2}{4} \right) + \frac{1}{2} - \frac{1}{2} {}_0F_2 \left(; \frac{1}{2}, \frac{1}{2}; \frac{v^2 t^2}{4} \right), \quad (2.44)$$

which agrees perfectly with Eq. (19) of Ref. [18].

2.4.3 A numerical method using Eq. (2.25)

We have from Eq. (2.25) that the averaged signal can be written as

$$\langle S(\Delta, t) \rangle = \int_0^\infty dy \frac{1}{\sqrt{\pi}} \exp\left(-\frac{y^2}{4}\right) S(\Delta, t)_{v^2 \rightarrow v^2/y^2}. \quad (2.45)$$

Then, using Eq. (2.6), we have

$$\langle S(\Delta, t) \rangle = \frac{4}{\sqrt{\pi}} \int_0^\infty dy \exp\left(-\frac{y^2}{4}\right) \frac{v^2 \sin^2\left(\frac{1}{2}\sqrt{\Delta^2 + 4\frac{v^2}{y^2}}t\right)}{\Delta^2 + 4\frac{v^2}{y^2}}. \quad (2.46)$$

We can rewrite this as

$$\begin{aligned} \langle S(\Delta, t) \rangle &= \frac{2}{\sqrt{\pi}} \int_0^\infty dy \exp\left(-\frac{y^2}{4}\right) \frac{\frac{v^2}{y^2}}{\Delta^2 + 4\frac{v^2}{y^2}} \left[1 - \cos\left(\sqrt{\Delta^2 + 4\frac{v^2}{y^2}}t\right)\right] \\ &= \frac{2}{\sqrt{\pi}} \int_0^\infty dy \exp\left(-\frac{y^2}{4}\right) \frac{\frac{v^2}{y^2}}{\Delta^2 + 4\frac{v^2}{y^2}} - \\ &\quad \frac{2}{\sqrt{\pi}} \operatorname{Re} \int_0^\infty dy \frac{\frac{v^2}{y^2}}{\Delta^2 + 4\frac{v^2}{y^2}} \exp\left(-\frac{y^2}{4} + it\sqrt{\Delta^2 + 4\frac{v^2}{y^2}}\right). \end{aligned} \quad (2.47)$$

If $\Delta = 0$, then we have

$$\langle S(\Delta = 0, t) \rangle = \frac{1}{2} - I(\Delta = 0, t), \quad (2.48)$$

where

$$I(\Delta = 0, t) = \frac{1}{2\sqrt{\pi}} \operatorname{Re} \int_0^\infty dy \exp\left(-\frac{y^2}{4} + 2it\frac{v}{y}\right). \quad (2.49)$$

We can change the path of integration from the positive real axis to a path where we start from the origin and proceed along the negative imaginary axis to the point $y = -i$, then proceed to the point $y = \infty - i$ along the line $\operatorname{Im} y = -i$. Then we have

$$\begin{aligned} I(\Delta = 0, t) &= \frac{1}{2\sqrt{\pi}} \operatorname{Re} \left[-\frac{1}{i} \int_0^1 dz \exp\left(\frac{z^2}{4} - 2t\frac{v}{z}\right) \right] + \\ &\quad \frac{1}{2\sqrt{\pi}} \operatorname{Re} \int_0^\infty dw \exp\left[-\frac{(w-i)^2}{4} + 2it\frac{v}{w-i}\right]. \end{aligned} \quad (2.50)$$

Clearly the integral over z is purely real, and so

$$\langle S(\Delta = 0, t) \rangle = \frac{1}{2} - \frac{1}{2\sqrt{\pi}} \operatorname{Re} \int_0^\infty dw \exp \left[-\frac{(w-i)^2}{4} + \frac{2ivt}{w-i} \right]. \quad (2.51)$$

Mathematica is quite adept at quickly evaluating this integral for any value of vt .

The case where $\Delta \neq 0$ is only slightly more complicated. We have from Eq. (2.47) that

$$\langle S(\Delta, t) \rangle = \frac{\sqrt{\pi}}{2} \frac{v}{\Delta} \exp \left(\frac{v^2}{\Delta^2} \right) \operatorname{erfc} \left(\frac{v}{\Delta} \right) - I(\Delta, t), \quad (2.52)$$

where

$$I(\Delta, t) = \frac{2}{\sqrt{\pi}} \operatorname{Re} \int_0^\infty dy \frac{1}{y^2} \frac{1}{\frac{\Delta^2}{v^2} + \frac{4}{y^2}} \exp \left(-\frac{y^2}{4} + ivt \sqrt{\frac{\Delta^2}{v^2} + \frac{4}{y^2}} \right). \quad (2.53)$$

The path we used in the resonant case will still work well for small Δ/v , but will fail for $\Delta \gtrsim 2v$. This is clear because the radicand $\frac{\Delta^2}{v^2} + \frac{4}{y^2}$ will change sign as y goes from zero to $-i$. By analogy with the resonant case and through a bit of trial and error, however, one finds that for $\Delta \gtrsim 2v$ the path where we start from the origin and proceed along the positive imaginary axis to the point $y = -\frac{iv}{2\Delta}$, then proceed to the point $y = \infty - \frac{iv}{2\Delta}$ along the line $\operatorname{Im} y = -\frac{iv}{2\Delta}$ works well. Using this path we have

$$\begin{aligned} I(\Delta, t) &= -\frac{2}{\sqrt{\pi}} \operatorname{Re} \left[-\frac{1}{i} \int_0^{\frac{iv}{2\Delta}} dz \frac{1}{z^2} \frac{1}{\frac{\Delta^2}{v^2} - \frac{4}{z^2}} \exp \left(\frac{z^2}{4} + ivt \sqrt{\frac{\Delta^2}{v^2} - \frac{4}{z^2}} \right) \right] + \\ &\quad \frac{2}{\sqrt{\pi}} \operatorname{Re} \int_0^\infty dw \frac{1}{\left(w - \frac{iv}{2\Delta}\right)^2} \left(\frac{\Delta^2}{v^2} + \frac{4}{\left(w - \frac{iv}{2\Delta}\right)^2} \right)^{-1} \times \\ &\quad \exp \left[-\frac{\left(w - \frac{iv}{2\Delta}\right)^2}{4} + ivt \sqrt{\frac{\Delta^2}{v^2} + \frac{4}{\left(w - \frac{iv}{2\Delta}\right)^2}} \right]. \end{aligned} \quad (2.54)$$

It is again the case that the z integral gives zero, and we have that

$$\begin{aligned} \langle S(\Delta, t) \rangle &= \frac{\sqrt{\pi}}{2} \frac{v}{\Delta} \exp \left(\frac{v^2}{\Delta^2} \right) \operatorname{erfc} \left(\frac{v}{\Delta} \right) - \\ &\quad \frac{2}{\sqrt{\pi}} \operatorname{Re} \int_0^\infty dw \frac{1}{\left(w - \frac{iv}{2\Delta}\right)^2} \left(\frac{\Delta^2}{v^2} + \frac{4}{\left(w - \frac{iv}{2\Delta}\right)^2} \right)^{-1} \times \\ &\quad \exp \left[-\frac{\left(w - \frac{iv}{2\Delta}\right)^2}{4} + ivt \sqrt{\frac{\Delta^2}{v^2} + \frac{4}{\left(w - \frac{iv}{2\Delta}\right)^2}} \right]. \end{aligned} \quad (2.55)$$

Mathematica is again fairly adept at evaluating this expression numerically for any values of vt and Δ/v , although the computation time increases with increasing Δ/v . In practice, we have used Eq. (2.51) for $\Delta < v$ and Eq. (2.55) for $\Delta > v$.

Note that, using this method, it is possible to obtain a plot of the resonance width versus time by solving numerically for a value of Δ such that

$$\langle S(\Delta, t) \rangle = \frac{1}{2} \langle S(0, t) \rangle, \quad (2.56)$$

at many values of t .

We can also use this method to obtain asymptotic expressions for the signal $\langle S(\Delta, t) \rangle$. Consider the resonant case. We see from Eqs. (2.48) and (2.49) that we want to obtain an asymptotic expression for the integral

$$I(\Delta = 0, t) = \frac{1}{2\sqrt{\pi}} \operatorname{Re} \int_0^\infty dy \exp[\phi(y)], \quad (2.57)$$

where

$$\phi(y) = -\frac{y^2}{4} + \frac{2ivt}{y}. \quad (2.58)$$

We can simply apply the method of steepest descent to this integral, as discussed on pages 82–90 of Ref. [43]. We see that

$$\phi'(y) = -\frac{y}{2} - \frac{2ivt}{y^2}, \quad (2.59)$$

and

$$\phi''(y) = -\frac{1}{2} + \frac{4it}{y^3}. \quad (2.60)$$

Thus we find that $\phi'(y)$ vanishes when $y^3 = -4ivt$. To ensure convergence, we want to pick the root closest to the original integration path in the lower half plane, and so we choose the root

$$y_0 = \exp\left(-\frac{i\pi}{6}\right) (4vt)^{1/3}. \quad (2.61)$$

We then have

$$\phi(y) \approx \phi(y_0) + \frac{1}{2} \phi''(y_0) (y - y_0). \quad (2.62)$$

Proceeding carefully we find that

$$\phi(y_0) = \frac{3}{2} \left(-1 + i\sqrt{3} \right) (vt)^{2/3}, \quad (2.63)$$

and

$$\phi''(y_0) = -6. \quad (2.64)$$

Finally there is only a Gaussian integral to do, and one easily finds that

$$\langle S(\Delta = 0, t) \rangle \approx \frac{1}{2} - \frac{1}{\sqrt{3}} \exp \left[-\frac{3}{2} (vt)^{2/3} \right] \cos \left[\frac{3\sqrt{3}}{2} (vt)^{2/3} \right], \quad (2.65)$$

for large t .

The same procedure can be applied when $\Delta \neq 0$, although this situation is somewhat more complicated because in order to determine the position of the saddle point one must first solve a cubic equation. This is best done numerically, and one finds that the result is qualitatively the same as Eq. (2.65).

2.4.4 Comparison of the three methods

Each of the three methods we have discussed has its drawbacks.

In order for the fast Fourier transform method of Section 2.4.1 to be practical, we must first subtract off certain parts of the Fourier transform that are not well behaved. For instance, we must subtract off the part of the Fourier transform that goes as $1/\omega$ at small ω . Because we must sample points over a wide range of values of ω in Fourier space in order to obtain an accurate picture of the signal in t space, however, we must also ensure that the Fourier transform falls off suitably fast as ω increases. We actually subtract off the quantity

$$-i \frac{\sqrt{\pi}}{2} \frac{\exp\left(\frac{1}{\Delta^2}\right) \operatorname{erfc}\left(\frac{1}{\Delta}\right)}{\Delta\omega + i \exp\left(\frac{1}{\Delta^2}\right) \operatorname{erfc}\left(\frac{1}{\Delta}\right) \omega^2}, \quad (2.66)$$

so that the coefficient of $1/\omega^2$ at large ω also vanishes. The parts that are subtracted off must have a known inverse transform, which at the end is added to the remaining part that is transformed by a fast Fourier transform algorithm. Finding a suitable subtraction is a rather cumbersome process. In addition, because the fast Fourier transform method is a numerical method (as opposed to an

analytical method), we do not obtain an explicit form for $\langle S(\Delta, t) \rangle$.

The series obtained using the method of Section 2.4.2, on the other hand, do give an explicit form for $\langle S(\Delta, t) \rangle$. Unfortunately, however, they have the very serious limitation that they do not always converge for larger values of t unless Δ is small.

The method discussed in Section 2.4.3 shares a drawback with the fast Fourier transform method, namely that unless the integral can be done analytically, an explicit form for $\langle S(\Delta, t) \rangle$ cannot be obtained. This method is, however, superior to the fast Fourier transform method because it does not require the cumbersome subtractions.

As a general rule, the series method of Section 2.4.2 is best when it converges, and the integral method of Section 2.4.3 is the best otherwise.

2.4.5 Plots and discussion

Plots of $\langle S(\Delta, t) \rangle$ for several values of Δ are shown in Fig. 2.1. Notice that the initial slope of the signal is independent of Δ . This feature translates into resonance widths that vary as $1/t$ for small t – the so-called transform broadening discussed by Thomson *et al.* [60, 59]. With v on the order of MHz, this initial rise occurs in a fraction of a μs . We will see later that when the $sp \rightarrow ps$ process is included, the initial rise is independent of both the detuning Δ and the strength of the $sp \rightarrow ps$ interaction. Another point of interest is that the averaging is much more effective at smoothing out the oscillations for $\Delta = 0$ than it is for $\Delta \neq 0$.

We can construct a measure of the width from the first two terms in the Δ -expansion, Eq. (2.41). If

$$\langle S(\Delta, t) \rangle = S_0(t) + \Delta^2 S_1(t) + \mathcal{O}(\Delta^4), \quad (2.67)$$

and we define

$$w = \sqrt{-\frac{S_0(t)}{S_1(t)}}, \quad (2.68)$$

then $2w$ would be the FWHM if the lineshape were Lorentzian. We note that the functions $S_0(t)$ and $S_1(t)$ are easily obtained in closed form, since they are essentially just the $m = 0$ and $m = 1$ terms in the sum of Eq. (2.41), respectively. The quantity w/v is plotted in Fig. 2.2 as the dashed curve. For small vt , we have explicitly $w = \sqrt{12}/t$. While the $1/t$ behavior follows from the transform broadening argument, or even simply from dimensional analysis, the coefficient $\sqrt{12}$ is a prediction of the detailed theory.

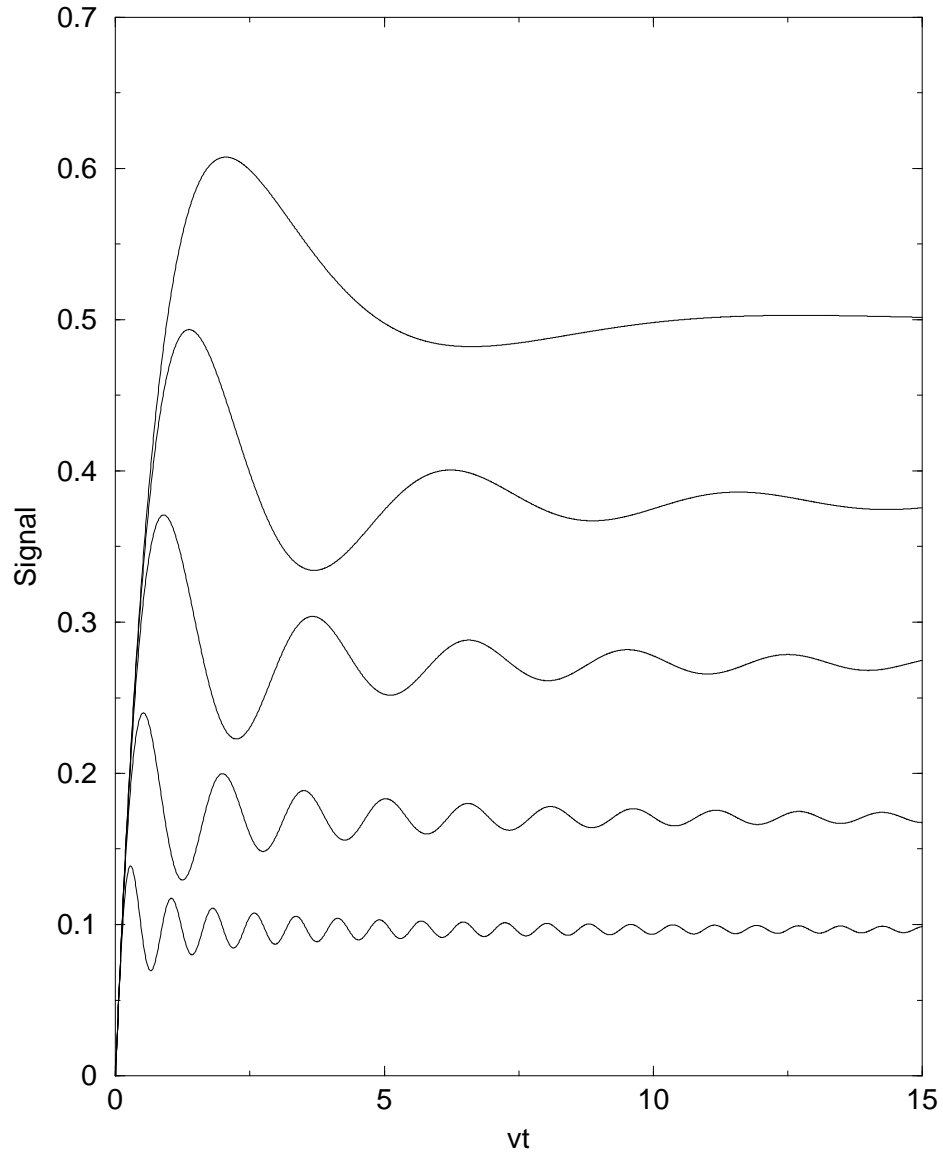


Figure 2.1: Averaged signal $S(\Delta, t)$ for (from top to bottom) $\Delta/v = 0, 1, 2, 4,$ and 8 , calculated using the method of Section 2.4.3 for the sparse limit. The $ss' \rightarrow pp'$ process is averaged, and the $sp \rightarrow ps$ process is neglected. The Rabi oscillations are not completely washed out by the averaging process and are more pronounced off resonance.

The solid curve in Fig. 2.2 is the exact half width, as determined using Eq. (2.56) of Section 2.4.3. We see that the width of Eq. (2.68) is a good approximation to the exact result only at small times.

The lineshape at saturation ($t \rightarrow \infty$) can be obtained directly from the first line of Eq. (2.47). For large times the cosine term averages to zero, giving

$$\langle S(\Delta, t \rightarrow \infty) \rangle = \frac{\sqrt{\pi}}{2} \frac{v}{\Delta} \exp\left(\frac{v^2}{\Delta^2}\right) \operatorname{erfc}\left(\frac{v}{\Delta}\right), \quad (2.69)$$

which can also be extracted from the small α behavior of Eq. (2.27). This lineshape is plotted in Fig. 2.3. The FWHM is approximately $4.6v$. Also plotted is a Lorentzian lineshape with the same height and FWHM. Notice that this lineshape is sharper than the Lorentzian for small Δ and falls off more slowly for large Δ .

2.5 Averaging more complicated interaction potentials

In Section 2.3 we averaged the quantity $e^{-\beta\mathcal{V}^2}$, where $\mathcal{V}^2 = \sum_{k=1}^N V_k^2$ and $V_k = \mu\mu'/r_k^3$. In this section we consider the problem of averaging a more complicated interaction potential. Here we perform the averaging procedure for a potential that varies as

$$V_k(\mathbf{r}_k) = \frac{C}{r_k^p} f(\theta_k, \phi_k), \quad (2.70)$$

where C is a constant and r_k , θ_k , and ϕ_k are the spherical coordinates corresponding to \mathbf{r}_k . We have seen that we can evaluate the average of the signal if we can compute the average of the quantity $\exp(-\beta\mathcal{V}^2)$. A careful look at Eq. (2.8) shows that the steps do not make any assumptions on how $V(\mathbf{r}_k)$ depends on \mathbf{r}_k , so this equation still holds and we have

$$\langle e^{-\beta\mathcal{V}^2} \rangle = \exp\left\{-\frac{N}{\Omega} \int d^3r \left[1 - e^{-\beta V^2(\mathbf{r})}\right]\right\}. \quad (2.71)$$

Thus we are left with the task of evaluating the integral

$$\begin{aligned} I &= \int d^3r \left[1 - e^{-\beta V^2(\mathbf{r})}\right] \\ &= \int_0^\infty dr r^2 \int_0^{2\pi} d\phi \int_0^\pi d\theta \sin\theta \left[1 - \exp\left(-\beta \frac{C^2}{r^{2p}} f^2(\theta, \phi)\right)\right]. \end{aligned} \quad (2.72)$$

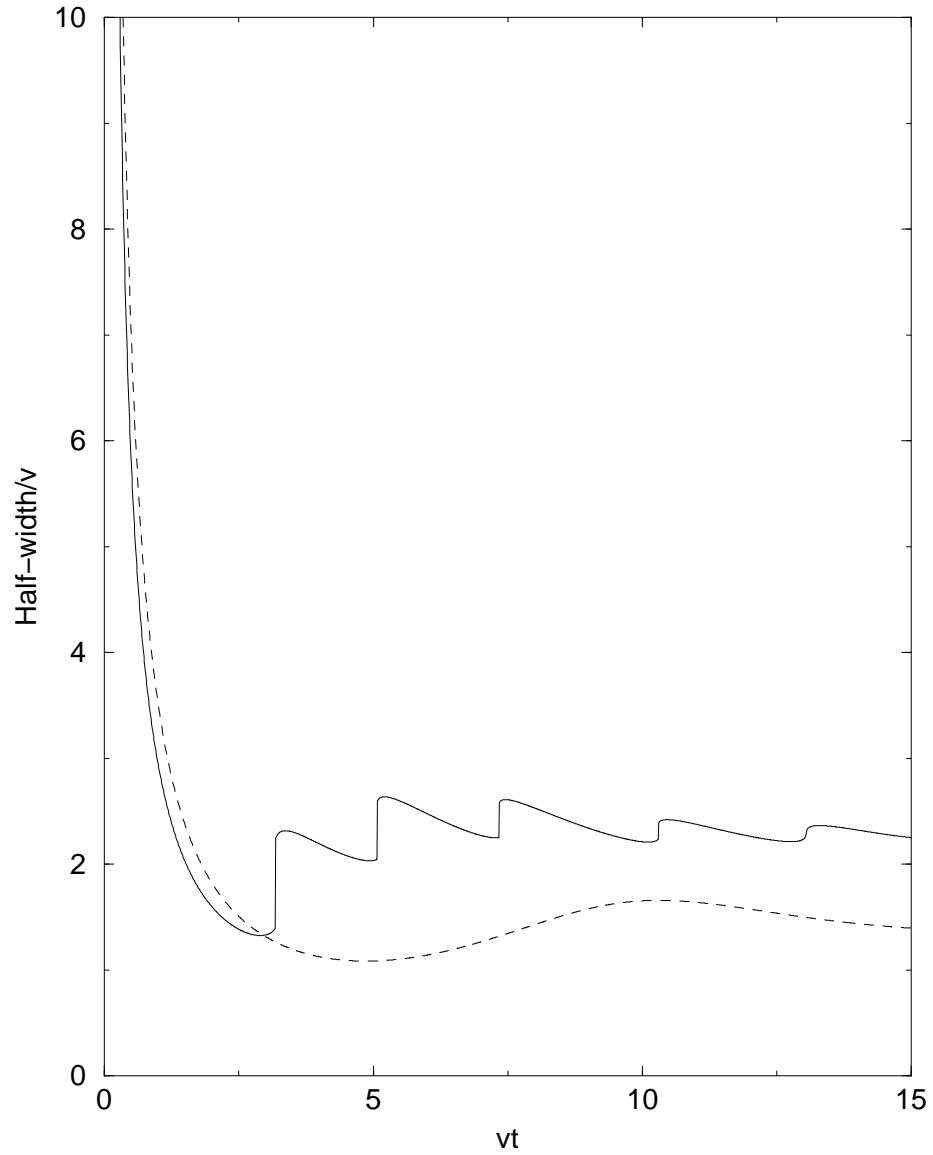


Figure 2.2: The dashed line is the width w , as given by Eq. (2.68), versus time. The solid line is the width as determined using Eq. (2.56) of Section 2.4.3. The “dip” seen in both curves is associated with the stronger and higher frequency oscillations seen at larger values of Δ , as shown in Fig. 2.1.

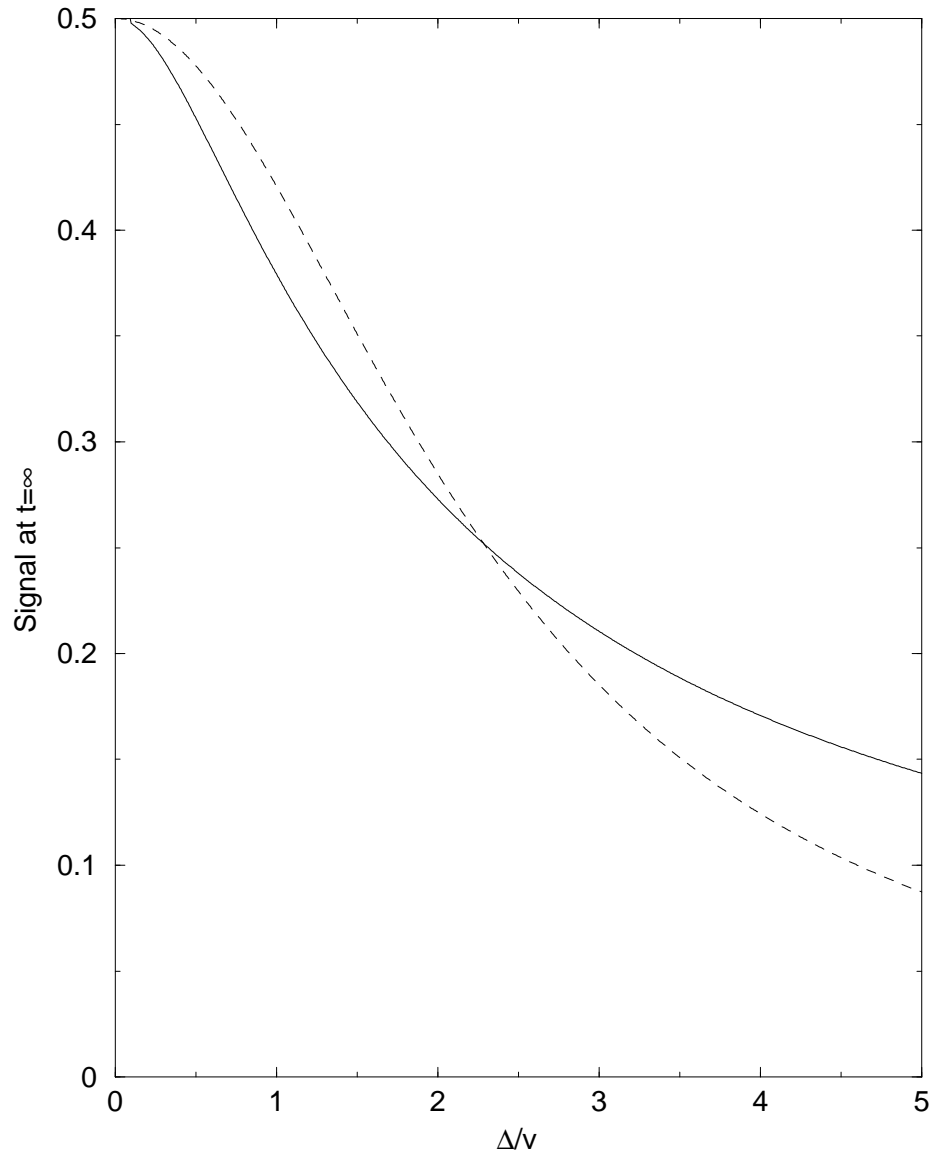


Figure 2.3: The solid curve is the saturation ($t \rightarrow \infty$) lineshape of Eq. (2.69). It is not a Lorentzian but a Lorentzian averaged as in Eq. (2.25). The dashed curve is a Lorentzian with the same height and FWHM, drawn for comparison.

We can define the variable $z = r^3 [C^2 f^2(\theta, \phi)]^{-3/2p}$, and then

$$\begin{aligned}
I &= \frac{1}{3} \int_0^\infty dz \int_0^{2\pi} d\phi \int_0^\pi d\theta \sin \theta [C^2 f^2(\theta, \phi) \beta]^{3/2p} \left[1 - \exp\left(-\frac{1}{z^{2p/3}}\right) \right] \\
&= \frac{1}{3} |C|^{3/p} \beta^{3/2p} \\
&\quad \left\{ \int_0^\infty dz \left[1 - \exp\left(-\frac{1}{z^{2p/3}}\right) \right] \right\} \left\{ \int_0^{2\pi} d\phi \int_0^\pi d\theta \sin \theta |f(\theta, \phi)|^{3/p} \right\}. \quad (2.73)
\end{aligned}$$

The remaining integrals over z and the angular variables can now be looked up in tables or done numerically.

It is very important to note that the introduction of an angular dependence into the potential does not affect the averaging process except to change the definition of the scaling parameter v by a constant factor. This means that we can, for simplicity, use a simple potential that contains no angular dependence to get an answer, and then take into account any angular dependence by simply changing the definition of v in the formulas.

2.5.1 Interaction potential of aligned dipoles

The induced dipoles in the magneto-optical trap become aligned when the applied electric field is sufficiently large that the Stark effect has passed from the quadratic to the linear regime. The aligned dipole case is the one considered in Refs. [32] and [54], for example. It is also the potential we use in performing the numerical simulations discussed in Chapter 7, for reasons that are explained fully in Section 7.2. Specifically, we have

$$V(\mathbf{r}) = -\frac{\mu_1 \mu_2}{r^3} (3 \cos^2 \theta - 1). \quad (2.74)$$

Thus we need to evaluate the integral

$$\begin{aligned}
&\frac{1}{3} \mu_1 \mu_2 \sqrt{\beta} \left\{ \int_0^\infty dz \left[1 - \exp\left(-\frac{1}{z^2}\right) \right] \right\} \left\{ \int_0^{2\pi} d\phi \int_0^\pi d\theta \sin \theta |3 \cos^2 \theta - 1| \right\} \\
&= \frac{1}{3} \mu_1 \mu_2 \sqrt{\beta} \{ \sqrt{\pi} \} \left\{ 2\pi \frac{8}{3\sqrt{3}} \right\} \\
&= \frac{16\pi^{3/2}}{9\sqrt{3}} \mu_1 \mu_2 \sqrt{\beta}. \quad (2.75)
\end{aligned}$$

We see that the additional angular dependence changes v by a factor of $4/3\sqrt{3} \approx 0.77$.

2.5.2 Effect of a different radial dependence on the initial rise

In this section, we want to determine the effect of a different radial dependence in the interaction potential on the initial rise. We saw that if the potential goes as $1/r^3$, then the signal starts linearly with t , with a slope that is independent of the detuning Δ . We will see that if the interaction potential goes as $1/r^p$, then the initial rise will go as $t^{3/p}$, with a coefficient that is again independent of the detuning.

Consider again Eq. (2.26) in the form

$$\tilde{S}(\Delta, \alpha) = \frac{1}{2\alpha} - \frac{\alpha^2 + \Delta^2}{2\alpha} \int_0^\infty d\beta e^{-\beta(\alpha^2 + \Delta^2 + 4\nu^2)}. \quad (2.76)$$

We noted previously that any angular dependence in the interaction potential will only change the scale factor ν , and will not change the functional form of the signal. Therefore we can simply consider a potential of the form

$$V(r_k) = \frac{C}{r_k^p}. \quad (2.77)$$

Of course, we can incorporate the effect of an angular contribution by simply rescaling C .

It follows, then, from Eqs. (2.71) and (2.73) that

$$\langle \tilde{S}(\Delta, \alpha) \rangle = \frac{1}{2\alpha} - \frac{\alpha^2 + \Delta^2}{2\alpha} \int_0^\infty d\beta e^{-\beta(\alpha^2 + \Delta^2) - \nu\beta^{3/2p}}, \quad (2.78)$$

where

$$\nu = 4\pi \frac{4^{3/2p}}{3} |C|^{3/p} \int_0^\infty dz \left[1 - \exp\left(-\frac{1}{z^{2p/3}}\right) \right]. \quad (2.79)$$

If we define $\xi = \beta(\alpha^2 + \Delta^2)$, then

$$\langle \tilde{S}(\Delta, \alpha) \rangle = \frac{1}{2\alpha} - \frac{1}{2\alpha} \int_0^\infty d\xi e^{-\xi} \exp\left(-\xi^{3/2p} \frac{\nu}{(\alpha^2 + \Delta^2)^{3/2p}}\right). \quad (2.80)$$

We want the behavior at small times, which corresponds to large α . Therefore we can replace $\alpha^2 + \Delta^2$ with α^2 and expand the second exponential, finding

$$\begin{aligned} \langle \tilde{S}(\Delta, \alpha) \rangle &= \frac{1}{2\alpha} - \frac{1}{2\alpha} \int_0^\infty d\xi e^{-\xi} \left[1 - \xi^{3/2p} \frac{\nu}{\alpha^{3/p}} + \dots \right] \\ &= \Gamma\left(1 + \frac{3}{2p}\right) \frac{\nu}{2\alpha^{1+3/p}} - \dots \end{aligned} \quad (2.81)$$

It immediately follows that

$$\langle S(\Delta, t) \rangle = \frac{\Gamma\left(1 + \frac{3}{2p}\right)}{2\Gamma\left(1 + \frac{3}{p}\right)} \nu t^{3/p} - \dots, \quad (2.82)$$

Thus we see that if the interaction potential goes as $1/r^p$, then the initial rise is independent of the detuning, Δ , and is proportional to $t^{3/p}$. As a check, we note that if $p = 3$, then we have

$$\begin{aligned} \langle S(\Delta, t) \rangle &= \frac{\Gamma\left(\frac{3}{2}\right)}{2\Gamma(2)} \nu t - \dots \\ &= \frac{\sqrt{\pi}}{4} \nu t - \dots, \end{aligned} \quad (2.83)$$

where

$$\begin{aligned} \nu &= 4\pi \frac{2}{3} |C| \int_0^\infty dz \left[1 - \exp\left(-\frac{1}{z^2}\right) \right] \\ &= \frac{8\pi^{3/2}}{3} |C|, \end{aligned} \quad (2.84)$$

and so

$$\langle S(\Delta, t) \rangle = \frac{\sqrt{\pi}}{2} \nu t - \dots, \quad (2.85)$$

which agrees perfectly with the $m = 0, n = 0$ term of Eq. (2.37).

2.6 Summary

In this chapter we discussed the case of a single s' atom interacting resonantly with a surrounding gas of s atoms, without the possibility of any $sp-ps$ interaction. The results, when averaged over the positions of the s atoms, are applicable to a sparse distribution of s' atoms among the s atoms (or vice versa, with the appropriate changes). This case is important to study for several reasons. First, exact analytical results can be obtained. This not only provides an excellent means for testing the validity of the numerical simulations discussed in Chapter 7, but it also provides a simpler arena for the development of the techniques that are used again and again in the more complicated models of the later chapters. Two key examples of the latter are the averaging technique of Sections 2.3 and 2.5, and the writing of sums as generalized hypergeometrics, as was done in Section 2.4.2.

The averaging is non-trivial because the interaction potential itself, being proportional to $1/r^3$, does not have an average value. Nevertheless, an effective average potential v given by Eq. (2.12) appears naturally in the theory. The basic averaging equation is Eq. (2.11), which enables the computation of averages of functions that depend on the sum of the squares of the interaction potentials in terms of v . This is equivalent to the distribution of Eq. (2.23) for the quantity $\mathcal{V}^2 = \sum_k V_k^2$, where V_k is the dipole-dipole interaction potential defined by Eq. (2.2). The initial rate of conversion from ss' to pp' is given by Eq. (2.37) or Eq. (2.85) to be $\sqrt{\pi}v/2$, and is independent of the detuning Δ . As we will see later, this initial rate remains the same even when the $sp-ps$ interaction is switched on.

Chapter 3

Localization in the Simple Model

3.1 Introduction

In this chapter we continue with our discussion of the simple model of Chapter 2 by examining the issue of localization. We want to determine the effective range, or localization length, of the disturbance caused by the presence of an s' atom in the frozen gas of s atoms. Since the $1/r^3$ interaction does not have a length scale, it follows that the localization length must be of the form $(\Omega/N)^{1/3} g(vt, \Delta/v)$, where N/Ω is the density of s atoms, t is the time, Δ is the detuning from resonance, and v is defined in Eq. (2.12), or more generally in Eq. (2.73). The task, then, is to give a precise definition of the localization length and to compute the function $g(vt, \Delta/v)$.

First, in Section 3.2 we compute a distribution function $\langle \mathcal{S}(\Delta, \mathbf{r}, t) \rangle$, which describes the contribution to the $ss' \rightarrow pp'$ process due to s atoms at position \mathbf{r} when the s' atom is at the origin. We begin by computing the Laplace transform of this function in Section 3.2.1, then we invert this Laplace transform in Section 3.2.2. In Section 3.2.3 we perform a check on the results of Section 3.2.1 and 3.2.2 by using them to rederive the result for the signal that was found in Chapter 2. In Section 3.2.4 we present plots of the distribution $\langle \mathcal{S}(\Delta, \mathbf{r}, t) \rangle$.

In Section 3.3 we compute the moments of the distribution $\langle \mathcal{S}(\Delta, \mathbf{r}, t) \rangle$. We again start by computing the Laplace transform of the moments in Section 3.3.1, then we invert this Laplace transform in Section 3.3.2. The result of Section 3.3.2 is rearranged in Section 3.3.3 to obtain a more convenient form, and in this section we also define localization lengths in terms of the moments in the usual way. The end result for the moments is checked in Section 3.3.4 by seeing that the zeroth

moment agrees with the result for the signal as a function of time that was found in Chapter 2. In Section 3.3.5 we present plots of the results.

The summary and conclusions are given in Section 3.4. It is possible to go to this section directly and refer back to final formulas and the plots of Section 3.3.5, skipping the intervening mathematics.

3.2 The function $\langle \mathcal{S}(\Delta, \mathbf{r}, t) \rangle$

In order to study localization in the simple model of Chapter 2, we consider the quantity

$$\langle \mathcal{S}(\Delta, \mathbf{r}, t) \rangle = \left\langle \sum_{k=1}^N |c_k(\Delta, t)|^2 \delta(\mathbf{r} - \mathbf{r}_k) \right\rangle. \quad (3.1)$$

As is illustrated explicitly below, the computation of the average is very similar to the computation of the average signal, $\langle \tilde{\mathcal{S}}(\Delta, \alpha) \rangle$, of Chapter 2.

3.2.1 Computation of the Laplace transform of $\langle \mathcal{S}(\Delta, \mathbf{r}, t) \rangle$

From Eq. (2.3) of this thesis or Eq. (3) of Ref. [18] we have that

$$\int_0^\infty dt e^{-\alpha t} |c_k(t)|^2 = \frac{1}{\alpha} \frac{2V_k^2}{\alpha^2 + \Delta^2 + 4\mathcal{V}^2}, \quad (3.2)$$

where $\mathcal{V}^2 = \sum_k V_k^2$. Therefore we define

$$\langle \tilde{\mathcal{S}}(\Delta, \mathbf{r}, \alpha) \rangle = \frac{1}{\Omega^N} \int d^3r_1 \cdots d^3r_N \frac{2}{\alpha} \sum_{k=1}^N \frac{V_k^2 \delta(\mathbf{r} - \mathbf{r}_k)}{\alpha^2 + \Delta^2 + 4\mathcal{V}^2}. \quad (3.3)$$

Consider for now just the $k = 1$ term in the sum. For convenience, we will call this term \mathcal{A} . We have

$$\mathcal{A} = \frac{2}{\alpha} \frac{1}{\Omega^N} \int d^3r_1 \cdots d^3r_N \frac{V^2(\mathbf{r}_1) \delta(\mathbf{r} - \mathbf{r}_1)}{\alpha^2 + \Delta^2 + 4V^2(\mathbf{r}_1) + 4 \sum_{l=2}^N V_l^2}, \quad (3.4)$$

where I have written V_1 as $V(\mathbf{r}_1)$ to be explicit. The integral over \mathbf{r}_1 is trivial, and we find

$$\mathcal{A} = \frac{2}{\alpha} V^2(\mathbf{r}) \frac{1}{\Omega^N} \int d^3r_2 \cdots d^3r_N \frac{1}{\alpha^2 + \Delta^2 + 4V^2(\mathbf{r}) + 4 \sum_{l=2}^N V_l^2}. \quad (3.5)$$

We observe now that we can write the denominator as an integral over an exponential and use the same averaging technique as in Chapter 2. The fact that the sum over l starts from $l = 2$ does not

affect the validity of Eq. (2.11), as long as N is large. Thus we have

$$\begin{aligned} \mathcal{A} &= \frac{2}{\alpha} V^2(\mathbf{r}) \frac{1}{\Omega^N} \int_0^\infty d\Lambda \int d^3r_2 \cdots d^3r_N \exp \left\{ -\Lambda \left[\alpha^2 + \Delta^2 + 4V^2(\mathbf{r}) + 4 \sum_{l=2}^N V_l^2 \right] \right\} \\ &= \frac{2}{\alpha} V^2(\mathbf{r}) \frac{1}{\Omega} \int_0^\infty d\Lambda \exp \left\{ -\Lambda \left[\alpha^2 + \Delta^2 + 4V^2(\mathbf{r}) \right] - 2v\sqrt{\Lambda} \right\}. \end{aligned} \quad (3.6)$$

It is clear that it did not matter that we chose the $k = 1$ term from the sum in Eq. (3.3). We would have gotten the result of Eq. (3.6) no matter which term we picked. It follows that all the terms are equal, and so

$$\langle \tilde{\mathcal{S}}(\Delta, \mathbf{r}, \alpha) \rangle = \frac{2}{\alpha} \frac{N}{\Omega} V^2(\mathbf{r}) \int_0^\infty d\Lambda \exp \left\{ -\Lambda \left[\alpha^2 + \Delta^2 + 4V^2(\mathbf{r}) \right] - 2v\sqrt{\Lambda} \right\}. \quad (3.7)$$

The remaining integral over Λ is familiar from Chapter 2 and can be looked up in tables (see, for example, Ref. [25]) or done by *Mathematica*. The result is

$$\begin{aligned} \langle \tilde{\mathcal{S}}(\Delta, \mathbf{r}, \alpha) \rangle &= \frac{N}{\Omega} \frac{2V^2(\mathbf{r})}{\alpha \left[\alpha^2 + \Delta^2 + 4V^2(\mathbf{r}) \right]} - \\ &\quad \frac{N}{\Omega} \frac{2v\sqrt{\pi}V^2(\mathbf{r})}{\alpha \left[\alpha^2 + \Delta^2 + 4V^2(\mathbf{r}) \right]^{3/2}} \times \\ &\quad \exp \left[\frac{v^2}{\alpha^2 + \Delta^2 + 4V^2(\mathbf{r})} \right] \operatorname{erfc} \left[\frac{v}{\sqrt{\alpha^2 + \Delta^2 + 4V^2(\mathbf{r})}} \right]. \end{aligned} \quad (3.8)$$

3.2.2 Inverting the Laplace transform

Now that we have $\langle \tilde{\mathcal{S}}(\Delta, \mathbf{r}, \alpha) \rangle$, the next step is to invert the Laplace transform. Because Eq. (3.8) is of a form that is similar to Eq. (2.27), we can again use Eqs. (2.31), (2.33), and (2.34) to achieve this.

Using Eq. (2.31), we have

$$\begin{aligned} \langle \tilde{\mathcal{S}}(\Delta, \mathbf{r}, \alpha) \rangle &= \frac{N}{\Omega} \frac{2V^2(\mathbf{r})}{\alpha \left[\alpha^2 + \Delta^2 + 4V^2(\mathbf{r}) \right]} - \\ &\quad \frac{N}{\Omega} \frac{2v\sqrt{\pi}V^2(\mathbf{r})}{\alpha \left[\alpha^2 + \Delta^2 + 4V^2(\mathbf{r}) \right]^{3/2}} \sum_{n=0}^{\infty} \frac{1}{\Gamma\left(\frac{n}{2} + 1\right)} \left[-\frac{v}{\sqrt{\alpha^2 + \Delta^2 + 4V^2(\mathbf{r})}} \right]^n \\ &= \frac{N}{\Omega} \frac{2V^2(\mathbf{r})}{\alpha \left[\alpha^2 + \Delta^2 + 4V^2(\mathbf{r}) \right]} - \\ &\quad \frac{N}{\Omega} 2v\sqrt{\pi}V^2(\mathbf{r}) \sum_{n=0}^{\infty} \frac{1}{\Gamma\left(\frac{n}{2} + 1\right)} \frac{(-v)^n}{\alpha \left[\alpha^2 + \Delta^2 + 4V^2(\mathbf{r}) \right]^{\frac{n+3}{2}}}. \end{aligned} \quad (3.9)$$

Next, using the fact (from Eq. (2.66) of Ref. [51]) that the inverse Laplace transform of Eq. (2.33) is Eq. (2.34), we see that

$$\begin{aligned}
\langle \mathcal{S}(\Delta, \mathbf{r}, t) \rangle &= \frac{N}{\Omega} 2V^2(\mathbf{r}) \frac{t^2}{\Gamma(3)} {}_1F_2 \left\{ 1; \frac{3}{2}, 2; -\frac{1}{4} [\Delta^2 + 4V^2(\mathbf{r})] t^2 \right\} - \\
&\quad \frac{N}{\Omega} 2v\sqrt{\pi}V^2(\mathbf{r}) \sum_{n=0}^{\infty} \frac{(-v)^n t^{n+3}}{\Gamma(\frac{n}{2} + 1) \Gamma(n+4)} \times \\
&\quad {}_1F_2 \left\{ \frac{n+3}{2}; \frac{n+4}{2}, \frac{n+5}{2}; -\frac{1}{4} [\Delta^2 + 4V^2(\mathbf{r})] t^2 \right\} \\
&= \frac{N}{\Omega} V^2(\mathbf{r}) t^2 {}_1F_2 \left\{ 1; \frac{3}{2}, 2; -\frac{1}{4} [\Delta^2 + 4V^2(\mathbf{r})] t^2 \right\} - \\
&\quad \frac{N}{\Omega} 2\sqrt{\pi}vV^2(\mathbf{r}) t^3 \sum_{n=0}^{\infty} \frac{(-vt)^n}{\Gamma(\frac{n}{2} + 1) \Gamma(n+4)} \times \\
&\quad {}_1F_2 \left\{ \frac{n+3}{2}; \frac{n+4}{2}, \frac{n+5}{2}; -\frac{1}{4} [\Delta^2 + 4V^2(\mathbf{r})] t^2 \right\}. \tag{3.10}
\end{aligned}$$

3.2.3 A check on the result for $\langle \tilde{\mathcal{S}}(\Delta, \mathbf{r}, \alpha) \rangle$

It is clear from Eq. (3.1) that

$$\int d^3r \langle \mathcal{S}(\Delta, \mathbf{r}, t) \rangle = \langle \mathcal{S}(\Delta, t) \rangle, \tag{3.11}$$

and since taking the Laplace transform with respect to time and integrating over the variable \mathbf{r} clearly commute, it must also be the case that

$$\int d^3r \langle \tilde{\mathcal{S}}(\Delta, \mathbf{r}, \alpha) \rangle = \langle \tilde{\mathcal{S}}(\Delta, \alpha) \rangle. \tag{3.12}$$

For the sake of completeness, we now check that this is true. We will also find this exercise useful in the next section. From Eq. (3.7) we have

$$\begin{aligned}
\int d^3r \langle \tilde{\mathcal{S}}(\Delta, \mathbf{r}, \alpha) \rangle &= \int d^3r \frac{N}{\Omega} \frac{2V^2(\mathbf{r})}{\alpha} \int_0^{\infty} d\Lambda \exp \left\{ -\Lambda [\alpha^2 + \Delta^2 + 4V^2(\mathbf{r})] - 2v\sqrt{\Lambda} \right\} \\
&= \frac{2}{\alpha} \int_0^{\infty} d\Lambda \exp \left[-\Lambda (\alpha^2 + \Delta^2) - 2v\sqrt{\Lambda} \right] \frac{N}{\Omega} \int d^3r V^2(\mathbf{r}) \exp \left[-4\Lambda V^2(\mathbf{r}) \right] \\
&= \frac{2}{\alpha} \int_0^{\infty} d\Lambda \exp \left[-\Lambda (\alpha^2 + \Delta^2) - 2v\sqrt{\Lambda} \right] \times \\
&\quad \left(-\frac{1}{4} \right) \frac{\partial}{\partial \Lambda} \left[\frac{N}{\Omega} \int d^3r \exp \left(-4\Lambda V^2(\mathbf{r}) \right) \right]. \tag{3.13}
\end{aligned}$$

We now recall from Eqs. (2.10) and (2.12), or more generally from Section 2.5 of this thesis, that

$$\frac{N}{\Omega} \int d^3r \left[1 - e^{-\beta V^2(\mathbf{r})} \right] = v\sqrt{\beta}. \quad (3.14)$$

It follows from this that

$$\frac{N}{\Omega} \int d^3r \exp[-4\Lambda V^2(\mathbf{r})] = N - 2v\sqrt{\Lambda}, \quad (3.15)$$

and so

$$\begin{aligned} \int d^3r \langle \tilde{\mathcal{S}}(\Delta, \mathbf{r}, \alpha) \rangle &= \frac{1}{2\alpha} \int_0^\infty d\Lambda \exp[-\Lambda(\alpha^2 + \Delta^2) - 2v\sqrt{\Lambda}] \left(-\frac{\partial}{\partial \Lambda} \right) (N - 2v\sqrt{\Lambda}) \\ &= \frac{v}{2\alpha} \int_0^\infty \frac{d\Lambda}{\sqrt{\Lambda}} \exp[-\Lambda(\alpha^2 + \Delta^2) - 2v\sqrt{\Lambda}]. \end{aligned} \quad (3.16)$$

The integral over Λ can again be found in tables or done by *Mathematica*. The result is

$$\begin{aligned} \int d^3r \langle \tilde{\mathcal{S}}(\Delta, \mathbf{r}, \alpha) \rangle &= \frac{\sqrt{\pi}}{2} \frac{v}{\alpha\sqrt{\alpha^2 + \Delta^2}} \exp\left(\frac{v^2}{\alpha^2 + \Delta^2}\right) \operatorname{erfc}\left(\frac{v}{\sqrt{\alpha^2 + \Delta^2}}\right) \\ &= \langle \tilde{\mathcal{S}}(\Delta, \alpha) \rangle, \end{aligned} \quad (3.17)$$

where we have used Eq. (2.27).

A similar check for $\langle \mathcal{S}(\Delta, \mathbf{r}, t) \rangle$ is carried out in Section 3.3.4.

3.2.4 Plots

In Fig. 3.1 we see plots of the dimensionless quantity

$$\left[\left(\frac{v}{\mu\mu'} \right)^{2/3} \frac{\Omega}{N} \right] r^2 \langle \mathcal{S}(\Delta, \mathbf{r}, t = \infty) \rangle, \quad (3.18)$$

as a function of $(v/\mu\mu')^{1/3} r$, for $\Delta = 0$, v , and $2v$. The quantity $\langle \mathcal{S}(\Delta, \mathbf{r}, t = \infty) \rangle$ is most easily computed by multiplying Eq. (3.8) by α and then taking the limit $\alpha \rightarrow 0$. We see that the peak of the distribution shifts to the left with increasing Δ .

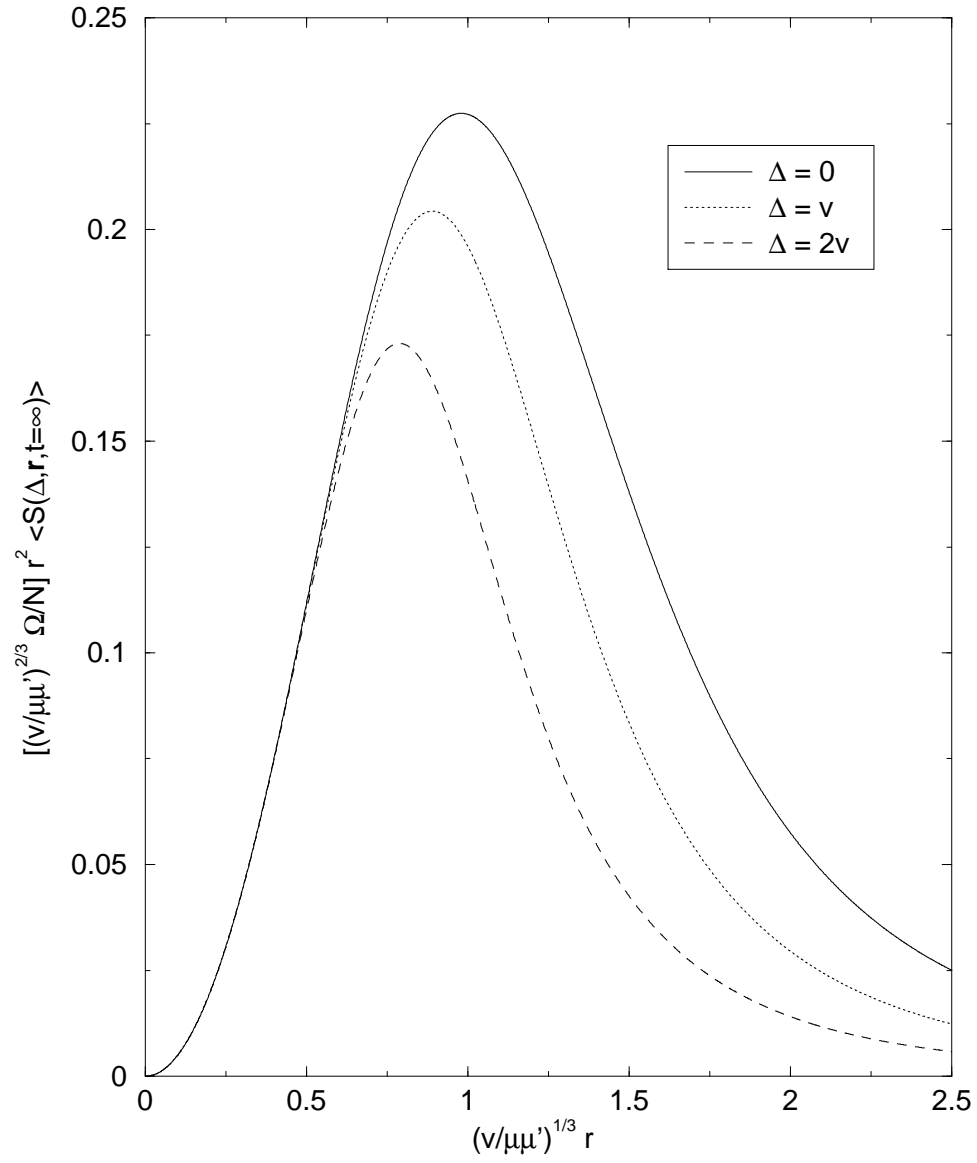


Figure 3.1: Plots of the quantity $r^2 \langle S(\Delta, r, t = \infty) \rangle$ as a function of r for Δ equal to 0, v , and $2v$.

3.3 The moments of $\langle \mathcal{S}(\Delta, \mathbf{r}, t) \rangle$

In order to compute the moments of $\langle \mathcal{S}(\Delta, \mathbf{r}, t) \rangle$, we first define

$$\tilde{\mathcal{M}}_p(\Delta, \alpha) = \int d^3r r^p \langle \tilde{\mathcal{S}}(\Delta, \mathbf{r}, \alpha) \rangle, \quad (3.19)$$

so that $\tilde{\mathcal{M}}_p(\Delta, \alpha)$ is the p th moment of $\langle \tilde{\mathcal{S}}(\Delta, \mathbf{r}, \alpha) \rangle$. We will see that we can then determine $\mathcal{M}_p(\Delta, t)$ by applying the inverse Laplace transform methods we have already refined.

3.3.1 Computation of $\tilde{\mathcal{M}}_p(\Delta, \alpha)$

Much of this computation is very similar to that done in Section 3.2.3. Using Eq. (3.7), we have

$$\begin{aligned} \tilde{\mathcal{M}}_p(\Delta, \alpha) &= \int d^3r r^p \frac{N}{\Omega} \frac{2V^2(\mathbf{r})}{\alpha} \int_0^\infty d\Lambda \exp \left[-\Lambda (\alpha^2 + \Delta^2 + 4V^2(\mathbf{r})) - 2v\sqrt{\Lambda} \right] \\ &= \frac{2}{\alpha} \int_0^\infty d\Lambda \exp \left[-\Lambda (\alpha^2 + \Delta^2) - 2v\sqrt{\Lambda} \right] \frac{N}{\Omega} \int d^3r r^p V^2(\mathbf{r}) \exp \left[-4\Lambda V^2(\mathbf{r}) \right] \\ &= \frac{2}{\alpha} \int_0^\infty d\Lambda \exp \left[-\Lambda (\alpha^2 + \Delta^2) - 2v\sqrt{\Lambda} \right] \times \\ &\quad \left(-\frac{1}{4} \frac{\partial}{\partial \Lambda} \right) \left\{ \frac{N}{\Omega} \int d^3r r^p \exp \left[-4\Lambda V^2(\mathbf{r}) \right] \right\}. \end{aligned} \quad (3.20)$$

We now note that

$$\int d^3r r^p \exp \left[-4\Lambda V^2(\mathbf{r}) \right] = \int d^3r r^p - \int d^3r r^p \{ 1 - \exp \left[-4\Lambda V^2(\mathbf{r}) \right] \}. \quad (3.21)$$

Although the first term diverges, it will disappear when we take the derivative over Λ because it does not depend on that variable.

We now need to compute the remaining integral over \mathbf{r} . I will compute it here for the case where $V(\mathbf{r}) = \mu\mu'/r^3$. If there is an angular dependence in the potential, then the computation is somewhat more complicated because the extra factors of r in the integrand will bring down extra angular factors when we apply the methods of Section 2.5. This is one case where we cannot simply rescale v to obtain the correct result when an angular dependence is introduced into the potential. With this in mind, we have

$$\int d^3r r^p \{ 1 - \exp \left[-4\Lambda V^2(\mathbf{r}) \right] \} = 4\pi \int dr r^{p+2} \left\{ 1 - \exp \left[-4\Lambda \frac{(\mu\mu')^2}{r^6} \right] \right\}$$

$$= \frac{4\pi}{3} [4\Lambda (\mu\mu')^2]^{\frac{p+3}{6}} \int dz z^{p/3} \left[1 - \exp\left(-\frac{1}{z^2}\right) \right], \quad (3.22)$$

where $z^2 = r^6/4\Lambda (\mu\mu')^2$. The remaining integral over z can be found in tables or done by *Mathematica*. The result is

$$\int d^3r r^p \{1 - \exp[-4\Lambda V^2(\mathbf{r})]\} = -\frac{1}{2}\Gamma\left(-\frac{p+3}{6}\right) \frac{4\pi}{3} [4\Lambda (\mu\mu')^2]^{\frac{p+3}{6}}, \quad (3.23)$$

for $p < 3$. This should suffice, since we will be primarily interested in $p = 1$ and $p = 2$.

Thus we have (for $p < 3$)

$$\begin{aligned} \tilde{\mathcal{M}}_p(\Delta, \alpha) &= \frac{1}{2\alpha} \int_0^\infty d\Lambda \exp[-\Lambda(\alpha^2 + \Delta^2) - 2v\sqrt{\Lambda}] \times \\ &\quad \frac{\partial}{\partial \Lambda} \left\{ -\frac{1}{2}\Gamma\left(-\frac{p+3}{6}\right) \frac{4\pi}{3} \frac{N}{\Omega} [4\Lambda (\mu\mu')^2]^{\frac{p+3}{6}} \right\} \\ &= -\frac{1}{2\alpha} [4(\mu\mu')^2]^{\frac{p+3}{6}} \frac{p+3}{12} \Gamma\left(-\frac{p+3}{6}\right) \times \\ &\quad \frac{4\pi}{3} \frac{N}{\Omega} \int_0^\infty d\Lambda \Lambda^{\frac{p-3}{6}} \exp[-\Lambda(\alpha^2 + \Delta^2) - 2v\sqrt{\Lambda}] \\ &= \frac{1}{\alpha} 2^{p/3} (\mu\mu')^{p/3} \frac{1}{2} \Gamma\left(\frac{3-p}{6}\right) \frac{v}{\sqrt{\pi}} \times \\ &\quad \int_0^\infty d\Lambda \Lambda^{\frac{p-3}{6}} \exp[-\Lambda(\alpha^2 + \Delta^2) - 2v\sqrt{\Lambda}], \end{aligned} \quad (3.24)$$

where in the last step we have used the fact that $\Gamma(n+1) = n\Gamma(n)$ and Eq. (2.12). For $p > -3$, we have from *Mathematica* that

$$\begin{aligned} \int_0^\infty d\Lambda \Lambda^{\frac{p-3}{6}} \exp[-\Lambda A^2 - 2v\sqrt{\Lambda}] &= \left(\frac{1}{A}\right)^{\frac{p+3}{3}} \Gamma\left(\frac{p+3}{6}\right) {}_1F_1\left(\frac{p+3}{6}; \frac{1}{2}; \frac{v^2}{A^2}\right) - \\ &\quad \frac{2v}{A^{\frac{p+6}{3}}} \Gamma\left(\frac{p+6}{6}\right) {}_1F_1\left(\frac{p+6}{6}; \frac{3}{2}; \frac{v^2}{A^2}\right), \end{aligned} \quad (3.25)$$

where as in Chapter 2, $A^2 = \alpha^2 + \Delta^2$. It follows that for $|p| < 3$, we have

$$\begin{aligned} \tilde{\mathcal{M}}_p(\Delta, \alpha) &= \frac{1}{\alpha} 2^{\frac{p-3}{3}} (\mu\mu')^{p/3} \Gamma\left(\frac{3-p}{6}\right) \frac{v}{\sqrt{\pi}} \times \\ &\quad \left[\left(\frac{1}{\alpha^2 + \Delta^2}\right)^{\frac{p+3}{6}} \Gamma\left(\frac{p+3}{6}\right) {}_1F_1\left(\frac{p+3}{6}; \frac{1}{2}; \frac{v^2}{\alpha^2 + \Delta^2}\right) - \right. \\ &\quad \left. \frac{2v}{(\alpha^2 + \Delta^2)^{\frac{p+6}{6}}} \Gamma\left(\frac{p+6}{6}\right) {}_1F_1\left(\frac{p+6}{6}; \frac{3}{2}; \frac{v^2}{\alpha^2 + \Delta^2}\right) \right]. \end{aligned} \quad (3.26)$$

3.3.2 Inverting the Laplace transform

We know from Eq. (2.35) that

$${}_1F_1(a, b, z) = \frac{\Gamma(b)}{\Gamma(a)} \sum_{j=0}^{\infty} \frac{\Gamma(j+a)}{\Gamma(j+b)\Gamma(j+1)} z^j, \quad (3.27)$$

so

$$\begin{aligned} \tilde{\mathcal{M}}_p(\Delta, \alpha) &= \frac{1}{\alpha} 2^{\frac{p-3}{3}} (\mu\mu')^{p/3} \Gamma\left(\frac{3-p}{6}\right) \frac{v}{\sqrt{\pi}} \times \\ &\quad \left[\left(\frac{1}{\alpha^2 + \Delta^2}\right)^{\frac{p+3}{6}} \Gamma\left(\frac{p+3}{6}\right) \frac{\Gamma(\frac{1}{2})}{\Gamma(\frac{p+3}{6})} \sum_{j=0}^{\infty} \frac{\Gamma(j + \frac{p+3}{6})}{\Gamma(j + \frac{1}{2})\Gamma(j+1)} \left(\frac{v^2}{\alpha^2 + \Delta^2}\right)^j - \right. \\ &\quad \left. \frac{2v}{(\alpha^2 + \Delta^2)^{\frac{p+6}{6}}} \Gamma\left(\frac{p+6}{6}\right) \frac{\Gamma(\frac{3}{2})}{\Gamma(\frac{p+6}{6})} \sum_{j=0}^{\infty} \frac{\Gamma(j + \frac{p+6}{6})}{\Gamma(j + \frac{3}{2})\Gamma(j+1)} \left(\frac{v^2}{\alpha^2 + \Delta^2}\right)^j \right] \\ &= \frac{1}{\alpha} 2^{\frac{p-3}{3}} (\mu\mu')^{p/3} \Gamma\left(\frac{3-p}{6}\right) \frac{v}{\sqrt{\pi}} \times \\ &\quad \left[\sqrt{\pi} \sum_{j=0}^{\infty} \frac{\Gamma(j + \frac{p+3}{6})}{\Gamma(j + \frac{1}{2})\Gamma(j+1)} \frac{v^{2j}}{(\alpha^2 + \Delta^2)^{j + \frac{p+3}{6}}} - \right. \\ &\quad \left. v\sqrt{\pi} \sum_{j=0}^{\infty} \frac{\Gamma(j + \frac{p+6}{6})}{\Gamma(j + \frac{3}{2})\Gamma(j+1)} \frac{v^{2j}}{(\alpha^2 + \Delta^2)^{j + \frac{p+6}{6}}} \right] \\ &= \frac{1}{\alpha} 2^{\frac{p-3}{3}} (\mu\mu')^{p/3} \Gamma\left(\frac{3-p}{6}\right) v \left[\sum_{j=0}^{\infty} \frac{\Gamma(j + \frac{p+3}{6})}{\Gamma(j + \frac{1}{2})\Gamma(j+1)} \frac{v^{2j}}{(\alpha^2 + \Delta^2)^{j + \frac{p+3}{6}}} - \right. \\ &\quad \left. \sum_{j=0}^{\infty} \frac{\Gamma(j + \frac{p+6}{6})}{\Gamma(j + \frac{3}{2})\Gamma(j+1)} \frac{v^{2j+1}}{(\alpha^2 + \Delta^2)^{j + \frac{p+6}{6}}} \right], \quad (3.28) \end{aligned}$$

where we have used the facts that $\Gamma(1/2) = \sqrt{\pi}$ and $\Gamma(3/2) = \sqrt{\pi}/2$.

Now we note that

$$\sum_{j=0}^{\infty} \frac{\Gamma(j + \frac{p+3}{6})}{\Gamma(j + \frac{1}{2})\Gamma(j+1)} \frac{v^{2j}}{(\alpha^2 + \Delta^2)^{j + \frac{p+3}{6}}} - \sum_{j=0}^{\infty} \frac{\Gamma(j + \frac{p+6}{6})}{\Gamma(j + \frac{3}{2})\Gamma(j+1)} \frac{v^{2j+1}}{(\alpha^2 + \Delta^2)^{j + \frac{p+6}{6}}} \quad (3.29)$$

can be rewritten as

$$\sum_{j=0}^{\infty} \frac{\Gamma(\frac{2j}{2} + \frac{p+3}{6})}{\Gamma(\frac{2j}{2} + \frac{1}{2})\Gamma(\frac{2j}{2} + 1)} \left(-\frac{v}{\sqrt{\alpha^2 + \Delta^2}}\right)^{2j} \left(\frac{1}{\alpha^2 + \Delta^2}\right)^{\frac{p+3}{6}} +$$

$$\sum_{j=0}^{\infty} \frac{\Gamma\left(\frac{2j+1}{2} + \frac{p+3}{6}\right)}{\Gamma\left(\frac{2j+1}{2} + 1\right) \Gamma\left(\frac{2j+1}{2} + \frac{1}{2}\right)} \left(-\frac{v}{\sqrt{\alpha^2 + \Delta^2}}\right)^{2j+1} \left(\frac{1}{\alpha^2 + \Delta^2}\right)^{\frac{p+3}{6}}, \quad (3.30)$$

and so Eq. (3.29) is equivalent to the single sum

$$\left(\frac{1}{\alpha^2 + \Delta^2}\right)^{\frac{p+3}{6}} \sum_{j=0}^{\infty} \frac{\Gamma\left(\frac{j}{2} + \frac{p+3}{6}\right)}{\Gamma\left(\frac{j}{2} + \frac{1}{2}\right) \Gamma\left(\frac{j}{2} + 1\right)} \left(-\frac{v}{\sqrt{\alpha^2 + \Delta^2}}\right)^j. \quad (3.31)$$

Therefore we have

$$\begin{aligned} \tilde{\mathcal{M}}_p(\Delta, \alpha) &= \frac{1}{\alpha} 2^{\frac{p-3}{3}} (\mu\mu')^{p/3} \Gamma\left(\frac{3-p}{6}\right) v \times \\ &\quad \left(\frac{1}{\alpha^2 + \Delta^2}\right)^{\frac{p+3}{6}} \sum_{j=0}^{\infty} \frac{\Gamma\left(\frac{j}{2} + \frac{p+3}{6}\right)}{\Gamma\left(\frac{j}{2} + \frac{1}{2}\right) \Gamma\left(\frac{j}{2} + 1\right)} \left(-\frac{v}{\sqrt{\alpha^2 + \Delta^2}}\right)^j. \end{aligned} \quad (3.32)$$

Using Eqs. (2.33) and (2.34), we see that the inverse Laplace transform of

$$\frac{1}{\alpha} \left(\frac{1}{\alpha^2 + \Delta^2}\right)^\nu \quad (3.33)$$

is

$$\frac{t^{2\nu}}{\Gamma(2\nu + 1)} {}_1F_2\left(\nu; \nu + \frac{1}{2}; \nu + 1; -\frac{1}{4}\Delta^2 t^2\right). \quad (3.34)$$

Therefore we have that

$$\begin{aligned} \mathcal{M}_p(\Delta, t) &= 2^{\frac{p-3}{3}} (\mu\mu')^{p/3} \Gamma\left(\frac{3-p}{6}\right) v \times \\ &\quad \sum_{j=0}^{\infty} (-v)^j \frac{\Gamma\left(\frac{j}{2} + \frac{p+3}{6}\right)}{\Gamma\left(\frac{j}{2} + \frac{1}{2}\right) \Gamma\left(\frac{j}{2} + 1\right) \Gamma\left(j + \frac{p+3}{3} + 1\right)} t^{j + \frac{p+3}{3}} \times \\ &\quad {}_1F_2\left(\frac{j}{2} + \frac{p+3}{6}; \frac{j}{2} + \frac{p+6}{6}; \frac{j}{2} + \frac{p+9}{6}; -\frac{1}{4}\Delta^2 t^2\right) \\ &= 2^{\frac{p-3}{3}} \Gamma\left(\frac{3-p}{6}\right) (\mu\mu')^{p/3} vt^{\frac{p+3}{3}} \times \\ &\quad \sum_{j=0}^{\infty} \frac{\Gamma\left(\frac{j}{2} + \frac{p+3}{6}\right)}{\Gamma\left(\frac{j}{2} + \frac{1}{2}\right) \Gamma\left(\frac{j}{2} + 1\right) \Gamma\left(j + \frac{p+3}{3} + 1\right)} (-vt)^j \times \\ &\quad {}_1F_2\left(\frac{j}{2} + \frac{p+3}{6}; \frac{j}{2} + \frac{p+6}{6}; \frac{j}{2} + \frac{p+9}{6}; -\frac{1}{4}\Delta^2 t^2\right). \end{aligned} \quad (3.35)$$

3.3.3 A more convenient form for $\mathcal{M}_p(\Delta, t)$

As we mentioned in Section 2.4.2, it is sometimes useful to have a result as a series in powers of the detuning squared. Now we exploit the method used there to obtain such a form for $\mathcal{M}_p(\Delta, t)$. For convenience, we define

$$\mathcal{B} = \sum_{j=0}^{\infty} \frac{\Gamma\left(\frac{j+1}{2} + \frac{p}{6}\right)}{\Gamma\left(\frac{j+1}{2}\right) \Gamma\left(\frac{j+2}{2}\right) \Gamma\left(j+2 + \frac{p}{3}\right)} (-vt)^j \times {}_1F_2\left(\frac{j+1}{2} + \frac{p}{6}; \frac{j+2}{2} + \frac{p}{6}, \frac{j+3}{2} + \frac{p}{6}; -\frac{1}{4}\Delta^2 t^2\right), \quad (3.36)$$

so that

$$\mathcal{M}_p(\Delta, t) = 2^{\frac{p-3}{3}} \Gamma\left(\frac{3-p}{6}\right) (\mu\mu')^{p/3} vt^{\frac{p+3}{3}} \mathcal{B} \quad (3.37)$$

We now recall from Eq. (2.35) that

$${}_1F_2(a; b, c; z) = \frac{\Gamma(b)\Gamma(c)}{\Gamma(a)} \sum_{k=0}^{\infty} \frac{\Gamma(k+a)}{\Gamma(k+b)\Gamma(k+c)\Gamma(k+1)} z^k, \quad (3.38)$$

and hence

$$\mathcal{B} = \sum_{j=0}^{\infty} \frac{\Gamma\left(\frac{j+2}{2} + \frac{p}{6}\right) \Gamma\left(\frac{j+3}{2} + \frac{p}{6}\right)}{\Gamma\left(\frac{j+1}{2}\right) \Gamma\left(\frac{j+2}{2}\right) \Gamma\left(j+2 + \frac{p}{3}\right)} (-vt)^j \times \sum_{k=0}^{\infty} \frac{\Gamma\left(k + \frac{j+1}{2} + \frac{p}{6}\right)}{\Gamma\left(k + \frac{j+2}{2} + \frac{p}{6}\right) \Gamma\left(k + \frac{j+3}{2} + \frac{p}{6}\right) \Gamma(k+1)} \left(-\frac{1}{4}\Delta^2 t^2\right)^k. \quad (3.39)$$

Recalling Eq. (2.30), we see that

$$\Gamma\left(j+2 + \frac{p}{3}\right) = \frac{1}{2\sqrt{\pi}} 2^{j+2+\frac{p}{3}} \Gamma\left(\frac{j+2}{2} + \frac{p}{6}\right) \Gamma\left(\frac{j+3}{2} + \frac{p}{6}\right), \quad (3.40)$$

and so

$$\begin{aligned} \mathcal{B} &= \frac{\sqrt{\pi}}{2^{\frac{p+3}{3}}} \sum_{k=0}^{\infty} \sum_{j=0}^{\infty} \frac{1}{\Gamma\left(\frac{j+1}{2}\right) \Gamma\left(\frac{j+2}{2}\right)} \left(-\frac{vt}{2}\right)^j \times \\ &\quad \frac{\Gamma\left(k + \frac{j+1}{2} + \frac{p}{6}\right)}{\Gamma\left(k + \frac{j+2}{2} + \frac{p}{6}\right) \Gamma\left(k + \frac{j+3}{2} + \frac{p}{6}\right) \Gamma(k+1)} \left(-\frac{1}{4}\Delta^2 t^2\right)^k \\ &= \frac{\sqrt{\pi}}{2^{\frac{p+3}{3}}} \sum_{k=0}^{\infty} \left(\frac{-\Delta^2 t^2}{4}\right)^k \frac{1}{\Gamma(k+1)} \times \end{aligned}$$

$$\sum_{j=0}^{\infty} \frac{\Gamma\left(\frac{j+1}{2} + k + \frac{p}{6}\right)}{\Gamma\left(\frac{j+1}{2}\right) \Gamma\left(\frac{j+2}{2}\right) \Gamma\left(\frac{j+2}{2} + k + \frac{p}{6}\right) \Gamma\left(\frac{j+3}{2} + k + \frac{p}{6}\right)} \left(-\frac{vt}{2}\right)^j. \quad (3.41)$$

Now we define

$$\mathcal{B}_k^{\text{odd}} = \sum_{j=0, j \text{ odd}}^{\infty} \frac{\Gamma\left(\frac{j+1}{2} + k + \frac{p}{6}\right)}{\Gamma\left(\frac{j+1}{2}\right) \Gamma\left(\frac{j+2}{2}\right) \Gamma\left(\frac{j+2}{2} + k + \frac{p}{6}\right) \Gamma\left(\frac{j+3}{2} + k + \frac{p}{6}\right)} \left(-\frac{vt}{2}\right)^j \quad (3.42)$$

and similarly,

$$\mathcal{B}_k^{\text{even}} = \sum_{j=0, j \text{ even}}^{\infty} \frac{\Gamma\left(\frac{j+1}{2} + k + \frac{p}{6}\right)}{\Gamma\left(\frac{j+1}{2}\right) \Gamma\left(\frac{j+2}{2}\right) \Gamma\left(\frac{j+2}{2} + k + \frac{p}{6}\right) \Gamma\left(\frac{j+3}{2} + k + \frac{p}{6}\right)} \left(-\frac{vt}{2}\right)^j, \quad (3.43)$$

so that

$$\mathcal{B} = \frac{\sqrt{\pi}}{2^{\frac{p+3}{3}}} \sum_{k=0}^{\infty} \left(-\frac{\Delta^2 t^2}{4}\right)^k \frac{1}{\Gamma(k+1)} (\mathcal{B}_k^{\text{odd}} + \mathcal{B}_k^{\text{even}}). \quad (3.44)$$

We then have (again using Eq. (2.35))

$$\begin{aligned} \mathcal{B}_k^{\text{odd}} &= -\frac{vt}{2} \sum_{j=0}^{\infty} \frac{\Gamma\left(j + k + \frac{p}{6} + 1\right)}{\Gamma(j+1) \Gamma\left(j + \frac{3}{2}\right) \Gamma\left(j + k + \frac{p}{6} + \frac{3}{2}\right) \Gamma\left(j + k + \frac{p}{6} + 2\right)} \left(\frac{v^2 t^2}{4}\right)^j \\ &= -\frac{vt}{2} \frac{\Gamma\left(k + \frac{p}{6} + 1\right)}{\Gamma\left(\frac{3}{2}\right) \Gamma\left(k + \frac{p}{6} + \frac{3}{2}\right) \Gamma\left(k + \frac{p}{6} + 2\right)} \times \\ &\quad {}_1F_3\left(k + \frac{p}{6} + 1; \frac{3}{2}, k + \frac{p}{6} + \frac{3}{2}, k + \frac{p}{6} + 2; \frac{v^2 t^2}{4}\right) \\ &= -\frac{vt}{\sqrt{\pi}} \frac{1}{\left(k + \frac{p}{6} + 1\right) \Gamma\left(k + \frac{p}{6} + \frac{3}{2}\right)} \times \\ &\quad {}_1F_3\left(k + \frac{p}{6} + 1; \frac{3}{2}, k + \frac{p}{6} + \frac{3}{2}, k + \frac{p}{6} + 2; \frac{v^2 t^2}{4}\right). \end{aligned} \quad (3.45)$$

Performing the analogous calculation for $\mathcal{B}_k^{\text{even}}$, we see that

$$\begin{aligned} \mathcal{B}_k^{\text{even}} &= \sum_{j=0}^{\infty} \frac{\Gamma\left(j + k + \frac{p}{6} + \frac{1}{2}\right)}{\Gamma\left(j + \frac{1}{2}\right) \Gamma(j+1) \Gamma\left(j + k + \frac{p}{6} + 1\right) \Gamma\left(j + k + \frac{p}{6} + \frac{3}{2}\right)} \left(\frac{v^2 t^2}{4}\right)^j \\ &= \frac{\Gamma\left(k + \frac{p}{6} + \frac{1}{2}\right)}{\Gamma\left(\frac{1}{2}\right) \Gamma\left(k + \frac{p}{6} + 1\right) \Gamma\left(k + \frac{p}{6} + \frac{3}{2}\right)} \times \\ &\quad {}_1F_3\left(k + \frac{p}{6} + \frac{1}{2}; \frac{1}{2}, k + \frac{p}{6} + 1, k + \frac{p}{6} + \frac{3}{2}; \frac{v^2 t^2}{4}\right) \\ &= \frac{1}{\sqrt{\pi}} \frac{1}{\left(k + \frac{p}{6} + \frac{1}{2}\right) \Gamma\left(k + \frac{p}{6} + 1\right)} \times \\ &\quad {}_1F_3\left(k + \frac{p}{6} + \frac{1}{2}; \frac{1}{2}, k + \frac{p}{6} + 1, k + \frac{p}{6} + \frac{3}{2}; \frac{v^2 t^2}{4}\right). \end{aligned} \quad (3.46)$$

Using Eq. (3.44), we arrive at

$$\begin{aligned}
\mathcal{B} &= \frac{1}{2^{\frac{p+3}{3}}} \sum_{k=0}^{\infty} \left(-\frac{\Delta^2 t^2}{4} \right)^k \frac{1}{\Gamma(k+1)} \left[\frac{1}{(k + \frac{p}{6} + \frac{1}{2}) \Gamma(k + \frac{p}{6} + 1)} \times \right. \\
&\quad {}_1F_3 \left(k + \frac{p}{6} + \frac{1}{2}; \frac{1}{2}, k + \frac{p}{6} + 1, k + \frac{p}{6} + \frac{3}{2}; \frac{v^2 t^2}{4} \right) - \\
&\quad \frac{vt}{(k + \frac{p}{6} + 1) \Gamma(k + \frac{p}{6} + \frac{3}{2})} \times \\
&\quad \left. {}_1F_3 \left(k + \frac{p}{6} + 1; \frac{3}{2}, k + \frac{p}{6} + \frac{3}{2}, k + \frac{p}{6} + 2; \frac{v^2 t^2}{4} \right) \right]. \tag{3.47}
\end{aligned}$$

Recalling Eq. (3.37), we obtain finally

$$\begin{aligned}
\mathcal{M}_p(\Delta, t) &= 2^{\frac{p-3}{3}} \Gamma\left(\frac{3-p}{6}\right) (\mu\mu')^{p/3} vt^{\frac{p+3}{3}} \times \\
&\quad \frac{1}{2^{\frac{p+3}{3}}} \sum_{k=0}^{\infty} \left(-\frac{\Delta^2 t^2}{4} \right)^k \frac{1}{\Gamma(k+1)} \left[\frac{1}{(k + \frac{p}{6} + \frac{1}{2}) \Gamma(k + \frac{p}{6} + 1)} \times \right. \\
&\quad {}_1F_3 \left(k + \frac{p}{6} + \frac{1}{2}; \frac{1}{2}, k + \frac{p}{6} + 1, k + \frac{p}{6} + \frac{3}{2}; \frac{v^2 t^2}{4} \right) - \\
&\quad \frac{vt}{(k + \frac{p}{6} + 1) \Gamma(k + \frac{p}{6} + \frac{3}{2})} \times \\
&\quad \left. {}_1F_3 \left(k + \frac{p}{6} + 1; \frac{3}{2}, k + \frac{p}{6} + \frac{3}{2}, k + \frac{p}{6} + 2; \frac{v^2 t^2}{4} \right) \right] \\
&= \frac{1}{4} \Gamma\left(\frac{3-p}{6}\right) \left(\frac{\mu\mu'}{v} \right)^{p/3} (vt)^{\frac{p+3}{3}} \times \\
&\quad \sum_{k=0}^{\infty} \left(-\frac{\Delta^2 t^2}{4} \right)^k \frac{1}{\Gamma(k+1)} \left[\frac{1}{(k + \frac{p}{6} + \frac{1}{2}) \Gamma(k + \frac{p}{6} + 1)} \times \right. \\
&\quad {}_1F_3 \left(k + \frac{p}{6} + \frac{1}{2}; \frac{1}{2}, k + \frac{p}{6} + 1, k + \frac{p}{6} + \frac{3}{2}; \frac{v^2 t^2}{4} \right) - \\
&\quad \frac{vt}{(k + \frac{p}{6} + 1) \Gamma(k + \frac{p}{6} + \frac{3}{2})} \times \\
&\quad \left. {}_1F_3 \left(k + \frac{p}{6} + 1; \frac{3}{2}, k + \frac{p}{6} + \frac{3}{2}, k + \frac{p}{6} + 2; \frac{v^2 t^2}{4} \right) \right]. \tag{3.48}
\end{aligned}$$

It is important to recall that this result is valid for $|p| < 3$.

The result of Eq. (3.48) shows that the p th moment \mathcal{M}_p is equal to the quantity $(\mu\mu'/v)^{p/3}$ multiplied by a dimensionless function. Since $\mu\mu'/v$ is proportional to Ω/N , as can be seen from Eq. (2.12), it follows that \mathcal{M}_p has the dimensions of length to the p th power as it should.

To extract a localization length l_p from the moment \mathcal{M}_p , we must first normalize the distribution

\mathcal{S} of Eq. (3.10). The localization length corresponding to the p th moment is thus given by

$$l_p(\Delta, t) = \left[\frac{\mathcal{M}_p(\Delta, t)}{\mathcal{M}_0(\Delta, t)} \right]^{1/p}. \quad (3.49)$$

For each value of p , this expression gives a somewhat different measurement of localization. The quantity l_p is proportional to $(\mu\mu'/v)^{1/3}$, which according to Eq. (2.12) is equal to $(3/4\pi^{3/2})^{1/3}(\Omega/N)^{1/3}$, or $0.5126(\Omega/N)^{1/3}$. Therefore we see that l_p has units of length for all values of p , as one would expect.

3.3.4 A check on the result for $\mathcal{M}_p(\Delta, t)$

We see from Eq. (3.11) that $\mathcal{M}_0(\Delta, t) = \langle S(\Delta, t) \rangle$, and this provides one way to check Eq. (3.48).

From Eq. (3.48) we have

$$\begin{aligned} \mathcal{M}_0(\Delta, t) &= \frac{1}{4}\Gamma\left(\frac{1}{2}\right)vt \sum_{k=0}^{\infty} \left(-\frac{\Delta^2 t^2}{4}\right)^k \frac{1}{\Gamma(k+1)} \times \\ &\quad \left[\frac{1}{(k+\frac{1}{2})\Gamma(k+1)} {}_1F_3\left(k+\frac{1}{2}; \frac{1}{2}, k+1, k+\frac{3}{2}; \frac{v^2 t^2}{4}\right) - \right. \\ &\quad \left. \frac{vt}{(k+1)\Gamma(k+\frac{3}{2})} {}_1F_3\left(k+1; \frac{3}{2}, k+\frac{3}{2}, k+2; \frac{v^2 t^2}{4}\right) \right] \\ &= \frac{\sqrt{\pi}}{4}vt \sum_{k=0}^{\infty} \left(-\frac{\Delta^2 t^2}{4}\right)^k \times \\ &\quad \left\{ \frac{1}{(k+\frac{1}{2})[\Gamma(k+1)]^2} {}_1F_3\left(k+\frac{1}{2}; \frac{1}{2}, k+1, k+\frac{3}{2}; \frac{v^2 t^2}{4}\right) - \right. \\ &\quad \left. \frac{vt}{\Gamma(k+\frac{3}{2})\Gamma(k+2)} {}_1F_3\left(k+1; \frac{3}{2}, k+\frac{3}{2}, k+2; \frac{v^2 t^2}{4}\right) \right\}, \end{aligned} \quad (3.50)$$

which agrees perfectly with Eq. (2.41).

3.3.5 Plots

Figs. 3.2 – 3.4 give plots of the dimensionless quantities

$$\left(\frac{v}{\mu\mu'}\right)^{p/3} \mathcal{M}_p(\Delta, t), \quad (3.51)$$

as a function of vt , for $p = -1, -1, 1$, and 2 and for $\Delta = 0, v$, and $2v$, respectively.

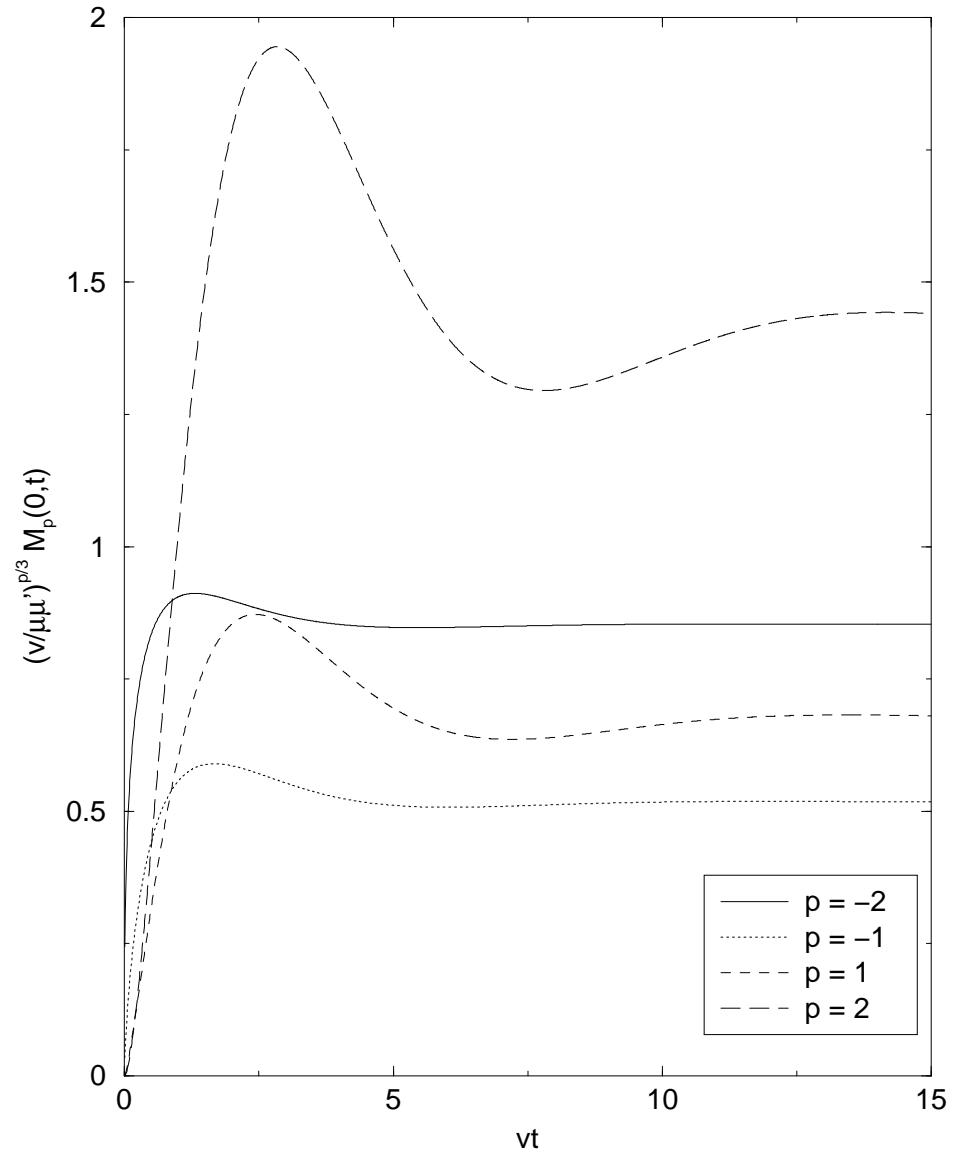
In Figs. 3.5 – 3.7 we see plots of the dimensionless quantities

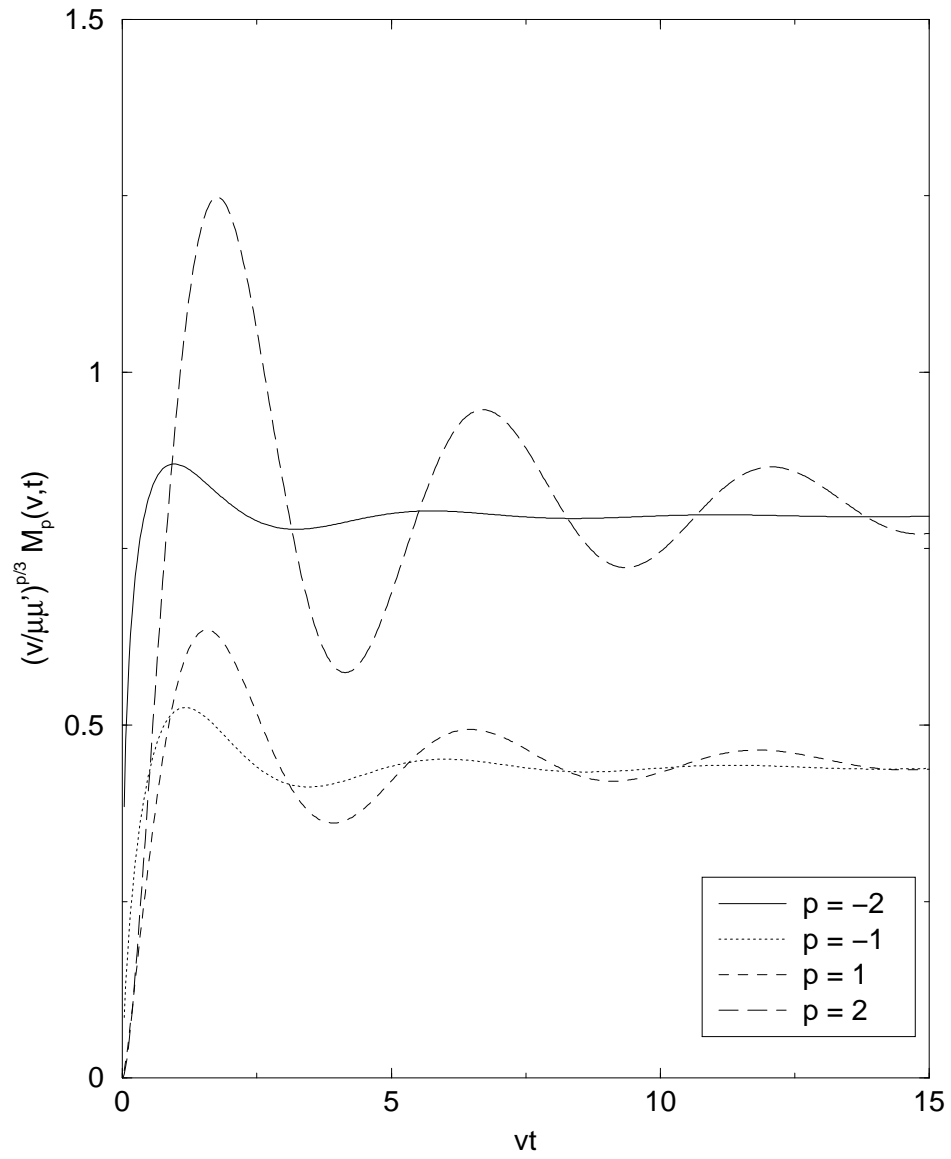
$$\left(\frac{v}{\mu\mu'}\right)^{1/3} l_p(\Delta, t), \quad (3.52)$$

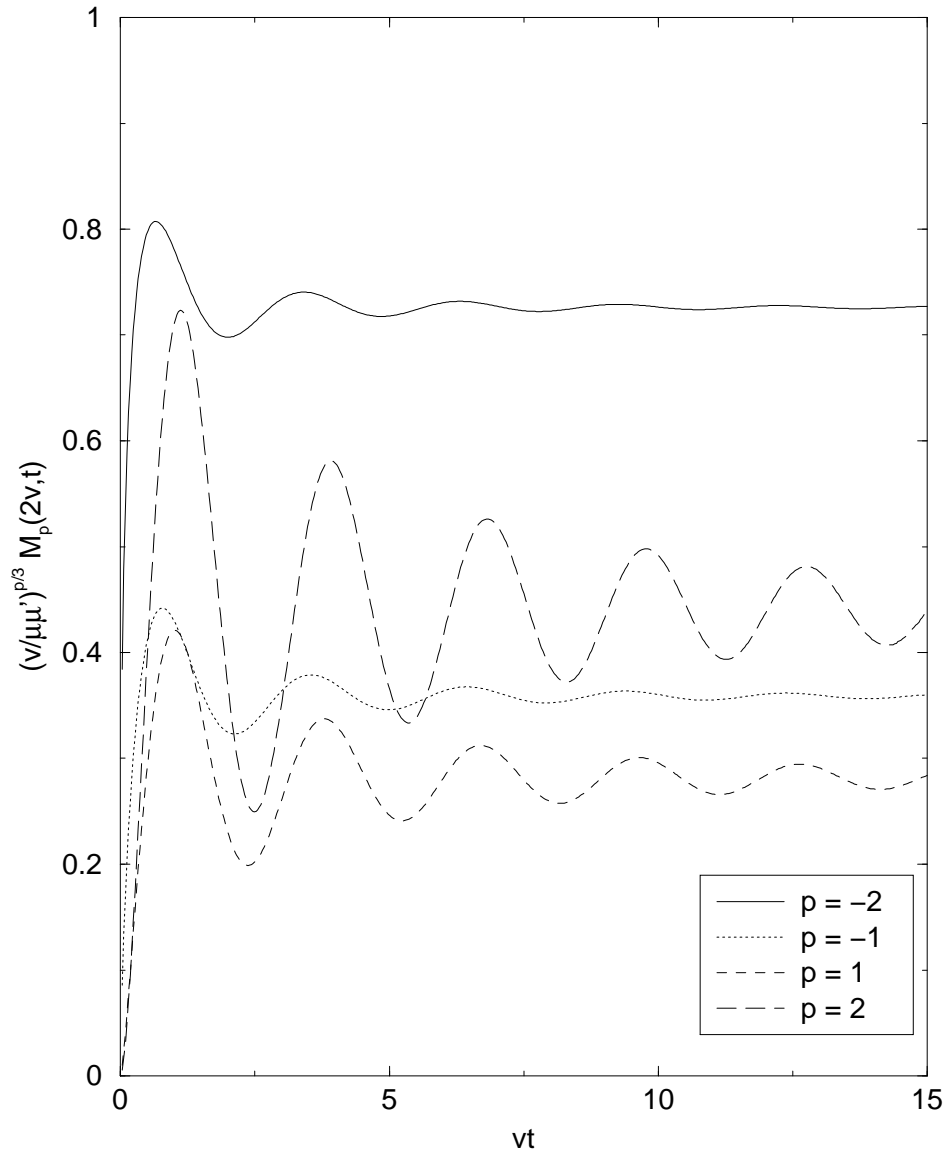
as a function of vt , for $\Delta = 0$, v , and $2v$, respectively. We see that all the plots initially rise rapidly like $(vt)^{1/3}$, and then oscillate around a value of order one that depends rather weakly on the detuning Δ .

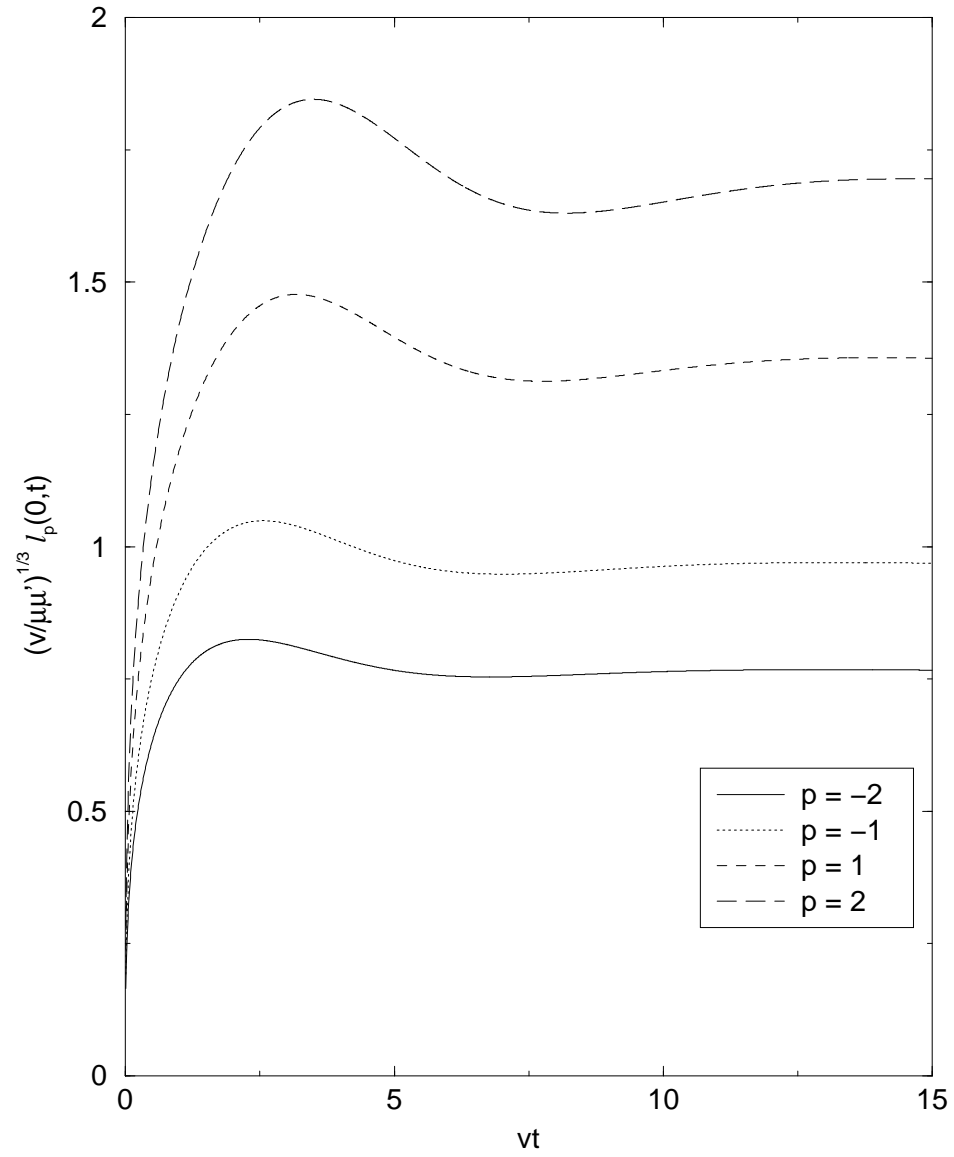
3.4 Summary

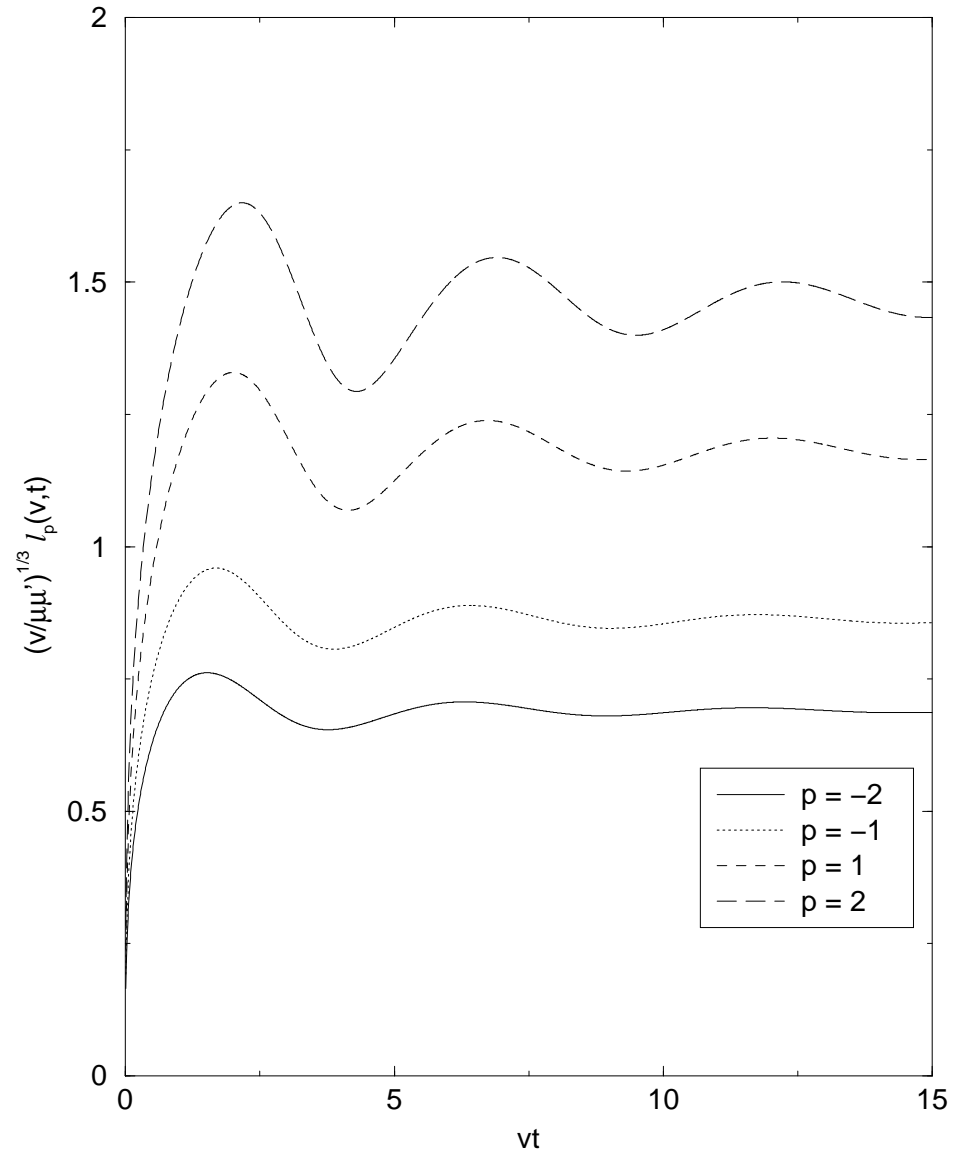
We study localization in this system because we need to have some idea of the relative importance of close pairs of atoms, as well as some idea of the effective range of the $1/r^3$ interaction. Naively, it seems that the close pairs are dominant and that the range of the $1/r^3$ potential is infinite because $1/r^3$ diverges at $r = 0$ and yet the integral $\int d^3r/r^3$ over all space diverges at both limits.

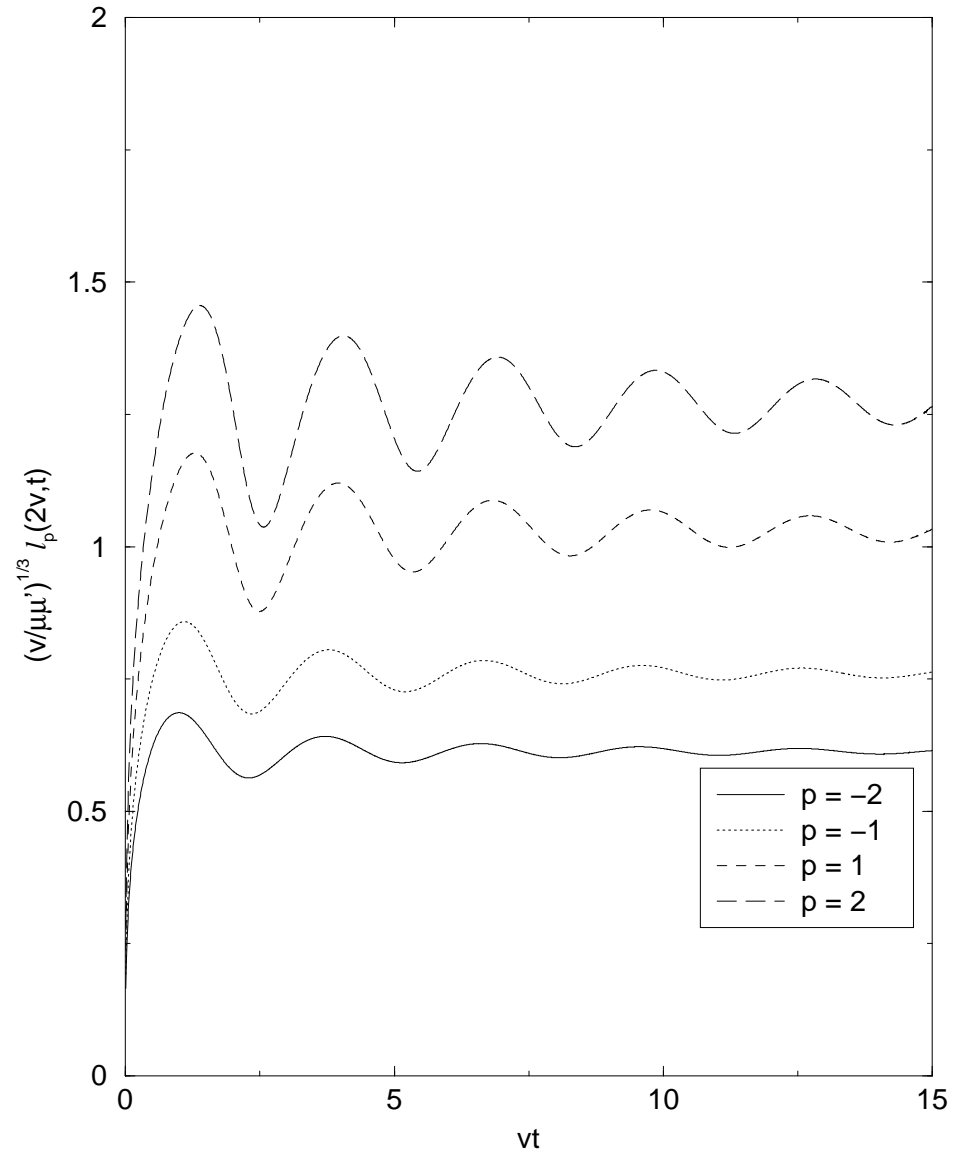
Figure 3.2: Plots of the moments $\mathcal{M}_p(0,t)$ for p equal to -2 , -1 , 1 , and 2 .

Figure 3.3: Plots of the moments $\mathcal{M}_p(v,t)$ for p equal to -2 , -1 , 1 , and 2 .

Figure 3.4: Plots of the moments $M_p(2v, t)$ for p equal to -2 , -1 , 1 , and 2 .

Figure 3.5: Plots of the localization lengths $l_p(0,t)$ for p equal to -2 , -1 , 1 , and 2 .

Figure 3.6: Plots of the localization lengths $l_p(v, t)$ for p equal to -2 , -1 , 1 , and 2 .

Figure 3.7: Plots of the localization lengths $l_p(2v, t)$ for p equal to -2 , -1 , 1 , and 2 .

Chapter 4

Sparse $ss' \rightarrow pp'$ Processes with U Interaction

4.1 Introduction

In this section we complicate the simple model of Chapter 2 by introducing the $sp \rightarrow ps$ process through the addition of an interaction potential U . The $sp \rightarrow ps$ process can be viewed as an exciton propagating through the medium [8, 15, 35], as was discussed in Ref. [17].

In Section 4.2 we discuss the Cayley tree approximation, starting with its justification in Section 4.2.1. In Sections 4.2.2 – 4.2.4 we solve for the Laplace transform of the probability amplitude in the case where Δ and V are both zero, the case where V is nonzero but Δ is still zero, and the case where both Δ and V are nonzero, respectively.

We consider a Hubbard band approximation in Section 4.3. In Section 4.3.1 we again solve for the Laplace transform of the probability amplitude in the case where Δ and V are both zero and in Section 4.3.2 we do the same for the case where V is nonzero but Δ is still zero. However, we note in this case that the latter solution is not consistent. In the case of the Hubbard approximation, we are also able to compute the square of the probability amplitude in the $V = \Delta = 0$ case, as is done in Section 4.3.3.

In Section 4.4 we consider a coherent potential approximation (CPA). In this approximation we are able to compute the probability amplitude in all cases. We will see in Section 4.6 that the CPA

results agree best with the results of the numerical simulations discussed in Chapter 7.

In Section 4.5 we compare the results of these three approximations. We see that they are in some ways rather similar, but that the differences are sufficiently large that it is easy to tell them apart, particularly when the $sp \rightarrow ps$ process is weak. This means that one approximation will fit the exact results better than the others, and in the case we are studying it is the CPA. Thus, in Section 4.6 we present plots of the CPA results in comparison with the results of the numerical simulations discussed in Chapter 7.

Finally, in Section 4.7 we summarize these results and conclude.

4.2 The Cayley tree approximation

4.2.1 Justification of the Cayley tree approximation

We start with the equations

$$i\dot{a}_0 = \Delta a_0 + \sum_{k=1}^N V_k c_k, \quad (4.1a)$$

$$i\dot{c}_k = V_k a_0 + \sum_{l \neq k} U_{kl} c_l. \quad (4.1b)$$

These are the same as Eqs. (2.1a) and (2.1b), except that we now allow for the $sp \rightarrow ps$ process by including the $\sum_l U_{kl} c_l$ term in the equation for c_k . For the purposes of compressing indices on sums and products, it is convenient to define U_{kl} to be zero when $k = l$. With this definition, the previous equation becomes

$$i\dot{a}_0 = \Delta a_0 + \sum_{k=1}^N V_k c_k, \quad (4.2a)$$

$$i\dot{c}_k = V_k a_0 + \sum_{l=1}^N U_{kl} c_l. \quad (4.2b)$$

Unfortunately the potential U makes the set of equations insoluble as they stand, so we cannot obtain an exact solution as we did in Chapter 2. However, the equations can be solved numerically, and one can also make quite a lot of progress by making approximations and proceeding analytically.

In developing approximations, it is useful to cast the problem in the standard Green's function language [16], as discussed in Section 3 of Ref. [11]. The Green's function of Eq. (4.2b) satisfies the

equation

$$\omega G_{ln} = \delta_{ln} + \sum_{m=1}^N U_{lm} G_{mn}, \quad (4.3)$$

and then

$$a_0(\Delta, \omega) = \frac{i}{\omega - \Delta - \sum_{lm} V_l G_{lm} V_m}. \quad (4.4)$$

Actually, $-ia_0$ is the 00 element of the Green's function for the entire set of $N + 1$ equations.

We can derive a convenient form for the on-site Green's function G_{nn} . From Eq. (4.3) we have, for $l = n$,

$$\omega G_{nn} = 1 + \sum_m U_{nm} G_{mn}, \quad (4.5)$$

and if we write separately the term containing G_{nn} , we obtain

$$\omega G_{ln} = U_{ln} G_{nn} + \sum_{m \neq n} U_{lm} G_{mn}, \quad (4.6)$$

for $l \neq n$. We note here that Eqs. (4.5) and (4.6) are the analogs of Eqs. (4.2a) and (4.2b), respectively.

Now we imagine removing the n th atom. The new Green's function for the remaining $N - 1$ atoms, which we will call $G_{lp,[n]}$, obeys the equation

$$\omega G_{lp,[n]} = \delta_{lp} + \sum_{m \neq n} U_{lm} G_{mp,[n]}, \quad (4.7)$$

where l and p are never equal to n . If we multiply both sides of this equation by $U_{pn} G_{nn}$ and sum over p , we obtain

$$\omega \sum_p G_{lp,[n]} U_{pn} G_{nn} = U_{ln} G_{nn} + \sum_{m \neq n} U_{lm} \sum_p G_{mp,[n]} U_{pn} G_{nn}. \quad (4.8)$$

Comparing this equation with Eq. (4.6), we see that for $m \neq n$

$$G_{mn} = \sum_p G_{mp,[n]} U_{pn} G_{nn}. \quad (4.9)$$

If we insert this result into Eq. (4.5), then we have finally that

$$\omega G_{nn} = 1 + \sum_m U_{nm} \sum_p G_{mp,[n]} U_{pn} G_{nn}, \quad (4.10)$$

and hence

$$G_{nn} = \frac{1}{\omega - \sum_{mp} U_{nm} G_{mp,[n]} U_{pn}}. \quad (4.11)$$

It is important to keep in mind that these Green's function equations are exact.

The Cayley approximation [1, 37, 38, 39] keeps only the diagonal ($l = m$) terms in the sum over l and m in Eqs. (4.4) and (4.11). It further assumes that each $G_{ll,[n]}$ is independently distributed, and that there are sufficiently many sites that $G_{ll,[n]}$ and G_{ll} have the same distribution.

We choose to set $\omega = i\alpha$ and work in Laplace space instead of Fourier space because this makes many of the integrals that follow more obviously convergent. Up to a point, the same analysis can be carried out with the Fourier analogs, but Laplace transforms are needed to solve the Cayley equations exactly in Section 4.2.2. We also work with the inverses of these Green's functions, setting $a_0(i\alpha) = 1/f_0(\alpha)$ and $G_{kk}(i\alpha) = i/f_k(\alpha)$, so in the Cayley approximation we have from Eqs. (4.7) and (4.8), respectively

$$f_0 = \alpha + i\Delta + \sum_{k=1}^N \frac{V_{0k}^2}{f_k}, \quad (4.12a)$$

$$f_k = \alpha + \sum_{l=1}^N \frac{U_{kl}^2}{f_l}. \quad (4.12b)$$

4.2.2 Cayley tree approximation with the U process only

First we consider just the U process and solve Eq. (4.12b), which is to say we look at the $sp \rightarrow ps$ process by itself. Note that f_k is always real and positive. The distribution of f_k is given by

$$P(f_k) = \int \left\langle \delta \left(f_k - \alpha - \sum_{l=1}^N \frac{U_{kl}^2}{f_l} \right) \right\rangle \prod_{m \neq k, m=1}^N P(f_m) df_m, \quad (4.13)$$

where for a uniform gas of volume Ω ,

$$\langle X \rangle = \frac{1}{\Omega^N} \int \prod_{j=1}^N d^3 r_j X. \quad (4.14)$$

Writing the delta function as a Fourier transform, we see that

$$\begin{aligned} P(f_k) &= \int_{-\infty}^{\infty} \frac{dq}{2\pi} \int \prod_{m \neq k, m=1}^N P(f_m) df_m e^{iq(f_k - \alpha)} \left\langle \exp \left(-iq \sum_{l=1}^N \frac{U_{kl}^2}{f_l} \right) \right\rangle \\ &= \int_{-\infty}^{\infty} \frac{dq}{2\pi} e^{iq(f_k - \alpha)} \int \prod_{m \neq k, m=1}^N P(f_m) df_m \times \\ &\quad \frac{1}{\Omega^{N-1}} \int \prod_{l \neq k, l=1}^N d^3 r_l \exp \left(-iq \frac{U_{kl}^2}{f_l} \right). \end{aligned} \quad (4.15)$$

Using the fact that $(\prod_m P_m)(\prod_l E_l) = \prod_m P_m E_m$, we can write

$$\begin{aligned} P(f_k) &= \int_{-\infty}^{\infty} \frac{dq}{2\pi} e^{iq(f_k - \alpha)} \prod_{m \neq k, m=1}^N \int P(f_m) df_m \frac{1}{\Omega} \int d^3 r_m \exp \left(-iq \frac{U_{km}^2}{f_m} \right) \\ &= \int_{-\infty}^{\infty} \frac{dq}{2\pi} e^{iq(f_k - \alpha)} \left[\int_0^{\infty} df_1 P(f_1) \frac{1}{\Omega} \int d^3 r_1 \exp \left(-iq \frac{U_{k1}^2}{f_1} \right) \right]^{N-1} \\ &= \int_{-\infty}^{\infty} \frac{dq}{2\pi} e^{iq(f_k - \alpha)} \times \\ &\quad \left(1 - \int_0^{\infty} df P(f) \frac{1}{\Omega} \int d^3 r \left\{ 1 - \exp \left[-iq \frac{U^2(r)}{f} \right] \right\} \right)^{N-1}, \end{aligned} \quad (4.16)$$

where in the last step we have simply changed variables from \mathbf{r}_1 to $\mathbf{r} = \mathbf{r}_1 - \mathbf{r}_k$. Using the averaging method detailed in Section 2.3, we see that¹

$$P(f) = \int_{-\infty}^{\infty} \frac{dq}{2\pi} e^{iq(f - \alpha)} \exp \left[-u \sqrt{iq} Q(\alpha) \right], \quad (4.17)$$

where

$$Q(\alpha) = \int_0^{\infty} \frac{df}{\sqrt{f}} P(f), \quad (4.18)$$

and

$$u = \frac{4\pi^{3/2}}{3} \mu^2 \frac{N}{\Omega}, \quad (4.19)$$

¹Of course, we must use the more elaborate averaging method of Section 2.5 if the potential U is more complicated.

if U is of the simple μ^2/r^3 form with no angular dependence, and is the equivalent of v in Eq. (2.73) otherwise. For A and B real, we have that

$$\int_{-\infty}^{\infty} \frac{dq}{2\pi} e^{iqA - \sqrt{iq}B} = \frac{1}{2\sqrt{\pi}} \frac{B}{A^{3/2}} \exp\left(-\frac{B^2}{4A}\right) \theta(A), \quad (4.20)$$

where this integral is evaluated by the same procedure used to evaluate the integral of Eq. (2.15).²

With this result, we have

$$P(f) = \frac{1}{2\sqrt{\pi}} \frac{uQ(\alpha)}{(f-\alpha)^{3/2}} \exp\left[-\frac{u^2Q^2(\alpha)}{4(f-\alpha)}\right] \theta(f-\alpha). \quad (4.21)$$

and so

$$\begin{aligned} Q(\alpha) &= \int_{\alpha}^{\infty} \frac{df}{\sqrt{f}} \frac{1}{2\sqrt{\pi}} \frac{uQ(\alpha)}{(f-\alpha)^{3/2}} \exp\left[-\frac{u^2Q^2(\alpha)}{4(f-\alpha)}\right] \\ &= \frac{1}{\sqrt{\alpha}} \exp\left[\frac{u^2Q^2(\alpha)}{4\alpha}\right] \operatorname{erfc}\left[\frac{uQ(\alpha)}{2\sqrt{\alpha}}\right]. \end{aligned} \quad (4.22)$$

We also have

$$\begin{aligned} \left\langle \frac{1}{f} \right\rangle &= \int_0^{\infty} \frac{df}{f} P(f) \\ &= \frac{1}{\alpha} - \frac{\sqrt{\pi}}{2} \frac{uQ(\alpha)}{\alpha^{3/2}} \exp\left[\frac{u^2Q^2(\alpha)}{4\alpha}\right] \operatorname{erfc}\left[\frac{uQ(\alpha)}{2\sqrt{\alpha}}\right], \end{aligned} \quad (4.23)$$

or

$$\left\langle \frac{1}{f} \right\rangle = \frac{1}{\alpha} \left[1 - \frac{\sqrt{\pi}}{2} uQ^2(\alpha) \right]. \quad (4.24)$$

Thus we can solve numerically the transcendental relation for $Q(\alpha)$ given in Eq. (4.22) and plug it into Eq. (4.24) to find $\langle 1/f \rangle$. It is important to note that Eq. (4.22) defines Q as an analytic function of α in the half-plane where $\operatorname{Re} \alpha > 0$. Thus $\langle 1/f \rangle$ can be analytically continued, in the variable $\omega = i\alpha$, from the positive imaginary axis to the entire upper half-plane.

²In case the reader is curious, the theta function appears here but is omitted in Eq. (2.23) because \mathcal{V}^2 is an intrinsically positive quantity.

4.2.3 Cayley tree approximation with U and V processes in the absence of Δ

Now we allow the V process to be present, but we still ignore the detuning, Δ . We start with the equations

$$f_0 = \alpha + \sum_{k=1}^N \frac{V_{0k}^2}{f_k}, \quad (4.25a)$$

$$f_k = \alpha + \sum_{l=1, l \neq k}^N \frac{U_{kl}^2}{f_l}. \quad (4.25b)$$

Repeating the analysis we did before, we have

$$P_0(f_0) = \int \left\langle \delta \left(f_0 - \alpha - \sum_{k=1}^N \frac{V_{0k}^2}{f_k} \right) \right\rangle \prod_{l=1}^N P(f_l) df_l, \quad (4.26)$$

which leads to the form

$$P_0(f_0) = \int_{-\infty}^{\infty} \frac{dq}{2\pi} e^{iq(f_0 - \alpha)} \left\{ \int_0^{\infty} df P(f) \frac{1}{\Omega} \int d^3r \exp \left[-iq \frac{V^2(r)}{f} \right] \right\}^N. \quad (4.27)$$

At this point it is clear from the work we did to obtain Eq. (4.21) from (4.16) that this equation leads to

$$P_0(f_0) = \frac{1}{2\sqrt{\pi}} \frac{vQ(\alpha)}{(f_0 - \alpha)^{3/2}} \exp \left[-\frac{v^2 Q^2(\alpha)}{4(f_0 - \alpha)} \right] \theta(f_0 - \alpha), \quad (4.28)$$

where $Q(\alpha)$ is still given by Eq. (4.22), and depends on u . Therefore we obtain the result

$$\begin{aligned} \left\langle \frac{1}{f_0} \right\rangle &= \int_0^{\infty} \frac{df_0}{f_0} P_0(f_0) \\ &= \frac{1}{\alpha} - \frac{\sqrt{\pi}}{2} \frac{vQ(\alpha)}{\alpha^{3/2}} \exp \left[\frac{v^2 Q^2(\alpha)}{4\alpha} \right] \operatorname{erfc} \left[\frac{vQ(\alpha)}{2\sqrt{\alpha}} \right], \end{aligned} \quad (4.29)$$

which again can be analytically continued.

4.2.4 Cayley tree approximation with U and V processes in the presence of Δ

If we further consider the effect of a detuning, Δ , then we have the full set of Eqs. (4.12a) and (4.12b). The equation for f_k is unchanged from the previous case, but because the equation for f_0 is now complex we have to consider a distribution in the two variables $f_0^R = \text{Re } f_0$ and $f_0^I = \text{Im } f_0$. We have

$$P_0(f_0^R, f_0^I) = \int \left\langle \delta \left(f_0^R - \alpha - \sum_{k=1}^N \frac{V_{0k}^2}{f_k} \right) \delta(f_0^I - \Delta) \right\rangle \prod_{l=1}^N P(f_l) df_l. \quad (4.30)$$

Clearly the delta function involving f_0^I does not participate in the averaging or in the integrations over f_l . Therefore we can treat the part involving f_0^R just as we did before, and the f_0^I part will just be carried along. Hence we find

$$P_0(f_0^R, f_0^I) = \frac{1}{2\sqrt{\pi}} \frac{vQ(\alpha)}{(f_0^R - \alpha)^{3/2}} \exp \left[-\frac{v^2 Q^2(\alpha)}{4(f_0^R - \alpha)} \right] \theta(f_0^R - \alpha) \delta(f_0^I - \Delta). \quad (4.31)$$

It follows, then, that

$$\begin{aligned} \left\langle \frac{1}{f_0} \right\rangle &= \int_0^\infty df_0^R \int_{-\infty}^\infty df_0^I \frac{1}{f_0^R + if_0^I} P_0(f_0^R, f_0^I) \\ &= \frac{1}{\alpha + i\Delta} - \frac{\sqrt{\pi}}{2} \frac{vQ(\alpha)}{(\alpha + i\Delta)^{3/2}} \exp \left[\frac{v^2 Q^2(\alpha)}{4(\alpha + i\Delta)} \right] \text{erfc} \left[\frac{vQ(\alpha)}{2\sqrt{\alpha + i\Delta}} \right]. \end{aligned} \quad (4.32)$$

4.3 The Hubbard approximation

It is also possible to make approximations other than the one we have chosen. For example, instead of working with Eq. (4.12b), one can instead choose to work with

$$f_k = \alpha + \sum_{l=1}^N \frac{U_{kl}^2}{f_k}, \quad (4.33)$$

which gives explicitly

$$f_k = \frac{1}{2} \left(\alpha + \sqrt{\alpha^2 + 4 \sum_l U_{kl}^2} \right). \quad (4.34)$$

This approximation corresponds to a Hubbard band.

4.3.1 Computation of $\langle 1/f \rangle$

It is possible to average Eq. (4.34), although it requires a little more manipulation than the averaging methods we have applied previously because of the presence of the square root. We first note that

$$\begin{aligned} \frac{1}{f_k} &= \frac{2}{\alpha + \sqrt{\alpha^2 + 4\mathcal{U}^2}} \\ &= \frac{1}{2\mathcal{U}^2} \left(\sqrt{\alpha^2 + 4\mathcal{U}^2} - \alpha \right), \end{aligned} \quad (4.35)$$

where

$$\mathcal{U}^2 = \sum_l U_{kl}^2. \quad (4.36)$$

Interestingly enough, the Laplace transform in Eq. (4.35) has a known inverse. We see from Eq. (2.1.35) of Ref. [51] that the inverse Laplace transform of Eq. (4.35) is

$$\frac{1}{\mathcal{U}t} J_1(2\mathcal{U}t). \quad (4.37)$$

We will use Eq. (4.37) in Section 4.3.3 to compute $\langle |a_0(\Delta = 0, t)|^2 \rangle$ in the case where only the U process is present.

We now note that

$$\sqrt{x^2 + y} - x = \frac{y}{2} \int_0^1 \frac{d\lambda}{\sqrt{\alpha^2 + \lambda y}}, \quad (4.38)$$

so we can rewrite Eq. (4.35) as

$$\frac{1}{f_k} = \int_0^1 \frac{d\lambda}{\sqrt{\alpha^2 + 4\lambda\mathcal{U}^2}}. \quad (4.39)$$

We introduce yet another integral by observing that

$$\frac{1}{\sqrt{\alpha^2 + C\lambda\mathcal{U}^2}} = \frac{2}{\sqrt{\pi}} \int_0^\infty d\beta \exp[-\beta^2(\alpha^2 + C\lambda\mathcal{U}^2)], \quad (4.40)$$

if $\text{Re}(C\lambda) > 0$, so

$$\frac{1}{f_k} = \frac{2}{\sqrt{\pi}} \int_0^\infty d\beta \int_0^1 d\lambda \exp[-\beta^2(\alpha^2 + 4\lambda\mathcal{U}^2)]. \quad (4.41)$$

From our previous experience with averaging over \mathcal{U} , we know that

$$\left\langle \frac{1}{f} \right\rangle = \frac{2}{\sqrt{\pi}} \int_0^\infty d\beta \int_0^1 d\lambda \exp\left(-\beta^2\alpha^2 + 2u\beta\sqrt{\lambda}\right). \quad (4.42)$$

Here we write $\langle 1/f \rangle$ in place of $\langle 1/f_k \rangle$ because the averages of all the f_k are equal. The integral over β is familiar to us, since it is the type of integral that shows up repeatedly in this averaging method. We have

$$\begin{aligned} \left\langle \frac{1}{f} \right\rangle &= \frac{2}{\sqrt{\pi}} \int_0^1 d\lambda \frac{\sqrt{\pi}}{2\alpha} \exp\left(\frac{u^2\lambda}{\alpha^2}\right) \operatorname{erfc}\left(\frac{u\sqrt{\lambda}}{\alpha}\right) \\ &= \frac{1}{\alpha} \int_0^1 d\lambda \exp\left(\frac{u^2\lambda}{\alpha^2}\right) \operatorname{erfc}\left(\frac{u\sqrt{\lambda}}{\alpha}\right). \end{aligned} \quad (4.43)$$

The remaining integral over λ can be done by parts, with the result that

$$\left\langle \frac{1}{f} \right\rangle = \frac{2}{u\sqrt{\pi}} + \frac{\alpha}{u^2} \left[\exp\left(\frac{u^2}{\alpha^2}\right) \operatorname{erfc}\left(\frac{u}{\alpha}\right) - 1 \right]. \quad (4.44)$$

We can also compute $\langle 1/f \rangle$ by first computing the distribution $P_H(f_k)$. It will turn out that knowing $P_H(f_k)$ will aid greatly in the computation of $1/f_0$ for this approximation, as we will see in Section 4.3.2. Because in this case f_k is explicitly given in terms of \mathcal{U}^2 through Eq. (4.34), we have

$$P_H(f_k) = \left\langle \delta\left(f_k - \frac{\alpha}{2} - \frac{1}{2}\sqrt{\alpha^2 + 4\mathcal{U}^2}\right) \right\rangle. \quad (4.45)$$

This average is easy to compute using the analog of Eq. (2.23) for the potential U . We have

$$\begin{aligned} P_H(f_k) &= \int_0^\infty d(\mathcal{U}^2) \delta\left(f_k - \frac{\alpha}{2} - \frac{1}{2}\sqrt{\alpha^2 + 4\mathcal{U}^2}\right) \frac{1}{2\sqrt{\pi}} \frac{u}{\mathcal{U}^3} \exp\left(-\frac{u^2}{4\mathcal{U}^2}\right) \\ &= \frac{1}{2\sqrt{\pi}} \frac{2f - \alpha}{[f(f - \alpha)]^{3/2}} \exp\left[-\frac{u^2}{4f(f - \alpha)}\right] \theta(f - \alpha), \end{aligned} \quad (4.46)$$

where we have used the fact that

$$\delta\left(f_k - \frac{\alpha}{2} - \frac{1}{2}\sqrt{\alpha^2 + 4\mathcal{U}^2}\right) = (2f - \alpha) \delta[\mathcal{U}^2 - f(f - \alpha)]. \quad (4.47)$$

The theta function is present in Eq. (4.46) because \mathcal{U}^2 and f are positive definite quantities, and hence $\delta[\mathcal{U}^2 - f(f - \alpha)]$ cannot be nonzero unless $f - \alpha > 0$.

Using the distribution of Eq. (4.46) we can compute

$$\left\langle \frac{1}{f} \right\rangle = \int_0^\infty \frac{df}{f} P_H(f)$$

$$\begin{aligned}
&= \int_0^\infty \frac{df}{f} \frac{1}{2\sqrt{\pi}} \frac{2f - \alpha}{[f(f - \alpha)]^{3/2}} \exp\left[-\frac{u^2}{4f(f - \alpha)}\right] \theta(f - \alpha) \\
&= \frac{1}{2\sqrt{\pi}} \int_\alpha^\infty \frac{df}{f} \frac{2f - \alpha}{[f(f - \alpha)]^{3/2}} \exp\left[-\frac{u^2}{4f(f - \alpha)}\right]. \tag{4.48}
\end{aligned}$$

This integral is very difficult to compute analytically in its present form, even by a computer package such as *Mathematica*. Therefore we change variables to $\chi = f(f - \alpha)$. Then $d\chi = (2f - \alpha)df$, and because f must be positive we have $f = \alpha + \sqrt{\alpha^2 + 4\chi}$. It follows that

$$\left\langle \frac{1}{f} \right\rangle = \frac{1}{2\sqrt{\pi}} \int_0^\infty \frac{d\chi}{\chi^{3/2}} \frac{1}{\alpha + \sqrt{\alpha^2 + 4\chi}} \exp\left(-\frac{u^2}{4\chi}\right). \tag{4.49}$$

This integral can now be done by *Mathematica*, and it gives exactly the result of Eq. (4.44).

4.3.2 Computation of $\langle 1/f_0 \rangle$

Going back to Eq. (4.12a), we see that

$$\frac{1}{f_0} = \left(\alpha + i\Delta + \sum_k \frac{V_k^2}{f_k} \right)^{-1}. \tag{4.50}$$

Since this is the same equation we considered for the Cayley approximation in Section 4.2.4 we see that the result for $P_{0,H}(f_0^R, f_0^I)$ is very similar to Eq. (4.31). Specifically, we have

$$P_{0,H}(f_0^R, f_0^I) = \frac{1}{2\sqrt{\pi}} \frac{vQ_H(\alpha)}{(f_0^R - \alpha)^{3/2}} \exp\left[-\frac{v^2Q_H^2(\alpha)}{4(f_0^R - \alpha)}\right] \theta(f_0^R - \alpha) \delta(f_0^I - \Delta), \tag{4.51}$$

where

$$Q_H(\alpha) = \int_0^\infty \frac{df}{\sqrt{f}} P_H(f). \tag{4.52}$$

It then follows from Eq. (4.32) that

$$\left\langle \frac{1}{f_0} \right\rangle = \frac{1}{\alpha + i\Delta} - \frac{\sqrt{\pi}}{2} \frac{vQ_H(\alpha)}{(\alpha + i\Delta)^{3/2}} \exp\left[\frac{v^2Q_H^2(\alpha)}{4(\alpha + i\Delta)}\right] \operatorname{erfc}\left[\frac{vQ_H(\alpha)}{2\sqrt{\alpha + i\Delta}}\right]. \tag{4.53}$$

One might think that because $P_H(f)$ is known explicitly in this case, instead of involving transcendental quantities as Eq. (4.21) does, it should be possible to compute the function $Q_H(\alpha)$ explicitly as well. Unfortunately the integral of Eq. (4.52) cannot be done analytically. If we make

the same change of variable that we did to obtain Eq. (4.49), however, then Eq. (4.52) becomes

$$Q_H(\alpha) = \frac{1}{2\sqrt{\pi}} \int_0^\infty \frac{d\chi}{\chi^{3/2}} \frac{1}{\sqrt{\alpha + \sqrt{\alpha^2 + 4\chi}}} \exp\left(-\frac{u^2}{4\chi}\right), \quad (4.54)$$

and this integral can be done numerically for a given value of α .

Thus $Q_H(\alpha)$ can be computed numerically, and the result substituted into Eq. (4.53) to obtain $\langle 1/f_0 \rangle$.

Although we have shown how to compute $\langle 1/f_0 \rangle$ for the Hubbard model using Eqs. (4.12a) and (4.34), we note that these equations are not consistent. Consistency demands that $\langle 1/f_0 \rangle$ reduces to $\langle 1/f \rangle$ when $u = v$ and $\Delta = 0$, and this is clearly not the case with Eqs. (4.53) and (4.33). In fact, one can see this inconsistency immediately from Eqs. (4.12a) and (4.34). If we set $\mathcal{U}^2 = \mathcal{V}^2$ and $\Delta = 0$ in these equations, then we have

$$f_0 = \alpha + \sum_{k=1}^N \frac{V_{0k}^2}{f_k}, \quad (4.55a)$$

$$f_k = \alpha + \frac{\mathcal{V}^2}{f_k}. \quad (4.55b)$$

We see that even in this limit, f_0 and f_k are still treated differently in this approximation. Therefore the Hubbard approximation is inconsistent, and to be safe one should disregard the result for $\langle 1/f_0 \rangle$ and only consider the result for $\langle 1/f \rangle$ of Section 4.3.1 as valid.

4.3.3 Computation of $\langle |a_0(\Delta, t)|^2 \rangle$ with the U process only at resonance

We saw in Eq. (4.37) that at resonance

$$a_0(0, t) = \frac{1}{\mathcal{U}t} J_1(2\mathcal{U}t), \quad (4.56)$$

and so

$$|a_0(0, t)|^2 = \frac{1}{\mathcal{U}^2 t^2} J_1^2(2\mathcal{U}t). \quad (4.57)$$

According to Eq. (10.1.1) of Ref [51], this function has the inverse Laplace transform

$$\frac{1}{\alpha} - \tilde{S}(0, \alpha) = \frac{1}{\pi\mathcal{U}} \int_0^\pi d\theta (1 + \cos\theta) \left[\sqrt{\frac{\alpha^2}{4\mathcal{U}^2} + 2 - 2\cos\theta} - \frac{\alpha}{2\mathcal{U}} \right]$$

$$= \frac{1}{2\pi\mathcal{U}^2} \int_0^\pi d\theta (1 + \cos\theta) \left[\sqrt{\alpha^2 + 8\mathcal{U}^2(1 - \cos\theta)} - \alpha \right]. \quad (4.58)$$

Now we again apply Eq. (4.38), with the result that

$$\begin{aligned} \tilde{S}(0, \alpha) &= \frac{1}{\alpha} - \frac{1}{2\pi\mathcal{U}^2} \int_0^\pi d\theta (1 + \cos\theta) 4(1 - \cos\theta) \mathcal{U}^2 \int_0^1 \frac{d\lambda}{\sqrt{\alpha^2 + 8\lambda\mathcal{U}^2(1 - \cos\theta)}} \\ &= \frac{1}{\alpha} - \frac{2}{\pi} \int_0^\pi d\theta \sin^2\theta \int_0^1 \frac{d\lambda}{\sqrt{\alpha^2 + 8\lambda\mathcal{U}^2(1 - \cos\theta)}}. \end{aligned} \quad (4.59)$$

At this point, we apply Eq. (4.40) to find that

$$\tilde{S}(0, \alpha) = \frac{1}{\alpha} - \frac{4}{\pi^{3/2}} \int_0^\pi d\theta \sin^2\theta \int_0^1 d\lambda \int_0^\infty d\beta e^{-\beta[\alpha^2 + 8\lambda\mathcal{U}^2(1 - \cos\theta)]}. \quad (4.60)$$

This expression can now be averaged. We find that

$$\langle \tilde{S}(0, \alpha) \rangle = \frac{1}{\alpha} - \frac{4}{\pi^{3/2}} \int_0^\pi d\theta \sin^2\theta \int_0^1 d\lambda \int_0^\infty d\beta e^{-\beta\alpha^2 - 2\sqrt{2}u\sqrt{\beta\lambda(1 - \cos\theta)}}. \quad (4.61)$$

The integration over β can be performed at this point, with the result that

$$\begin{aligned} \langle \tilde{S}(0, \alpha) \rangle &= \frac{1}{\alpha} - \frac{4}{\pi^{3/2}} \int_0^\pi d\theta \sin^2\theta \int_0^1 d\lambda \frac{\sqrt{\pi}}{2} \frac{1}{\alpha} \times \\ &\quad \exp\left[\frac{2\lambda u^2}{\alpha^2}(1 - \cos\theta)\right] \operatorname{erfc}\left[\frac{u}{\alpha}\sqrt{2\lambda(1 - \cos\theta)}\right] \\ &= \frac{1}{\alpha} - \frac{2}{\pi} \frac{1}{\alpha} \int_0^\pi d\theta \sin^2\theta \int_0^1 d\lambda \exp\left[\frac{2\lambda u^2}{\alpha^2}(1 - \cos\theta)\right] \times \\ &\quad \operatorname{erfc}\left[\frac{u}{\alpha}\sqrt{2\lambda(1 - \cos\theta)}\right]. \end{aligned} \quad (4.62)$$

The λ integral can be done by parts. The result is

$$\begin{aligned} \langle \tilde{S}(0, \alpha) \rangle &= \frac{1}{\alpha} - \frac{2}{\pi} \frac{1}{\alpha} \int_0^\pi d\theta \sin^2\theta \left\{ \frac{\alpha^2}{2u^2(1 - \cos\theta)} \exp\left[\frac{2u^2}{\alpha^2}(1 - \cos\theta)\right] \times \right. \\ &\quad \left. \operatorname{erfc}\left[\frac{u}{\alpha}\sqrt{2(1 - \cos\theta)}\right] - \frac{\alpha^2}{2u^2(1 - \cos\theta)} + \sqrt{\frac{2}{\pi}} \frac{\alpha}{u\sqrt{1 - \cos\theta}} \right\} \\ &= \frac{1}{\alpha} - \frac{1}{\pi} \frac{\alpha}{u^2} \int_0^\pi d\theta \frac{\sin^2\theta}{1 - \cos\theta} \exp\left[\frac{2u^2}{\alpha^2}(1 - \cos\theta)\right] \operatorname{erfc}\left[\frac{u}{\alpha}\sqrt{2(1 - \cos\theta)}\right] + \\ &\quad \frac{1}{\pi} \frac{\alpha}{u^2} \int_0^\pi d\theta (1 + \cos\theta) - \left(\frac{2}{\pi}\right)^{3/2} \frac{1}{u} \int_0^\pi d\theta \frac{\sin^2\theta}{\sqrt{1 - \cos\theta}}. \end{aligned} \quad (4.63)$$

The last two terms are standard integrals, and we have that

$$\begin{aligned} \langle \tilde{S}(0, \alpha) \rangle &= \frac{1}{\alpha} - \frac{1}{\pi} \frac{\alpha}{u^2} \int_0^\pi d\theta (1 + \cos \theta) \exp \left[\frac{2u^2}{\alpha^2} (1 - \cos \theta) \right] \operatorname{erfc} \left[\frac{u}{\alpha} \sqrt{2(1 - \cos \theta)} \right] + \\ &\quad \frac{\alpha}{u^2} - \frac{16}{3\pi^{3/2}} \frac{1}{u}. \end{aligned} \quad (4.64)$$

Now we consider the remaining integral

$$\Lambda = \frac{1}{\pi} \frac{\alpha}{u^2} \int_0^\pi d\theta (1 + \cos \theta) \exp \left[\frac{2u^2}{\alpha^2} (1 - \cos \theta) \right] \operatorname{erfc} \left[\frac{u}{\alpha} \sqrt{2(1 - \cos \theta)} \right]. \quad (4.65)$$

First we define $\phi = \theta/2$, so that $d\theta = 2 d\phi$. Thus $1 + \cos \theta = 2 \cos^2 \phi$ and similarly $1 - \cos \theta = 2 \sin^2 \phi$. In addition, since $0 \leq \theta \leq \pi$, it follows that $0 \leq \phi \leq \pi/2$, and hence both $\cos \phi$ and $\sin \phi$ are positive quantities. With this substitution we have

$$\Lambda = \frac{4}{\pi} \frac{\alpha}{u^2} \int_0^{\pi/2} d\phi \cos^2 \phi \exp \left(\frac{4u^2}{\alpha^2} \sin^2 \phi \right) \operatorname{erfc} \left(\frac{2u}{\alpha} \sin \phi \right). \quad (4.66)$$

Using Eq. (2.31), we see that

$$\begin{aligned} \Lambda &= \frac{4}{\pi} \frac{\alpha}{u^2} \int_0^{\pi/2} d\phi \cos^2 \phi \sum_{n=0}^{\infty} \frac{1}{\Gamma(\frac{n+2}{2})} \left(-\frac{2u}{\alpha} \sin \phi \right)^n \\ &= \frac{4}{\pi} \frac{\alpha}{u^2} \sum_{n=0}^{\infty} \frac{1}{\Gamma(\frac{n+2}{2})} \left(-\frac{2u}{\alpha} \right)^n \int_0^{\pi/2} d\phi \cos^2 \phi \sin^n \phi. \end{aligned} \quad (4.67)$$

The integral over ϕ is a standard one, and we find that

$$\begin{aligned} \Lambda &= \frac{1}{\sqrt{\pi}} \frac{\alpha}{u^2} \sum_{n=0}^{\infty} \frac{\Gamma(\frac{n+1}{2})}{\Gamma(\frac{n+2}{2}) \Gamma(\frac{n+4}{2})} \left(-\frac{2u}{\alpha} \right)^n \\ &= \frac{\alpha}{u^2} - \frac{16}{3\pi^{3/2}} \frac{1}{u} + \frac{1}{\alpha} + \frac{1}{\sqrt{\pi}} \frac{\alpha}{u^2} \sum_{n=3}^{\infty} \frac{\Gamma(\frac{n+1}{2})}{\Gamma(\frac{n+2}{2}) \Gamma(\frac{n+4}{2})} \left(-\frac{2u}{\alpha} \right)^n \\ &= \frac{\alpha}{u^2} - \frac{16}{3\pi^{3/2}} \frac{1}{u} + \frac{1}{\alpha} - \frac{8}{\sqrt{\pi}} \frac{u}{\alpha^2} \sum_{n=0}^{\infty} \frac{\Gamma(\frac{n+4}{2})}{\Gamma(\frac{n+5}{2}) \Gamma(\frac{n+7}{2})} \left(-\frac{2u}{\alpha} \right)^n. \end{aligned} \quad (4.68)$$

Substituting this back into Eq. (4.64), we see that

$$\langle \tilde{S}(0, \alpha) \rangle = \frac{8}{\sqrt{\pi}} \frac{u}{\alpha^2} \sum_{n=0}^{\infty} \frac{\Gamma(\frac{n+4}{2})}{\Gamma(\frac{n+5}{2}) \Gamma(\frac{n+7}{2})} \left(-\frac{2u}{\alpha} \right)^n. \quad (4.69)$$

At this point we can invert this Laplace transform term by term, using the fact that the inverse Laplace transform of $\alpha^{-\nu}$ is $t^{\nu-1}/\Gamma(\nu)$. We finally arrive at

$$\langle S(0, t) \rangle = \frac{8}{\sqrt{\pi}} ut \sum_{n=0}^{\infty} \frac{\Gamma\left(\frac{n+4}{2}\right)}{\Gamma\left(\frac{n+5}{2}\right) \Gamma\left(\frac{n+7}{2}\right) \Gamma(n+2)} (-2ut)^n. \quad (4.70)$$

The even terms in this sum reduce to

$$\begin{aligned} S_{\text{H, even}} &= \frac{8}{\sqrt{\pi}} ut \sum_{n=0}^{\infty} \frac{\Gamma\left(\frac{2n+4}{2}\right)}{\Gamma\left(\frac{2n+5}{2}\right) \Gamma\left(\frac{2n+7}{2}\right) \Gamma(2n+2)} (-2ut)^{2n} \\ &= 4ut \sum_{n=0}^{\infty} \frac{\Gamma(n+2)}{\Gamma\left(n+\frac{5}{2}\right) \Gamma\left(n+\frac{7}{2}\right) \Gamma(n+1) \Gamma\left(n+\frac{3}{2}\right)} (4u^2t^2)^n \\ &= \frac{256}{45\pi^{3/2}} ut {}_1F_3\left(2; \frac{3}{2}, \frac{5}{2}, \frac{7}{2}; u^2t^2\right), \end{aligned} \quad (4.71)$$

where in the third step we have used Eq. (2.30) and in the final step we have used Eq. (2.35).

Similarly, the odd terms in this sum reduce to

$$\begin{aligned} S_{\text{H, odd}} &= \frac{8}{\sqrt{\pi}} ut \sum_{n=0}^{\infty} \frac{\Gamma\left(\frac{2n+5}{2}\right)}{\Gamma\left(\frac{2n+6}{2}\right) \Gamma\left(\frac{2n+8}{2}\right) \Gamma(2n+3)} (-2ut)^{2n+1} \\ &= -4u^2t^2 \sum_{n=0}^{\infty} \frac{\Gamma\left(n+\frac{5}{2}\right)}{\Gamma(n+3) \Gamma(n+4) \Gamma\left(n+\frac{3}{2}\right) \Gamma(n+2)} (u^2t^2)^n \\ &= -4 \sum_{n=1}^{\infty} \frac{\Gamma\left(n+\frac{3}{2}\right)}{\Gamma(n+2) \Gamma(n+3) \Gamma\left(n+\frac{1}{2}\right) \Gamma(n+1)} (u^2t^2)^n \\ &= 1 - {}_1F_3\left(\frac{3}{2}; \frac{1}{2}, 2, 3; u^2t^2\right), \end{aligned} \quad (4.72)$$

and so we have finally that

$$\langle S(0, t) \rangle = 1 + \frac{256}{45\pi^{3/2}} ut {}_1F_3\left(2; \frac{3}{2}, \frac{5}{2}, \frac{7}{2}; u^2t^2\right) - {}_1F_3\left(\frac{3}{2}; \frac{1}{2}, 2, 3; u^2t^2\right). \quad (4.73)$$

Figure 4.1 shows a plot of this result as a function of time. Looking back to Fig. 1.3, we see that this signal saturates too quickly to provide a good fit to the experimental data. In fact, looking ahead to Fig. 7.3, we see that it reaches saturation too quickly to favorably compare with the numerical simulation results for $u = 0$ at resonance.

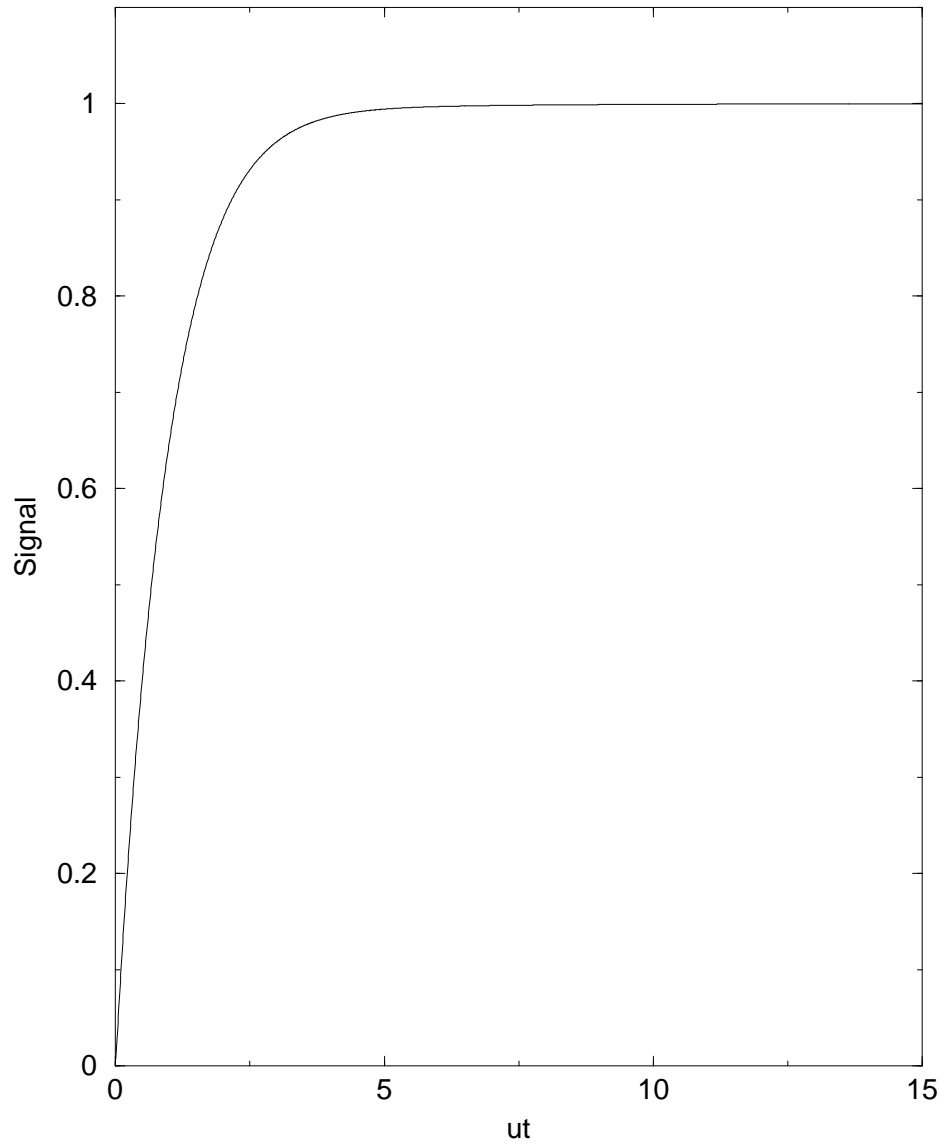


Figure 4.1: A plot of the averaged signal as a function of time for $u = v$ and $\Delta = 0$ in the Hubbard approximation.

4.4 The coherent potential approximation

Instead of making the Hubbard substitution of Eq. (4.33), we can replace $1/f_l$ by its average in Eq. (4.12b), obtaining

$$f_k = \alpha + \sum_{l=1}^N U_{kl}^2 \left\langle \frac{1}{f_l} \right\rangle. \quad (4.74)$$

This corresponds to a coherent potential approximation (CPA).

4.4.1 Computation of $\langle 1/f \rangle$

We have from Eq. (4.74) that

$$\frac{1}{f_k} = \frac{1}{\alpha + \sum_{l=1}^N U_{kl}^2 \left\langle \frac{1}{f} \right\rangle}. \quad (4.75)$$

We again note that $\langle 1/f_k \rangle$ is independent of k , so we drop the subscript and we see that

$$\left\langle \frac{1}{f} \right\rangle = \left\langle \frac{1}{\alpha + \mathcal{U}^2 \left\langle \frac{1}{f} \right\rangle} \right\rangle. \quad (4.76)$$

The averaging procedure of Section 2.3 is by now second nature, and we see that

$$\begin{aligned} \left\langle \frac{1}{f} \right\rangle &= \left\langle \int_0^\infty d\beta \exp \left[-\beta \left(\alpha + \mathcal{U}^2 \left\langle \frac{1}{f} \right\rangle \right) \right] \right\rangle \\ &= \int_0^\infty d\beta \exp \left(-\beta \alpha - u \sqrt{\beta \left\langle \frac{1}{f} \right\rangle} \right) \\ &= \frac{1}{\alpha} - \frac{\sqrt{\pi}}{2} \frac{u}{\alpha^{3/2}} \sqrt{\left\langle \frac{1}{f} \right\rangle} \exp \left(\frac{u^2}{4\alpha} \left\langle \frac{1}{f} \right\rangle \right) \operatorname{erfc} \left(\frac{u}{2\sqrt{\alpha}} \sqrt{\left\langle \frac{1}{f} \right\rangle} \right). \end{aligned} \quad (4.77)$$

This is an implicit equation for $\langle 1/f \rangle$, which can be rearranged to give

$$\alpha \left\langle \frac{1}{f} \right\rangle + \frac{\sqrt{\pi}}{2} \frac{u}{\sqrt{\alpha}} \sqrt{\left\langle \frac{1}{f} \right\rangle} \exp \left(\frac{u^2}{4\alpha} \left\langle \frac{1}{f} \right\rangle \right) \operatorname{erfc} \left(\frac{u}{2\sqrt{\alpha}} \sqrt{\left\langle \frac{1}{f} \right\rangle} \right) = 1. \quad (4.78)$$

Eq. (4.78) can then be solved numerically for $\langle 1/f \rangle$.

4.4.2 Computation of $\langle 1/f_0 \rangle$

Just as we saw when considering the Hubbard approximation, the modification of Eq. (4.12b) to Eq. (4.74) makes the latter equation inconsistent with Eq. (4.12a). It is possible to use Eq. (4.78)

coupled with Eq. (4.12a) to obtain an expression for $\langle 1/f_0 \rangle$, but it does not reduce to Eq. (4.78) when we take the limit $\Delta = 0$ and $u = v$. In this case, however, we can modify Eq. (4.12a) to

$$f_0 = \alpha + i\Delta + \mathcal{V}^2 \left\langle \frac{1}{f} \right\rangle, \quad (4.79)$$

so that it and Eq. (4.74) are again consistent.

Proceeding as we did in going from Eq. (4.76) to 4.77, we have

$$\begin{aligned} \left\langle \frac{1}{f_0} \right\rangle &= \left\langle \frac{1}{\alpha + i\Delta + \mathcal{V}^2 \left\langle \frac{1}{f} \right\rangle} \right\rangle \\ &= \left\langle \int_0^\infty d\beta \exp \left[-\beta \left(\alpha + i\Delta + \mathcal{V}^2 \left\langle \frac{1}{f} \right\rangle \right) \right] \right\rangle \\ &= \int_0^\infty d\beta \exp \left[-\beta (\alpha + i\Delta) - v \sqrt{\beta \left\langle \frac{1}{f} \right\rangle} \right], \end{aligned} \quad (4.80)$$

and hence

$$\begin{aligned} \left\langle \frac{1}{f_0} \right\rangle &= \frac{1}{\alpha + i\Delta} - \frac{\sqrt{\pi}}{2} \frac{v}{(\alpha + i\Delta)^{3/2}} \sqrt{\left\langle \frac{1}{f} \right\rangle} \times \\ &\quad \exp \left[\frac{v^2}{4(\alpha + i\Delta)} \left\langle \frac{1}{f} \right\rangle \right] \operatorname{erfc} \left(\frac{v}{2\sqrt{\alpha + i\Delta}} \sqrt{\left\langle \frac{1}{f} \right\rangle} \right). \end{aligned} \quad (4.81)$$

4.5 Comparison of the Cayley, Hubbard, and CPA approximations

We have examined these approximations and found that the results that agree best with the simulations are those obtained using the CPA approximation. In fact, as we will see in Section 4.6, the CPA results agree strikingly well with the simulations. This is somewhat surprising, since in the Cayley equations (4.12a) and (4.12b) the on-site Green's functions for the U problem are allowed to vary from site to site, whereas in Eqs. (4.33) and (4.74) they are not. However, the Cayley tree approximation is exact in a one-dimensional system with nearest neighbor interactions and becomes increasingly inaccurate as the dimensionality of the problem and the range of the interaction increase. The CPA, on the other hand, is a mean field approximation, and it becomes accurate for higher dimensional problems and long-range interactions.

We see in Fig. 4.2 plots of $\text{Re} \langle a_0(\Delta, \omega) \rangle$ for $u = 0$ and several values of Δ . The Cayley and CPA approximations coincide in this case. The exact result for $u = 0$ can actually be obtained analytically by the methods for computing $\langle \tilde{S}(\Delta, \alpha) \rangle$ used in Ref. [18] and described in detail in Chapter 2. We reproduce here the result of Eq. (2.28), which is

$$\langle \tilde{a}_0(\Delta, \alpha) \rangle = \frac{1}{\alpha + i\Delta} - \frac{\sqrt{\pi}}{2} \frac{v}{(\alpha + i\Delta)^{3/2} \sqrt{\alpha}} \exp\left[\frac{v^2}{4\alpha(\alpha + i\Delta)}\right] \text{erfc}\left[\frac{v}{2\sqrt{\alpha(\alpha + i\Delta)}}\right]. \quad (4.82)$$

As one would expect, this agrees with Eq. (4.32) for $Q(\alpha) = 1/\sqrt{\alpha}$ and with Eq. (4.81) for $\langle 1/f \rangle = 1/\alpha$.

We note the ‘‘gap’’ that is present in each of the curves, and we also note that the width of the gap increases with Δ . This effect can be seen analytically from Eq. (4.82). We start by converting from Laplace to Fourier space by making the substitution $\alpha = \omega/i$, so that we have

$$\langle a_0(\Delta, \omega) \rangle = \frac{i}{\omega - \Delta} + \frac{\sqrt{\pi}}{2} \frac{v}{(\omega - \Delta)^{3/2} \sqrt{\omega}} \exp\left[-\frac{v^2}{4\omega(\omega - \Delta)}\right] \text{erfc}\left[i\frac{v}{2\sqrt{\omega(\omega - \Delta)}}\right]. \quad (4.83)$$

Using Eq. (2.31), we see that

$$\text{Re} \langle a_0(\Delta, \omega) \rangle = \text{Re} \left\{ \frac{\sqrt{\pi}}{2} \frac{v}{(\omega - \Delta)^{3/2} \sqrt{\omega}} \exp\left[-\frac{v^2}{4\omega(\omega - \Delta)}\right] \right\}, \quad (4.84)$$

which reduces to

$$\text{Re} \langle a_0(\Delta, \omega) \rangle = \frac{\sqrt{\pi}}{2} \frac{v}{(\omega - \Delta)^{3/2} \sqrt{\omega}} \exp\left[-\frac{v^2}{4\omega(\omega - \Delta)}\right], \quad (4.85)$$

if $\omega > \Delta$, and zero otherwise. This explains the gaps seen in the $\Delta = v$ and $\Delta = 2v$ curves. For $\Delta = 0$, Eq. (4.85) becomes

$$\text{Re} \langle a_0(\Delta, \omega) \rangle = \frac{\sqrt{\pi}}{2} \frac{v}{\omega^2} \exp\left(-\frac{v^2}{4\omega^2}\right), \quad (4.86)$$

which produces the quasigap around $\omega = 0$ seen in the resonance curve.

In Fig. 4.3, which presents plots of $\text{Re} \langle a_0(\Delta, t) \rangle$ for $u = 0.25v$ and several values of Δ , we begin to see differences between the CPA and Cayley approximations. We see that the CPA results retain the gap structure of the $u = 0$ case somewhat, while the only vestiges of the gap remaining in the

Cayley results are the dimple in the $\Delta = 0$ curve at $\omega/v = 0$ and a barely perceptible bend in the $\Delta = v$ curve at $\omega/v = 0$. The off-resonant CPA results are also noticeably asymmetric around $\omega = \Delta$.

In Fig. 4.4 we see plots for $u = v$, and many of the trends of Fig. 4.3 continue. The off-resonant CPA results continue to retain some memory of the gap and are still asymmetric around $\omega = \Delta$. The gap structure is no longer evident in the on-resonance curve. For $\Delta = 0$ the result for the Hubbard approximation is also shown.

We see that the CPA and Cayley results look the most similar in Fig. 4.5, where $u = 4v$. However, upon careful examination one notes that the CPA results are still slightly asymmetric about $\omega = \Delta$. The peaks are also slightly wider for the CPA results.

4.6 Plots

4.6.1 The averaged amplitude $\langle a_0 \rangle$ as a function of time

Figs. 4.6 and 4.7 display the numerical simulations of $\text{Re} \langle a_0(\Delta, t) \rangle$ and $\text{Im} \langle a_0(\Delta, t) \rangle$, respectively, for $u/v = 0, 0.25, 1$, and 4 . We recall that $\langle a_0(\Delta, t) \rangle$ is the probability amplitude that the $ss' \rightarrow pp'$ has not occurred during the time t . The striking feature of these graphs is that, off-resonance, oscillations with an approximate period Δ persist for a long time, not only when the exciton does not propagate ($u = 0$), but even for $u = 4v$.

The graphs for $u = 0$ can be obtained analytically by the methods for computing $\langle S(\Delta, t) \rangle$ used in Ref. [18] and described in detail in Chapter 2. In fact, we have obtained $\langle a_0(\Delta, t) \rangle$ by expanding Eq. (4.82) (or, equivalently, Eq. (2.28)) in powers of $1/\alpha$ and inverting the Laplace transform term by term. As in Chapter 2, various formulas involving special functions can also be obtained. The exact analytical results in this case (not shown here) agree with the numerical simulations about as well as in Fig. 7.1. The initial dependence on time is given by

$$\langle a_0(\Delta, t) \rangle \approx 1 - \frac{\sqrt{\pi}}{2} vt - i\Delta t \quad (4.87)$$

Looking at the graphs, it seems that the initial decrease of $\text{Re} \langle a_0(\Delta, t) \rangle$ depends on u , but this perception only indicates that the range of validity of the linear approximation Eq. (4.87) is small. On the other hand, the graphs of $1 - \langle |a_0|^2 \rangle$ as a function of time in Figs. 7.1–7.5 look linear and

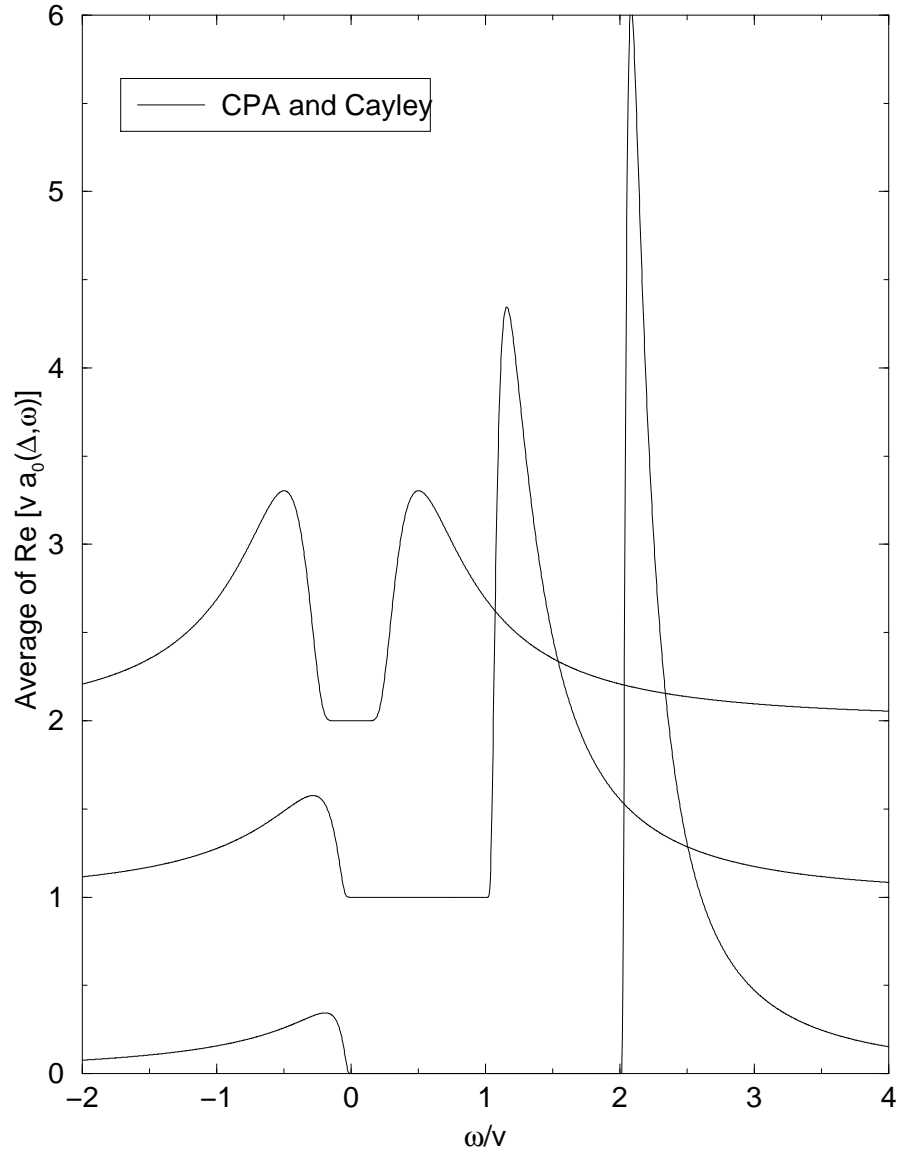


Figure 4.2: Plots of $\text{Re} \langle \text{Re} a_0(\Delta, \omega) \rangle$ for $u = 0$ and, from left to right, $\Delta = 0, v,$ and $2v$. The $\Delta = v$ curve has been shifted vertically upward by 1, and the $\Delta = 2v$ curve by 2. The results are exact in this case.

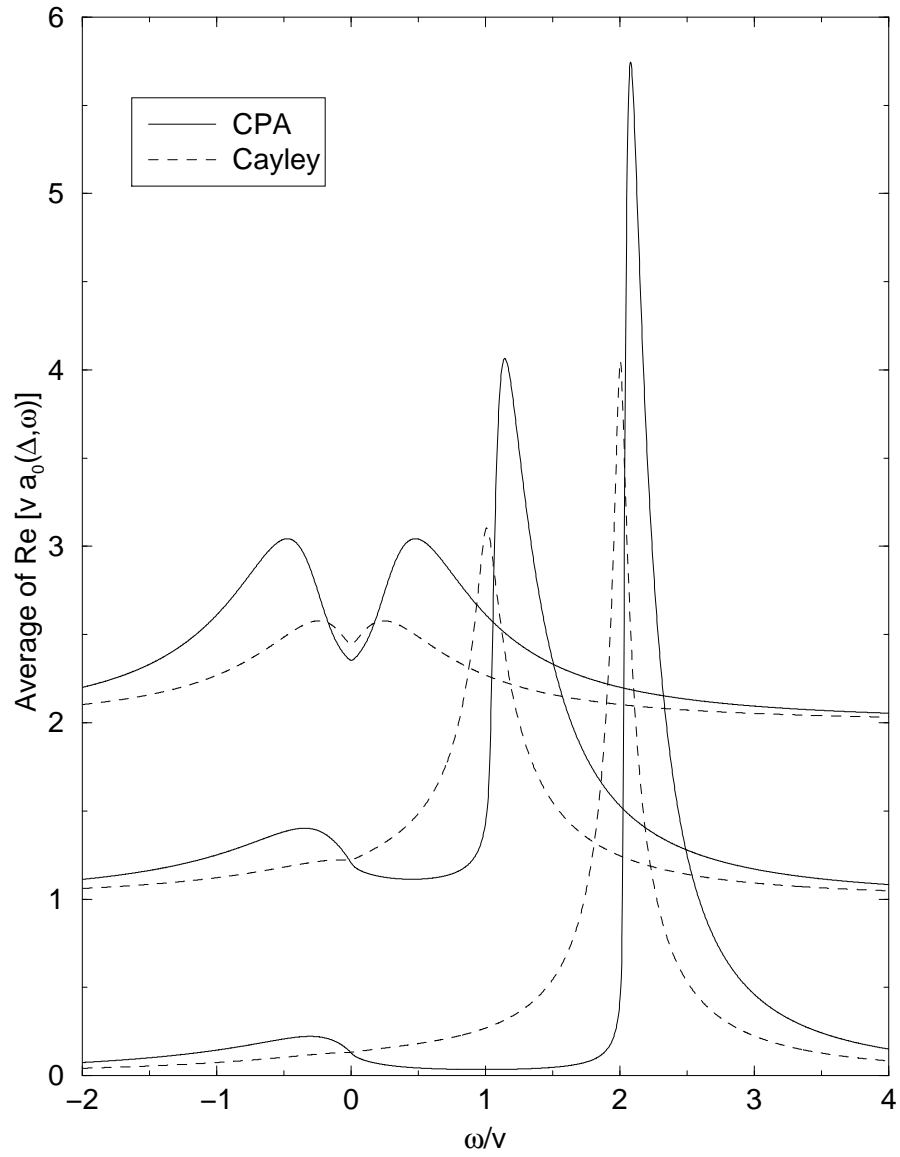


Figure 4.3: Plots of $\text{Re} \langle a_0(\Delta, \omega) \rangle$ for $u = 0.25v$ and, from left to right, $\Delta = 0, v,$ and $2v$. The $\Delta = v$ curve has been shifted vertically upward by 1, and the $\Delta = 2v$ curve by 2.

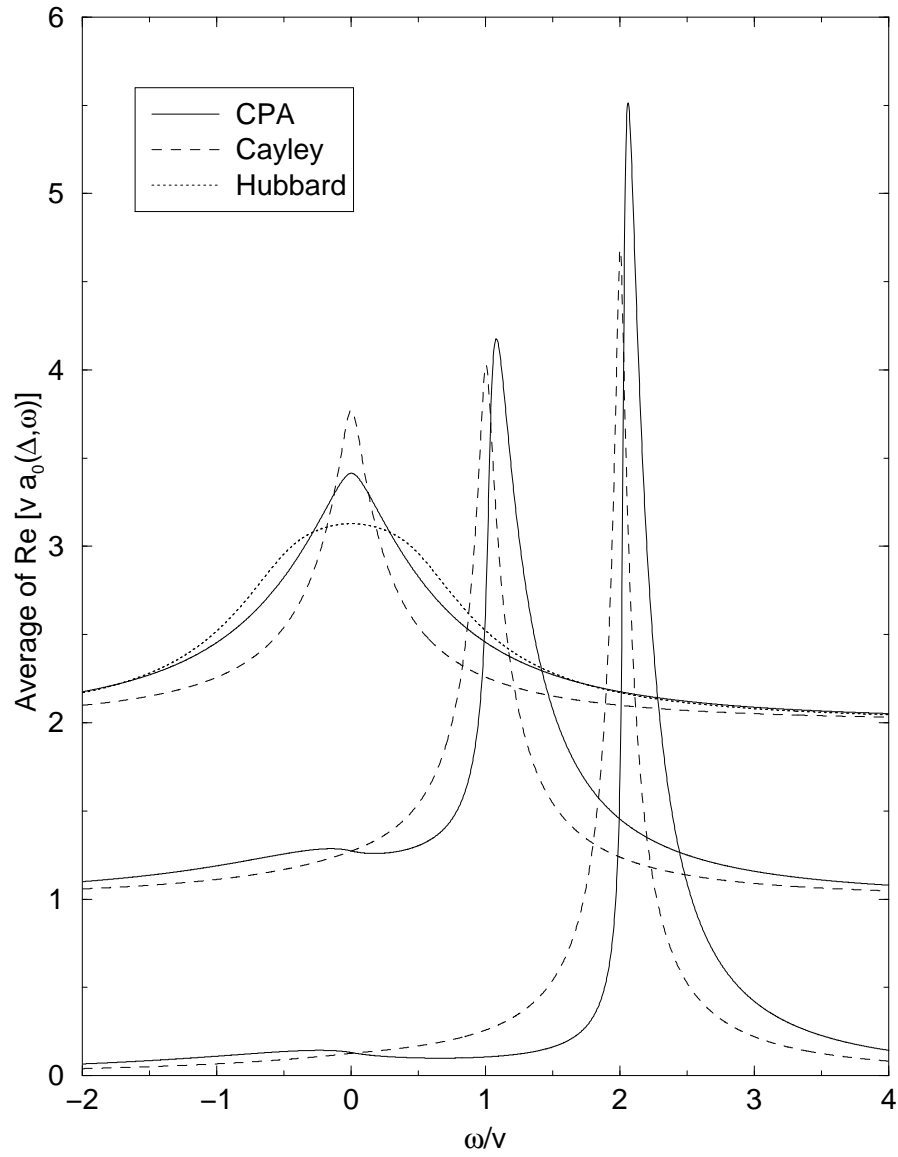


Figure 4.4: Plots of $\text{Re} \langle a_0(\Delta, \omega) \rangle$ for $u = v$ and, from left to right, $\Delta = 0, v,$ and $2v$. The $\Delta = v$ curve has been shifted vertically upward by 1, and the $\Delta = 2v$ curve by 2.

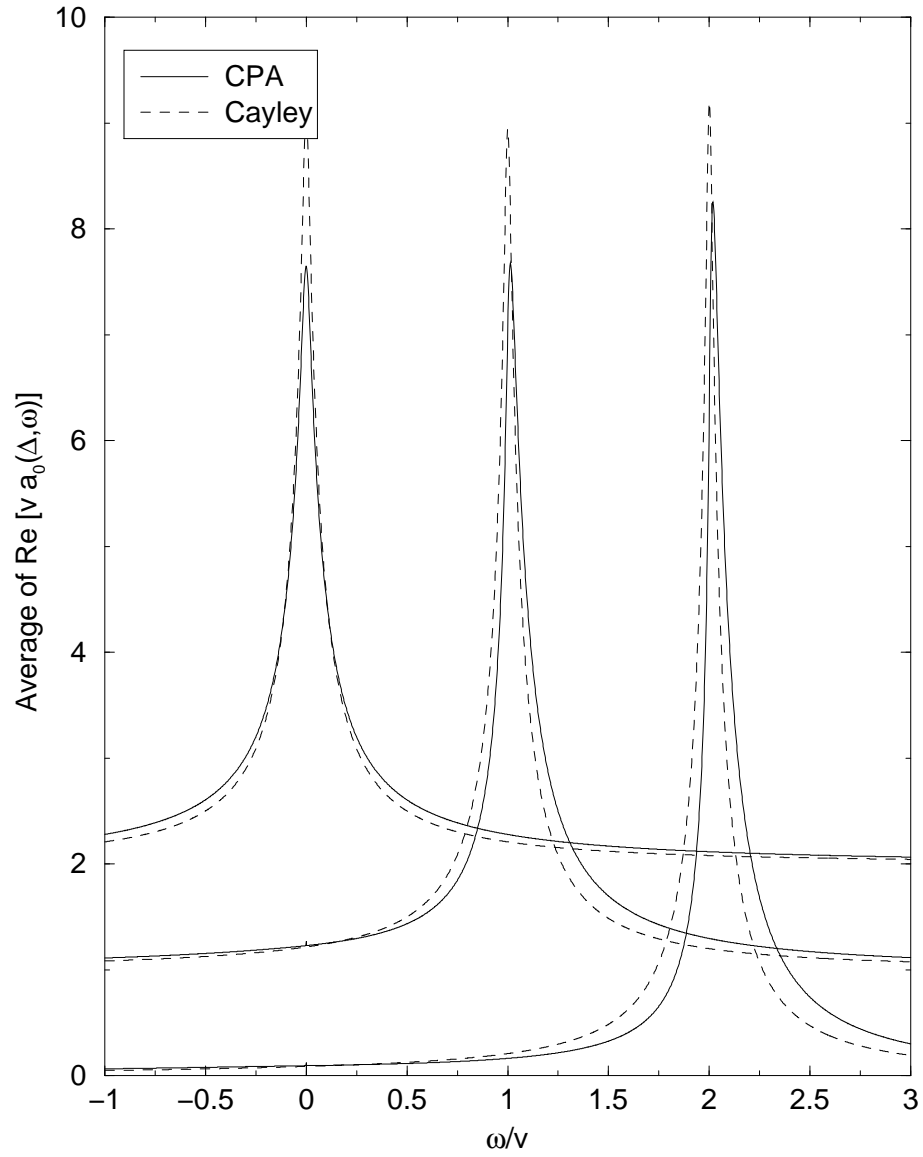


Figure 4.5: Plots of $\text{Re} \langle a_0(\Delta, \omega) \rangle$ for $u = 4v$ and, from left to right, $\Delta = 0, v,$ and $2v$. The $\Delta = v$ curve has been shifted vertically upward by 1, and the $\Delta = 2v$ curve by 2.

independent of u over a wide range of vt . Note also that $|\langle a_0(\Delta, t) \rangle|^2 \approx 1 - \sqrt{\pi}vt$ decreases initially twice as fast as $\langle |a_0(\Delta, t)|^2 \rangle \approx 1 - (\sqrt{\pi}/2)vt$. Of course, it must be true that the mod square of the average is smaller than or equal to the average of the square, but the above result shows that $|\langle a_0(\Delta, t) \rangle|^2$ is not even a fair approximation to $\langle |a_0(\Delta, t)|^2 \rangle$.

4.6.2 The averaged amplitude $\langle a_0 \rangle$ as a function of frequency

Figs. 4.8–4.11 present graphs of $\text{Re} \langle a_0(\Delta, \omega) \rangle$ that correspond to the graphs of $\langle a_0(\Delta, t) \rangle$ in Figs. 4.6 and 4.7. For $u = v$ and $\Delta = 0$, $\text{Re} \langle a_0(\Delta, \omega) \rangle$ is the exciton spectral density (times π); more generally, it is an excitation spectral density for the resonant process $ss' \rightarrow pp'$. Each figure gives a comparison of the numerical simulation with the CPA approximation, which in particular for $u = 0$ reduces correctly to the real part of the exact result of Eq. (4.82), with $\alpha = \omega/i$. We compare spectral densities, rather than time graphs, in part because obtaining $\langle a_0(\Delta, t) \rangle$ for the CPA approximation is laborious, and in part because the comparison of spectral densities is instructive, as we now discuss.

In the notation of Section 7.3, the spectral density is obtained numerically from Eq. (7.7) as

$$\text{Re } a_0(\Delta, \omega + i\varepsilon) = \text{Im} \sum_{m=0}^N \frac{\beta_{m0}\beta_{0m}}{\omega - \lambda_m + i\varepsilon} \quad (4.88)$$

in the limits $\varepsilon \rightarrow 0$ and $N \rightarrow \infty$. In practice it is difficult to go beyond $N = 10^3$, and one must choose ε to be fairly large to obtain a smooth plot for the spectral density where the eigenvalues are sparse, even after averaging over 10^4 realizations. On the other hand, the distribution of eigenvalues for a random dipolar gas is highly structured near $\omega = 0$, and if ε is too large this structure will be missed. Rather than spending much time to go to large N and refine the numerical technique, we set $N = 100$, plot the results for $\varepsilon/v = 0.1$ and 0.01 , and let the eye extrapolate to the correct limit. It is remarkable that the CPA approximation agrees best with the smallest value of ε/v , except for wiggles that are usually in regions of sparse eigenvalues. This is exactly how the exact spectral density is expected to compare with a calculation for finite N . A finite ε can also be viewed as a simulation of the decoherence introduced by atomic motions, or of losses to other channels, such as the decay of the excited atomic states due to blackbody radiation as described in Chapter 5 of Ref. [22]. Thus, ε is almost equivalent to the γ of the Lorentzian broadening model of Ref. [18], the difference being that in Ref. [18] $i\gamma$ is added to ω for the Fourier transform of Eq. (2.1b) only, while

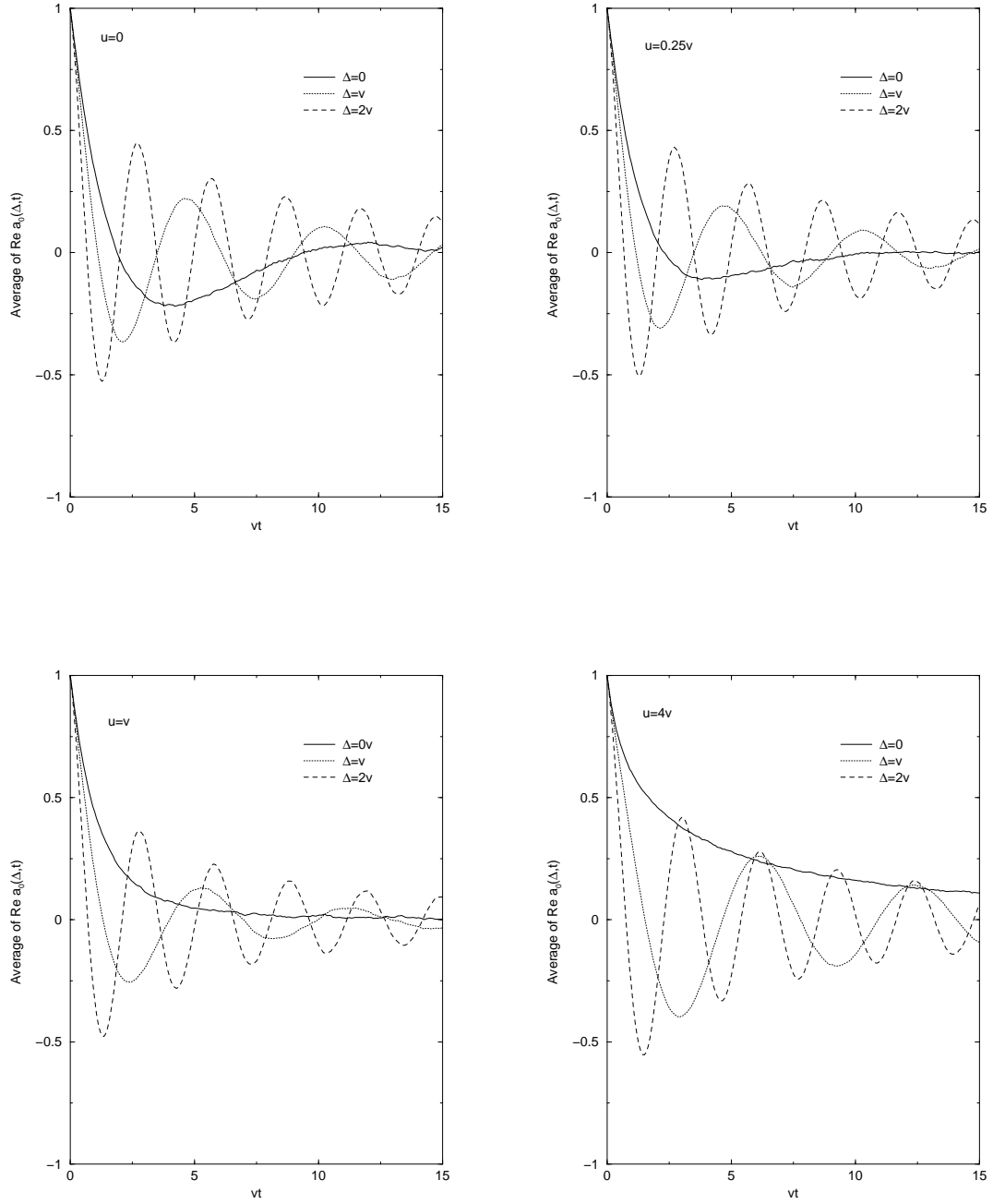


Figure 4.6: Plots of the real part of $\langle a_0(\Delta, t) \rangle$ for $u = 0$, $u = 0.25v$, $u = v$, and $u = 4v$.

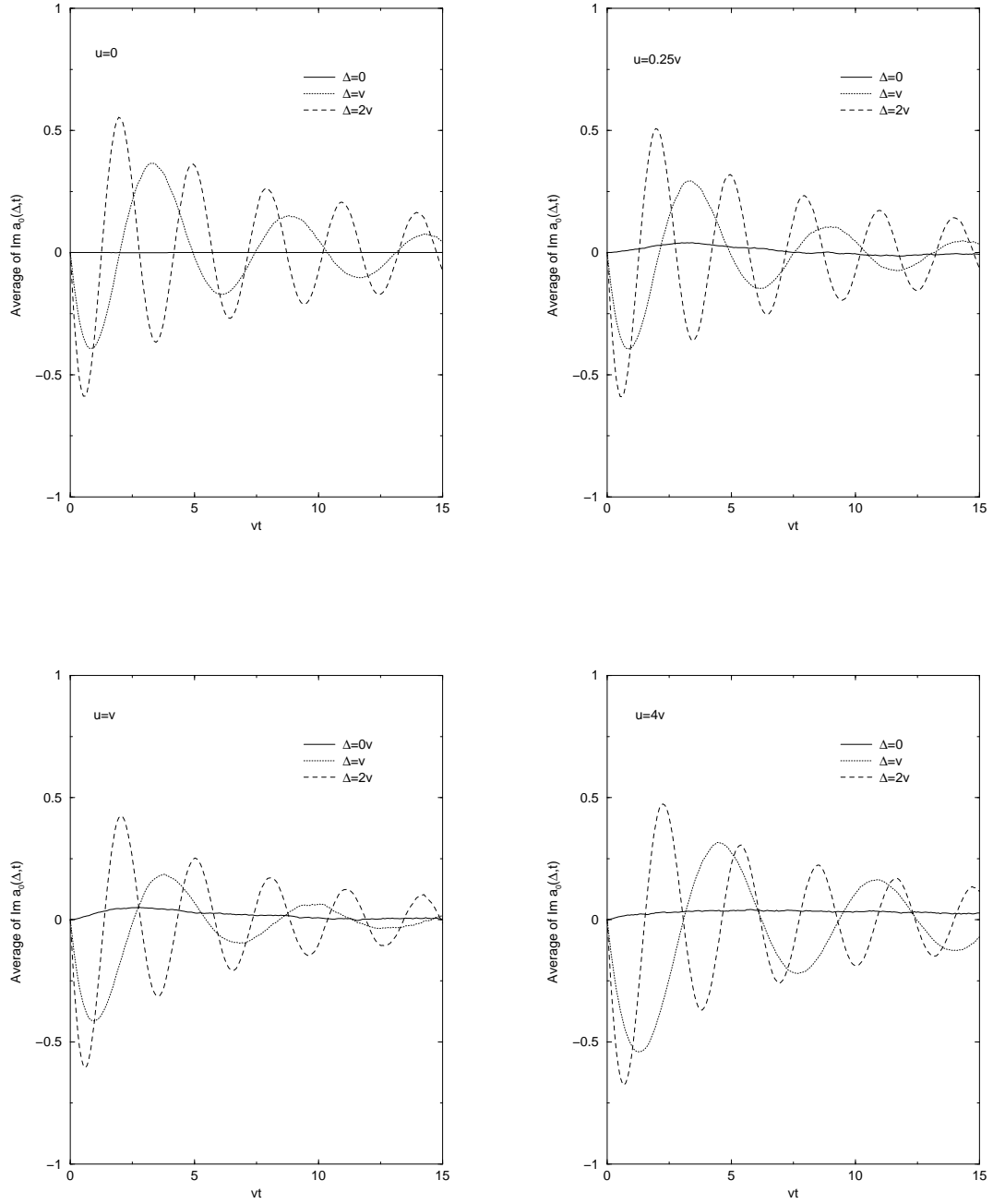


Figure 4.7: Plots of the imaginary part of $\langle a_0(\Delta, t) \rangle$ for $u = 0$, $u = 0.25v$, $u = v$, and $u = 4v$.

here $i\varepsilon$ is added to every ω that appears. As ε increases, the highly structured spectral densities of the ideal frozen gas become increasingly similar to Lorentzian lines. Because of unavoidable losses and incoherences, the experimental spectral densities will resemble the results of the simulations for some finite ε .

In Fig. 4.8, where results are presented for $u = 0$, the spectral density is quite different from a Lorentzian. At $\Delta = 0$ there is a quasi-gap around $\omega = 0$. As Δ increases the gap extends from $\omega = 0$ to $\omega = \Delta$, as was described in Section 4.5.

In Fig. 4.9 are presented results for $u = 0.25v$. We see that the sharp features of the $u = 0$ spectrum are rounded off and the gap is beginning to be filled, but is still recognizable.

Results for $u = v$ are presented in Fig. 4.10. We note that the spectrum at $\Delta = 0$ has the appearance of a single, asymmetric line. At $\Delta = v$ and $\Delta = 2v$ a shoulder on the left of the line is the remnant of the gap of Fig. 4.8.

Fig. 4.11 contains results for $u = 4v$. We see that there is a single line for any value of Δ , which becomes increasingly sharp as u increases. The lineshape is not Lorentzian, but even a small additional broadening will make it nearly so, as indicated by the calculation for $\varepsilon/v = 0.01$. This sharp line leads to the damped sinusoidal oscillations seen in the $u = 4v$ graphs of Figs. 4.6 and 4.7. The general phenomenon of line narrowing can be discussed using the simple Lorentzian model for the exciton band, in which Eq. (1b) of Ref. [18] is replaced by

$$i\dot{c}_k = V_k a_0 - i\gamma c_k. \quad (4.89)$$

Solving the equations in this limit, one finds a pole at

$$\omega = -i \frac{\gamma \sum_k V_k^2}{\gamma^2 + \Delta^2} + \Delta, \quad (4.90)$$

which gives a decreasing width as u increases, since γ is proportional to u . One cannot simply replace $\sum_k V_k^2$ by its average, which does not even exist. Instead, one can Fourier transform the average to find the time dependence

$$\exp(-i\Delta t - \sqrt{\gamma e q t}), \quad (4.91)$$

where

$$\gamma_{eq} = \frac{v^2 \gamma}{\gamma^2 + \Delta^2}, \quad (4.92)$$

and v has been defined in Eq. (2.12). A similar argument was applied in Ref. [18] to find the time dependence of $\langle |a_0|^2 \rangle$.

From the comparison with the simulations, it is apparent that a shortcoming of the CPA approximation is that it gives a symmetric spectral density at resonance ($\Delta = 0$), while the correct spectral density is slightly asymmetric, except for $u = 0$. Correspondingly, $\langle a_0(\Delta, t) \rangle$ is not purely real at resonance, as can be seen in Fig. 4.7. For $\Delta \neq 0$, the spectral density at $\omega < \Delta$ is underestimated by the CPA approximation.

Clearly, the asymmetry of the spectral density at $\Delta = 0$ comes from the terms with $l \neq m$ in the denominator of Eq. (4.4), which are neglected in the CPA approximation. It is surprising that these terms have such small effect on $\langle a_0(\Delta, \omega) \rangle$ at $\Delta = 0$. At finite Δ , the underestimate of $\text{Re} \langle a_0(\Delta, \omega) \rangle$ for $\omega < \Delta$ is probably due to the neglect of these same terms. We have already shown how to include these terms in the CPA formulation [11], but in practice, when the simple CPA is not adequate one can just as well use the numerical simulations.

4.7 Summary

In this chapter we have extended the simple model of Chapter 2 by allowing the $sp \rightarrow ps$ process to take place. Although this complication no longer allows a direct analytical solution of the problem, we consider three approximations, each of which allows us to make some progress. We compare these approximations with the results of numerical simulations, which are carried out for a finite number of atoms by the methods described later in Chapter 7 of this thesis.

The results of the Cayley tree approximation are not found to give the best results for the problem we are considering here, but they are still extremely worthwhile results. They extend the Cayley tree results of Ref. [1], which are used extensively, for example, in the study of dipolar liquids [12, 28, 31, 30, 37, 39, 58].

The results of the Hubbard approximation are somewhat disappointing, since in this case we can obtain an explicit expression for the exciton spectrum ($1/f_l$) but we are not able to obtain a consistent result when the effects of the $ss' \rightarrow pp'$ process are included. However, in this approximation we can obtain the average of $|a_0|^2$ as a function of time when the V process is absent, and perhaps in

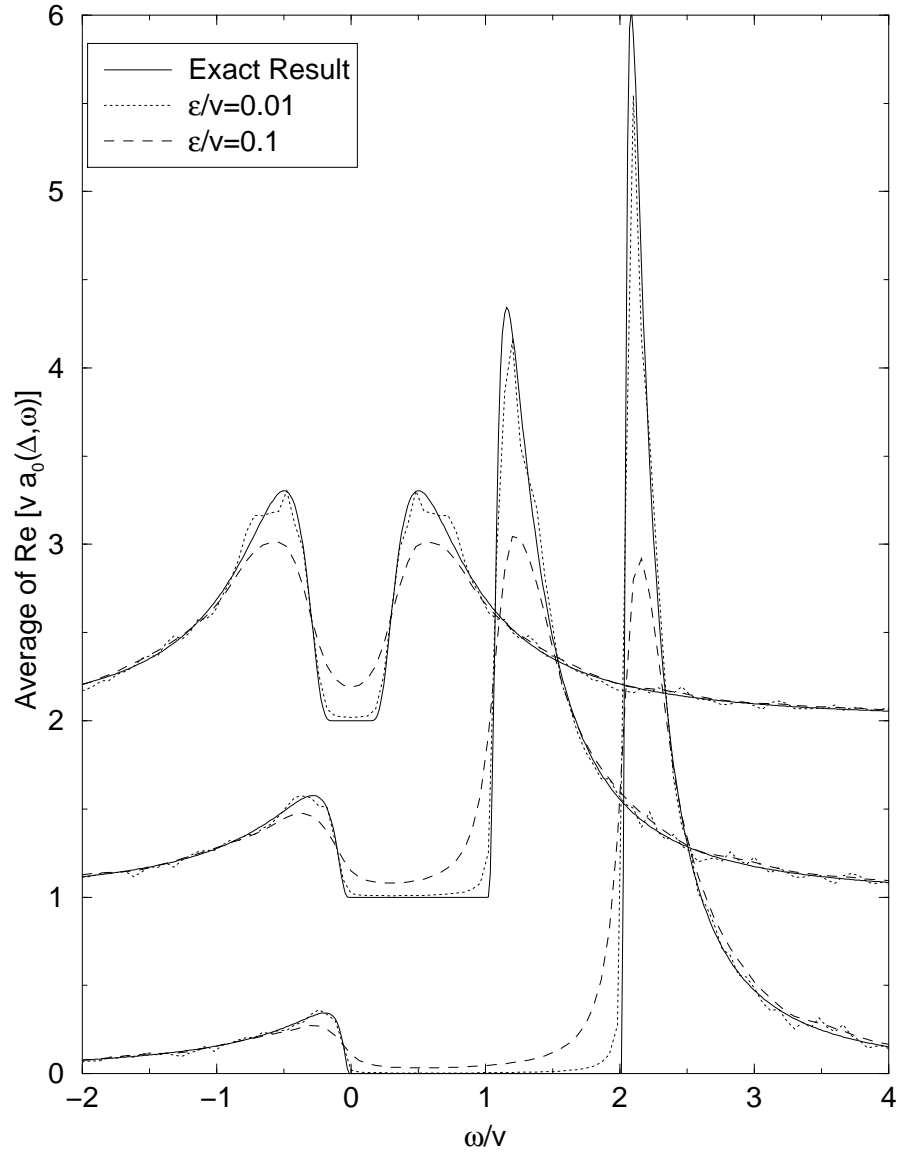


Figure 4.8: A plot of the real part of $\langle a_0(\Delta, \omega) \rangle$ for $u = 0$ and, from left to right, $\Delta = 0, v,$ and $2v$. To aid the eye in separating the curves, the $\Delta = 0$ curve has been vertically offset by 2 and the $\Delta = v$ curve by 1.

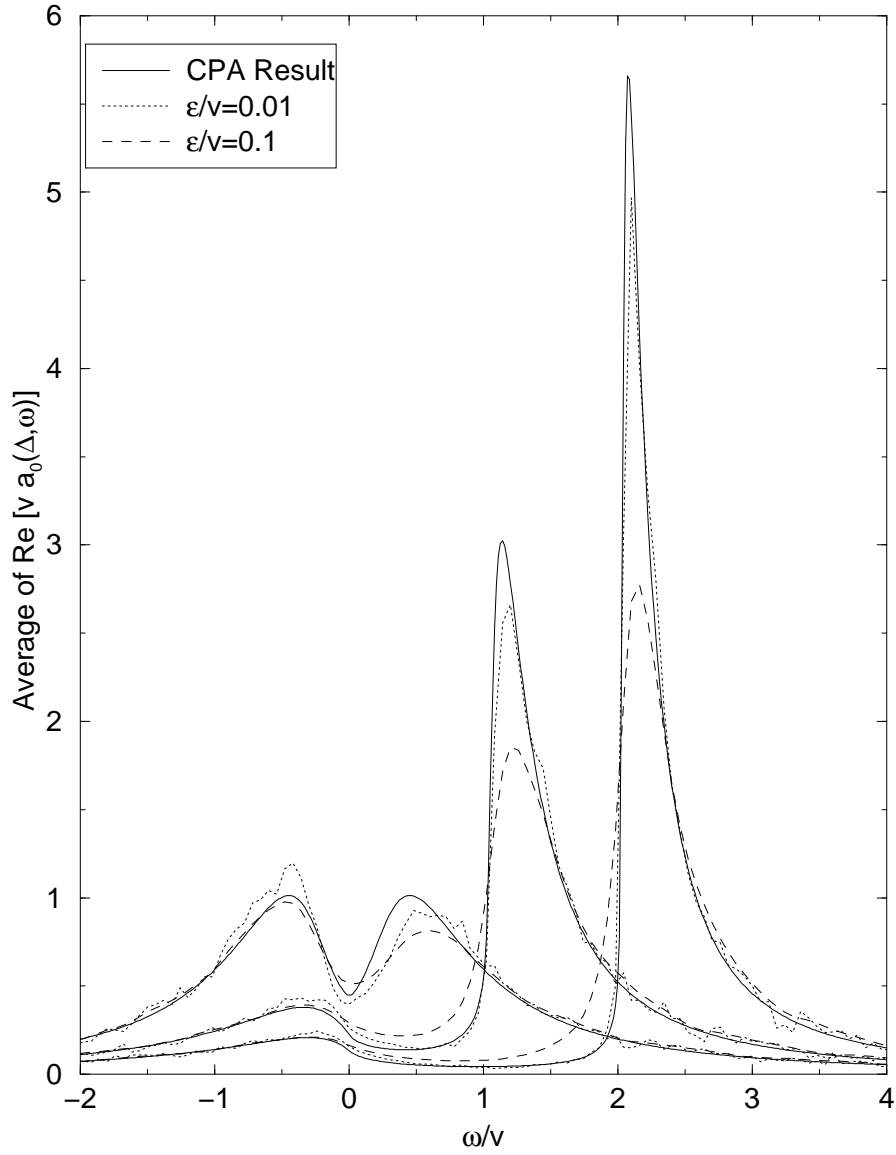


Figure 4.9: A plot of the real part of $\langle a_0(\Delta, \omega) \rangle$ for $u = 0.25v$ and, from left to right, $\Delta = 0, v$, and $2v$.

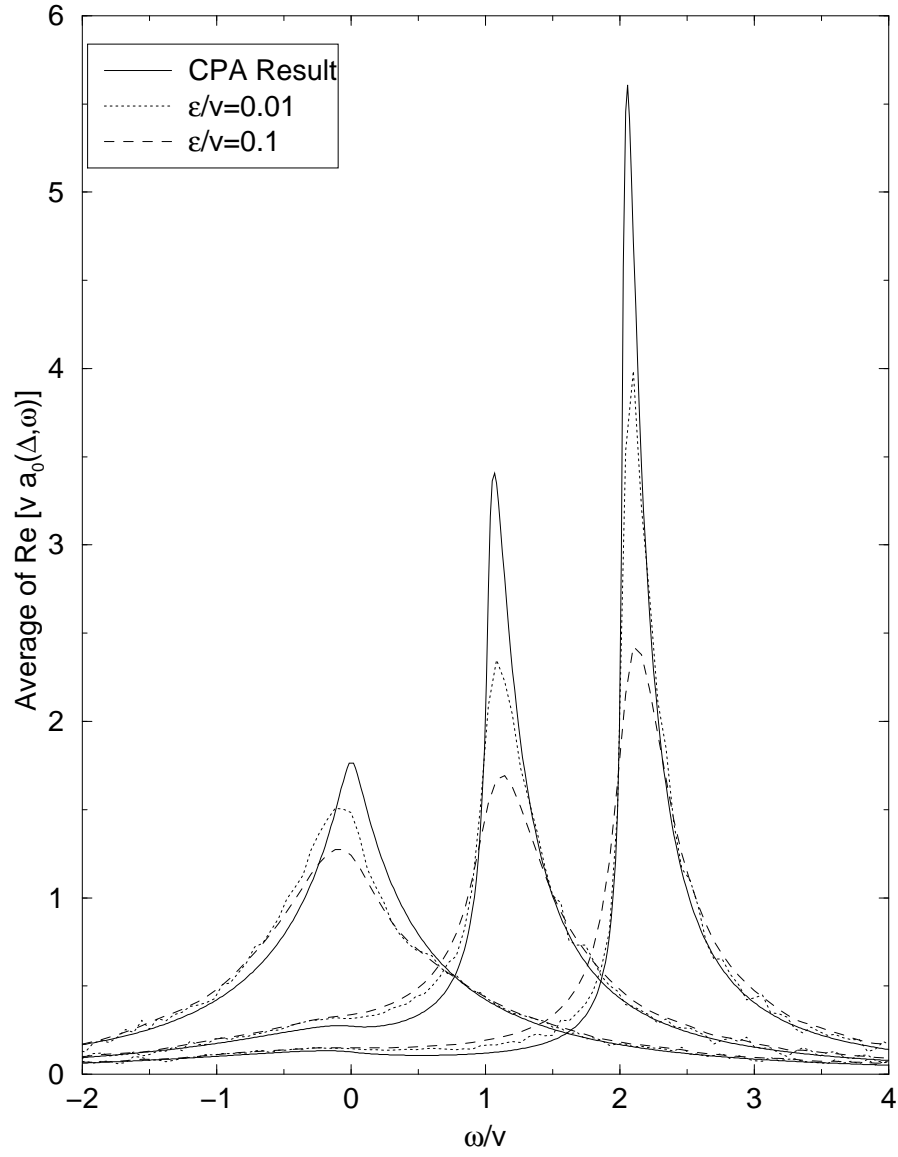


Figure 4.10: A plot of the real part of $\langle a_0(\Delta, \omega) \rangle$ for $u = v$ and, from left to right, $\Delta = 0, v,$ and $2v$.

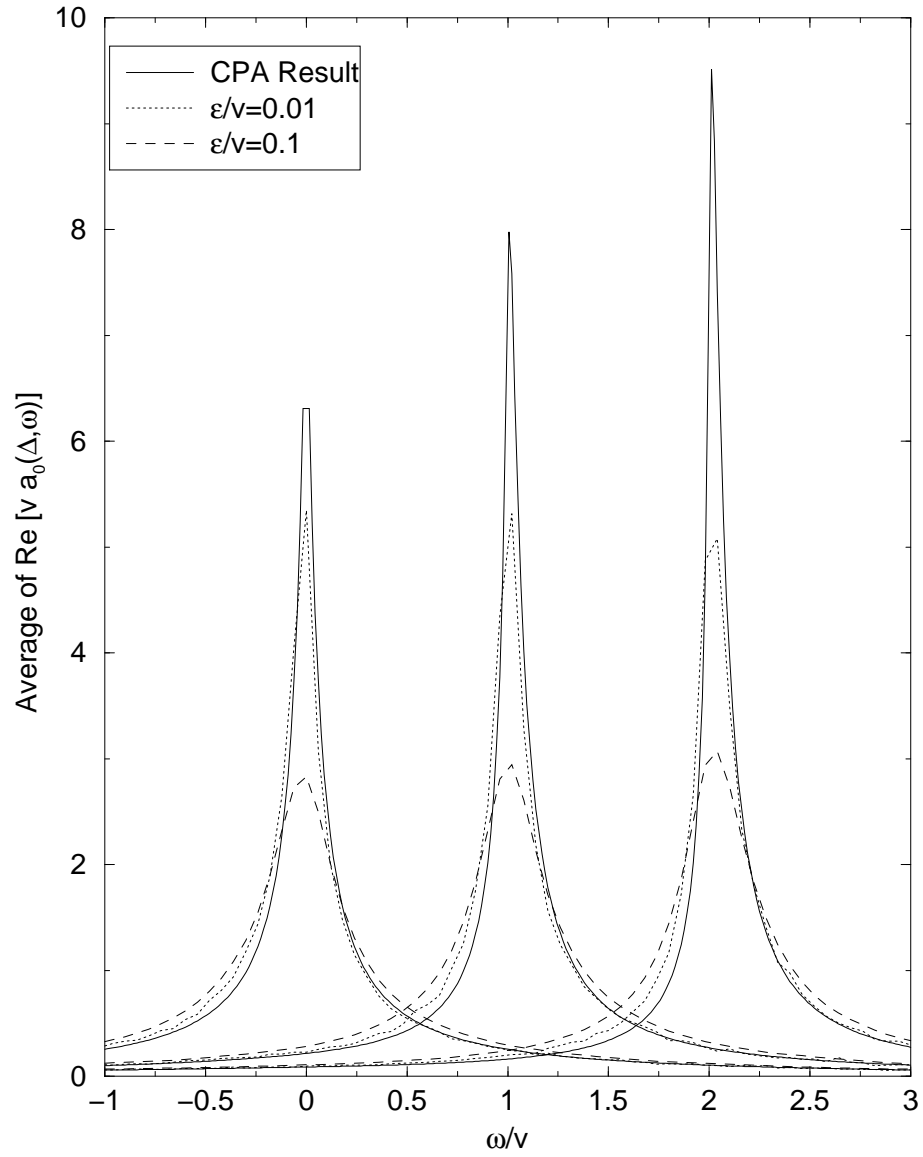


Figure 4.11: A plot of the real part of $\langle a_0(\Delta, \omega) \rangle$ for $u = 4v$ and, from left to right, $\Delta = 0, v,$ and $2v$.

the future this will lead to a more general technique that will allow this quantity to be computed in the other approximations as well.

The CPA approximation is found to agree best with the results of the numerical simulations, and we are able to carry our computations in this approximation just as far as in the Cayley tree approximation. It seems at first strange that the CPA approximation gives better results than the Cayley, since in the Cayley equations (4.12a) and (4.12b) the on-site Green's functions for the U problem are allowed to vary from site to site, whereas in Eqs. (4.33) and (4.74) they are not. However, the Cayley tree approximation is exact in a one-dimensional system with nearest neighbor interactions and becomes increasingly inaccurate as the dimensionality of the problem and the range of the interaction increase. The CPA, on the other hand, is a mean field approximation, and it becomes accurate for higher dimensional problems and long-range interactions. It may also happen that, when the off-diagonal terms of Eqs. (4.4) and (4.11) are included, the Cayley is found to be the better approximation.

Chapter 5

Analogy With Spin Glasses

5.1 Introduction

In this chapter, we examine a correspondence between the atomic system we are seeking to model and spin glasses. We start in Section 5.2 by considering the rubidium experiments of Anderson *et al.* [5, 6] and Lowell *et al.* [40]. In Section 5.2.1 we derive in a rather straightforward manner a Hamiltonian that describes these experiments as a system of two interpenetrating spin glasses. We also determine the corresponding equations of motion. In Section 5.2.2 we illustrate how the results of Section 5.2.1 reduce to those of Chapter 4 in the appropriate limit. We derive a new, and seemingly more cumbersome Hamiltonian in Section 5.2.3 that also describes the rubidium experiments and is entirely equivalent to the Hamiltonian of Section 5.2.1. The method used to generate the new Hamiltonian is more generally applicable, however, as we demonstrate in Section 5.3 by using the new method to construct a spin Hamiltonian that describes the cesium experiments of Mourachko *et al.* [45, 44]. Finally, we conclude in Section 5.4.

5.2 The rubidium system as a spin glass

5.2.1 Spin glass Hamiltonian and equations of motion

We consider N atoms at positions \mathbf{r}_k which are initially in state s , and N' atoms at positions $\mathbf{r}_{k'}$ which are initially in state s' . We represent the s and p states at \mathbf{r}_k with the down and up states of an effective spin σ_k , respectively, and similarly represent the s' and p' states at $\mathbf{r}_{k'}$ with a spin $\sigma_{k'}$.

The Hamiltonian that describes this system with the $ss' \rightarrow pp'$ and $sp \rightarrow ps$ processes mediated by dipole-dipole interaction potentials V and U , respectively, is then

$$H = \sum_{k=1}^N [\varepsilon_s + (\varepsilon_p - \varepsilon_s) \sigma_k^+ \sigma_k^-] + \sum_{k'=1}^{N'} [\varepsilon'_s + (\varepsilon'_p - \varepsilon'_s) \sigma_{k'}^+ \sigma_{k'}^-] + \sum_{k,k'} V_{kk'} [\sigma_k^+ \sigma_{k'}^+ + \sigma_k^- \sigma_{k'}^-] + \sum_{k,l \neq k} U_{kl} \sigma_k^+ \sigma_l^-, \quad (5.1)$$

where

$$V_{kk'} = \frac{\mu\mu'}{|\mathbf{r}_k - \mathbf{r}_{k'}|^3}, \quad (5.2)$$

and

$$U_{kl} = \frac{\mu^2}{|\mathbf{r}_k - \mathbf{r}_l|^3}, \quad (5.3)$$

if $l \neq k$ and $U_{kl} = 0$ otherwise.¹ This is precisely the Hamiltonian for two interpenetrating spin glasses that interact via dipole-dipole potentials.

For the experiments under consideration $\mu \approx 4\mu'$, and the $sp \rightarrow ps$ coupling μ^2 , which leads to “spin diffusion,” is larger than the $ss' \rightarrow pp'$ coupling $\mu\mu'$ that is responsible for the resonant energy transfer.

We can write down basic equations of motion such as

$$i \frac{d}{dt} \sigma_{k'}^+ = \Delta \sigma_{k'}^+ + \sigma_{k'}^z \sum_{k=1}^N V_{k'k} \sigma_k^-, \quad (5.4)$$

$$i \frac{d}{dt} \sigma_k^+ = \sigma_k^z \sum_{k'} V_{kk'} \sigma_{k'}^- + \sigma_k^z \sum_{l \neq k} U_{kl} \sigma_l^+, \quad (5.5)$$

and

$$i \frac{d}{dt} \sigma_{k'}^z = 2 \sum_{k=1}^N V_{k'k} (\sigma_k^+ \sigma_{k'}^+ - \sigma_k^- \sigma_{k'}^-), \quad (5.6)$$

where Δ is the detuning from resonance.² From these we can obtain

$$\begin{aligned} \frac{1}{2} \frac{d^2}{dt^2} \sigma_{k'}^z &= - \sum_{kl'} V_{k'k} V_{kl'} \sigma_k^z (\sigma_{k'}^- \sigma_{l'}^+ + \sigma_{k'}^+ \sigma_{l'}^-) - \sum_{kl} V_{k'k} V_{lk'} \sigma_{k'}^z (\sigma_k^- \sigma_l^+ + \sigma_k^+ \sigma_l^-) + \\ &\quad - \sum_{k,l \neq k} V_{k'k} U_{kl} \sigma_k^z (\sigma_k^+ \sigma_l^+ + \sigma_{k'}^- \sigma_l^-) - \Delta \sum_k V_{k'k} (\sigma_{k'}^+ \sigma_k^+ + \sigma_{k'}^- \sigma_k^-). \end{aligned} \quad (5.7)$$

¹Of course, the $1/r^3$ potentials of Eqs. (5.2) and (5.3) are just the simplest examples of dipole-dipole interaction potentials. We are free to choose more complicated potentials if we so desire.

²To obtain these expressions we take the equations of motion that come about naturally from the Hamiltonian in Eq. (5.1) and introduce a phase $\exp[-i(\varepsilon_p - \varepsilon_s)t]$ into the definitions of σ_k^+ and $\sigma_{k'}^+$.

These differential equations are rather difficult to work with, but we have already discussed one possible approximation scheme in Ref. [18].

5.2.2 Reduction to the sparse limit

We now show explicitly how the general spin-variable formalism of Section 5.2.1 relates to the coefficients a_0 and c_k of Eqs. (4.1a) and (4.1b) when there is only a single atom that can be in the s', p' pair of states (i.e., when only a single spin variable of the type $\sigma_{k'}$ is present.) The key to the correspondence is that in this case the initial state $|i\rangle$, which consists of all spins down, evolves to

$$|t\rangle = \left(a_0(\Delta, t) + \sum_q c_q(\Delta, t) \sigma_{k'}^+ \sigma_q^+ \right) |i\rangle, \quad (5.8)$$

at time t , where the spin variables now denote time-independent Schrödinger operators. With the understanding that $\mathbf{r}_{k'} = 0$, we have:

$$\langle i | \sigma_{k'}^z(t) | i \rangle = \langle t | \sigma_{k'}^z | t \rangle = 1 - 2 |a_0(\Delta, t)|^2, \quad (5.9)$$

$$\langle t | \sigma_k^z | t \rangle = 2 |c_k(\Delta, t)|^2 - 1, \quad (5.10)$$

and

$$\langle t | \sigma_{k'}^+ \sigma_k^+ | t \rangle = c_k^\dagger(\Delta, t) a_0(\Delta, t). \quad (5.11)$$

It is then clear that the expectation value of Eq. (5.6) is equivalent to

$$i \frac{d}{dt} |a_0(\Delta, t)|^2 = \sum_k V_k \left[a_0^\dagger(\Delta, t) c_k(\Delta, t) - c_k^\dagger(\Delta, t) a_0(\Delta, t) \right], \quad (5.12)$$

where V_k is short for $V_{k'k}$. This equation is itself a consequence of Eq. (4.1a). Similarly, the equations for $\langle t | \sigma_k^z | t \rangle$ and $\langle t | \sigma_{k'}^+ \sigma_k^+ | t \rangle$ are equivalent to the equations for $|c_k(\Delta, t)|^2$ and $c_k(\Delta, t)^\dagger a_0(\Delta, t)$ that follow from Eqs. (4.1a) and (4.1b).

5.2.3 Another spin glass Hamiltonian for the rubidium system

In the rubidium experiments of Anderson *et al.* [5, 6] and Lowell *et al.* [40] there are the four states s, p, s' , and p' . Therefore we can define a column vector of length four for each site, so that if an

atom at site Λ is in the s , p , s' , or p' state, then the column vector corresponding to that site is $(0, 0, 0, 1)^T$, $(0, 0, 1, 0)^T$, $(0, 1, 0, 0)^T$, or $(1, 0, 0, 0)^T$, respectively. The Hamiltonian for this system can then be written

$$H_{\text{Rb}} = \sum_{\Lambda} \epsilon_{\Lambda} + \sum_{\Lambda_1, \Lambda_2} V_{\Lambda_1 \Lambda_2} \left[(\sigma_{sp}^+)_{\Lambda_1} (\sigma_{s'p'}^+)_{\Lambda_2} + \text{h.c.} \right] + \sum_{\Lambda_1, \Lambda_2} U_{\Lambda_1 \Lambda_2} \left[(\sigma_{sp}^+)_{\Lambda_1} (\sigma_{sp}^-)_{\Lambda_2} + \text{h.c.} \right], \quad (5.13)$$

where ϵ , σ_{sp}^{\pm} , and $\sigma_{s'p'}^{\pm}$ are the 4×4 matrices

$$\epsilon = \begin{pmatrix} \epsilon_{p'} & 0 & 0 & 0 \\ 0 & \epsilon_{s'} & 0 & 0 \\ 0 & 0 & \epsilon_p & 0 \\ 0 & 0 & 0 & \epsilon_s \end{pmatrix}, \quad (5.14)$$

$$\sigma_{sp}^{\pm} = \begin{pmatrix} 0 & 0 & 0 & 0 \\ 0 & 0 & 0 & 0 \\ 0 & 0 & & \sigma^{\pm} \\ 0 & 0 & & \end{pmatrix}, \quad (5.15)$$

and

$$\sigma_{s'p'}^{\pm} = \begin{pmatrix} & \sigma^{\pm} & 0 & 0 \\ & & 0 & 0 \\ 0 & 0 & 0 & 0 \\ 0 & 0 & 0 & 0 \end{pmatrix}, \quad (5.16)$$

and the subscripts on these matrices indicate on which site they are to be applied. The quantities $V_{\Lambda_1 \Lambda_2}$ and $U_{\Lambda_1 \Lambda_2}$ are defined to be zero if $\Lambda_1 = \Lambda_2$, and are the interaction potentials

$$V_{\Lambda_1 \Lambda_2} = \frac{\mu \mu'}{|\mathbf{r}_{\Lambda_1} - \mathbf{r}_{\Lambda_2}|^3}, \quad (5.17)$$

and

$$U_{\Lambda_1 \Lambda_2} = \frac{\mu^2}{|\mathbf{r}_{\Lambda_1} - \mathbf{r}_{\Lambda_2}|^3}, \quad (5.18)$$

otherwise. In the interest of completeness, we note that we could also include the $s'p' \rightarrow p's'$ interaction by adding a term

$$\sum_{\Lambda_1, \Lambda_2} W_{\Lambda_1 \Lambda_2} \left[\left(\sigma_{s'p'}^+ \right)_{\Lambda_1} \left(\sigma_{s'p'}^- \right)_{\Lambda_2} + \text{h.c.} \right] \quad (5.19)$$

to the Hamiltonian of Eq. (5.13).

The Hamiltonian of Eq. (5.13) is entirely equivalent to the Hamiltonian of Eq. (5.1). The fact that Eq. (5.1) contains one set of spins corresponding to the primed sites and another set of spins corresponding to the unprimed sites is seen to arise from the fact that Eq. (5.13) can be viewed as containing two distinct types of operators. One type operates only on the s' and p' states and hence only on primed sites, while the other acts only on the s and p states and hence only on the unprimed sites. Eq. (5.13) appears more complicated than Eq. (5.1), but it actually embodies the general technique for constructing spin Hamiltonians for these systems, as we will see in Section 5.3.

5.3 Spin glass model for the cesium system

In the cesium experiments of Mourachko *et al.* [45, 44], there are three states that contribute to the experimental results. These are the $23s$, $23p$, and the $24s$ states, which we refer to as the s , p , and s' states, respectively. The processes $pp \rightarrow ss'$, $ps \rightarrow sp$, and $ps' \rightarrow s'p$ can occur. The $pp \rightarrow ss'$ process can be tuned in and out of resonance via the Stark shift by application of an electric field, while the $ps \rightarrow sp$ and $ps' \rightarrow s'p$ processes are always resonant. In the case of the cesium experiments, the $ps \rightarrow sp$ and $ps' \rightarrow s'p$ processes are of comparable strength and both must be considered.

Just as we did in Section 5.2, we define a column vector of length three for each site. If an atom at site Λ is in the s , p , or s' state, then the column vector corresponding to that site is $(0, 0, 1)^T$, $(0, 1, 0)^T$, or $(1, 0, 0)^T$, respectively. The Hamiltonian for this system is then

$$\begin{aligned} H_{\text{Cs}} = & \sum_{\Lambda} \epsilon_{\Lambda} + \\ & \sum_{\Lambda_1, \Lambda_2} V_{\Lambda_1 \Lambda_2} \left[\left(\sigma_{ps'}^+ \right)_{\Lambda_1} \left(\sigma_{ps}^- \right)_{\Lambda_2} + \text{h.c.} \right] + \sum_{\Lambda_1, \Lambda_2} U_{\Lambda_1 \Lambda_2} \left[\left(\sigma_{ps'}^+ \right)_{\Lambda_1} \left(\sigma_{ps'}^- \right)_{\Lambda_2} + \text{h.c.} \right] + \\ & \sum_{\Lambda_1, \Lambda_2} W_{\Lambda_1 \Lambda_2} \left[\left(\sigma_{ps}^- \right)_{\Lambda_1} \left(\sigma_{ps}^+ \right)_{\Lambda_2} + \text{h.c.} \right], \end{aligned} \quad (5.20)$$

where ϵ , $\sigma_{ps'}^\pm$, and σ_{ps}^\pm are the 3×3 matrices

$$\epsilon = \begin{pmatrix} \epsilon_{s'} & 0 & 0 \\ 0 & \epsilon_p & 0 \\ 0 & 0 & \epsilon_s \end{pmatrix}, \quad (5.21)$$

$$\sigma_{ps'}^\pm = \begin{pmatrix} \sigma^\pm & 0 \\ & 0 \\ 0 & 0 & 0 \end{pmatrix}, \quad (5.22)$$

and

$$\sigma_{ps}^\pm = \begin{pmatrix} 0 & 0 & 0 \\ 0 & & \sigma^\pm \\ 0 & & \end{pmatrix}, \quad (5.23)$$

and the interaction potentials $V_{\Lambda_1\Lambda_2}$, $U_{\Lambda_1\Lambda_2}$, and $W_{\Lambda_1\Lambda_2}$ are zero if $\Lambda_1 = \Lambda_2$ and otherwise are the potentials corresponding to the $pp \rightarrow ss'$, $ps' \rightarrow s'p$, and $ps \rightarrow sp$ processes, respectively.

The equations of motion can be determined in this case as well, simply by computing commutators.

5.4 Summary

We have seen in this chapter how the frozen dipolar gases studied by Anderson *et al.* [5, 6] and Lowell *et al.* [40], as well as Mourachko *et al.* [45, 44], are completely equivalent to systems of interpenetrating spin glasses. Casting the problem in this form has the advantage that it becomes possible to at least write down equations that go beyond the sparse model of Chapters 2 and 4.

Chapter 6

The Effect of Spin

6.1 Introduction

Throughout most of Chapter 2, we used an interaction potential that varied as $1/r^3$, with no angular dependence. In Section 2.5 we discussed how to deal with interaction potentials that have a more complicated dependence on r , depend on the angular variables, or both. In this chapter we determine exactly what the spin-dependent interatomic potentials are for the $ss' \rightarrow pp'$ and $sp \rightarrow ps$ processes in the experiment we are modeling [5, 6, 40]. The interaction potential depends directly on the m_j values for the states involved, where m_j is the projection of the total angular momentum in the direction of the applied electric field. For states with $l = 0$, m_j is just the projection of the outer electron's spin. For states with $l = 1$, the spin-orbit coupling separates the states with $j = 3/2$ from the states with $j = 1/2$. Further, we assume that for $j = 3/2$, the applied electric field splits the states with $|m_j| = 3/2$ from those with $|m_j| = 1/2$. As is illustrated in Fig. 1.1, this is the case for the $34p$ states of Rb under the conditions of the experiments in which we are interested. Then, for each of the states we consider, $|m_j|$ is fixed and m_j can only take on the values $\pm|m_j|$, so that it is effectively equivalent to a spin of $1/2$. When we refer to spin effects in this chapter we mean, more precisely, the effects due to m_j which are derived from the spin-orbit coupling.

We start in Section 6.2 by examining the matrix elements of the dipole-dipole interaction in more detail, and taking into account the effect of the various atomic spin states. The techniques we use for doing this are inspired by Ref. [46], which we found to be extremely helpful in that it pointed us in the right direction when we began our study of spin effects in the frozen system. In

In Section 6.2.1 we recall the form of the dipole-dipole interaction potential and in Section 6.2.2 we begin the calculation of the dipolar matrix elements with the effects of the atomic states taken into consideration. This computation requires a change of basis of the atomic spin states, as explained in Section 6.2.3. In Section 6.2.4 the laborious procedure necessary to compute the individual matrix elements is explained, and the results are presented in tabular form.

Next, in Section 6.3 we attempt to determine the effective interaction potential for the resonant and nonresonant processes. We start in Section 6.3.1 by determining the states and probability amplitudes of the system when the complications due to the presence of atomic spin are taken into account. We proceed in Section 6.3.2 to discuss the corresponding equations of motion. We find, as expected, that in general the quantity m_j is not conserved. Therefore the number of interacting states for a system of $N + 1$ atoms is 2^{N+1} , whereas it is only $N + 1$ when the effects of spin are neglected. However, when states of $|m_j| = 3/2$ are involved it is still possible to obtain exact formulas as we did in Chapter 2, provided that the quantity V is replaced by an effective interaction. We refer to this case as the separable case, for reasons that will become apparent in Section 6.3.4. Section 6.3.3 concerns the properties of Dirac matrices, which are instrumental in our discussion of separability and its applicability to averaging in Section 6.3.4. In Section 6.3.5 we determine the effective interaction potential in the separable case. Finally, we summarize and conclude in Section 6.4.

6.2 Matrix elements for the $ss' \rightarrow pp'$ and $sp \rightarrow ps$ processes

6.2.1 The dipole-dipole interaction

We consider two atoms, the first with its nucleus located at \mathbf{x}_{nuc} and outer electron located at \mathbf{x}_{elec} , and the second with nucleus located at \mathbf{x}'_{nuc} and outer electron located at $\mathbf{x}'_{\text{elec}}$. Next we define

$$\mathbf{R} = \mathbf{x}_{\text{nuc}} - \mathbf{x}'_{\text{nuc}}, \quad (6.1)$$

$$\mathbf{r} = \mathbf{x}_{\text{elec}} - \mathbf{x}_{\text{nuc}}, \quad (6.2)$$

and

$$\mathbf{r}' = \mathbf{x}'_{\text{elec}} - \mathbf{x}'_{\text{nuc}}. \quad (6.3)$$

The potential for the electrostatic interaction between the two atoms is then, in atomic units,

$$U(\mathbf{r}, \mathbf{r}', \mathbf{R}) = \frac{1}{R} + \frac{1}{|\mathbf{R} + \mathbf{r}' - \mathbf{r}|} - \frac{1}{|\mathbf{R} + \mathbf{r}'|} - \frac{1}{|\mathbf{R} - \mathbf{r}|}. \quad (6.4)$$

The first two terms on the right hand side represent the interaction between the two nuclei and the interaction between the two electrons, respectively. The last two terms represent the interactions between a nucleus and the electron that belongs to the other atom.

As is shown on page 283 of Ref. [56] and in more detail on page 260 of Ref. [55], expanding Eq. (6.4) and keeping terms only to leading order in r/R and r'/R gives

$$U(\mathbf{r}, \mathbf{r}', \mathbf{R}) = \frac{\mathbf{r} \cdot \mathbf{r}' - 3(\hat{\mathbf{R}} \cdot \mathbf{r})(\hat{\mathbf{R}} \cdot \mathbf{r}')}{R^3}. \quad (6.5)$$

This is the well known result for the dipole-dipole potential between two atoms.

It is important to note that, although Eq. (6.5) is the same potential used in the derivation of the van der Waals interaction, the effects we study are transient effects that take place after the atoms have been allowed to interact only a very short time. Therefore they are quite different from the steady-state van der Waals effect.

6.2.2 Dipolar matrix elements

We will later be averaging over the positions of the atoms, so we only want to determine the angular dependence of the matrix elements. Thus the $1/R^3$ factor can be ignored until averaging, and we need only consider matrix elements of the type

$$\langle p | \langle p' | \mathbf{r} \cdot \mathbf{r}' - 3(\mathbf{r} \cdot \hat{\mathbf{R}})(\mathbf{r}' \cdot \hat{\mathbf{R}}) | s' \rangle | s \rangle, \quad (6.6)$$

or

$$\langle p | \langle s | \mathbf{r} \cdot \mathbf{r}' - 3(\mathbf{r} \cdot \hat{\mathbf{R}})(\mathbf{r}' \cdot \hat{\mathbf{R}}) | p \rangle | s \rangle. \quad (6.7)$$

Here we note that when we write the states $|a\rangle|b\rangle$ and $\langle c|\langle d|$ we really mean $|a\rangle \otimes |b\rangle$ and $\langle c| \otimes \langle d|$, respectively. In Section 6.2.4, where we deal with products of a great many states and the tensor products are more urgently called for, we will write the tensor product symbols out explicitly. For now, however, since we are only dealing with products of two states at a time, we omit them to save

space and make the notation a little simpler.

We now recall that, in the experiments we are modeling, s , s' , p , and p' refer to the $25s$, $33s$, $24p_{1/2}$, and $34p_{3/2}$ states, respectively. We also recall that there are really two distinct resonances in the $ss' \rightarrow pp'$ interaction, corresponding to whether $|m_j| = 1/2$ or $|m_j| = 3/2$ for the p' atom. The complication for the interaction potential enters through the p and p' states. Clearly the matrix element in Eq. (6.7) will be different for the case where the p state on the left has $m_j = 1/2$ and the one on the right has $m_j = -1/2$ than for the case where both p states have $m_j = 1/2$, because the p state with $m_j = 1/2$ will involve a different mixture of the p_x , p_y , and p_z states than the state where $m_j = -1/2$. The matrix element in Eq. (6.6) will similarly depend on the m_j values of the p and p' states, although there is some simplification because we are able to consider the p' states with $|m_j| = 1/2$ and those with $|m_j| = 3/2$ separately.

For simplicity, we define

$$\rho = \mathbf{r} \cdot \mathbf{r}' - 3 \left(\mathbf{r} \cdot \hat{\mathbf{R}} \right) \left(\mathbf{r}' \cdot \hat{\mathbf{R}} \right), \quad (6.8)$$

and we note that

$$\rho = xx' + yy' + zz' - 3 \left(x\hat{R}_x + y\hat{R}_y + z\hat{R}_z \right) \left(x'\hat{R}_x + y'\hat{R}_y + z'\hat{R}_z \right), \quad (6.9)$$

where $\hat{R}_x = \sin \theta \cos \phi$, $\hat{R}_y = \sin \theta \sin \phi$, and $\hat{R}_z = \cos \theta$.

Consider for a moment the matrix element

$$\langle p_a | \langle p'_b | xx' | s' \rangle | s \rangle = \langle p_a | x | s \rangle \langle p'_b | x' | s' \rangle, \quad (6.10)$$

where a and b can be x , y , or z . We can apply the usual parity argument to determine that $\langle p_a | x | s \rangle$ is nonzero only if $a = x$, and in that case is equal to the dipole moment μ . Similarly, $\langle p'_b | x' | s' \rangle$ is nonzero only if $b = x$, and in that case is equal to the dipole moment μ' . Thus we have

$$\begin{aligned} \langle p_a | \langle p'_b | xx' | s' \rangle | s \rangle &= \langle p_a | x | s \rangle \langle p'_b | x' | s' \rangle \\ &= \mu \mu' \delta_{ax} \delta_{bx}. \end{aligned} \quad (6.11)$$

Analogously,

$$\begin{aligned}\langle p_b | \langle s | x x' | p_a \rangle | s \rangle &= \langle p_b | x | s \rangle \langle s | x' | p_a \rangle \\ &= \mu^2 \delta_{ax} \delta_{bx}.\end{aligned}\quad (6.12)$$

In fact, the matrix elements we consider are a little more complicated than this. The atoms have a total spin $\mathbf{J} = \mathbf{L} + \mathbf{S}$. The potential ρ changes \mathbf{L} , but does not at all affect \mathbf{S} and therefore cannot change s or m_s . Therefore the matrix elements we really consider are of the form

$$\begin{aligned}\langle p_a, \alpha | \langle p'_b, \beta | x x' | s', \gamma \rangle | s, \epsilon \rangle &= \langle p_a, \alpha | x | s, \epsilon \rangle \langle p'_b, \beta | x' | s', \gamma \rangle \\ &= \mu \mu' \delta_{ax} \delta_{bx} \delta_{\alpha\epsilon} \delta_{\beta\gamma},\end{aligned}\quad (6.13)$$

where, for example, $|s, \alpha\rangle$ is short for $|s, m_s = \alpha\rangle$. Analogously,

$$\begin{aligned}\langle p_a, \alpha | \langle s, \beta | x x' | p_b, \gamma \rangle | s, \epsilon \rangle &= \langle p_a, \alpha | x | s, \epsilon \rangle \langle s, \beta | x' | p_b, \gamma \rangle \\ &= \mu^2 \delta_{ax} \delta_{bx} \delta_{\alpha\epsilon} \delta_{\beta\gamma}.\end{aligned}\quad (6.14)$$

Using Eqs. (6.13) and (6.14), it is trivial to see that

$$\langle p_a, \alpha | \langle p'_b, \beta | \rho | s', \gamma \rangle | s, \epsilon \rangle = \mu \mu' \left(\delta_{ab} - 3 \hat{R}_a \hat{R}_b \right) \delta_{\alpha\epsilon} \delta_{\beta\gamma}, \quad (6.15)$$

and

$$\langle p_a, \alpha | \langle s, \beta | \rho | p_b, \gamma \rangle | s, \epsilon \rangle = \mu^2 \left(\delta_{ab} - 3 \hat{R}_a \hat{R}_b \right) \delta_{\alpha\epsilon} \delta_{\beta\gamma}. \quad (6.16)$$

6.2.3 A change of basis

We can easily write out the states s , s' , p , and p' in terms of states of the form $|j, l, m_j\rangle$. For example, the state s denotes the pair of states $|j = 1/2, l = 0, m_j = 1/2\rangle$ and $|j = 1/2, l = 0, m_j = -1/2\rangle$, while the state s' denotes the pair of states $|j' = 1/2, l' = 0, m_j = 1/2\rangle$ and $|j' = 1/2, l' = 0, m_j = -1/2\rangle$. Similarly, p denotes the pair of states $|j = 1/2, l = 1, m_j = 1/2\rangle$ and $|j = 1/2, l = 1, m_j = -1/2\rangle$. Recalling that the p' states with $|m_j| = 3/2$ are treated separately from those with $|m_j| = 1/2$, we see that p' denotes either the pair of states $|j' = 3/2, l' = 1, m_j = 3/2\rangle$ and $|j' = 3/2, l' = 1, m_j = -3/2\rangle$, or the pair of states $|j' = 3/2, l' = 1, m_j = 1/2\rangle$ and $|j' = 3/2, l' = 1, m_j = -1/2\rangle$. In order to use

State	Decomposition
$ j = \frac{3}{2}, m_j = \frac{3}{2}\rangle$	$-\frac{1}{\sqrt{2}} (p_x, \frac{1}{2}\rangle + i p_y, \frac{1}{2}\rangle)$
$ j = \frac{3}{2}, m_j = -\frac{3}{2}\rangle$	$\frac{1}{\sqrt{2}} (p_x, -\frac{1}{2}\rangle - i p_y, -\frac{1}{2}\rangle)$
$ j = \frac{3}{2}, m_j = \frac{1}{2}\rangle$	$\sqrt{\frac{2}{3}} p_z, \frac{1}{2}\rangle - \frac{1}{\sqrt{6}} (p_x, -\frac{1}{2}\rangle + i p_y, -\frac{1}{2}\rangle)$
$ j = \frac{3}{2}, m_j = -\frac{1}{2}\rangle$	$\sqrt{\frac{2}{3}} p_z, -\frac{1}{2}\rangle + \frac{1}{\sqrt{6}} (p_x, \frac{1}{2}\rangle - i p_y, \frac{1}{2}\rangle)$
$ j = \frac{1}{2}, m_j = \frac{1}{2}\rangle$	$-\frac{1}{\sqrt{3}} p_z, \frac{1}{2}\rangle - \frac{1}{\sqrt{3}} (p_x, -\frac{1}{2}\rangle + i p_y, -\frac{1}{2}\rangle)$
$ j = \frac{1}{2}, m_j = -\frac{1}{2}\rangle$	$\frac{1}{\sqrt{3}} p_z, -\frac{1}{2}\rangle - \frac{1}{\sqrt{3}} (p_x, \frac{1}{2}\rangle - i p_y, \frac{1}{2}\rangle)$

Table 6.1: The decomposition of all p and p' states into linear combinations of states of the form $|p_a, m_s\rangle$.

Eqs. (6.15) and (6.16), we have to write the p and p' states as linear combinations of states of the form $|p_a, m_s\rangle$. This is easily done by consulting a table of Clebsch-Gordan coefficients, as can be found on pages 76–77 of Ref. [14]. Using such a table, we determine the decompositions in Table 6.1.

6.2.4 The $ss' \rightarrow pp'$ and $sp \rightarrow ps$ matrix elements

With the decomposition of Table 6.1 and the rules of Eqs. (6.15) and (6.16) in hand, it is now possible to compute the matrix elements we need. I will first show how to compute one matrix element, as an example, then present all the matrix elements in table form.

Consider the matrix element

$$\left\langle p, m_j = -\frac{1}{2} \left| \left\langle p', m_j = \frac{3}{2} \left| \frac{\rho}{\mu\mu'} \right| s', m_j = \frac{1}{2} \right\rangle \right| s, m_j = -\frac{1}{2} \right\rangle. \quad (6.17)$$

We have from Table 6.1 that

$$\left| p', m_j = \frac{3}{2} \right\rangle = -\frac{1}{\sqrt{2}} \left(\left| p'_x, \frac{1}{2} \right\rangle + i \left| p'_y, \frac{1}{2} \right\rangle \right), \quad (6.18)$$

and

$$\left| p, m_j = -\frac{1}{2} \right\rangle = \frac{1}{\sqrt{3}} \left| p_z, -\frac{1}{2} \right\rangle - \frac{1}{\sqrt{3}} \left(\left| p_x, \frac{1}{2} \right\rangle - i \left| p_y, \frac{1}{2} \right\rangle \right). \quad (6.19)$$

Dropping the occurrences of “ $m_j =$ ” that appear to save space, we see that

$$\begin{aligned} \left\langle p, -\frac{1}{2} \left| \left\langle p', \frac{3}{2} \right| \right. &= \left[\frac{1}{\sqrt{3}} \left| p_z, -\frac{1}{2} \right\rangle - \frac{1}{\sqrt{3}} \left(\left| p_x, \frac{1}{2} \right\rangle - i \left| p_y, \frac{1}{2} \right\rangle \right) \right]^\dagger \times \\ &\left[-\frac{1}{\sqrt{2}} \left(\left| p'_x, \frac{1}{2} \right\rangle + i \left| p'_y, \frac{1}{2} \right\rangle \right) \right]^\dagger \end{aligned}$$

$\rho/(\mu\mu')$	$ s', \frac{1}{2}\rangle s, \frac{1}{2}\rangle$	$ s', \frac{1}{2}\rangle s, -\frac{1}{2}\rangle$	$ s', -\frac{1}{2}\rangle s, \frac{1}{2}\rangle$	$ s', -\frac{1}{2}\rangle s, -\frac{1}{2}\rangle$
$\langle p, \frac{1}{2} \langle p', \frac{3}{2} $	$-\sqrt{\frac{3}{2}} \cos \theta \sin \theta e^{i\phi}$	$-\sqrt{\frac{3}{2}} \sin^2 \theta e^{2i\phi}$	0	0
$\langle p, -\frac{1}{2} \langle p', \frac{3}{2} $	$-\frac{1}{\sqrt{6}} (1 - 3 \cos^2 \theta)$	$\sqrt{\frac{3}{2}} \cos \theta \sin \theta e^{i\phi}$	0	0
$\langle p, \frac{1}{2} \langle p', -\frac{3}{2} $	0	0	$\sqrt{\frac{3}{2}} \cos \theta \sin \theta e^{-i\phi}$	$\frac{1}{\sqrt{6}} (1 - 3 \cos^2 \theta)$
$\langle p, -\frac{1}{2} \langle p', -\frac{3}{2} $	0	0	$\sqrt{\frac{3}{2}} \sin^2 \theta e^{-2i\phi}$	$-\sqrt{\frac{3}{2}} \cos \theta \sin \theta e^{-i\phi}$

Table 6.2: The matrix elements $\langle p, m_j | \langle p', m_j | \rho/(\mu\mu') | s', m_j \rangle | s, m_j \rangle$ for the $ss' \rightarrow pp'$ process when $|m_j| = 3/2$ for the p' atom.

$$\begin{aligned}
&= \left[\frac{1}{\sqrt{3}} \left\langle p_z, -\frac{1}{2} \right| - \frac{1}{\sqrt{3}} \left(\left\langle p_x, \frac{1}{2} \right| + i \left\langle p_y, \frac{1}{2} \right| \right) \right] \times \\
&\quad \left[-\frac{1}{\sqrt{2}} \left(\left\langle p'_x, \frac{1}{2} \right| - i \left\langle p'_y, \frac{1}{2} \right| \right) \right] \\
&= \frac{1}{\sqrt{6}} \left\{ -\left\langle p_z, -\frac{1}{2} \right| \left\langle p'_x, \frac{1}{2} \right| + \left\langle p_x, \frac{1}{2} \right| \left\langle p'_x, \frac{1}{2} \right| + i \left\langle p_y, \frac{1}{2} \right| \left\langle p'_x, \frac{1}{2} \right| + \right. \\
&\quad \left. i \left\langle p_z, -\frac{1}{2} \right| \left\langle p'_y, \frac{1}{2} \right| - i \left\langle p_x, \frac{1}{2} \right| \left\langle p'_y, \frac{1}{2} \right| + \left\langle p_y, \frac{1}{2} \right| \left\langle p'_y, \frac{1}{2} \right| \right\}. \quad (6.20)
\end{aligned}$$

Now we simply apply Eq. (6.15) to each matrix element corresponding to a term in the sum of Eq. (6.20). For example, the first term in the sum corresponds to the matrix element

$$-\frac{1}{\sqrt{6}} \left\langle p_z, -\frac{1}{2} \right| \left\langle p'_x, \frac{1}{2} \right| \frac{\rho}{\mu\mu'} \left| s', \frac{1}{2} \right\rangle \left| s, -\frac{1}{2} \right\rangle, \quad (6.21)$$

which according to Eq. (6.15) is equal to

$$-\frac{1}{\sqrt{6}} \left(-3\hat{R}_x \hat{R}_z \right) = \sqrt{\frac{3}{2}} \sin \theta \cos \theta \cos \phi. \quad (6.22)$$

Computing the other terms similarly and summing them, we determine one of the matrix elements for the $ss' \rightarrow pp'$ process.

The process is straightforward, albeit laborious, and one obtains the matrix elements presented in the Tables 6.2 – 6.4.

6.3 Determining the potential

$\rho/(\mu\mu')$	$ s', \frac{1}{2}\rangle s, \frac{1}{2}\rangle$	$ s', \frac{1}{2}\rangle s, -\frac{1}{2}\rangle$	$ s', -\frac{1}{2}\rangle s, \frac{1}{2}\rangle$	$ s', -\frac{1}{2}\rangle s, -\frac{1}{2}\rangle$
$\langle p, \frac{1}{2} \langle p', \frac{1}{2} $	$-\frac{\sqrt{2}}{3} (1 - 3 \cos^2 \theta)$	$\sqrt{2} \cos \theta \sin \theta e^{i\phi}$	$-\frac{1}{\sqrt{2}} \cos \theta \sin \theta e^{i\phi}$	$-\frac{1}{\sqrt{2}} \sin^2 \theta e^{2i\phi}$
$\langle p, -\frac{1}{2} \langle p', \frac{1}{2} $	$\sqrt{2} \cos \theta \sin \theta e^{-i\phi}$	$\frac{\sqrt{2}}{3} (1 - 3 \cos^2 \theta)$	$-\frac{1}{3\sqrt{2}} (1 - 3 \cos^2 \theta)$	$\frac{1}{\sqrt{2}} \cos \theta \sin \theta e^{i\phi}$
$\langle p, \frac{1}{2} \langle p', -\frac{1}{2} $	$\frac{1}{\sqrt{2}} \cos \theta \sin \theta e^{-i\phi}$	$\frac{1}{3\sqrt{2}} (1 - 3 \cos^2 \theta)$	$-\frac{\sqrt{2}}{3} (1 - 3 \cos^2 \theta)$	$\sqrt{2} \cos \theta \sin \theta e^{i\phi}$
$\langle p, -\frac{1}{2} \langle p', -\frac{1}{2} $	$\frac{1}{\sqrt{2}} \sin^2 \theta e^{-2i\phi}$	$-\frac{1}{\sqrt{2}} \cos \theta \sin \theta e^{-i\phi}$	$\sqrt{2} \cos \theta \sin \theta e^{-i\phi}$	$\frac{\sqrt{2}}{3} (1 - 3 \cos^2 \theta)$

Table 6.3: The matrix elements $\langle p, m_j | \langle p', m_j | \rho/(\mu\mu') | s', m_j \rangle | s, m_j \rangle$ for the $ss' \rightarrow pp'$ process when $|m_j| = 1/2$ for the p' atom.

ρ/μ^2	$ p, \frac{1}{2}\rangle s, \frac{1}{2}\rangle$	$ p, \frac{1}{2}\rangle s, -\frac{1}{2}\rangle$	$ p, -\frac{1}{2}\rangle s, \frac{1}{2}\rangle$	$ p, -\frac{1}{2}\rangle s, -\frac{1}{2}\rangle$
$\langle p, \frac{1}{2} \langle s, \frac{1}{2} $	$\frac{1}{3} (1 - 3 \cos^2 \theta)$	$-\cos \theta \sin \theta e^{-i\phi}$	$-\cos \theta \sin \theta e^{-i\phi}$	$-\sin^2 \theta e^{-2i\phi}$
$\langle p, \frac{1}{2} \langle s, -\frac{1}{2} $	$-\cos \theta \sin \theta e^{i\phi}$	$-\frac{1}{3} (1 - 3 \cos^2 \theta)$	$-\frac{1}{3} (1 - 3 \cos^2 \theta)$	$\cos \theta \sin \theta e^{-i\phi}$
$\langle p, -\frac{1}{2} \langle s, \frac{1}{2} $	$-\cos \theta \sin \theta e^{i\phi}$	$-\frac{1}{3} (1 - 3 \cos^2 \theta)$	$-\frac{1}{3} (1 - 3 \cos^2 \theta)$	$\cos \theta \sin \theta e^{-i\phi}$
$\langle p, -\frac{1}{2} \langle s, -\frac{1}{2} $	$-\sin^2 \theta e^{2i\phi}$	$\cos \theta \sin \theta e^{i\phi}$	$\cos \theta \sin \theta e^{i\phi}$	$\frac{1}{3} (1 - 3 \cos^2 \theta)$

Table 6.4: The matrix elements $\langle p, m_j | \langle s, m_j | \rho/(\mu^2) | p, m_j \rangle | s, m_j \rangle$ for the $sp \rightarrow ps$ process.

6.3.1 States and probability amplitudes with spin included

In the initial state, the system is labeled by an index $|s', m_j\rangle$ representing the state of the s' atom and a set of N indices $\{|s, m_j\rangle\}$ representing the states of the N s atoms. In the absence of an applied magnetic field, the initial values of these indices are random. The state corresponding to the configuration where the primed atom is in the s' state with $m_j = \alpha_0$ and the unprimed atoms are all in the s state with $\{m_j\} = \{\alpha_0; \alpha_1, \dots, \alpha_N\}$ is

$$|s', \alpha_0\rangle \otimes |s, \alpha_1\rangle \otimes \dots \otimes |s, \alpha_N\rangle. \quad (6.23)$$

Of course, because the s and s' states have total spin $1/2$, all α_k are required to have the value $1/2$ or $-1/2$. The probability amplitude corresponding to this state is

$$a_{\{\alpha_0; \alpha_1, \dots, \alpha_N\}}(t) = \langle s, \alpha_N | \otimes \dots \otimes \langle s, \alpha_1 | \otimes \langle s', \alpha_0 | \psi(t), \quad (6.24)$$

where $|\psi(t)\rangle$ is the state of the system at time t .

Because the system is allowed to make $ss' \rightarrow pp'$ transitions, we must also consider states in which the primed atom is in the state p' and a single unprimed atom is in the state p . This state is labeled by the indices $|p', m_j\rangle$ and $|p, m_j\rangle$, together with the indices $\{|s, m_j\rangle\}$ corresponding to the s atoms not involved in the $ss' \rightarrow pp'$ transition. The state corresponding to the configuration

where the primed atom is in the p' state with $m_j = \beta_0$ and all the unprimed atoms except for the k th are in the s state while the k th unprimed atom is in the p state with $m_j = \beta_k$ is

$$|p', \beta_0\rangle \otimes |s, \beta_1\rangle \otimes \cdots \otimes |s, \beta_{k-1}\rangle \otimes |p, \beta_k\rangle \otimes |s, \beta_{k+1}\rangle \otimes \cdots \otimes |s, \beta_N\rangle. \quad (6.25)$$

The quantities $\beta_1, \dots, \beta_{k-1}, \beta_{k+1}, \dots, \beta_N$ are restricted to the values $\pm 1/2$ because the s state has total spin $1/2$. Because the p state also has total spin $1/2$, β_k is similarly restricted to the values $\pm 1/2$. The p' state has total spin $3/2$, and the quantity β_0 is restricted to the values $\pm 3/2$ or $\pm 1/2$, depending on whether we are considering the $|m_j| = 3/2$ or $|m_j| = 1/2$ resonance, respectively. Similarly to Eq. (6.24), the probability amplitude corresponding to the state in Eq. (6.25) is

$$c_{k; \{\beta_0; \beta_1, \dots, \beta_N\}}(t) = \langle s, \beta_N | \otimes \cdots \otimes \langle s, \beta_{k+1} | \otimes \langle p, \beta_k | \otimes \langle s, \beta_{k-1} | \otimes \cdots \otimes \langle p', \beta_0 | \} |\psi(t)\rangle, \quad (6.26)$$

where $|\psi(t)\rangle$ is again the state of the system at time t .

6.3.2 Equations of motion

In the interest of brevity, we denote the subscript lists

$$\{\alpha_0; \alpha_1, \dots, \alpha_N\}, \quad (6.27)$$

and

$$\{\gamma_0; \beta_1, \dots, \beta_{k-1}, \gamma_k, \beta_{k+1}, \dots, \beta_N\} \quad (6.28)$$

by A and $B_k(\gamma_0, \gamma_k)$, respectively. We label the 0th and k th components of $B_k(\gamma_0, \gamma_k)$ with a different symbol than the rest because we will sum over $B_k(\gamma_0, \gamma_k)$, and it will turn out that the $B_k(\gamma_0, \gamma_k)$ term in the sum corresponds to the s' atom at the origin and the s atom at position \mathbf{r}_k making the $ss' \rightarrow pp'$ transition. Thus the use of a different symbol serves as a reminder of which atoms are involved in the transition.

The equations of motion for the a and c coefficients of Eqs. (6.24) and Eqs. (6.26) in Fourier space are then

$$(\omega - \Delta) a_A = i \prod_{m=0}^N \delta_{\alpha_m, \alpha_m^{(i)}} + \sum_{k=1}^N \sum_{B_k(\gamma_0, \gamma_k)} V_k M_{A, B_k(\gamma_0, \gamma_k)}^{(k)} c_{k; B_k(\gamma_0, \gamma_k)}, \quad (6.29a)$$

$$\omega c_{k;B_k(\gamma_0,\gamma_k)} = \sum_{A'} V_k M_{B_k(\gamma_0,\gamma_k),A'}^{(k)} a_{A'}, \quad (6.29b)$$

where $\alpha_m^{(i)}$ is the initial m_j value for the m th atom and

$$V_k = \frac{\mu\mu'}{r_k^3} \quad (6.30)$$

is just the radial part of the interaction potential. Here we have defined $A' = \{\alpha'_0; \alpha'_1, \dots, \alpha'_N\}$ to be another set of indices subject to the same constraints as A . The matrix $M_{B_k(\gamma_0,\gamma_k),A}^{(k)}$ is a $2^{N+1} \times 2^{N+1}$ matrix that is constructed from the 4×4 matrix formed by Table 6.2 or 6.3, depending on whether we are considering the case where the p' atom has $|m_j| = 3/2$ or $|m_j| = 1/2$. Explicitly, if the set of

$$m_{\{\beta,\beta'\},\{\alpha,\alpha'\}}(\theta_k, \phi_k) = \left\langle p, \beta \left| \left\langle p', \beta' \left| \frac{\rho}{\mu\mu'} \right| s', \alpha' \right\rangle \right| s, \alpha \right\rangle \quad (6.31)$$

are the elements belonging to the 4×4 matrix that corresponds to the value of $|m_j|$ that we want for the p' state, then

$$M_{B_k(\gamma_0,\gamma_k),A}^{(k)} = m_{\{\gamma_0,\gamma_k\},\{\alpha_0,\alpha_k\}}(\theta_k, \phi_k) \prod_{l=1, l \neq k}^N \delta_{\alpha_l \beta_l}. \quad (6.32)$$

We see immediately from Eqs. (6.32) and (6.31) that

$$M_{A,B_k(\gamma_0,\gamma_k)}^{(k)} = \left[M_{B_k(\gamma_0,\gamma_k),A}^{(k)} \right]^*. \quad (6.33)$$

Multiplying both sides of Eq. (6.29b) by $V_k M_{A,B_k(\gamma_0,\gamma_k)}^{(k)}$ and summing over k and $B_k(\gamma_0, \gamma_k)$, we see that

$$\omega \sum_{k=1}^N \sum_{B_k(\gamma_0,\gamma_k)} V_k M_{A,B_k(\gamma_0,\gamma_k)}^{(k)} c_{k;B_k(\gamma_0,\gamma_k)} = \sum_{k=1}^N \sum_{A'} V_k^2 P_{A,A'}^{(k)} a_{A'}, \quad (6.34)$$

where

$$P_{A,A'}^{(k)} = \sum_{B_k(\gamma_0,\gamma_k)} M_{A,B_k(\gamma_0,\gamma_k)}^{(k)} M_{B_k(\gamma_0,\gamma_k),A'}^{(k)}. \quad (6.35)$$

Using Eq. (6.33) we see that, in terms of matrices, Eq. (6.35) is equivalent to

$$P^{(k)} = \left[M^{(k)} \right]^\dagger M^{(k)}. \quad (6.36)$$

Plugging the result of Eq. (6.34) into Eq. (6.29a), we see that

$$\omega(\omega - \Delta)a_A = i\omega \prod_{m=0}^N \delta_{\alpha_m, \alpha_m^{(i)}} + \sum_{k=1}^N \sum_{A'} V_k^2 P_{A,A'}^{(k)} a_{A'}. \quad (6.37)$$

For $N + 1$ atoms, this represents 2^{N+1} equations.

The quantity a_A actually depends on the two sets of indices A and $A^{(i)} = \{\alpha_0^{(i)}; \alpha_1^{(i)}, \dots, \alpha_N^{(i)}\}$, as is clear from the first term on the right hand side of Eq. (6.37). Therefore we can consider a to be a matrix, and we can write

$$\omega(\omega - \Delta)a = i\omega + \sum_{k=1}^N V_k^2 P^{(k)} a. \quad (6.38)$$

At this point we solve this equation formally and switch to Laplace space by making the substitution $\omega = i\alpha$. We find

$$\begin{aligned} a &= \frac{\alpha}{\alpha(\alpha + i\Delta) + \sum_{k=1}^N V_k^2 P^{(k)}} \\ &= \alpha \int_0^\infty d\beta \exp[-\beta\alpha(\alpha + i\Delta)] \exp\left[-\beta \sum_{k=1}^N V_k^2 P^{(k)}\right]. \end{aligned} \quad (6.39)$$

Because Eq. (6.29b) is coupled to Eq. (6.29a), $c_{k,B_k(\gamma_0, \gamma_k)}$ also depends on the set of indices $A^{(i)}$. Thus c_k can also be considered a matrix, and we can rewrite Eqs. (6.29a) and (6.29b) in the matrix form

$$(\omega - \Delta)a = i + \sum_{k=1}^N V_k \left[M^{(k)} \right]^\dagger c_k, \quad (6.40a)$$

$$\omega c_k = V_k M^{(k)} a. \quad (6.40b)$$

We note that these equations correspond to Eqs. (2.1a) and (2.1b), and so we hope to obtain an expression for $\tilde{S}(\Delta, \alpha)$ analogous to Eq. (2.7). We have to exercise a little caution, however, since Eqs. (2.1a) and (2.1b) are equations for scalar quantities while Eqs. (6.40a) and (6.40b) are matrix equations. First consider Eq. (6.39) in the rational form we had before we introduced the integral over β . Because the matrix $\sum_{k=1}^N V_k^2 P^{(k)}$ is Hermitian we can diagonalize it. If we let $|\lambda\rangle$ be the

eigenstate of $\sum_{k=1}^N V_k^2 P^{(k)}$ with eigenvalue λ , then

$$\langle \lambda | a | \lambda \rangle = \frac{\alpha}{\alpha(\alpha + i\Delta) + \lambda^2}. \quad (6.41)$$

The quantity $\langle \lambda | a | \lambda \rangle$ is just a scalar, so we can certainly invert this Laplace transform, take the mod square, and Laplace transform again just as we did in Section 2.2. In this way we find that

$$\langle \lambda | \tilde{S}(\Delta, \alpha) | \lambda \rangle = \frac{1}{2\alpha} \left[1 - \frac{\alpha^2 + \Delta^2}{\alpha^2 + \Delta^2 + 4\lambda^2} \right]. \quad (6.42)$$

We could do this for any of the eigenvectors $|\lambda\rangle$, and so it follows that

$$\begin{aligned} \tilde{S}(\Delta, \alpha) &= \frac{1}{2\alpha} \left[1 - \frac{\alpha^2 + \Delta^2}{\alpha^2 + \Delta^2 + 4 \sum_{k=1}^N V_k^2 P^{(k)}} \right] \\ &= \frac{1}{2\alpha} - \frac{\alpha^2 + \Delta^2}{2\alpha} \int_0^\infty d\beta \exp[-\beta(\alpha^2 + \Delta^2)] \exp \left[-4\beta \sum_{k=1}^N V_k^2 P^{(k)} \right], \end{aligned} \quad (6.43)$$

which looks very much like Eq. (2.7).

To obtain results that can be compared with the experiments, we also want to average over initial spin configurations and sum over final spin configurations. Thus we want to compute the quantity

$$\begin{aligned} \frac{1}{2^{N+1}} \text{Tr} \tilde{S}(\Delta, \alpha) &= \frac{1}{2\alpha} - \frac{\alpha^2 + \Delta^2}{2\alpha} \int_0^\infty d\beta \exp[-\beta(\alpha^2 + \Delta^2)] \times \\ &\quad \frac{1}{2^{N+1}} \text{Tr} \exp \left[-4\beta \sum_{k=1}^N V_k^2 P^{(k)} \right]. \end{aligned} \quad (6.44)$$

6.3.3 Dirac matrices

Before we go any further with Eq. (6.44), we first examine some properties of 4×4 matrices. It will turn out that this will aid us greatly in carrying out the average of Eq. (6.44).

We know from pages 211–213 of Ref. [7] that any 4×4 matrix can be written as a unique linear combination of the sixteen Dirac matrices. These matrices are of the form $\sigma_\alpha \otimes \sigma_\beta$, where α and β range from zero to three. Here we define σ_α to be the 2×2 unit matrix if $\alpha = 0$ and the usual Pauli matrix otherwise. Thus, if we have any 4×4 matrix Q then we can write

$$Q = \sum_{\alpha=0}^3 \sum_{\beta=0}^3 q_{\alpha\beta} \sigma_\alpha \otimes \sigma_\beta, \quad (6.45)$$

$P_{ss' \rightarrow pp', 3/2}$	$ s', \frac{1}{2}\rangle s, \frac{1}{2}\rangle$	$ s', \frac{1}{2}\rangle s, -\frac{1}{2}\rangle$	$ s', -\frac{1}{2}\rangle s, \frac{1}{2}\rangle$	$ s', -\frac{1}{2}\rangle s, -\frac{1}{2}\rangle$
$\langle s, \frac{1}{2} \langle s', \frac{1}{2} $	$\frac{3}{2} \sin^2 \theta$	$-\frac{1}{2} \sin(2\theta) e^{-i\phi}$	0	0
$\langle s, -\frac{1}{2} \langle s', \frac{1}{2} $	$-\frac{1}{2} \sin(2\theta) e^{i\phi}$	$\frac{1}{12} [5 + 3 \cos(2\theta)]$	0	0
$\langle s, \frac{1}{2} \langle s', -\frac{1}{2} $	0	0	$\frac{1}{12} [5 + 3 \cos(2\theta)]$	$\frac{1}{2} \sin(2\theta) e^{-i\phi}$
$\langle s, -\frac{1}{2} \langle s', -\frac{1}{2} $	0	0	$\frac{1}{2} \sin(2\theta) e^{i\phi}$	$\frac{3}{2} \sin^2 \theta$

Table 6.5: The P matrix for the $ss' \rightarrow pp'$ process when $|m_j| = 3/2$.

$P_{ss' \rightarrow pp', 1/2}$	$ s', \frac{1}{2}\rangle s, \frac{1}{2}\rangle$	$ s', \frac{1}{2}\rangle s, -\frac{1}{2}\rangle$	$ s', -\frac{1}{2}\rangle s, \frac{1}{2}\rangle$	$ s', -\frac{1}{2}\rangle s, -\frac{1}{2}\rangle$
$\langle s, \frac{1}{2} \langle s', \frac{1}{2} $	$\frac{1}{36} [29 + 3 \cos(2\theta)]$	$-\frac{1}{6} \sin(2\theta) e^{-i\phi}$	$-\frac{1}{3} \sin(2\theta) e^{-i\phi}$	$-\frac{2}{3} \sin^2 \theta e^{-2i\phi}$
$\langle s, -\frac{1}{2} \langle s', \frac{1}{2} $	$-\frac{1}{6} \sin(2\theta) e^{i\phi}$	$\frac{5}{36} [5 + 3 \cos(2\theta)]$	$\frac{1}{9} [5 + 3 \cos(2\theta)]$	$\frac{1}{3} \sin(2\theta) e^{-i\phi}$
$\langle s, \frac{1}{2} \langle s', -\frac{1}{2} $	$-\frac{1}{3} \sin(2\theta) e^{i\phi}$	$\frac{1}{9} [5 + 3 \cos(2\theta)]$	$\frac{2}{36} [5 + 3 \cos(2\theta)]$	$\frac{1}{6} \sin(2\theta) e^{-i\phi}$
$\langle s, -\frac{1}{2} \langle s', -\frac{1}{2} $	$-\frac{2}{3} \sin^2 \theta e^{2i\phi}$	$\frac{1}{3} \sin(2\theta) e^{i\phi}$	$\frac{1}{6} \sin(2\theta) e^{i\phi}$	$\frac{1}{36} [29 + 3 \cos(2\theta)]$

Table 6.6: The P matrix for the $ss' \rightarrow pp'$ process when $|m_j| = 1/2$.

for some coefficients $q_{\alpha\beta}$. These coefficients are in fact easy to determine, since

$$q_{\alpha\beta} = \frac{1}{4} \text{Tr} [Q(\sigma_\alpha \otimes \sigma_\beta)]. \quad (6.46)$$

Eq. (6.46) follows easily from the well-known properties of the Pauli matrices and the facts that

$$(A \otimes B)(C \otimes D) = (AC) \otimes (BD), \quad (6.47)$$

and

$$\text{Tr}(A \otimes B) = (\text{Tr} A)(\text{Tr} B). \quad (6.48)$$

Let $M_{ss' \rightarrow pp', \frac{3}{2}}$, $M_{ss' \rightarrow pp', \frac{1}{2}}$, and $M_{sp \rightarrow ps}$ be the 4×4 matrices determined by Tables 6.2 – 6.4.

Then define

$$P_{ss' \rightarrow pp', \frac{3}{2}} = M_{ss' \rightarrow pp', \frac{3}{2}}^\dagger M_{ss' \rightarrow pp', \frac{3}{2}}, \quad (6.49)$$

and similarly for $P_{ss' \rightarrow pp', \frac{1}{2}}$ and $P_{sp \rightarrow ps}$. We will see in Section 6.3.4 that these three matrices are very important when it comes to averaging Eq. (6.44). Therefore we present the three P matrices in Tables 6.5–6.7.

We will also see in Section 6.3.4 that in order to obtain the average of Eq. (6.44) we will need the decompositions of the P matrices into linear combinations of the Dirac matrices. We have seen that we can use Eqs. (6.45) and (6.46) to determine these linear combinations, and in this way we

$P_{sp \rightarrow ps}$	$ p, \frac{1}{2}\rangle s, \frac{1}{2}\rangle$	$ p, \frac{1}{2}\rangle s, -\frac{1}{2}\rangle$	$ p, -\frac{1}{2}\rangle s, \frac{1}{2}\rangle$	$ p, -\frac{1}{2}\rangle s, -\frac{1}{2}\rangle$
$\langle s, \frac{1}{2} \langle p, \frac{1}{2} $	$\frac{1}{9} [7 - 3 \cos(2\theta)]$	$-\frac{1}{3} \sin(2\theta) e^{-i\phi}$	$-\frac{1}{3} \sin(2\theta) e^{-i\phi}$	$-\frac{2}{3} \sin^2 \theta e^{-2i\phi}$
$\langle s, -\frac{1}{2} \langle p, \frac{1}{2} $	$-\frac{1}{3} \sin(2\theta) e^{i\phi}$	$\frac{1}{9} [5 + 3 \cos(2\theta)]$	$\frac{1}{9} [5 + 3 \cos(2\theta)]$	$\frac{1}{3} \sin(2\theta) e^{-i\phi}$
$\langle s, \frac{1}{2} \langle p, -\frac{1}{2} $	$-\frac{1}{3} \sin(2\theta) e^{i\phi}$	$\frac{1}{9} [5 + 3 \cos(2\theta)]$	$\frac{1}{9} [5 + 3 \cos(2\theta)]$	$\frac{1}{3} \sin(2\theta) e^{-i\phi}$
$\langle s, -\frac{1}{2} \langle p, -\frac{1}{2} $	$-\frac{2}{3} \sin^2 \theta e^{2i\phi}$	$\frac{1}{3} \sin(2\theta) e^{i\phi}$	$\frac{1}{3} \sin(2\theta) e^{i\phi}$	$\frac{1}{9} [7 - 3 \cos(2\theta)]$

Table 6.7: The P matrix for the $sp \rightarrow ps$ process.

Dirac Matrix	Projection
$\sigma_0 \otimes \sigma_0$	$\frac{1}{12} [7 - 3 \cos(2\theta)]$
$\sigma_0 \otimes \sigma_1$	0
$\sigma_0 \otimes \sigma_2$	0
$\sigma_0 \otimes \sigma_3$	0
$\sigma_1 \otimes \sigma_0$	0
$\sigma_1 \otimes \sigma_1$	0
$\sigma_1 \otimes \sigma_2$	0
$\sigma_1 \otimes \sigma_3$	0
$\sigma_2 \otimes \sigma_0$	0
$\sigma_2 \otimes \sigma_1$	0
$\sigma_2 \otimes \sigma_2$	0
$\sigma_2 \otimes \sigma_3$	0
$\sigma_3 \otimes \sigma_0$	0
$\sigma_3 \otimes \sigma_1$	$-\frac{1}{2} \sin(2\theta) \cos \phi$
$\sigma_3 \otimes \sigma_2$	$-\frac{1}{2} \sin(2\theta) \sin \phi$
$\sigma_3 \otimes \sigma_3$	$\frac{1}{6} [1 - 3 \cos(2\theta)]$

Table 6.8: Projections of the 4×4 matrix P onto the Dirac matrices for the $ss' \rightarrow pp'$ process when $|m_j| = 3/2$ for the p' atom.

obtain Tables 6.8–6.10.

6.3.4 Separability

At this point we would like to write

$$\exp \left[-\beta \sum_k V_k^2 P^{(k)} \right] = \prod_k \exp \left[-\beta V_k^2 P^{(k)} \right], \quad (6.50)$$

so that we can perform our usual averaging procedure as described in Section 2.3. Unfortunately, Eq. (6.50) does not hold unless the commutator of $P^{(k)}$ with $P^{(l)}$ is a c -number. We can use Tables 6.8–6.10 to check if this is the case for our three potentials.

Because it is the simplest, we first consider the potential for the $ss' \rightarrow pp'$ process when $|m_j| =$

<i>Dirac Matrix</i>	<i>Projection</i>
$\sigma_0 \otimes \sigma_0$	$\frac{1}{4} [3 + \cos(2\theta)]$
$\sigma_0 \otimes \sigma_1$	0
$\sigma_0 \otimes \sigma_2$	0
$\sigma_0 \otimes \sigma_3$	0
$\sigma_1 \otimes \sigma_0$	0
$\sigma_1 \otimes \sigma_1$	$\frac{1}{18} [5 + 3 \cos(2\theta) - 6 \sin^2 \theta \cos(2\phi)]$
$\sigma_1 \otimes \sigma_2$	$-\frac{1}{3} \sin^2 \theta \sin(2\phi)$
$\sigma_1 \otimes \sigma_3$	$-\frac{1}{3} \sin(2\theta) \cos \phi$
$\sigma_2 \otimes \sigma_0$	0
$\sigma_2 \otimes \sigma_1$	$-\frac{1}{3} \sin^2 \theta \sin(2\phi)$
$\sigma_2 \otimes \sigma_2$	$\frac{1}{18} [5 + 3 \cos(2\theta) + 6 \sin^2 \theta \cos(2\phi)]$
$\sigma_2 \otimes \sigma_3$	$-\frac{1}{3} \sin(2\theta) \sin \phi$
$\sigma_3 \otimes \sigma_0$	0
$\sigma_3 \otimes \sigma_1$	$-\frac{1}{6} \sin(2\theta) \cos \phi$
$\sigma_3 \otimes \sigma_2$	$-\frac{1}{6} \sin(2\theta) \sin \phi$
$\sigma_3 \otimes \sigma_3$	$\frac{1}{18} [1 - 3 \cos(2\theta)]$

Table 6.9: Projections of the 4×4 matrix P onto the Dirac matrices for the $ss' \rightarrow pp'$ process when $|m_j| = 1/2$ for the p' atom.

<i>Dirac Matrix</i>	<i>Projection</i>
$\sigma_0 \otimes \sigma_0$	$\frac{2}{3}$
$\sigma_0 \otimes \sigma_1$	0
$\sigma_0 \otimes \sigma_2$	0
$\sigma_0 \otimes \sigma_3$	0
$\sigma_1 \otimes \sigma_0$	0
$\sigma_1 \otimes \sigma_1$	$\frac{1}{18} [5 + 3 \cos(2\theta) - 6 \cos(2\phi) \sin^2 \theta]$
$\sigma_1 \otimes \sigma_2$	$-\frac{1}{3} \sin^2 \theta \sin(2\phi)$
$\sigma_1 \otimes \sigma_3$	$-\frac{1}{3} \sin(2\theta) \cos \phi$
$\sigma_2 \otimes \sigma_0$	0
$\sigma_2 \otimes \sigma_1$	$-\frac{1}{3} \sin^2 \theta \sin(2\phi)$
$\sigma_2 \otimes \sigma_2$	$\frac{1}{18} [5 + 3 \cos(2\theta) + 6 \cos(2\phi) \sin^2 \theta]$
$\sigma_2 \otimes \sigma_3$	$-\frac{1}{3} \sin(2\theta) \sin \phi$
$\sigma_3 \otimes \sigma_0$	0
$\sigma_3 \otimes \sigma_1$	$-\frac{1}{3} \sin(2\theta) \cos \phi$
$\sigma_3 \otimes \sigma_2$	$-\frac{1}{3} \sin(2\theta) \sin \phi$
$\sigma_3 \otimes \sigma_3$	$\frac{1}{9} [1 - 3 \cos(2\theta)]$

Table 6.10: Projections of the 4×4 matrix P onto the Dirac matrices for the $sp \rightarrow ps$ process.

3/2. Using Table 6.8 we see that

$$P^{(k)} = p_{00}^{(k)} \left\{ \sigma_0^{(0)} \otimes \sigma_0^{(k)} \right\} + p_{31}^{(k)} \left\{ \sigma_3^{(0)} \otimes \sigma_1^{(k)} \right\} + p_{32}^{(k)} \left\{ \sigma_3^{(0)} \otimes \sigma_2^{(k)} \right\} + p_{33}^{(k)} \left\{ \sigma_3^{(0)} \otimes \sigma_3^{(k)} \right\}, \quad (6.51)$$

for some coefficients $p_{00}^{(k)}$, $p_{31}^{(k)}$, $p_{32}^{(k)}$, and $p_{33}^{(k)}$ that depend on θ_k and ϕ_k . We also define

$$\left\{ \sigma_\alpha^{(0)} \otimes \sigma_\beta^{(k)} \right\} = \sigma_\alpha^{(0)} \otimes \sigma_0^{(1)} \otimes \cdots \otimes \sigma_0^{(k-1)} \otimes \sigma_\beta^{(k)} \otimes \sigma_0^{(k+1)} \otimes \cdots \otimes \sigma_0^{(N)}. \quad (6.52)$$

Similarly, we have

$$P^{(l)} = p_{00}^{(l)} \left\{ \sigma_0^{(0)} \otimes \sigma_0^{(l)} \right\} + p_{31}^{(l)} \left\{ \sigma_3^{(0)} \otimes \sigma_1^{(l)} \right\} + p_{32}^{(l)} \left\{ \sigma_3^{(0)} \otimes \sigma_2^{(l)} \right\} + p_{33}^{(l)} \left\{ \sigma_3^{(0)} \otimes \sigma_3^{(l)} \right\}. \quad (6.53)$$

Because σ_0 is just the 2×2 identity matrix, it follows that $\left\{ \sigma_0^{(0)} \otimes \sigma_0^{(k)} \right\}$ is just the $2^{N+1} \times 2^{N+1}$ identity matrix. Thus $\left\{ \sigma_0^{(0)} \otimes \sigma_0^{(k)} \right\}$ will commute with anything. Now consider the product

$$\Pi = \left\{ \sigma_3^{(0)} \otimes \sigma_\alpha^{(k)} \right\} \left\{ \sigma_3^{(0)} \otimes \sigma_\beta^{(l)} \right\}. \quad (6.54)$$

Although the result does not depend on it, we assume for convenience that $k \leq l$. We also expand each of the terms in Eq. (6.54) and apply Eq. (6.47). We find that

$$\begin{aligned} \Pi &= \left[\sigma_3^{(0)} \otimes \sigma_0^{(1)} \otimes \cdots \otimes \sigma_0^{(k-1)} \otimes \sigma_\alpha^{(k)} \otimes \sigma_0^{(k+1)} \otimes \cdots \otimes \sigma_0^{(N)} \right] \times \\ &\quad \left[\sigma_3^{(0)} \otimes \sigma_0^{(1)} \otimes \cdots \otimes \sigma_0^{(l-1)} \otimes \sigma_\beta^{(l)} \otimes \sigma_0^{(l+1)} \otimes \cdots \otimes \sigma_0^{(N)} \right] \\ &= \left(\sigma_3^{(0)} \sigma_3^{(0)} \right) \otimes \sigma_0^{(1)} \otimes \cdots \otimes \sigma_0^{(k-1)} \otimes \sigma_\alpha^{(k)} \otimes \sigma_0^{(k+1)} \otimes \cdots \otimes \\ &\quad \sigma_0^{(l-1)} \otimes \sigma_\beta^{(l)} \otimes \sigma_0^{(l+1)} \otimes \cdots \otimes \sigma_0^{(N)}, \end{aligned} \quad (6.55)$$

since σ_0 is just the identity matrix. Note that if we had considered instead the product

$$\left\{ \sigma_3^{(0)} \otimes \sigma_\beta^{(l)} \right\} \left\{ \sigma_3^{(0)} \otimes \sigma_\alpha^{(k)} \right\}, \quad (6.56)$$

then we would have obtained the same result. Therefore each term in $P^{(k)}$ commutes with each of the

terms in $P^{(l)}$. It follows that $P^{(k)}$ commutes with $P^{(l)}$, and hence we can perform the decomposition of Eq. (6.50) in this case.

Now consider the potential for the $ss' \rightarrow pp'$ process when $|m_j| = 1/2$. Using Table 6.9 we see that

$$\begin{aligned}
P^{(k)} = & p_{00}^{(k)} \left\{ \sigma_0^{(0)} \otimes \sigma_0^{(k)} \right\} + p_{11}^{(k)} \left\{ \sigma_1^{(0)} \otimes \sigma_1^{(k)} \right\} + p_{12}^{(k)} \left\{ \sigma_1^{(0)} \otimes \sigma_2^{(k)} \right\} + p_{13}^{(k)} \left\{ \sigma_1^{(0)} \otimes \sigma_3^{(k)} \right\} + \\
& p_{21}^{(k)} \left\{ \sigma_2^{(0)} \otimes \sigma_1^{(k)} \right\} + p_{22}^{(k)} \left\{ \sigma_2^{(0)} \otimes \sigma_2^{(k)} \right\} + p_{23}^{(k)} \left\{ \sigma_2^{(0)} \otimes \sigma_3^{(k)} \right\} + p_{31}^{(k)} \left\{ \sigma_3^{(0)} \otimes \sigma_1^{(k)} \right\} + \\
& p_{32}^{(k)} \left\{ \sigma_3^{(0)} \otimes \sigma_2^{(k)} \right\} + p_{33}^{(k)} \left\{ \sigma_3^{(0)} \otimes \sigma_3^{(k)} \right\}, \tag{6.57}
\end{aligned}$$

and similarly for $P^{(l)}$. Examining the product

$$\Pi = \left\{ \sigma_1^{(0)} \otimes \sigma_3^{(k)} \right\} \left\{ \sigma_2^{(0)} \otimes \sigma_1^{(l)} \right\}, \tag{6.58}$$

we see that

$$\begin{aligned}
\Pi = & \left(\sigma_1^{(0)} \sigma_2^{(0)} \right) \otimes \sigma_0^{(1)} \otimes \cdots \otimes \sigma_0^{(k-1)} \otimes \sigma_3^{(k)} \otimes \sigma_0^{(k+1)} \otimes \cdots \otimes \\
& \sigma_0^{(l-1)} \otimes \sigma_1^{(l)} \otimes \sigma_0^{(l+1)} \otimes \cdots \otimes \sigma_0^{(N)}, \tag{6.59}
\end{aligned}$$

while if we had multiplied the factors in the opposite order we would have obtained

$$\begin{aligned}
& \left(\sigma_2^{(0)} \sigma_1^{(0)} \right) \otimes \sigma_0^{(1)} \otimes \cdots \otimes \sigma_0^{(k-1)} \otimes \sigma_3^{(k)} \otimes \sigma_0^{(k+1)} \otimes \cdots \otimes \\
& \sigma_0^{(l-1)} \otimes \sigma_1^{(l)} \otimes \sigma_0^{(l+1)} \otimes \cdots \otimes \sigma_0^{(N)}. \tag{6.60}
\end{aligned}$$

Since $\sigma_1^{(0)} \sigma_2^{(0)} = i\sigma_3^{(0)}$, while $\sigma_2^{(0)} \sigma_1^{(0)} = -i\sigma_3^{(0)}$, we see that the commutator of $\left\{ \sigma_1^{(0)} \otimes \sigma_3^{(k)} \right\}$ and $\left\{ \sigma_2^{(0)} \otimes \sigma_1^{(l)} \right\}$ is not a c -number. Because the set of $\left\{ p_{\alpha\beta}^{(k)} \right\}$ is not the same as the set of $\left\{ p_{\alpha\beta}^{(l)} \right\}$, it follows that the commutator of $P^{(k)}$ and $P^{(l)}$ cannot be a c -number. Hence we cannot perform the separation of Eq. (6.50) in this case.

Considering the potential for the $sp \rightarrow ps$ process and consulting Table 6.9, we see that the coefficients of $\sigma_1 \otimes \sigma_3$ and $\sigma_2 \otimes \sigma_1$ are both nonzero. Therefore the argument of the previous paragraph will hold here too, and again we cannot perform the separation of Eq. (6.50).

6.3.5 Averaging the $ss' \rightarrow pp'$ process when $|m_j| = 3/2$ for the p' atom

In this case we can perform the separation of Eq. (6.50), and so we see from Eq. (6.44) that the averaging problem reduces the computation of the average of

$$\frac{1}{2^{N+1}} \text{Tr} \prod_{k=1}^N \exp \left[-\beta V_k^2 P^{(k)} \right]. \quad (6.61)$$

Using Table 6.8, we can write

$$\begin{aligned} \exp \left[-\beta V_k^2 P^{(k)} \right] &= \exp \left[-\beta v_{00}^{(k)} \left\{ \sigma_0^{(0)} \otimes \sigma_0^{(k)} \right\} - \beta \sum_{b=1}^3 v_{3b}^{(k)} \left\{ \sigma_3^{(0)} \otimes \sigma_b^{(k)} \right\} \right] \\ &= \exp \left[-\beta v_{00}^{(k)} \right] \exp \left[-\beta \sum_{b=1}^3 v_{3b}^{(k)} \left\{ \sigma_3^{(0)} \otimes \sigma_b^{(k)} \right\} \right], \end{aligned} \quad (6.62)$$

since $\left\{ \sigma_0^{(0)} \otimes \sigma_0^{(k)} \right\}$ is just the $2^{N+1} \times 2^{N+1}$ identity matrix, which certainly commutes with $\left\{ \sigma_3^{(0)} \otimes \sigma_b^{(k)} \right\}$.

Here $v_{\alpha\beta}^{(k)}$ depends on \mathbf{r}_k , and specifically

$$v_{\alpha\beta}^{(k)} = \frac{\mu\mu'}{r_k^3} p_{\alpha\beta}^{(k)}, \quad (6.63)$$

where $p_{\alpha\beta}^{(k)}$ is the same quantity as in Eq. (6.53).

If we define

$$\mathbf{v}^{(k)} = \sum_{b=1}^3 v_{3b}^{(k)} \hat{\mathbf{e}}_b \quad (6.64)$$

and

$$\boldsymbol{\sigma}^{(k)} = \sum_{b=1}^3 \sigma_{3b}^{(k)} \hat{\mathbf{e}}_b, \quad (6.65)$$

then we can rewrite Eq. (6.62) as

$$\exp \left[-\beta V_k^2 P^{(k)} \right] = \exp \left[-\beta v_{00}^{(k)} \right] \exp \left(\left\{ \sigma_3^{(0)} \otimes \left[-\beta \mathbf{v}^{(k)} \cdot \boldsymbol{\sigma}^{(k)} \right] \right\} \right). \quad (6.66)$$

Now we note that

$$\begin{aligned} \exp(\sigma_3 \otimes A) &= \sum_{j=0}^{\infty} \frac{1}{j!} (\sigma_3 \otimes A)^j \\ &= \sum_{j=0}^{\infty} \frac{1}{j!} (\sigma_3)^j \otimes (A)^j \end{aligned}$$

$$\begin{aligned}
&= \sum_{k=0}^{\infty} \frac{\sigma_0 \otimes (A)^{2k}}{(2k)!} + \sum_{l=0}^{\infty} \frac{\sigma_3 \otimes (A)^{2l+1}}{(2l+1)!} \\
&= \sigma_0 \otimes \cosh A + \sigma_3 \otimes \sinh A,
\end{aligned} \tag{6.67}$$

so that

$$\exp \left(\left\{ \sigma_3^{(0)} \otimes \left[-\beta \mathbf{v}^{(k)} \cdot \sigma^{(k)} \right] \right\} \right) = \sigma_0^{(0)} \otimes \cosh \left[-\beta \Sigma^{(k)} \right] + \sigma_3^{(0)} \otimes \sinh \left[-\beta \Sigma^{(k)} \right], \tag{6.68}$$

where to save space we define

$$\Sigma^{(k)} = \sigma_0^{(1)} \otimes \dots \otimes \sigma_0^{(k-1)} \otimes \left[\mathbf{v}^{(k)} \cdot \sigma^{(k)} \right] \otimes \sigma_0^{(k+1)} \otimes \dots \otimes \sigma_0^{(N)}. \tag{6.69}$$

A derivation very similar to that of Eq. (6.67) shows that

$$\cosh (\sigma_0 \otimes A) = \sigma_0 \otimes \cosh A, \tag{6.70}$$

and

$$\sinh (\sigma_0 \otimes A) = \sigma_0 \otimes \sinh A, \tag{6.71}$$

and by repeated application of these last two relations we finally arrive at

$$\begin{aligned}
\exp \left(\left\{ \sigma_3^{(0)} \otimes \left[-\beta \mathbf{v}^{(k)} \cdot \sigma^{(k)} \right] \right\} \right) &= \left\{ \sigma_0^{(0)} \otimes \cosh \left[-\beta \mathbf{v}^{(k)} \cdot \sigma^{(k)} \right] \right\} - \\
&\quad \left\{ \sigma_3^{(0)} \otimes \sinh \left[-\beta \mathbf{v}^{(k)} \cdot \sigma^{(k)} \right] \right\}.
\end{aligned} \tag{6.72}$$

From page 166 of Ref. [53] we have the familiar result that

$$\left(\mathbf{v}^{(k)} \cdot \sigma^{(k)} \right)^n = \begin{cases} 1 & \text{if } n \text{ is even,} \\ \mathbf{v}^{(k)} \cdot \sigma^{(k)} & \text{if } n \text{ is odd.} \end{cases} \tag{6.73}$$

From this it is easy to show that

$$\cosh \left[-\beta \mathbf{v}^{(k)} \cdot \sigma^{(k)} \right] = \cosh \left[\beta v^{(k)} \right], \tag{6.74}$$

and

$$\sinh \left[-\beta \mathbf{v}^{(k)} \cdot \boldsymbol{\sigma}^{(k)} \right] = -\hat{\mathbf{v}}^{(k)} \cdot \boldsymbol{\sigma}^{(k)} \sinh \left[\beta v^{(k)} \right]. \quad (6.75)$$

Thus we see that

$$\begin{aligned} \exp \left(\left\{ \sigma_3^{(0)} \otimes \left[-\beta \mathbf{v}^{(k)} \cdot \boldsymbol{\sigma}^{(k)} \right] \right\} \right) &= \cosh \left[\beta v^{(k)} \right] - \\ &\quad \sinh \left[\beta v^{(k)} \right] \left\{ \sigma_3^{(0)} \otimes \hat{\mathbf{v}}^{(k)} \cdot \boldsymbol{\sigma}^{(k)} \right\}, \end{aligned} \quad (6.76)$$

and hence

$$\begin{aligned} \exp \left[-\beta V_k^2 P^{(k)} \right] &= \exp \left[-\beta v_{00}^{(k)} \right] \cosh \left[\beta v^{(k)} \right] - \\ &\quad \exp \left[-\beta v_{00}^{(k)} \right] \sinh \left[\beta v^{(k)} \right] \left\{ \sigma_3^{(0)} \otimes \hat{\mathbf{v}}^{(k)} \cdot \boldsymbol{\sigma}^{(k)} \right\}. \end{aligned} \quad (6.77)$$

We now note that because $\text{Tr} \sigma_a = 0$ if a is equal to 1, 2, or 3, it follows that when we expand the product

$$\left[a_{00}^{(k)} \left\{ \sigma_0^{(0)} \otimes \sigma_0^{(k)} \right\} + \left\{ \sigma_3^{(0)} \otimes \mathbf{a}^{(k)} \cdot \boldsymbol{\sigma}^{(k)} \right\} \right] \left[a_{00}^{(l)} \left\{ \sigma_0^{(0)} \otimes \sigma_0^{(l)} \right\} + \left\{ \sigma_3^{(0)} \otimes \mathbf{a}^{(l)} \cdot \boldsymbol{\sigma}^{(l)} \right\} \right] \quad (6.78)$$

and take the trace, only the term

$$a_{00}^{(k)} a_{00}^{(l)} \text{Tr} \left\{ \sigma_0^{(0)} \otimes \sigma_0^{(k)} \right\} = 2^{N+1} a_{00}^{(k)} a_{00}^{(l)} \quad (6.79)$$

survives. This together with Eqs. (6.61) and (6.77) implies that

$$\frac{1}{2^{N+1}} \text{Tr} \prod_{k=1}^N \exp \left[-\beta V_k^2 P^{(k)} \right] = \prod_{k=1}^N \exp \left[-\beta v_{00}^{(k)} \right] \cosh \left[\beta v^{(k)} \right]. \quad (6.80)$$

We can now change variables so that

$$\left\langle \prod_{k=1}^N \exp \left[-\beta v_{00}^{(k)} \right] \cosh \left[\beta v^{(k)} \right] \right\rangle \quad (6.81)$$

is equal to a product of N copies of

$$\int_0^\infty dr_k r_k^2 \int_0^\pi d\theta_k \sin \theta_k \int_0^{2\pi} d\phi_k \exp \left[-\beta v_{00}^{(k)} \right] \cosh \left[\beta v^{(k)} \right]. \quad (6.82)$$

This integral, in turn, is equal to the sum of the integrals

$$\frac{1}{2\Omega} \int_0^\infty dr_k r_k^2 \int_0^\pi d\theta_k \sin \theta_k \int_0^{2\pi} d\phi_k \exp \left\{ -\beta \left[v_{00}^{(k)} - v^{(k)} \right] \right\}, \quad (6.83)$$

and

$$\frac{1}{2\Omega} \int_0^\infty dr_k r_k^2 \int_0^\pi d\theta_k \sin \theta_k \int_0^{2\pi} d\phi_k \exp \left\{ -\beta \left[v_{00}^{(k)} + v^{(k)} \right] \right\}. \quad (6.84)$$

Once again using the coefficients of Table 6.8, we find that

$$v_{00}^{(k)} = \frac{\mu\mu'}{r_k^3} \frac{1}{12} [7 - 3 \cos(2\theta_k)], \quad (6.85)$$

and

$$v^{(k)} = \frac{\mu\mu'}{r_k^3} \frac{1}{3\sqrt{3}} \sqrt{5 - 3 \cos(2\theta_k)}. \quad (6.86)$$

The integrals of Eqs. (6.83) and (6.84) are now of a familiar type, and they can be done using the methods explained in Sections 2.3 and 2.5. Unfortunately the angular integrals have to be done numerically, but the result is that¹

$$\frac{1}{\Omega} \int_0^\infty dr_k r_k^2 \int_0^\pi d\theta_k \sin \theta_k \int_0^{2\pi} d\phi_k \exp \left[-\beta v_{00}^{(k)} \right] \cosh \left[\beta v^{(k)} \right] = 1 - 5.18061 \frac{\mu\mu'}{\Omega} \sqrt{\beta}. \quad (6.87)$$

It follows that

$$\frac{1}{2^{N+1}} \text{Tr} \prod_{k=1}^N \exp \left[-\beta V_k^2 P^{(k)} \right] = \exp \left(-v_{\text{spin}} \sqrt{\beta} \right), \quad (6.88)$$

where

$$v_{\text{spin}} = 5.18061 \mu\mu' \frac{N}{\Omega}. \quad (6.89)$$

Recalling Eq. (2.12), we see that when we used the simple $\mu\mu'/r^3$ interaction potential of Chapter 2, we obtained

$$v = \frac{4\pi^{3/2}}{3} \mu\mu' \frac{N}{\Omega} = 7.42444 \mu\mu' \frac{N}{\Omega}. \quad (6.90)$$

Hence we arrive at

$$v_{\text{spin}} = 0.697778 v. \quad (6.91)$$

¹The astute reader will be relieved to know that the quantities $v_{00}^{(k)} + v^{(k)}$ and $v_{00}^{(k)} - v^{(k)}$ are both positive for all values of θ_k and ϕ_k , and so there is no difficulty in applying the methods of Sections 2.3 and 2.5 here.

Inserting our averaged result back into Eq. (6.44), we see that

$$\left\langle \frac{1}{2^{N+1}} \text{Tr} \tilde{S}(\alpha) \right\rangle = \frac{1}{2\alpha} - \frac{\alpha^2 + \Delta^2}{2\alpha} \int_0^\infty d\beta \exp \left[-\beta (\alpha^2 + \Delta^2) - 2v_{\text{spin}} \sqrt{\beta} \right]. \quad (6.92)$$

Comparing with Eq. (2.27), one immediately sees that Eq. (6.92) gives the same results as the signal computed in Chapter 2 but with the quantity v_{spin} appearing in place of v .

6.4 Summary

In this chapter we have considered the detailed effects of spin on the system we are studying. We were only able to fully average the $ss' \rightarrow pp'$ process when $|m_j| = 3/2$ for the p' atom, but we can see from Fig. 1.4 that the case where $|m_j| = 1/2$ for the p' atom is not very different. In the case that we could treat fully, we found that the effect of the spin was to change the value of the parameter v by a factor of 0.697778 from the simple case where we neglect the effects of spin and consider an angular independent $1/r^3$ interaction potential.

The consideration of the effects of spin becomes extremely important when a magnetic field is applied to the system. It was reported by Renn *et al.* [50] that the introduction of a magnetic field greatly proliferates the number of nondegenerate states present in a room temperature Rydberg gas. One can imagine applying a magnetic field that is parallel to the detuning electric field and of sufficient strength to lift the m_j degeneracy. The form of the $ss' \rightarrow pp'$ interaction would then be given by the appropriate matrix element of Table 6.2 or 6.3, and the form of the $sp \rightarrow ps$ interaction would similarly be found in Table 6.4. Thus we see that this is one possible scheme for selecting the angular form of the interaction potential.

Chapter 7

Numerical Simulations

7.1 Introduction

In this chapter we discuss numerical simulations of the system we are considering. We start by describing in detail how the simulations are carried out, then we present the results, including comparisons of the simulations with the experimental data.

7.2 Review of theoretical model

Before discussing exactly how the simulations are carried out, we review the basic elements of the theory presented at the beginning of Sections 2.2 and 4.2.1 of this thesis. We consider one atom at the origin, initially in the state s' , in interaction with a gas of s atoms through a resonant $ss' \rightarrow pp'$ dipole-dipole interaction V . We also allow for interaction among the unprimed atoms via an $sp \rightarrow ps$ process mediated by another dipole-dipole potential U . This system is described by Eqs. (4.1a) and (4.1b), which are

$$i \dot{a}_0 = \Delta a_0 + \sum_{k=1}^N V_k c_k, \quad (7.1a)$$

$$i \dot{c}_k = V_k a_0 + \sum_{l=1}^N U_{kl} c_l. \quad (7.1b)$$

Here $a_0(\Delta, t)$ is the amplitude of the state in which the atom at the origin is in state s' and all other atoms are in state s , while $c_k(\Delta, t)$ is the amplitude of the state in which the atom at the origin is in state p' and the atom at \mathbf{r}_k is in state p , while all the others remain in state s . The quantities V_k and U_{kl} are the interaction potentials and $\Delta = \epsilon_{p'} + \epsilon_p - \epsilon_{s'} - \epsilon_s$ is the detuning from resonance.

The simplest possibilities for the dipole-dipole interactions V and U are

$$V_k = -\frac{\mu\mu'}{r_k^3}, \quad (7.2)$$

and

$$U_{kl} = -\frac{\mu^2}{r_{kl}^3}. \quad (7.3)$$

Here μ is the dipole matrix element connecting the s and p states, and μ' is the dipole matrix element connecting the s' and p' states. We also define $U_{ll} = 0$, so that the restriction $l \neq k$ is automatic in sums of the type appearing in Eq. (7.1b). The atoms are assumed to be sufficiently cold that during the time scale of interest they move only a very small fraction of their separation, and therefore V_k and U_{kl} can be taken to be independent of time.

As was stated in Section 2.5.1, the induced dipoles in the magneto-optical trap become aligned if the applied electric field is sufficiently large that the Stark effect has passed from the quadratic to the linear regime. This is the case considered, for example, in Refs. [32] and [54]. For the numerical simulation results of this thesis we use the slightly more complicated dipole-dipole interaction potential corresponding to this case, which is

$$V_k = -\frac{2\mu\mu'}{r_k^3} P_2(\cos \theta_k), \quad (7.4)$$

where θ_k is the angle between \mathbf{r}_k and the applied electric field. Similarly, U_{kl} is of the form

$$U_{kl} = -\frac{2\mu^2}{r_{kl}^3} P_2(\cos \theta_{kl}), \quad (7.5)$$

for $l \neq k$, and $U_{kk} = 0$. These formulas for V and U are also valid, in some cases, in the quadratic Stark regime if a magnetic field parallel to the electric field is used to align the total angular momentum of the atoms, as we now discuss more fully.

We will show below that, using interactions such as Eqs. (7.2) and (7.3), or Eqs. (7.4) and (7.5), we are able to reduce the computation of any quantity to the diagonalization of an $(N + 1) \times (N + 1)$ matrix. On the other hand, we saw in Chapter 6 that in the quadratic Stark regime the actual interaction potentials depend on the quantum numbers m_j of the atoms involved. A complete consideration of the spins would require the diagonalization of a $2^{N+1} \times 2^{N+1}$ matrix in this case, which is computationally prohibitive to say the least. The problem can be reduced again to $\mathcal{O}(N \times N)$ by applying a magnetic field that is parallel to the electric field and of sufficient strength to lift the m_j degeneracy. The V interaction is then given by the appropriate matrix element of Table 6.2 or 6.3, and the U interaction is similarly found in Table 6.4. We see from these tables that for many matrix elements the angular dependence is the same as in Eqs. (7.4) and (7.5), which can therefore be taken as representative. We have also shown in Section 6.3.5 that, when a p' state with $|m_j| = 3/2$ is involved, each s atom interacts separately with the s' atom and, as the system evolves, the average number of p' states is the same as for a simple spin-independent interaction, but with an effective V_k . The resulting effective interaction energy v_{spin} is given by Eq. (6.91) to be $0.698 v$, where v is the effective interaction energy for the interaction potential of Eq. (7.2) and is defined explicitly in Eq. (2.12). For comparison, the effective interaction energy for the interaction potential of Eq. (7.4) is given by Eq. (2.75) to be $0.770 v$. Thus we see that the exact angular form of the interaction potential for V does not greatly affect the results. The numerical simulations reported in this chapter show that the same is true for the angular form of U .

7.3 Description of method

If we consider a column vector $C(\Delta, t) = (a_0(\Delta, t), c_1(\Delta, t), c_2(\Delta, t), \dots, c_N(\Delta, t))^T$, then clearly we can construct a matrix H such that the set of $N + 1$ coupled differential equations of Eqs. (7.1a) and (7.1b) can be written in the form $i \dot{C} = HC$. If we let $\{\lambda_m\}$ and $\{\theta_m\}$ be the eigenvalues and eigenvectors (represented as column vectors) of the real Hermitian matrix H , respectively, and if we further define e_n to be the column vector of length $N + 1$ with the n th entry set equal to one and all others set equal to zero, then we can write $e_n = \sum_{m=0}^N \beta_{mn} \theta_m$ and $\theta_m = \sum_{n=0}^N \beta_{nm} e_n$, where $\beta_{mn} = \theta_m^T e_n$. The system starts off in the state described by e_0 , so it follows that

$$C(\Delta, t) = \exp(-iHt) e_0$$

$$\begin{aligned}
&= \sum_{m=0}^N \beta_{m0} \exp(-i\lambda_m t) \theta_m \\
&= \sum_{m=0}^N \sum_{n=0}^N \beta_{m0} \beta_{nm} \exp(-i\lambda_m t) e_n.
\end{aligned} \tag{7.6}$$

The quantity $a_0(\Delta, t)$ is just the e_0 component of this expression, so

$$a_0(\Delta, t) = e_0^T C(\Delta, t) = \sum_{m=0}^N \beta_{m0} \beta_{0m} \exp(-i\lambda_m t). \tag{7.7}$$

Thus we see that, in this form, solving for a_0 at a given time becomes just a matter of diagonalizing the matrix H .

To carry out the numerical simulations, we first generate a set of random positions for the unprimed atoms. For the results presented in this Sections 7.5 and 7.6, these random positions are uniformly distributed so that the results can be more easily compared with the analytical results of previous chapters. However, when proceeding numerically it is just as easy to compute random positions for a gas blob with any given density profile. For the experiments we are modeling [5, 6, 40], the density profile is a Gaussian with an aspect ratio of approximately 1 : 1 : 5 [23], and so this is what we use to generate the results of Section 7.7. Once the atomic positions are generated, they are used to compute the interaction potentials V_k and U_{kl} , and these are in turn used to compute the matrix H . We then diagonalize H and construct the quantity a_0 at a set of values of t using Eq. (7.7). We do this for the same set of times for many random distributions of the unprimed atoms and thereby obtain an average of the quantities $a_0(\Delta, t)$ and $|a_0(\Delta, t)|^2$ at a given set of times over many configurations of the system. The signal measured by the experiments is then proportional to the average of $1 - |a_0(\Delta, t)|^2$. We can further obtain plots of the linewidth as a function of time by generating signal versus time curves for many values of the detuning, Δ , and then determining for each value of time which of these signals is equal to one half the value of the resonance signal. One can also directly generate Fourier transforms from Eq. (7.7), as we did in Section 4.6.2.

By comparing the results of the simulations to the analytical results of Chapter 2 we find that an average over 10^4 realizations, each consisting of a single s' atom and 100 s atoms, is sufficient, as can be seen in Fig. 7.1. These are the parameters we have used for all the simulation plots presented in this thesis, although we have run the simulations for as many as 800 s atoms.

The simulations are written in *Fortran 90*, and the computation process is greatly accelerated

by the use of a *Beowulf* cluster of thirteen *Linux* machines. Using this cluster, the computation can be carried out in parallel, as we now describe. A master program is started on one of the machines. The master then starts up a slave program on each machine in the cluster. The master initializes the slaves by sending them seeds for their random number generators.¹ The slaves then generate random distributions for the atoms, compute whatever quantity is required, and send the result back to the master. The master collects and averages the results returned by the slaves and saves the result to a data file. The master also takes care of any interaction with the user. The passing of messages and data between the master and slave processes is handled through the software program *Parallel Virtual Machine (PVM)* [24].

We use the (parallel) random number generation routines *gasdev* and *ran1* described in Refs. [47] and [48] to generate the random distributions of atoms. The routine *gasdev* generates Gaussian deviates with unit standard deviation, while *ran1* generates uniform deviates between zero and one. The computation of eigenvalues and eigenvectors for the matrix H corresponding to each realization is performed using the *ssyevx* routine of the *LAPACK* package, which is described in Ref. [4].

7.4 The effect of many s' atoms

7.4.1 The chemical argument

Considering the $ss' \rightarrow pp'$ process as a chemical reaction, we have the rate equation

$$\frac{dN_{p'}}{dt} = k(N_s N_{s'} - N_p N_{p'}), \quad (7.8)$$

where k is a constant with the units of inverse time, which is equivalent to energy since we take \hbar equal to unity. There are similar rate equations for N_p , N_s , and $N_{s'}$, but it is sufficient to consider only one of these because of the following constraints.

We know that $N_p = N_{p'}$, since if there is a p or p' atom present it can only have been produced as a result of a pair of atoms in the s and s' states making the $ss' \rightarrow pp'$ transition. We also know that $N = N_s + N_p = N_s + N_{p'}$ and $N' = N_{s'} + N_{p'}$, since primed and unprimed atoms can change

¹It is vital that the master control the random number generator seeds, since each slave program must be seeded differently so that each generates a different set of realizations for the atomic positions.

from s to p states and vice versa, but can never be created or destroyed. Therefore we have

$$\begin{aligned}\frac{dN_{p'}}{dt} &= k [(N - N_p) (N' - N_{p'}) - N_p N_{p'}] \\ &= k [(N - N_{p'}) (N' - N_{p'}) - N_{p'} N_{p'}] \\ &= k [NN' - (N + N') N_{p'}].\end{aligned}\tag{7.9}$$

With the initial condition $N_{p'} = 0$ at $t = 0$, this gives

$$N_{p'} = \frac{NN'}{N + N'} \left[1 - e^{-(N+N')kt} \right],\tag{7.10}$$

and at small times

$$N_{p'} = NN'kt.\tag{7.11}$$

7.4.2 Extrapolation to many s' atoms

In our case, the reaction rate is not constant and the approach to equilibrium is not accurately described by Eq. (7.10). However, the result we have from Chapter 2 in the limit $N' \ll N$ starts off at small times as

$$N_{p'} = C\mu\mu' \frac{N}{\Omega} N' t,\tag{7.12}$$

where C is a numerical constant that does not concern us here. This expression is fine for all values of N and N' , and in particular satisfies the requirement that $N_p = N_{p'}$. It is of the same form as Eq. (7.11) and shows that at small times we have

$$k = C \frac{\mu\mu'}{\Omega}.\tag{7.13}$$

Furthermore, we can write

$$N_{p'} = \frac{NN'}{N + N'} F \left(\mu\mu' \frac{N + N'}{\Omega} t, \dots \right),\tag{7.14}$$

where the dots indicate that the function F depends on other dimensionless ratios that characterize the system but do not involve t . The prefactor $NN'/(N + N')$ and the characteristic energy $\mu\mu'(N + N')/\Omega$ are suggested by the chemical argument of Section 7.4.1, since these factors are

explicitly seen in Eq. (7.10) if we keep in mind Eq. (7.13). The full function $F(x, \dots)$ is computable only in the dilute limits $N' \ll N$ or $N \ll N'$, but we know in general that it starts off linearly in x .

For large values of t we have, again for $N' \ll N$,

$$N_{p'} = N' f \left(\frac{\Delta}{\mu \mu' \frac{N}{\Omega}}, \frac{\mu}{\mu'} \right), \quad (7.15)$$

where $f(y, z)$ is some function that can be computed numerically using the methods of Section 7.3. This result cannot be correct for all values of N/N' . In fact, for $N \ll N'$ we can compute N_p and we find

$$N_p = N f \left(\frac{\Delta}{\mu \mu' \frac{N'}{\Omega}}, \frac{\mu}{\mu'} \right). \quad (7.16)$$

Since $N_{p'}$ is equal to N_p , we see that this (correct) result is quite different from what one would obtain using Eq. (7.15), which is incorrect in this limit. Interpolating between the limits given by Eqs. (7.15) and (7.16), we postulate that for large t

$$N_{p'} = \frac{NN'}{N + N'} f \left(\frac{\Delta}{\mu \mu' \frac{N+N'}{\Omega}}, \frac{\mu}{\mu'} \right). \quad (7.17)$$

We can join this result smoothly to the small t result of Eq. (7.12) by postulating a general result of the form

$$N_{p'} = \frac{NN'}{N + N'} F \left(\mu \mu' \frac{N + N'}{\Omega} t, \frac{\Delta}{\mu \mu' \frac{N+N'}{\Omega}}, \frac{N}{N + N'} \frac{\mu}{\mu'} + \frac{N'}{N + N'} \frac{\mu'}{\mu} \right), \quad (7.18)$$

where the function $F(x, y, z)$ is proportional to x for small x and approaches $f(y, z)$ for large x . We have also used the same scaling for the quantities t and Δ , so that $xy = \Delta t$.

With this approach we can use the function $F(x, y, z)$, which can be computed numerically in the dilute limit, as a reasonable guess for the functional dependence on the suitable dimensionless variables for any value of N'/N .

The combination

$$\frac{N}{N + N'} \frac{\mu}{\mu'} + \frac{N'}{N + N'} \frac{\mu'}{\mu} \quad (7.19)$$

is just an interpolation between the correct results in the limits of small N and small N' . It is reasonable, however, since the quantities

$$N \mu^2 \frac{N}{\Omega}, \quad (7.20)$$

$$N' (\mu')^2 \frac{N'}{\Omega}, \quad (7.21)$$

and

$$N' \mu \mu' \frac{N}{\Omega} \quad (7.22)$$

give the effective U for the $sp \rightarrow ps$ interaction for a fraction $N'/(N + N')$ of the atoms, the effective U' for the $s'p' \rightarrow p's'$ interaction for a fraction $N/(N + N')$ of the atoms, and the V interaction for the $ss' \rightarrow pp'$ process for all the atoms. The quantity of Eq. (7.19) is obtained by taking the ratio

$$\frac{N \mu^2 \frac{N}{\Omega} + N' (\mu')^2 \frac{N'}{\Omega}}{N' \mu \mu' \frac{N}{\Omega}}. \quad (7.23)$$

7.5 Results of simulations for the signal

For the results of this section, as well as those of Section 7.6, we use the interaction potentials of Eqs. (7.4) and (7.5). We also use a uniform distribution to generate the random atomic positions, so that the results can be more easily compared with the analytical results of previous chapters.

Figs. 7.1–7.5 display the numerical simulations of $1 - \langle |a_0|^2 \rangle$, corresponding to the experimental signal $N_{p'}/N'$, as a function of vt for $u/v = 0, 1/4, 1, 2,$ and 4 , and enough values of the detuning Δ to give an idea of the resonance width in each case. The FWHM at large t can be directly deduced from the intercepts of the graphs with the right edge of the figure, as is discussed more fully below.

In addition, Fig. 7.1 shows the exact results for $u = 0$ that were discussed in Chapter 2. Comparison with the numerical simulations, which were carried out for $N = 100$, shows that the infinite system is already well simulated, but that noticeable wiggles remain after averaging over 10^4 realizations. The reason for this persistence of fluctuations is that most realizations do not look at all like the average. In fact, the variance with realization is comparable to the average. In particular, for small t the average is given by $(\sqrt{\pi}/2) vt$ while each realization is quadratic in t , as already discussed in Ref. [18]. It can be seen from the graphs that the linear rise law, $(\sqrt{\pi}/2) vt$, is independent both of Δ and of u and holds for a substantial range of vt .

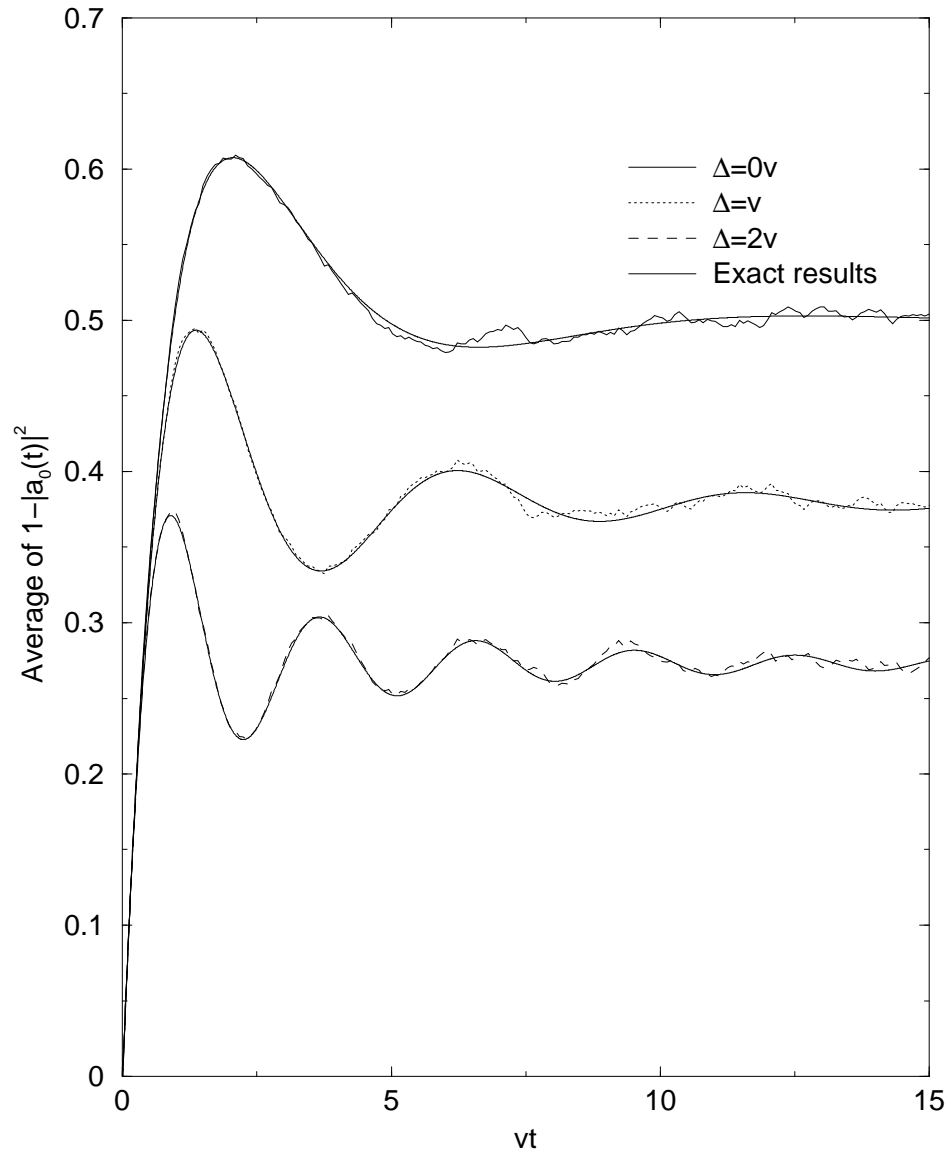


Figure 7.1: Plots of $1 - \langle |a_0(\Delta, t)|^2 \rangle$ for $u = 0$ and several values of the detuning Δ . The exact results of Chapter 2 are shown for comparison.

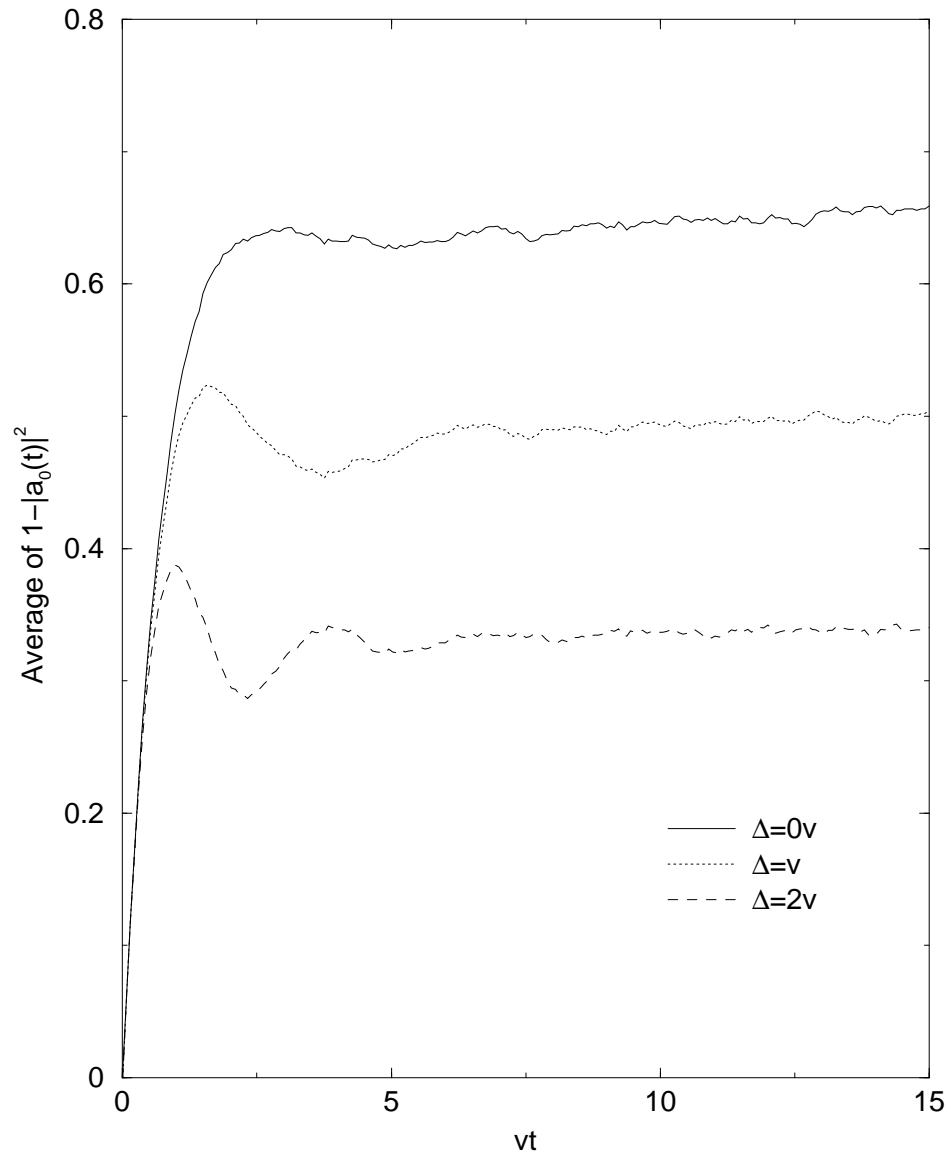


Figure 7.2: Plots of $1 - \langle |a_0(\Delta, t)|^2 \rangle$ for $u = 0.25v$ and several values of the detuning Δ .

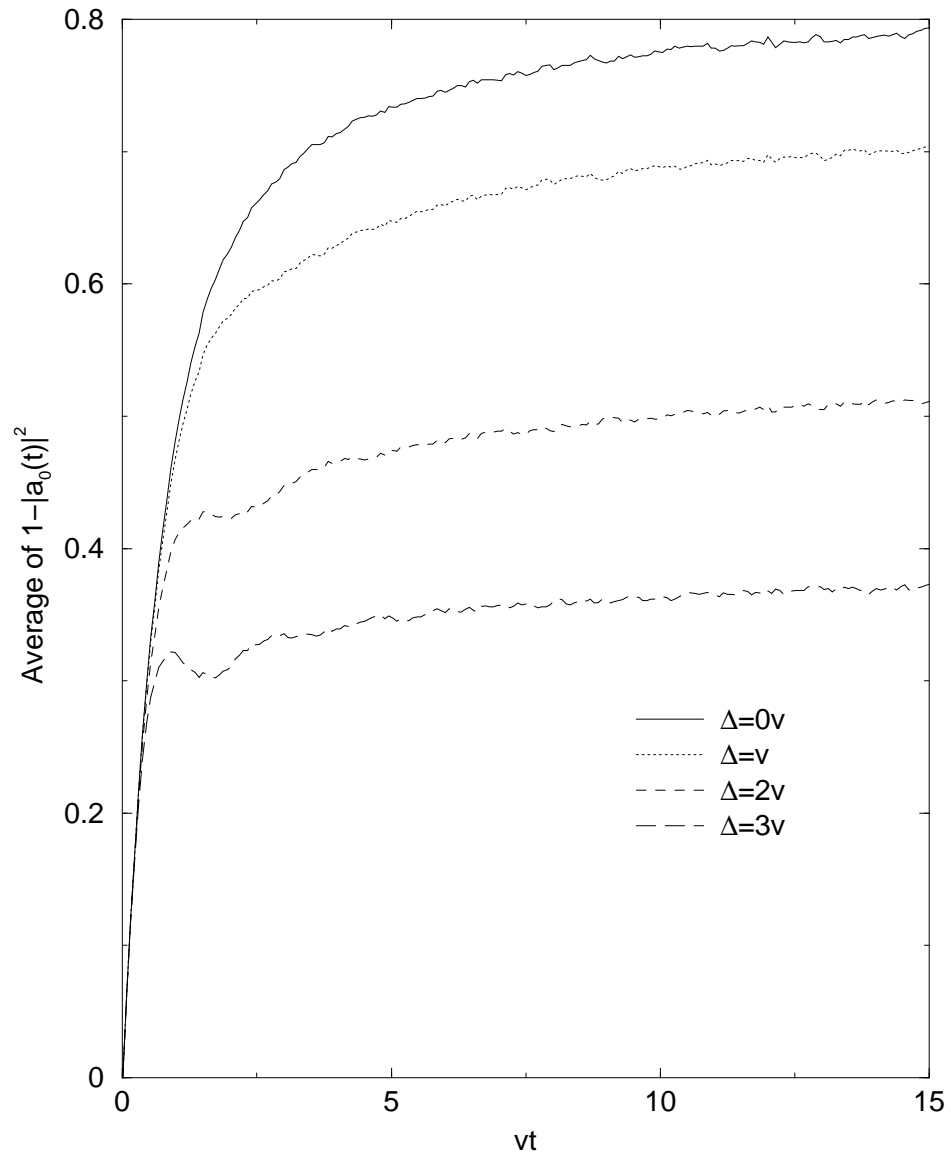


Figure 7.3: Plots of $1 - \langle |a_0(\Delta, t)|^2 \rangle$ for $u = v$ and several values of the detuning Δ .

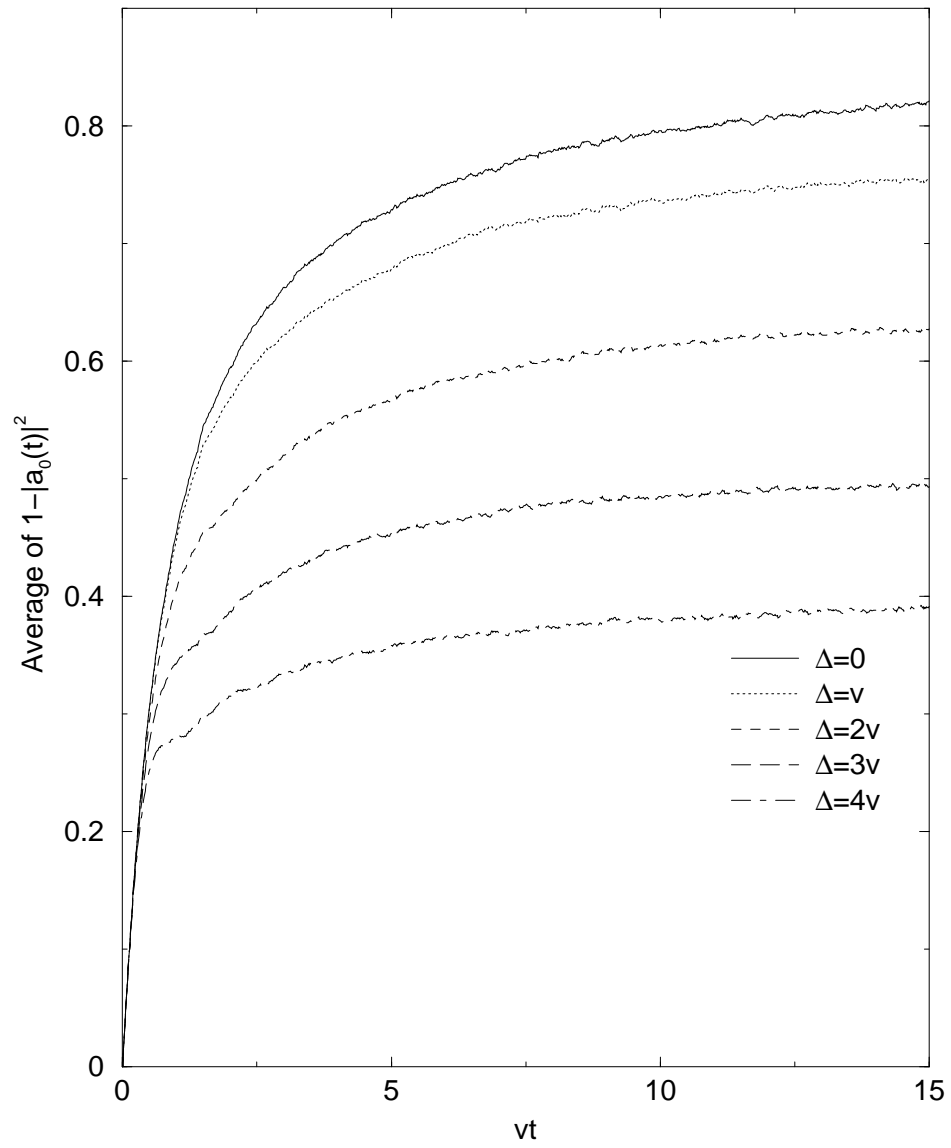


Figure 7.4: Plots of $1 - \langle |a_0(\Delta, t)|^2 \rangle$ for $u = 2v$ and several values of the detuning Δ .

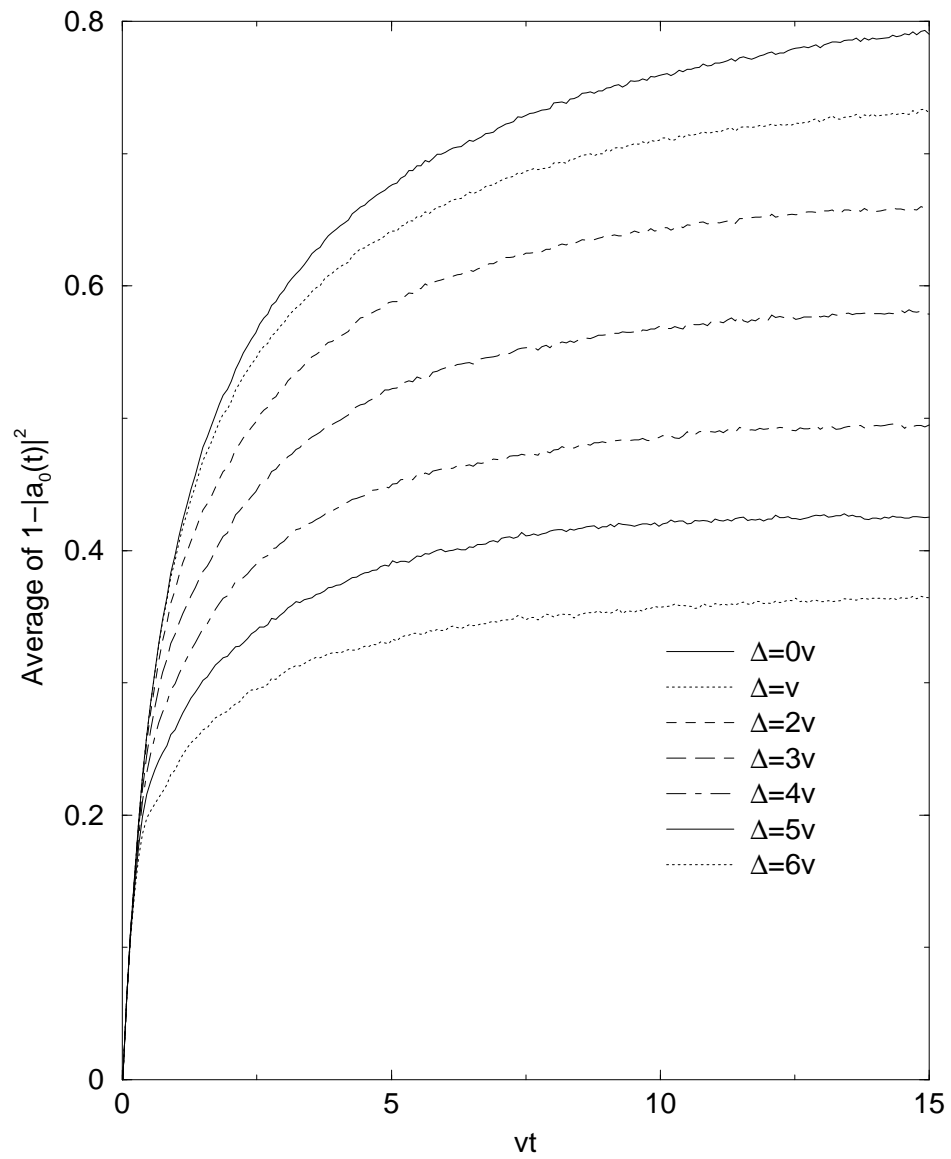


Figure 7.5: Plots of $1 - \langle |a_0(\Delta, t)|^2 \rangle$ for $u = 4v$ and several values of the detuning Δ .

7.6 Results of simulations for the width

The time-dependent resonance lineshape is obtained from the ordinates of the curves in Figs. 7.1–7.5 at a given vt . In general the lineshape is not Lorentzian, but we never find a split line with a minimum at resonance as reported in Ref. [45]. Thus it is fair to characterize the line by its FWHM. This cannot be directly compared with an experimental width, which is usually the FWHM of a Lorentzian fitted to a noisy experimental line, but it is indicative of trends. For a more accurate comparison with experiment, one should of course convolute the calculated lineshape with the broadening due to other effects.

Fig. 7.6 shows one half of the FWHM, w , as a function of vt for $u = 4v$. One sees the typical decrease of w from a universal t^{-1} behavior at small vt towards an asymptotic value, which is almost reached at $vt = 15$. The t^{-1} law, which results simply from the uncertainty principle [6, 60], has already been discussed in Ref. [18] where on the basis of a small Δ expansion it was estimated that $w = \sqrt{12}/t$ for small t . This t^{-1} behavior was observed experimentally by Renn *et al.* [60] in a different system, and was later observed by Anderson *et al.* [6, 5] in the Rb system.

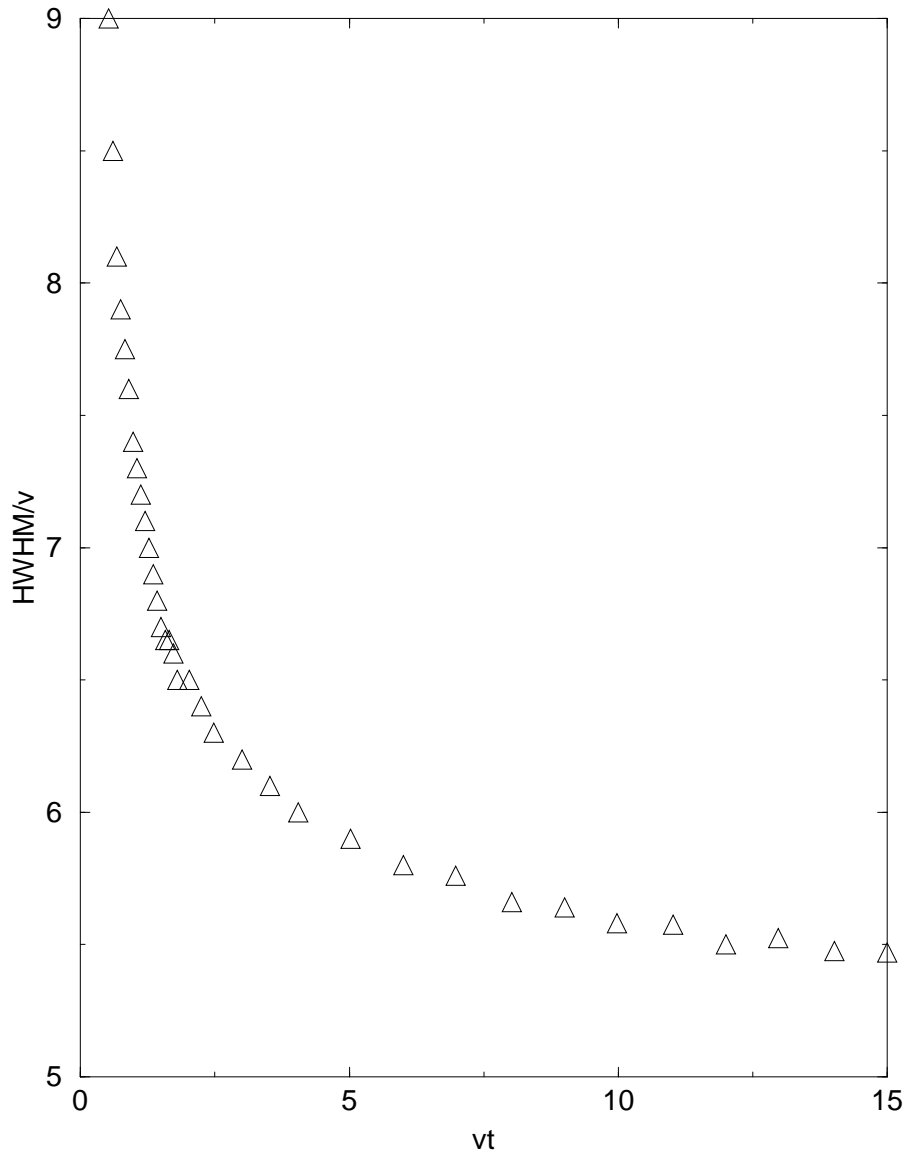
The near-asymptotic value of the FWHM at $vt = 15$ is shown in Fig. 7.7 as a function of u/v . Overall, the graph is roughly linear except at small u/v , although a careful examination shows that there are really two linear regimes with somewhat different slopes that meet at $u/v \approx 3.5$. There is an unexpected minimum around $u = v/4$, which is not a numerical artifact, but can be seen directly from Figs. 7.1–7.5 by comparing the plot for $u = v/4$ with those for $u = 0$ and $u = v$. What happens is that the resonance line always grows taller and wider as u increases, but for small u its height (the signal at $\Delta = 0$) grows faster than its width.

7.7 Comparison with experimental data

For the results in this section, we use the interaction potentials of Eqs. (7.4) and (7.5). Because it corresponds more closely to the experimental situation, we also use a Gaussian distribution with aspect ratio 1 : 1 : 5 to generate the random atomic positions.

Figs. 7.8 and 7.9 show the experimental signal as a function of time, together with a signal computed using the numerical simulations and fit to the data. The experimental data for both graphs are the data of Fig. 3.8 on page 71 of Ref. [40], but we show here all the data points.

The fits are made by first determining the vertical coordinates where the experimental signal

Figure 7.6: A plot of the width as a function of time for $u = 4v$.

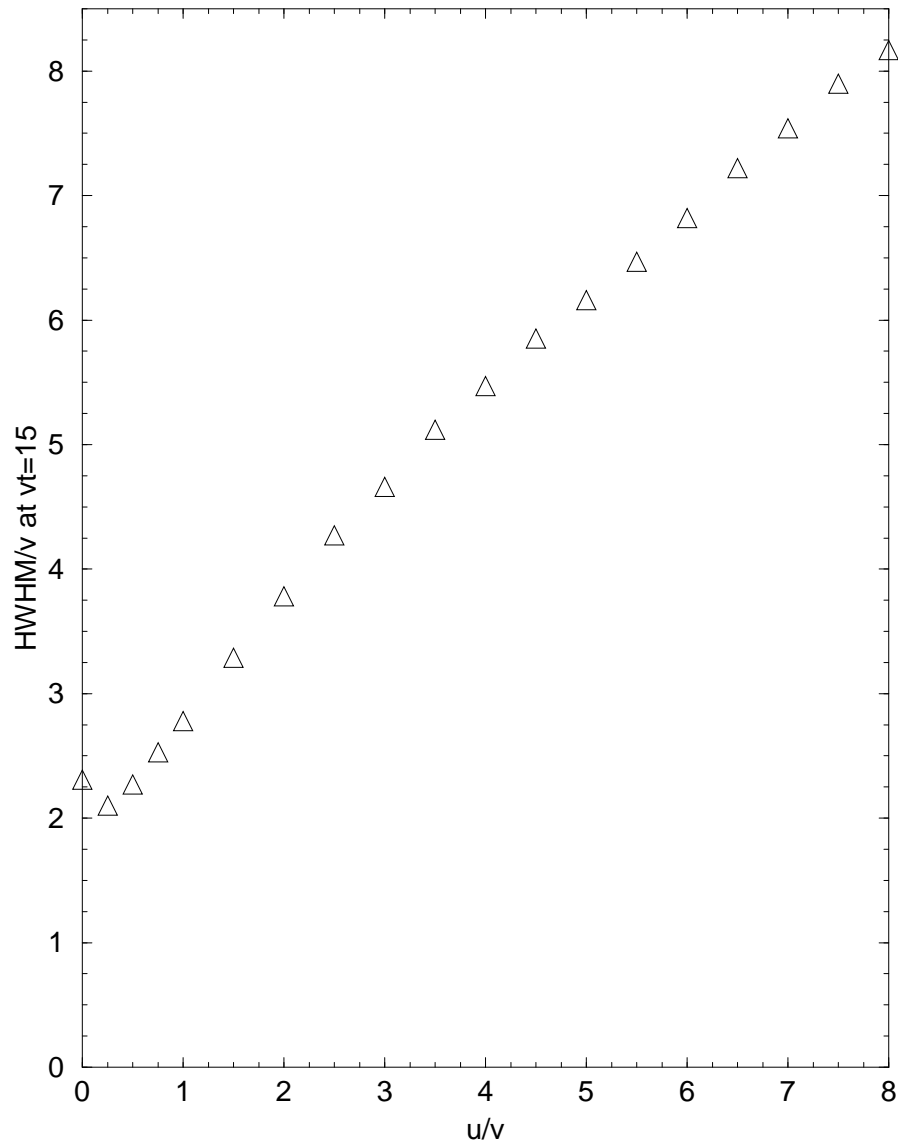


Figure 7.7: A plot of the width at $vt = 15$ as a function of the ratio u/v .

starts and stops. The difference between the two gives the vertical scale of the experimental signal, which is necessary because as one can see the experimental signal does not simply start at zero and rise to some value less than one. For example, in Fig. 7.8 we assumed that the experimental signal started at 900 and ended at 1850 so that the vertical scale was 950. The initial slope is then determined by fitting the first several points to a straight line. For Fig. 7.8 we obtained an initial slope of $4107 \mu\text{s}^{-1}$. We then have

$$\frac{\sqrt{\pi} v}{2 \hbar} = 3.83115 \mu\text{s}^{-1}, \quad (7.24)$$

which gives a value for the parameter v and hence the density N/Ω . This fixes the horizontal scale, and so all that remains is to adjust the parameter u/v until we find a good fit.

Fig. 7.10 shows the experimental width as a function of time. The data of Anderson *et al.* are taken from Fig. 4-18 on page 149 of Ref. [5], while the data of Lowell *et al.* are taken from Fig. 3.10 on page 75 of Ref. [40]. The discrepancy between the two sets of data has not yet been resolved by the experimentalists. Although the result of the simulations fit Anderson's data quite well for the parameters $u = 4v$ and $N/\Omega = 2 \times 10^9 \text{ cm}^{-3}$, it is important to note that these data are for rather small times, and are within or very close to the region where the universal t^{-1} behavior discussed in Section 7.6 is present. Thus for a wide range of values of the parameter u there will exist densities N/Ω that produce a good fit to the Anderson data.

7.8 Summary

We have seen in this chapter how to develop numerical simulations to solve Eqs. (7.1a) and (7.1b) for any quantity we want and average the result over many realizations of the system. Although Eqs. (7.1a) and (7.1b) apply to the sparse case where we begin initially with a single s' atom in a sea of s atoms, we have also discussed in this chapter how to extend these results to the nonsparse case. The simulation results agree very well with the exact analytical results of Chapter 2, as well as with the approximate analytical results of Chapter 4. The results of the simulations can also be compared with the experimental data of Anderson *et al.* [5, 6] and Lowell *et al.* [40], and we find that the agreement is again quite good.

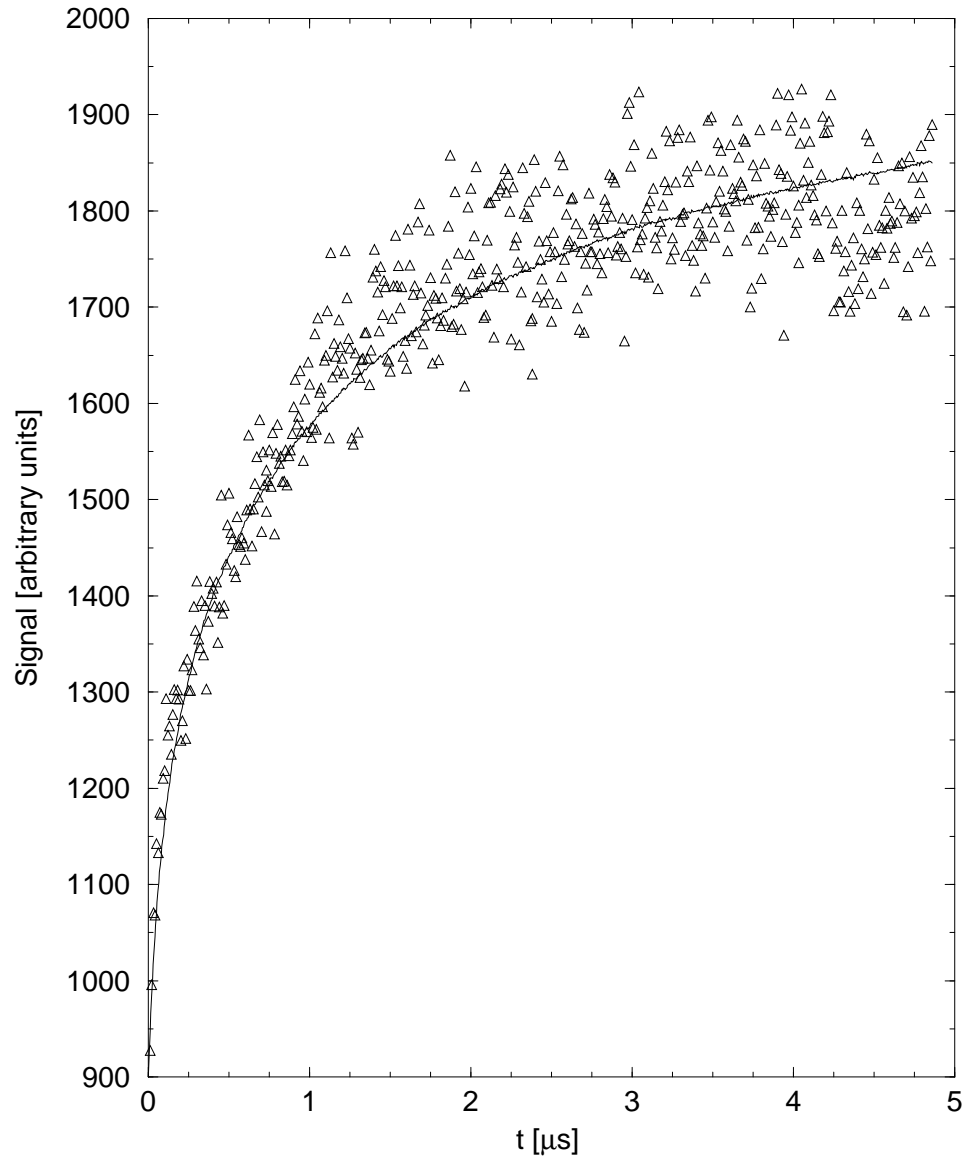


Figure 7.8: The experimental signal as a function of time (triangles), together with a signal curve computed using the numerical simulations and fit to the data. The fit parameters are $u = 12v$ and $N/\Omega = 2.25 \times 10^9 \text{ cm}^{-3}$.

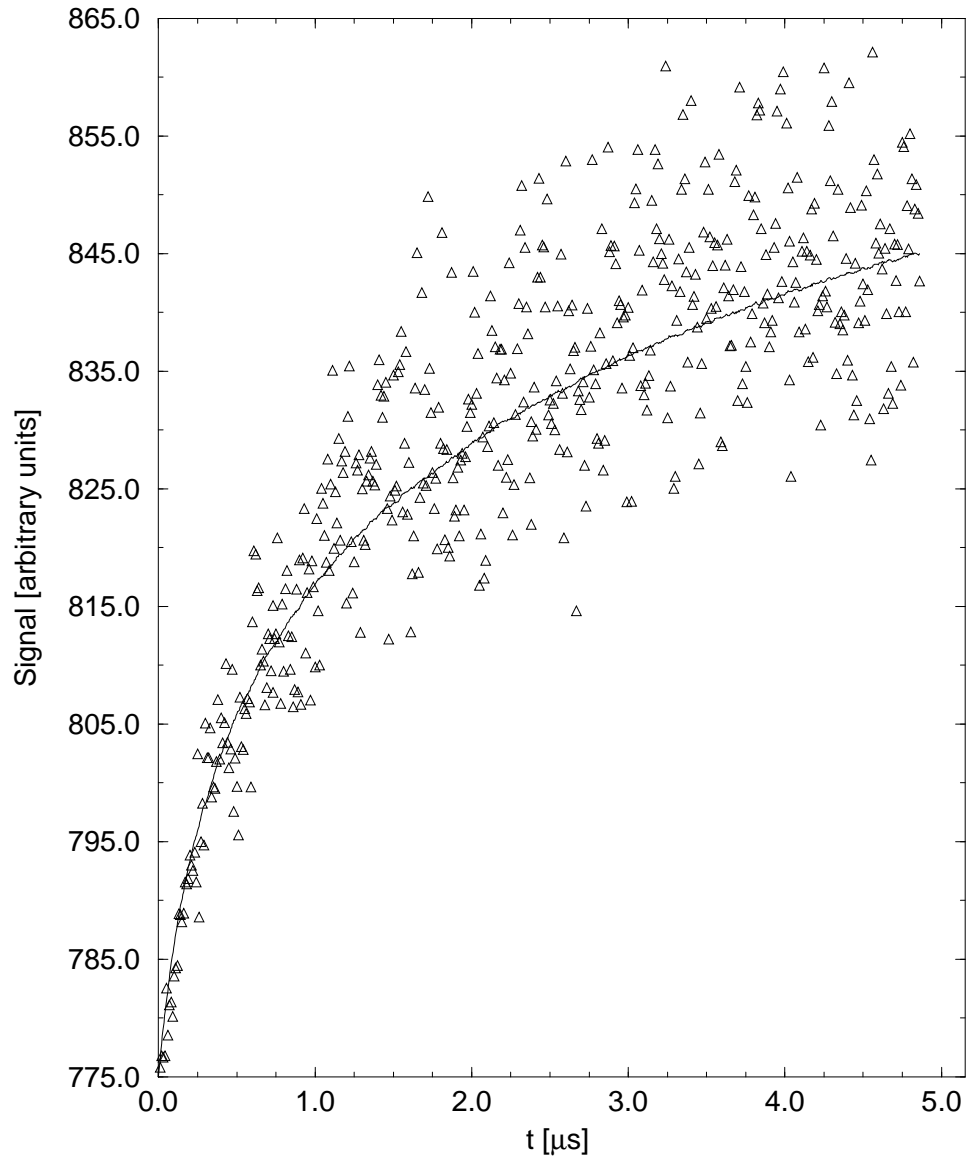


Figure 7.9: The experimental signal as a function of time (triangles), together with a signal curve computed using the numerical simulations and fit to the data. The fit parameters are $u = 12v$ and $N/\Omega = 6.70 \times 10^8 \text{ cm}^{-3}$.

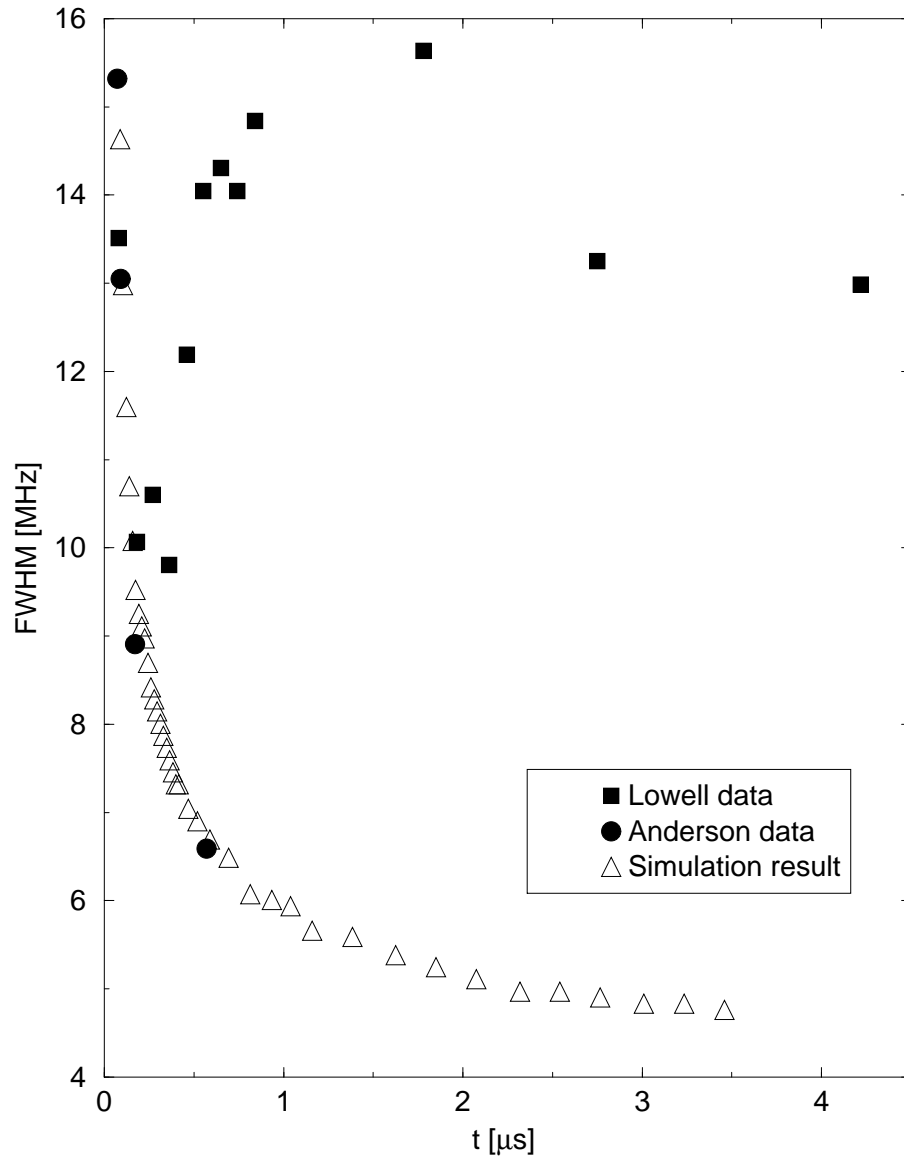


Figure 7.10: The experimental width as a function of time. The circles are the data of Anderson *et al.* [5, 6], while the squares are the data of Lowell [40]. The triangles are a width curve computed using the numerical simulations and fit to the data. The fit parameters are $u = 4v$ and $N/\Omega = 2 \times 10^9 \text{ cm}^{-3}$.

Chapter 8

Final Thoughts

Although we have focused chiefly on resonant dipole-dipole interactions among frozen Rydberg atoms in this thesis, there are many connections of this work with related experiments, as well as more general applications of the techniques we have developed.

In this thesis we have always considered the atoms to be frozen in place. It is true that the atoms are sufficiently cold that they move only a small fraction of their average interatomic spacing during the course of the experiment, but close pairs of atoms can be separated by distances considerably smaller than this, and hence the effects of interatomic motion can be considered. Certainly this would be a worthwhile endeavor, since one would ideally like to eventually have a theory that reduces to the frozen results of this thesis at low temperatures and, as the temperature increases, eventually makes the transition to the high-temperature regime where the results are dominated by binary atomic collisions. Some ideas for the inclusion of finite temperature effects can be gleaned from the extensive literature on dipolar liquids [12, 28, 31, 30, 37, 39, 58].

Dipole-dipole interactions among frozen Rydberg atoms may one day be useful for quantum computing, as methods for producing entanglement in such systems have already been studied theoretically [10, 32, 41] as well as experimentally [42]. This method for quantum computing has advantages over others that have been proposed. Entanglement of photon pairs, for example, has the disadvantage that the production of such pairs is not very efficient.

Experiments have been done recently that illustrate the creation of ultracold plasmas using Rydberg atoms [34, 36], and even the spontaneous evolution of Rydberg atoms into an ultracold plasma [52]. Unlike in a high-temperature plasma where the kinetic energy of the particles always

dominates, an ultracold plasma can be strongly coupled because the Coulomb interaction between neighboring particles can exceed their kinetic energy. Therefore such plasmas are of theoretical interest because they exhibit qualitatively different features than their high-temperature counterparts.

Although we have averaged over random distributions of atoms in this work, it is also possible to construct periodic optical potentials [26, 29, 33, 61] and even quasiperiodic optical lattices [27]. In the periodic case it is necessary to, instead of averaging, consider instead the appropriate dipolar sums for regular lattices, which are discussed in Refs. [13] and [20].

Bibliography

- [1] R. Abou-Chacra, P. W. Anderson, and D. J. Thouless. A self-consistent theory of localization. *J. Phys. C*, 6:1734, 1973.
- [2] Milton Abramowitz and Irene A. Stegun, editors. *Handbook of Mathematical Functions with Formulas, Graphs, and Mathematical Tables*. Dover, 1972.
- [3] V. M. Akulin, F. de Tomasi, I. Mourachko, and P. Pillet. Level-band problem and many-body effects in cold Rydberg atoms. *Physica D*, 131:125, 1999.
- [4] E. Anderson, Z. Bai, C. Bischof, S. Blackford, J. Demmel, J. Dongarra, J. Du Croz, A. Greenbaum, S. Hammarling, A. McKenney, and D. Sorensen. *LAPACK Users' Guide*. Society for Industrial & Applied Mathematics, 1999.
- [5] W. R. Anderson. *Resonant Dipole-Dipole Collisions of Magneto-Optically Trapped Rydberg Atoms*. PhD thesis, University of Virginia, 1996.
- [6] W. R. Anderson, J. R. Veale, and T. F. Gallagher. Resonant dipole-dipole energy transfer in a nearly frozen Rydberg gas. *Phys. Rev. Lett.*, 80:249, 1998.
- [7] George Arfken. *Mathematical Methods for Physicists*. Academic Press, 1985.
- [8] F. Bassani, G. Pastori Parravicini, and R. A. Ballinger. *Electronic States and Optical Transitions in Solids*. Pergamon, 1975.
- [9] Hans A. Bethe and Edwin A. Salpeter. *Quantum Mechanics of One- and Two-Electron Atoms*. Plenum Publishing Corporation, 1977.
- [10] Gavin K. Brennan and Ivan H. Deutsch. Entangling dipole-dipole interactions for quantum logic with neutral atoms. *Phys. Rev. A*, 61:062309, 2000.
- [11] V. Celli and J. S. Frasier. Laser excitation of polarization waves in a frozen gas. *cond-mat/9908230*, 1999.
- [12] D. Chandler, K. S. Schweizer, and P. G. Wolynes. Electronic states of a topologically disordered system: Exact solution of the mean spherical model for liquids. *Phys. Rev. Lett.*, 49:1100, 1982.
- [13] M. H. Cohen and F. Keffer. Dipolar sums in the primitive cubic lattices. *Phys. Rev.*, 99:1128, 1955.
- [14] E. U. Condon and G. H. Shortley. *The Theory of Atomic Spectra*. Cambridge University Press, 1964.
- [15] D. L. Dexter and R. S. Knox. *Excitons*. John Wiley & Sons, 1965.
- [16] E. N. Economou. *Green's Functions in Quantum Physics*. Springer, 1983.

- [17] J. S. Frasier and V. Celli. Resonant processes and exciton propagation in a frozen gas. *cond-mat/0008433*, 2000.
- [18] J. S. Frasier, V. Celli, and T. Blum. Resonant processes in a frozen gas. *Phys. Rev. A*, 59:4358, 1999.
- [19] Harald Friedrich. *Theoretical Atomic Physics*. Springer-Verlag, 1991.
- [20] N. M. Fujuki, K. De'Bell, and D. J. W. Geldart. Lattice sums for dipolar systems. *Phys. Rev. B*, 36:8512, 1987.
- [21] T. F. Gallagher. Resonant collisional energy transfer between Rydberg atoms. *Phys. Rep.*, 210:319, 1992.
- [22] T. F. Gallagher. *Rydberg Atoms*. Cambridge University Press, 1994.
- [23] T. F. Gallagher and M. P. Robinson. Private communication.
- [24] Al Geist, Adam Beguelin, Jack Dongarra, Weicheng Jiang, Robert Manchek, and Vaidy Sunderam. *PVM: Parallel Virtual Machine – A Users' Guide and Tutorial for Networked Parallel Computing*. MIT Press, 1994.
- [25] I. S. Gradshteyn and I. M. Ryzhik. *Table of Integrals, Series, and Products*. Academic, 1994.
- [26] G. Grynberg, B. Lounis, P. Verkerk, J.-Y. Courtois, and C. Salomon. Quantized motion of cold cesium atoms in two- and three-dimensional optical potentials. *Phys. Rev. Lett.*, 70:2249, 1993.
- [27] L. Guidoni, C. Triché, P. Verkerk, and G. Grynberg. Quasiperiodic optical lattices. *Phys. Rev. Lett.*, 79:3363, 1997.
- [28] R. W. Hall and P. G. Wolynes. Solvent influence on atomic spectra: The effect of finite size. *J. Chem. Phys.*, 83:3214, 1985.
- [29] A. Hemmerich and T. W. Hänsch. Two-dimensional atomic crystal bound by light. *Phys. Rev. Lett.*, 70:410, 1993.
- [30] J. S. Høye and K. Olaussen. Eigenmodes of the quantized polarizable fluid. *J. Chem. Phys.*, 77:2583, 1982.
- [31] J. S. Høye and G. Stell. Quantum statistical model for polarizable fluids. *J. Chem. Phys.*, 75:5133, 1981.
- [32] D. Jaksch, J. I. Cirac, P. Zoller, R. Côté, and M. D. Lukin. Fast quantum gates for neutral atoms. *Phys. Rev. Lett.*, 85:2208, 2000.
- [33] A. Kastberg, W. D. Phillips, S. L. Rolston, R. Spreew, and P. S. Jessen. Adiabatic cooling of cesium to 700 nK in an optical lattice. *Phys. Rev. Lett.*, 74:1542, 1995.
- [34] T. C. Killian, S. Kulin, S. D. Bergeson, L. A. Orozco, C. Orzel, and S. L. Rolston. Creation of an ultracold neutral plasma. *Phys. Rev. Lett.*, 83:4776, 1999.
- [35] Robert S. Knox. *Theory of Excitons*. Academic, 1963.
- [36] S. Kulin, T. C. Killian, S. D. Bergeson, and S. L. Rolston. Plasma oscillations and expansion of an ultracold neutral plasma. *Phys. Rev. Lett.*, 85:318, 2000.
- [37] D. E. Logan and P. G. Wolynes. Localizability and dephasing of dipolar excitons in topologically disordered systems. *J. Chem. Phys.*, 87:7199, 1987.

- [38] David E. Logan and Peter G. Wolynes. Anderson localization in topologically disordered systems. *Phys. Rev. B*, 31:2437, 1985.
- [39] David E. Logan and Peter G. Wolynes. Dephasing and Anderson localization in topologically disordered systems. *Phys. Rev. B*, 36:4135, 1987.
- [40] J. R. Lowell. *Dipole-Dipole Interactions in a Frozen Rydberg Gas*. PhD thesis, University of Virginia, 1998.
- [41] M. D. Lukin and P. R. Hemmer. Quantum entanglement via optical control of atom-atom interactions. *Phys. Rev. Lett.*, 84:2818, 2000.
- [42] X. Maître, E. Hagley, C. Wunderlich, P. Goy, M. Brune, J. M. Raimond, and S. Haroche. Quantum memory with a single photon in a cavity. *Phys. Rev. Lett.*, 79:769, 1997.
- [43] Jon Matthews and R. L. Walker. *Mathematical Methods of Physics*. W. A. Benjamin, Inc., 1970.
- [44] I. Mourachko. *Contribution Expérimentale et Théoretique à l'Etude des Effets à N Corps dans un Gaz de Rydberg Gelé de Césium*. PhD thesis, Université Paris XI Orsay, 1999.
- [45] I. Mourachko, D. Comparat, F. de Tomasi, A. Fioretti, P. Nosbaum, V. M. Akulin, and P. Pillet. Many-body effects in a frozen Rydberg gas. *Phys. Rev. Lett.*, 80:253, 1998.
- [46] M. Movre and G. Pichler. Resonance interaction and self-broadening of alkali resonance lines I. Adiabatic potential curves. *J. Phys. B*, 10:2631, 1977.
- [47] William H. Press, Saul A. Teukolsky, William T. Vetterling, and Brian P. Flannery. *Numerical Recipes in Fortran 77: The Art of Scientific Computing*. Cambridge University Press, 1992.
- [48] William H. Press, Saul A. Teukolsky, William T. Vetterling, and Brian P. Flannery. *Numerical Recipes in Fortran 90: The Art of Parallel Scientific Computing*. Cambridge University Press, 1996.
- [49] F. Reif. *Fundamentals of Statistical and Thermal Physics*. McGraw-Hill, 1963.
- [50] M. J. Renn, Q. S. Sun, and T. F. Gallagher. Resonant collisions of Na Rydberg atoms in electric and magnetic fields. *Phys. Rev. A*, 50:4077, 1994.
- [51] G. E. Roberts and H. Kaufman. *Table of Laplace Transforms*. W. B. Saunders, 1966.
- [52] M. P. Robinson, B. Laburthe Tolra, Michael W. Noel, T. F. Gallagher, and P. Pillet. Spontaneous evolution of Rydberg atoms into an ultracold plasma. *Phys. Rev. Lett.*, 85:4466, 2000.
- [53] J. J. Sakurai. *Modern Quantum Mechanics*. Addison-Wesley, 1994.
- [54] L. Santos, G. V. Shlyapnikov, P. Zoller, and M. Lewenstein. Bose-Einstein condensation in trapped dipolar gases. *Phys. Rev. Lett.*, 85:1791, 2000.
- [55] Leonard Schiff. *Quantum Mechanics*. McGraw-Hill, 1960.
- [56] Franz Schwabl. *Quantum Mechanics*. Springer-Verlag, 1995.
- [57] R. C. Stoneman, M. D. Adams, and T. F. Gallagher. Resonant-collision spectroscopy of Rydberg atoms. *Phys. Rev. Lett.*, 58:1324, 1987.
- [58] M. J. Thompson, K. S. Schweizer, and D. Chandler. Quantum theory of polarization in liquids: Exact solution of the mean spherical and related approximations. *J. Chem. Phys.*, 76:1128, 1982.

- [59] D. S. Thomson. *Resonant Collisions of Rydberg Atoms*. PhD thesis, University of Virginia, 1990.
- [60] D. S. Thomson, M. J. Renn, and T. F. Gallagher. Transform-limited collisions of K Rydberg atoms. *Phys. Rev. Lett.*, 65:3273, 1990.
- [61] P. Verkerk, B. Lounis, C. Salomon, C. Cohen-Tannoudji, J.-Y. Courtois, and G. Grynberg. Dynamics and spatial order of cold cesium atoms in a periodic optical potential. *Phys. Rev. Lett.*, 68:3861, 1992.
- [62] Stephen Wolfram. *The Mathematica Book, 3rd ed.* Wolfram Media/Cambridge University Press, 1996.